DEVELOPMENT OF SUSTAINABLE SOLID ACID AND BASE CARBON CATALYSTS FOR THE SYNTHESIS OF VALUE-ADDED CHEMICALS AND AVIATION FUELS

by

SARADA SRIPADA

(Under the direction of DR. JAMES R KASTNER)

ABSTRACT

This work developed synthesis methods for sustainable solid acid and base carbon catalysts from wood-based activated carbon in granular (GAC) and monolith (ACM) forms, and applications in continuous esterification (acid catalyzed esters) and condensation (base catalyzed aviation fuels). Solid acid carbon catalysts were synthesized by modified hydrothermal or low temperature hydrogen and water vapor plasma techniques. The catalytic activity of the hydrothermal and plasma sulfonated carbons was compared to commercial Amberlyst-15 in batch esterification reactions of 2-hydroxyisobutyric acid (2-HIBA) with ethanol. The hydrothermally sulfonated GAC (sGAC) and ACM (sACM) displayed reaction rates and ester yields comparable to Amberlyst-15 (150 °C, 1 h). Plasma methods successfully sulfonated the carbon materials at much lower temperatures and treatment times, yet generated low ester yields due to low acid site density. In the continuous esterification of 2-HIBA, the sACM displayed a higher space-time-yield of 96 g $Lcat^{-1}$ h^{-1} and selectivity of 76% compared to the sGAC (87 g $Lcat^{-1}$ h^{-1}, 60%) at

150 °C, 300 psig, and 3 mL min^{-1}. Time-on-stream studies suggested greater catalytic stability of the sulfonated carbons over Amberlyst-15 and significantly lower production of unwanted by-products. A kinetic model was developed for 2-HIBA esterification over the sulfonated carbons for use in scale-up and reactor design. Both Eley-Rideal and Langmuir-Hinshelwood models agreed with the experimental data. The catalytic activity of sGAC and sACM for pyruvic acid esterification (a possible fermentation derived biochemical) was also compared to Amberlyst-15. The sulfonated carbons displayed similar pyruvic acid conversion and selectivity, significantly higher turnover frequencies, lower water inhibition, yet lower ester yield than Amberlyst-15. Fermentation residuals including water and salts (phosphates and sulfates) reduced catalytic activity, suggesting side reactions and accelerated ester hydrolysis. Solid base ACM supported hydrotalcite catalysts (HT/ACM) were synthesized using traditional calcination, rehydration and sustainable air plasma techniques and demonstrated for continuous cyclopentanone self-condensation. The HT/ACM activated by air plasma (100 W,1 min) displayed higher catalytic efficiency than the calcined (500 °C, 4 h) and rehydrated ACM. The solid acid and base carbons synthesized in this work are promising catalysts for the catalytic upgrading of bio-based organic acids and cyclic and linear ketones.

INDEX WORDS: Activated Carbon Monolith, Continuous flow technology, Esterification, Condensation

DEVELOPMENT OF SUSTAINABLE SOLID ACID AND BASE CARBON CATALYSTS FOR THE SYNTHESIS OF VALUE-ADDED CHEMICALS AND AVIATION FUELS

by

SARADA SRIPADA

B.S., Amity University, India, 2012

M.S., Anna University, India, 2014

A Dissertation Submitted to the Graduate Faculty of the University of Georgia in Partial Fulfillment of the Requirements for the Degree

DOCTOR OF PHILOSOPHY

ATHENS, GEORGIA

2023

DEVELOPMENT OF SUSTAINABLE SOLID ACID AND BASE CARBON CATALYSTS FOR THE SYNTHESIS OF VALUE-ADDED CHEMICALS AND AVIATION FUELS

by

SARADA SRIPADA

Major Professor: James R Kastner

Advisory Committee: Mark Eiteman

William Kisaalita

Eric Ferreira

Brandon Rotavera

Electronic Version Approved:

Ron Walcott

Vice Provost for Graduate Education and Dean of the Graduate School

The University of Georgia

December 2023

ACKNOWLEDGEMENTS

I would like to express my gratitude to my advisor, Dr. James Kastner, for his guidance and support throughout my Ph.D. and graduate school. His mentorship has been truly valuable and helped me grow professionally. I am very thankful to him for giving me the opportunity to work in his lab.

I want to thank my committee members, Dr. Mark Eiteman, Dr. William Kisaalita, Dr. Brandon Rotavera, and Dr. Eric Ferreira, for their guidance and valuable suggestions that helped shape the course of my Ph.D. research.

I thank my former lab mates Maryam Pirmoradi, Nida Janualitis, and Seyedehsaan Vasefi for their assistance and support throughout my Ph.D.

I am incredibly thankful to my late father, Dr. Sripada V. Mani, my mother, Dr. Sripada Swarnalata, and my grandparents for their constant encouragement and support in all my academic pursuits.

Also, my friends Dr. Hemshikha Rajpurohit and Rashmi Pandey have been an instrumental part of my Ph.D. and have been family away from home. I thank them and all my other friends for their support throughout this incredible journey.

TABLE OF CONTENTS

Page

LIST OF TABLES

LIST OF FIGURES

CHAPTER 1

INTRODUCTION

Homogeneous acids (H_2SO_4, HCl, and H_3PO_4) and bases (NaOH and KOH) have been widely employed in various organic reactions such as esterification, transesterification, hydrolysis, condensation, etc. Although these liquid catalysts possess high catalytic efficiency, their usage presents several limitations including equipment corrosion, catalyst reuse and recycling, and treatment of the spent effluent. Moreover, liquid catalysts may react with other functional groups in the reaction mixture, generating unwanted byproducts. For instance, liquid sulfuric acid may interact with ethanol to produce ethylene or diethyl ether. To be well-suited for industrial applications, a catalyst should possess high activity, selectivity, stability, and longevity, while causing minimal environmental impact. In this regard, heterogeneous solid acid and base catalysts are advantageous as they facilitate easier product separation, ensure catalyst recyclability, and generate lesser waste, circumventing the environmental concerns associated with their homogeneous counterparts.

Most of the solid acid and base catalysts currently being used present certain drawbacks such as low porosity and surface area, low acid site density, poor stability, low tolerance to water, low thermal stability, high cost of preparation and synthesis from fossil-based resources (e.g., ion exchange resins such as Amberlyst-15). Activated carbon (AC) has emerged as a material of choice, both as a catalyst and catalyst support due to its high specific surface area and porosity, chemical inertness, stability under acidic and basic conditions, and inexpensive synthesis from

renewable biomass. Further, in monolith form (ACM), activated carbon offers the advantages of high external surface area, high mass transfer rates and low pressure drop, facilitating its application in continuous processes.

The preparation of solid acids and bases employs large quantities of harsh chemical reagents (e.g., H_2SO_4 for sulfonated carbons), and requires high temperatures/calcination and long durations. These challenges can be overcome by modifying some of the current preparation methods, as well as exploring new catalyst design tools such as plasma functionalization/activation. Plasma technology can be used to functionalize activated carbon at low temperatures and pressures, within shorter durations.

This work focuses on developing green routes for the synthesis of solid acid (sulfonated carbon) and base (hydrotalcite/carbon) activated carbon catalysts using granular and structured carbon (ACM) derived from woody biomass as platform catalysts.

The specific goals of this work include:

1) To compare the catalytic performance of hydrothermal and plasma sulfonated carbon catalysts in granular and monolith forms with an industrial benchmark catalyst Amberlyst-15 in the batch esterification of 2-hydroxyisobutyric acid (2-HIBA).

2) To demonstrate the continuous esterification of 2-HIBA using the solid acid carbon monolith catalyst and compare the performance and longevity of this catalyst with granular forms and a commercial catalyst.

3) To develop a kinetic model for 2-HIBA esterification over the sulfonated carbon catalysts (GAC and ACM), to aid in reactor design and scale-up.

4) To investigate the applications of the solid acid carbon catalysts in the esterification of pyruvic acid and study the impact of potential catalyst poisons (fermentation medium components) on catalytic activity.

5) To demonstrate the continuous condensation of cyclopentanone for the synthesis of high-density aviation fuels using solid base carbon monolith catalysts.

The novel aspects of this work include (1) the development of more sustainable wood-based solid acid activated carbon (monolith) catalysts by modified hydrothermal & plasma methods for the catalytic esterification of less-explored bio-based organic acids (e.g., 2-HIBA, pyruvic acid), (2) design of a continuous esterification process using the solid acid carbon monolith, (3) development of an esterification kinetic model over the solid acid carbon monolith and (4) development of a continuous condensation process using solid base carbon monolith catalysts.

CHAPTER 2

BACKGROUND AND LITERATURE REVIEW

There has been a paradigm shift to employing solid heterogeneous catalysts in the fine and specialty chemical industry to combat the limitations posed by homogeneous liquid catalysts. The following sections introduce solid catalysts, their preparation methods, and the support materials currently used in the chemical industry. The advantages of renewable activated carbon as a catalyst support, particularly in monolith forms, are discussed. Conventionally employed solid acid and base carbon catalysts, their preparation methods, and the need for more sustainable catalyst design tools are emphasized. The advantages of employing structured catalysts in continuous processes are also highlighted. The applications of solid acid carbons (sulfonated carbons) in esterification reactions and solid base (carbon-supported hydrotalcite) carbon catalysts in condensation reactions are discussed. In addition, the reaction mechanisms of solid acids, catalyst deactivation, and mitigation strategies are detailed.

2.1 Solid Catalysts

Solid acid/base heterogeneous catalysts pose several advantages over their homogeneous counterparts, the most significant being ease of catalyst recovery and reuse, which lowers operating costs.[1] The catalytic properties of solid catalysts depend greatly on the preparation steps as well as the purity/impurity of the precursor materials. Solid catalysts can be categorized into two main classes based on their preparation methods; bulk catalysts and impregnated/supported catalysts. Bulk catalysts, in which the entire catalyst is made of the active

material are generally prepared by precipitation/co-precipitation and hydrothermal synthesis, whereas impregnation methods involve introducing the active phase onto a porous bulk support. The support could be an oxide such as silica, activated carbon or a polymer resin.[2] In addition, extrusion is used for the synthesis of structured catalysts such as monoliths. The methods commonly used for the preparation of solid catalysts are discussed below.

Precipitation/Co-precipitation

Precipitation is one of the most frequently used methods for the preparation of solid catalysts including aluminum and silicon oxides.[3] This technique involves mixing precursor solutions (aqueous salt solutions), followed by precipitation of the desired salt by adding another reagent (e.g., acid/base). The precipitate is aged, filtered, washed, dried, and finally calcined to give the desired catalyst. Co-precipitation involves the simultaneous precipitation of more than one component and has been used for the synthesis of catalysts such as Ni/Al_2O_3, Cu/ZnO, and Mg-Al hydrotalcites.[3,4] Precipitation can yield high purity materials while co-precipitation can generate stoichiometric mixtures with well-defined mixed crystallites. [2]

Hydrothermal Synthesis

Hydrothermal treatments involve heating of precipitates or flocculates in the presence of water and are typically carried out in an autoclave between 100-300 °C. These treatments bring about structural changes in the catalyst such as crystal/particle growth and transformation of amorphous solids to crystalline materials. Hydrothermal synthesis has been widely applied in the synthesis of solid acid zeolites such as HZSM-5 (synthesis steps depicted in Figure 2.1) and sulfonated carbon catalysts.[2,5]

Impregnation

In impregnation techniques, the catalyst support is contacted with a precursor solution. Impregnation can be performed in two ways; wet impregnation, in which an excess amount of precursor solution is used, and incipient wetness or pore-volume impregnation, where only the pores of the catalyst support are filled with the precursor solution.[6] A limitation with wet impregnation is the generation of large volumes of aqueous waste, which can be overcome by the incipient wetness method. [6]

Extrusion

In this method, the catalyst powder is made into a paste with a binder material. Typically, clay, starch, and alumina are used as binders, depending on the mechanical and rheological properties required. The paste is forced through a former to yield extrudates, which are cut, dried, and calcined to give the final catalyst. [2] Extrusion molding, a common monolithic integration technology, has been applied for the synthesis of monoliths.[7] Catalysts, binders and pore-forming agents are extruded from a mold and cut into the desired shape. However, monoliths fabricated using this technology contain the catalyst both in the bulk and on the surface, reducing the utilization rate of the catalyst. This limitation can be overcome by deposition of the active phase on the monolith support, increasing catalyst utilization. [8]

Drying, Calcination, Activation

The preparation of solid catalysts generally involves a drying step, to eliminate solvents (mainly water) from the pores of the solid catalyst. Calcination, which involves drying at high temperatures (300-800 ºC) in air/N_2 eliminates water from the catalyst and decomposes carbonate and nitrate precursors, forming metal-oxide links in the support material. Based on the

final application, the catalyst may need to be activated prior to introducing the active phase or initiating the reaction. Activation of hydrotalcite catalysts by air calcination is an example. [2]

The catalyst preparation method adopted can strongly influence the performance of the catalyst, as very different conversions can be obtained with different sized particles and distributions. Further, the catalytic activity of solid acids and bases is influenced by the concentration and strength of Lewis/Bronsted acid/base sites. Catalyst support materials such as TiO_2, mesoporous silica and γ- alumina have been widely used in the chemical industry. To reduce the dependence on fossil fuels, the chemical industry is transitioning to renewable feedstocks for manufacturing value-added chemicals and fuels. However, these oxide supports are unstable in hydrothermal conditions, commonly encountered in biomass transformation reactions.[9] These materials do not retain their structural integrity, leading to decreased catalyst performance and difficulty in catalyst recovery and reuse. To overcome these limitations, activated carbon is gaining significance as a catalyst support material.[9]

2.2 Activated Carbon (AC) as a Catalyst Support

Activated carbon (AC) or activated charcoal is an amorphous, non-graphitic, black carbonaceous solid material with a high surface area (200-1500 m^2/g), excellent electron conductivity, chemical inertness, and well-developed porosity. In addition, AC is stable under acidic, basic, and aqueous environments.[10] These properties make AC a valuable support for biomass transformation reactions. The surface of AC generally comprises chemical groups such as carboxyl (COOH) and phenolic (OH) groups which may play an important role in catalytic reactions.[11] In addition, introducing heteroatoms onto the carbon surface can induce different types of active phase-support interactions, which is possible only to a certain extent in catalyst supports such as silica or alumina.[10] Moreover, activated carbon can be synthesized from

renewable biomass, reducing both the cost and carbon footprint of catalyst and chemical manufacturing processes. Despite the numerous advantages of activated carbon, less than 1% of the globally produced AC is used as a catalyst support, possibly due to the difficulty in reproducibility owing to the inconsistency of carbon precursor compositions.[10]

2.2.1 Preparation of AC

Some of the precursor materials commonly used for AC synthesis include fossil-based resources such as coal, and renewable agricultural waste/ biomass resources such as wood, straw, rice husk, coconut shells, corn cobs and olive stones.[10,11] Agricultural and industrial wastes have tremendous potential as raw materials for the synthesis of AC, especially in developing countries, due to their wide availability and low-cost.[12] The synthesis of AC occurs in two steps: carbonization and activation. Carbonization involves pyrolysis of the carbon precursors at temperatures ranging from 300-900 °C and reduces the volatile content of the raw materials. Activation improves the specific surface area or pore volume of the carbon material, by opening new pores and developing the existing pores in AC and imparts unique chemical characteristics to the carbon surface. The most used techniques for the activation of carbon are (i) physical activation, and (ii) chemical activation.[13] Physical activation involves carbonization in the presence of an inert gas such as N_2 or Ar, followed by activation in the presence of an oxidizing gas (O_2, CO_2, H_2O, steam) at temperatures ranging from 800-1200 °C. The formation of pores during physical activation is mostly due to removal of carbon atoms by gasification.[13] In chemical activation methods, carbonization and activation occur simultaneously at temperatures ranging between 450-850 °C. The carbon material is impregnated with a chemical reagent (which causes dehydration of the carbon precursor), followed by thermal activation to generate the pore structure.[14] Several chemical reagents have been employed for carbon activation

including, alkaline (e.g., KOH, K_2CO_3, NaOH), acidic (e.g., H_3PO_4, H_2SO_4, HNO_3), and neutral agents (e.g., $ZnCl_2$, $MgCl_2$, $CaCl_2$). [13] H_3PO_4 and KOH have been widely used for synthesizing AC with a high specific surface area and well-developed porosity. While KOH is advantageous as it develops high microporosity, the yield of AC impregnated with KOH is lower than AC activated by H_3PO_4 at high temperatures (>650 ºC), i.e., the carbon content is lower than the fixed carbon in the raw material.[15]

AC is traditionally synthesized in the form of powder, pellets, and granules (Figure 2.2). In general, powdered forms of carbon are employed in batch slurry reactors while granular forms are used in trickle bed reactors. However, it is difficult to use powdered forms of carbon in continuous processing, due to particle attrition and difficulty in recovering and reusing the catalyst. Trickle bed reactors with granular carbon present limitations of pressure drop and intraparticle mass transfer limitations. AC in monolith form can overcome the limitations with the powdered/ granular forms in continuous processes.[16]

2.3 Monolithic Catalysts

A monolith is a single block of catalytic material with straight parallel channels through which reactants and products are transported by convective means. The active phase is usually applied as a coating (e.g., washcoat) or deposited in the channels of the monolith, in which case the channel walls serve as the catalyst and permit gas/liquid flow.[7] Monoliths are commonly manufactured in ceramic/metallic (Figure 2.3) forms and have been primarily implemented in catalytic converters for exhaust gas abatement.[7] The commercial use of monoliths as catalytic supports in the chemical industry is limited, owing to the high cost of catalyst preparation in

comparison to pellets/powders. Akzo Nobel uses a monolithic catalyst for the hydrogenation of anthraquinones in hydrogen peroxide production.[17]

2.3.1 Advantages of the Monolith Structure

Monoliths offer multifold advantages over granular/pellet catalysts including a large geometric surface area, controlled reaction environment, short intraparticle diffusional distances in the catalytically active layer, high mass transfer rates in the capillaries, large contact area between the catalyst support and reactants, and high volumetric productivity for a smaller amount of catalyst. Further, the open structure of the monolith without bends offers minimal obstruction to flow, resulting in low pressure drop, and thereby lower energy requirements.[18] Structured catalysts also provide good mechanical strength compared to traditional catalyst powders /pellets. In addition, monoliths enable the integration of the catalyst with the reactor, circumventing issues with separation and attrition and extending the longevity of the catalyst. In monolithic packings, the reactants are mixed before coming into contact with the catalyst, which prevents local high concentrations of reactants, and thereby undesired side reactions.[19, 20]

Monoliths are characterized by their (i) channel shape, (ii) cell density, measured as cells per square inch (cpsi) which varies from 5-900 cpsi and (iii) wall thickness. The channels are generally square, triangular, rectangular, cylindrical, or hexagonal. From these three parameters, the monolithic characteristics such as open frontal area (OFA), geometric surface area (GSA), characteristic diffusion length, void fraction, and hydraulic diameter can be measured, which determine the performance of the monolithic catalyst (Figure 2.3).[21]

2.3.2 Carbon-based Monoliths

Although monoliths are primarily fabricated in ceramic and metallic forms, they can also be extruded from other materials including zeolites and carbon.[7] Carbon-based monoliths are

gaining attention as catalyst supports. Apart from providing the benefits of a monolith structure, they have well developed porosity, high surface area, can be synthesized from renewable carbon sources, and are highly stable in aqueous, acidic, and basic environments.[16] Carbon-based monoliths can be distinguished as carbon-coated and integral carbon monoliths. Carbon-coated monoliths are synthesized by dip-coating or chemical vapor deposition (CVD). Dip-coating involves immersing and soaking ceramic honeycomb monoliths in a phenolic resin, followed by carbonization and activation.[22] The CVD method involves dipping the ceramic monolith in an alumina or silica suspension followed by impregnation with a transition metal salt, that acts as a catalyst to grow carbon nanofibers on the monolith support. The synthesis of integral carbon monoliths involves mixing the carbon material/precursor with binders and organic/inorganic fillers followed by extrusion, drying, carbonization and sometimes activation, to enhance the support porosity and surface area. By this method, the carbon material is uniformly distributed throughout the monolith, reducing the number of preparation steps. [22] Activated carbon monoliths have been used in gas phase applications for the adsorption of volatile organic compounds.[23, 24]

2.4 Solid Acid Catalysts

Solid acid catalysts are characterized based on various properties such as their turnover frequency (TOF), Brønsted/Lewis acidity, porosity, strength and concentration of catalytic sites, and surface area. Modification of these properties can lead to enhanced catalytic activity and product selectivity. Solid acids have been employed in several industrial chemical processes such as catalytic cracking in petroleum refining, alkylation, esterification, etherification, amination, and isomerization.[25] Over 180 industrial processes in operation employ solid acid catalysts including zeolites, mixed oxides, heteropolyacids, and phosphates.[26]

Several solid acids have been studied as substitutes for homogeneous H_2SO_4 including metal oxides, heteropoly acids, sulfated zirconia, zeolites, and acidic ion exchange resins (e.g., Amberlyst-15) in various acid-catalyzed reactions such as alkylation, isomerization, esterification, hydration, hydrolysis, and transesterification (biodiesel synthesis).[27,28,29,30,31] For instance, mixed metal oxides such as mesoporous Nb-W with Brønsted and Lewis acid sites have displayed high catalytic performance in sugar conversion reactions, Friedel-Crafts alkylation, hydrolysis, and esterification owing to their mesoporous nature and acid properties.[32,33] Sulfated zirconia has been found to be an effective solid acid for the dehydration of fructose to 5-hydroxymethylfurfural and fatty acid esterification[34,35] showing good thermal stability (170 °C), and catalytic activity. Acidic ion exchange resins such as Amberlyst-15 have been applied for the double bond isomerization of linear 1-alkenes,[36] and in the esterification of various carboxylic acids.[31,37] However, most catalysts including conventional oxide-based solid acids are limited by low surface areas and low porosities. Further, sulfated zirconia preparation uses toxic gaseous SO_3 or requires high temperature calcination (650 °C). This catalyst also undergoes deactivation in the presence of water, a common challenge with many solid acid catalysts.[35,38] In addition, ion exchange resins such as Amberlyst-15 are limited by their low thermal stability. Carbon-supported solid acids are receiving a lot of attention as they are highly stable, inexpensive, widely available, and have strong protonic acid sites on the surface. Solid acid carbon catalysts have been employed in condensation, hydrolysis, and esterification reactions.[39]

2.4.1 Sulfonated Carbon Catalysts (SC)

Solid acid sulfonated carbon (SC) catalysts have received wide attention as potential substitutes for H_2SO_4 for catalytic reactions, including esterification, transesterification, hydrolysis, and nitration.[40] SC catalysts are characterized by a Brønsted acidity like concentrated sulfuric acid, [41]

and hold the advantages of a carbon support in terms of a large surface area, and stability under acidic and basic conditions.[42] Carbon supported catalysts are also stable in aqueous environments, a prerequisite for equilibrium-limiting esterification reactions that generate water as a byproduct.[43] SCs possess strong Brønsted acid SO_3H groups as the key active sites, along with weakly acidic -COOH and phenolic -OH groups, a distinct feature from other conventional solid acids comprising single functional groups. These weak acidic groups enhance the accessibility of hydrophilic reactants to the active sites, favoring catalytic performance.[44]

2.4.2 Preparation of sulfonated carbons

Sulfonated carbons are generally prepared by the carbonization of organic raw materials, followed by treatment with a sulfonating agent to introduce SO_3H groups into the carbon support. Recently, several studies have focused on the synthesis of sulfonated carbons from renewable biomass-based sources such as rice-husk,[45] corncob,[5] palm-kernel shell,[46] and wood sawdust.[47] Catalysts manufactured from wood/biomass are non-toxic, inexpensive, environmentally benign, and biodegradable, which facilitates easier disposal once the catalyst is no longer active.[48] Various sulfonating agents such as chlorosulfonic acid,[49] fuming sulfuric acid/oleum,[50] sulfuric acid and gaseous SO_3[42] have been used for the sulfonation of carbon.

SC preparation generally involves subjecting the raw materials to carbonization either by pyrolysis or a hydrothermal process at temperatures ranging between 240-700 °C for 5-10 h, followed by sulfonation.[5] Conventionally, sulfonation is performed hydrothermally, by wet impregnation of carbon in an activating agent such as concentrated or fuming sulfuric acid at elevated temperatures (80-250 °C) for long durations (10-24 h). For instance, Kitano and co-workers heated activated carbon in fuming H_2SO_4 (30 mL H_2SO_4/g catalyst) at 80 °C for 10 h

under N_2.[51] Similarly, Adhikari et al. refluxed carbon fibers in concentrated H_2SO_4 (50 mL H_2SO_4/g catalyst) for 12 h at 150 °C.[52] The sulfonated carbons synthesized by these methods are washed repeatedly in deionized water until impurities such as sulfate ions are no longer detected in the wash water, followed by drying at 100-105 °C to obtain the SC catalyst.[51]

Carbon-based monolithic solid acid catalysts have been applied in dehydration and esterification reactions. Ibeh and co-workers synthesized an activated carbon monolith by the extrusion of biomass-based materials including Kraft lignin and H_3PO_4 activated-olive stones and investigated its catalytic activity in the dehydration of methanol.[53] Nakhate and Yadav synthesized a solid acid carbon-based graphene oxide monolith by solvothermal carbonization of glucose, followed by sulfonation with chlorosulfonic acid. The catalytic efficiency of the sulfonated monolith was assessed in the esterification of levulinic acid with benzyl alcohol.[54]

2.5 Solid Base Catalysts

While solid acid catalysis has received widespread attention on account of its applications in petroleum refining and petrochemical processes, catalysis by solid bases has been less explored. Studies on solid base catalysis are gaining momentum, as they play a key role in several reactions critical for fine-chemical synthesis.[55] Solid base catalysts are advantageous over their liquid base counterparts in having simpler separation and recovery processes and enabling high productivity through the use of flow reactors. Further, neutralization of the base is not necessary, minimizing waste generation. Moreover, high temperature reactions can be carried out with solid bases, a major constraint with liquid bases, where reaction temperature is limited by the boiling point of solvents used in the reaction mixture. Solid base catalysts have also gained significant attention for various industrial processes owing to their large specific surface area, uniform pore

size distribution, and strong alkalinity. Another advantage is the co-existence of acidic and basic sites on the catalytic surface, [55] conferring bifunctional characteristics.

Solid bases such as alkali earth metal oxides (MgO), calcined/activated hydrotalcites, base zeolites, and mixed oxides find widespread applications in organic reactions including aldol condensation, Michael addition, transesterification, and Knoevenagel condensation (Figure 2.4).[56,57,58,59] Hydrotalcites (HT's) have attracted a lot of attention due to their ease of preparation, high thermal stability, low environmental impact and cost, and ease of biodegradation.[60]

2.5.1 Hydrotalcites

Hydrotalcites (HT) are layered double-metal hydroxides (LDHs) comprising alternating $Mg_6Al_2(OH)_{16}^{2+}$ as the brucite ($Mg(OH)_2$) layer, intercalated with anionic CO_3^{2-}. A schematic view of the structure of hydrotalcites is presented in Figure 2.5. Bivalent and trivalent cations (Mg^{2+} and Al^{3+}) are sixfold coordinated to form octahedra that share edges forming infinite layers, while small spheres in the interlayers represent CO_3^{2-} anions.[60] HTs are generally synthesized by the coprecipitation of a solution of magnesium nitrate and aluminum nitrate using a solution of potassium hydroxide and potassium carbonate. The LDH structure of hydrotalcites confers several unique characteristics, including uniform dispersion of M^{2+} and M^{3+} cations, tunable surface basicity, excellent cation-exchange ability, and good adsorption capacity.[61] Hydrotalcites have been employed as photocatalysts in CO_2 conversion, and in the catalytic upgrading of biomass platform chemicals such as furfural for the synthesis of biofuels. [58,62]

HT is usually activated by heat treatment/calcination, in which the layered structure is destroyed to form a mixed oxide. Calcined HTs act as strong base/weak Lewis acid catalysts. They possess

medium-strong Lewis basic O^{2-} - Mn^{+} pairs, strongly basic O^{2-} ions that operate as active basic sites, and Al^{3+} ions that serve as weak Lewis acid sites. Calcination also results in the formation of weakly basic OH^{-} ions in the interlayers.[60] The acidic-basic nature of HTs depends on their composition, i.e., the nature and ratio of cations and the compensating interlayer anions, which can be tailored according to the target reaction. With Mg-Al HTs, increasing the Mg/Al molar ratio increases the number of strong basic sites on the catalyst. Further, the anion basicity influences the overall basicity of HT, which can be tuned by changing the compensating anion in the interlayers. For instance, HTs with intercalated OH^{-} or CO_3^{2-} ions are more basic than materials with Cl^{-} ions. Further, calcined HT displays a characteristic 'memory effect' by which the original hydrotalcite structure can be recovered by rehydration.[60] Performing rehydration in the liquid or vapor phase restores the original HT structure and incorporates Bronsted base sites (OH^{-}) by excluding CO_2 and other anions.[63] The presence of strong Bronsted base sites makes these catalysts useful for a wide range of base-catalyzed reactions including Michael addition,[64] Knoevenagel[65] and Claisen-Smith condensation[66] reactions. Tichit and coworkers previously reported higher catalytic activity with rehydrated Mg Al HT compared to the mixed oxide in the self-condensation of acetone.[67]

2.5.2 Carbon Supported Hydrotalcites

Hydrotalcite powders synthesized by traditional methods have low specific surface areas. In addition, the utilization of HT in slurry/liquid phase processes is limited by its low mechanical strength, which poses difficulty in catalyst separation and recovery. Further, the active sites of hydrotalcites are located on the edge of the HT platelets. Although several authors have tried to increase the number of edge sites of the platelets, the exposed edge area is limited by the lateral size of the HT crystallites. [63] While efforts have been made to reduce the lateral size of the HT

crystallites, further reducing the size can create difficulties in catalyst recovery in liquid phase reactions.[63] Consequently, there has been a rising interest in synthesizing supported HT's, i.e., introducing HT onto support materials such as silica[68] and carbon[63] to improve the surface area and confer the desired mechanical properties on the catalyst. Activated carbon has been gaining attention as a catalyst support for hydrotalcite due to its large surface area and well-developed porosity.[10] HT has been supported on carbon nanofibers/activated carbon and successfully applied for CO_2 adsorption and aldol condensation reactions.[63,69]

2.6 Novel Catalysts Design Tools: Plasma Technology

Recent efforts towards novel and sustainable strategies for catalyst fabrication have led to the emergence of plasma technology as a design tool for surface modification. Plasma comprises highly reactive species including electrons, photons, ions, and free radicals that can tune the pore size distribution, wettability, and selectivity of the catalyst.[70] Particularly, non-thermal plasmas (NTP), characterized by a thermodynamic non-equilibrium (electrons are at a much higher temperature (1-10 eV) than the other plasma species) are receiving much attention for catalyst design. NTP permits catalyst synthesis at low temperatures and pressures, in shorter durations, with limited use of hazardous reagents, thereby minimizing waste generation.[71] In addition, catalysts synthesized by NTP have smaller particle size, better dispersion, and have shown enhanced catalytic activity, selectivity, and stability. This makes NTP an attractive alternative to the conventional high temperature, long duration thermal methods. Further, there has been a lot of interest in coupling plasma reactors with renewable energy. With the drastic drop in electricity costs, electricity-driven plasma processes will become more attractive. In addition, plasma reactors allow rapid switch on/off (turnkey process), and involve very low investment and operating costs, with almost no economies of scale.[72]

Plasma has been employed for different stages of catalyst preparation such as grafting functional groups on the support, reduction, oxidation, as well as catalyst regeneration. Catalyst supports can be functionalized with various groups depending on the plasma gases used. For instance, oxygen containing groups such as C-O, C=O and O-C=O were introduced onto the surface of carbon nanotubes by an Ar/O_2 plasma.[73] Sabat et al. employed a non-thermal hydrogen plasma for the reduction of cobalt oxide to metallic cobalt. Low-temperature plasma reduction confers thermodynamic and kinetic advantages, apart from reducing atmospheric pollution.[74] Plasma oxidation can be employed for regeneration of coked catalysts without significantly affecting the catalyst structure. Srour and coworkers employed a dibarrier discharge NTP for the regeneration of a coked hydrodesulfurization catalyst ($CoMoP/Al_2O_3$).[75] Cold plasma techniques have also been investigated as an alternative to thermal calcination as they allow a reduction of treatment time and temperature, and chemical activation. Further, plasma reactions (between the plasma active species and catalyst precursors) are much faster in comparison to calcination processes, permitting rapid crystal nucleation (e.g., metal-based catalysts, hydrotalcite, etc.) during catalyst preparation. Low temperature cold plasma enables slow crystal growth, which allows small catalyst size or high dispersion. Size reduction of the crystals favors stronger active site (e.g., metal) and support interactions, providing greater sintering and coking resistance, thereby imparting greater catalyst stability and durability. [76]

2.6.1 Mechanism

Plasma is created by applying a high voltage to a gas/gas mixture for ionization. The electrons in the plasma have a much higher mobility compared to the ions and other reactive species, causing the electrons to migrate towards the catalyst surface, imparting a negative charge.[71] Consequently, an electric field is established, which slows down the electrons and accelerates the

positively charged ions, resulting in a dynamic equilibrium with equal electron and ion fluxes (Figure 2.6). This results in the formation of a positively charged sheath near the catalyst surface, which is critical in determining the energies and fluxes of the charged species reaching the surface. Therefore, plasma-catalyst interactions depend on the electric field distribution, and plasma characteristics including power, gas pressure and chemical composition of the plasma.[71]

2.6.2 Plasma Functionalization of Carbon

More recently, there has been a lot of interest in the plasma functionalization of carbon, for the synthesis of solid acid and base catalysts. While investigating the synthesis of solid acid, sulfonated carbon catalysts, Li and co-workers performed the plasma sulfonation of carbon black in a dilute sulfuric acid solution (0.1-1 M) for a 30 min processing time in ambient air. It was proposed that hydrogen radicals formed in the plasma react with sulfuric acid on the carbon to form sulfonic acid (SO_3H) groups, which attack the carbon forming -SO_3H on the catalyst surface.[77] In a follow up study, Qin et al. established a gas-liquid interfacial plasma process in dilute H_2SO_4 (1 M) using a mixture of N_2/Ar for sulfonating carbon materials. The plasma sulfonated carbon catalysts exhibited similar catalytic activity, yet greater stability in comparison to their hydrothermally synthesized counterparts in the hydrolysis of decrystallized cellulose, [78] implying the potential of NTP for replacing conventional thermal methods. A few studies have also investigated the plasma synthesis of solid base catalysts and the possibility of replacing conventional thermal calcination with plasma methods. Luo et al. used a cold air plasma to synthesize Cu/ZnO/C catalysts with strong basic sites for the hydrogenation of CO_2 to methanol in a fixed-bed reactor. The plasma catalyst resulted in space time yields about 1.5 times that of the calcined catalyst.[79] Similarly, Hajkova et al. used an air plasma to synthesize basic, hydrotalcite-type catalysts and investigated their catalytic activity in the aldol condensation of

furfural and acetone. The plasma modified catalyst (4 s treatment time) performed better (over 1.6 times furfural conversion) in comparison to calcined hydrotalcite (450 °C, 6 h).[60]

2.7 Catalyst Characterization

The most common characterization methods employed for understanding the surface morphology and chemical composition of solid catalysts include Brunauer-Emmett-Teller (BET) and Barrett-Joyner-Halenda (BJH) analysis, scanning/transmission/ scanning-transmission electron microscopy techniques (SEM/TEM/STEM), X-ray Photoelectron Spectroscopy (XPS), Fourier Transform Infrared Spectroscopy (FTIR), X-ray Diffraction (XRD), Inductively Coupled Plasma Optical Emission Spectroscopy (ICP-OES), and Boehm Titration.

BET surface area & BJH pore size and volume analysis provide information on the specific surface area of the sample by multilayer adsorption, measured as a function of relative pressure. The pore volume and pore size distribution are determined by gas (N_2) adsorption while the hysteresis of the adsorption isotherm can provide information on the pore shape.[2] The morphology of solid catalysts can be studied by electron microscopy techniques such as SEM, TEM, and STEM. While SEM gives information on the sample surface and composition, TEM/STEM provide valuable information on the inner structure of the sample such as the crystal structure and morphology. Further, STEM is advantageous over SEM imaging in providing better spatial resolution. Energy Dispersive X-ray Spectroscopy (EDS) is generally used in conjunction with SEM/TEM/STEM to determine the elemental or compositional analysis of the sample.[80] Another elemental analysis technique is ICP-OES in which the constituent elements are identified by emission spectra of a sample. ICP-OES has the advantages of good selectivity and lower detection limits.[81] Further, XPS can determine the elemental composition and

oxidation states of a material, as well as provide basic chemical bond information. Each element is characterized by a set of bonding energies, and the XPS peak areas can be used to determine the surface composition of the material.[2] FTIR has been widely used for determining the surface chemistry of heterogeneous catalysts and can provide information on the catalyst structure and chemical species adsorbed on the catalyst surface.[82] Further, surface sites can be characterized by FTIR spectroscopy of probe molecules. For instance, pyridine (Pyridine-FTIR) has been used to determine the type of acid sites (Bronsted/Lewis), while CO_2 adsorption has been used to determine the basic sites (e.g., surface oxygen atoms in oxides) on the catalyst surface. [82] XRD can be used to identify the crystalline phases of solid catalysts,[2] while Boehm titration is used to quantify acidic/basic oxygen functional groups on the surface of the catalyst.[10]

2.8 Continuous Processes using Monolithic Catalysts

Most fine and specialty chemicals, and pharmaceuticals are being synthesized in liquid phase batch processes.[83] However, with the growing demand for sustainability, chemical industries are shifting from batch to continuous flow processing.[84] In comparison to batch operation, continuous processes are safer due to the lower reaction volumes, better temperature control (advantageous for exothermic reactions) and ability to perform reactions under high pressure without risk. In addition, high mass transfer rates can be achieved due to the lower reaction volume and increased contact area. Enhanced heat and mass transfer improve product selectivity and yield. Other advantages of continuous technologies over batch processes include reduced downtimes, real-time process control, process intensification, and automation of manufacturing operations, thereby reducing the operating expenditure.[84] Moreover, process intensification enables waste minimization through coupling of unit operations and recycling streams,[85] leading to the design of environmentally benign processes with low carbon footprint.

Employing continuous flow processes with leach proof, heterogeneous solid catalysts can provide numerous technical and economic benefits to the fine and specialty chemical industries.[86] Most continuous flow processes utilize reactors with slurry catalysts or randomly packed catalytic beds (granules, beads). However, slurry catalysts pose a difficulty in separating the product from the catalyst, and attrition. An alternative to slurry catalysts is employing granular catalysts in trickle bed reactors. However, large particles must be used to minimize pressure drop, which can result in intraparticle mass transfer limitations. Moreover, randomly packed beds typically show uncontrolled fluid dynamics, leading to stagnation zones and hot spots, low selectivity, and process efficiency. In comparison to granular catalysts, monoliths are characterized by a large open frontal area that enables a low pressure-drop, and short diffusion paths enabling high mass transfer rates, which facilitates their use in continuous processes.[87] Further, the large surface area to volume ratio of monoliths ensures high product space time yields, selectivity, and productivity. Continuous flow technologies using advanced structured catalysts such as monoliths can lead to decentralized, smaller production plants for manufacturing low-volume, high value chemicals with limited waste generation.[86] Monolith reactors have previously been demonstrated to have higher productivities in comparison to batch or packed bed reactors for transesterification, Diels-Alder reaction and Knoevenagel condensation.[88]

2.9 Esterification Reactions

Esterification is an acid-catalyzed chemical reaction in which a carboxylic acid and alcohol react to yield an organic ester and water. Esterification is a slow, equilibrium-limited, reversible reaction, generally performed in the liquid phase.[89] To shift the equilibrium towards product formation, an excess amount of one of the reactants (e.g., alcohol) is used, or one of the products,

particularly water, is continuously removed.[89,90] Esterification can also be performed in the vapor phase by heating a mixture of a carboxylic acid, alcohol, and catalyst to the desired reaction temperature. Vapor phase esterification is thermodynamically favorable, due to the higher values of the equilibrium constants in comparison to the liquid phase. This process is also advantageous in preventing reactor corrosion, minimizing the cost of materials, saving energy, and simplifying the process.[90] Depending on the scale of operation, esterification reactions are generally carried out in batch or continuous reactors. There is a growing interest in continuous over batch processing owing to easier automation, safer long-term operation, and reproducibility.[88] Further, the use of continuous-flow technology affords the economically viable and environmentally benign production of specialty chemicals such as esters. Reactive distillation (RD) has also gained a lot of attention for esterification in shifting the reaction towards complete conversion by continuous removal of the products. RD can use the ratio of the stoichiometric reactants to push the equilibrium to high conversions instead of using an excess of one of the reactants.[91]

Organic esters have been widely employed in food, flavor, pharmaceutical, solvent, cosmetic, lubricant, and biofuel industries.[92] For instance, the ethyl esters of butyric acid find applications as green solvents and are promising replacements for halogenated petroleum-based solvents.[93] Monoethyl and dimethyl fumarate have applications in dermatology for the treatment of diseases such as psoriasis and multiple sclerosis.[94] Further, esters of hydroxyacids have valuable industrial and medical applications.[95] Eastman Chemical developed an organic cleaning solvent butyl 3-hydroxybutyrate, marketed under the trade name Omnia^{TM}, by esterifying a diketene with butanol and hydrogenation.[96] 2-hydroxyisobutyric acid (2-HIBA) is gaining significance as a platform chemical and has been identified as a building block for polymer synthesis.[97] The

methyl ester of 2-HIBA is produced from 2-hydroxyisobutyramide and methyl formate, and finds applications in electronic materials, agrochemicals, and medicine.[98]

2.9.1 Esterification of Carboxylic acids using Sulfonated Carbon Catalysts

Sulfonated carbons (SC) have been widely investigated for the esterification of fatty acids in biodiesel synthesis. Several studies have reported better catalytic performance with SC in comparison to commercial catalysts such as Amberlyst-15 and Nafion. For instance, Tamborini and co-workers used a sulfonated nanoporous carbon catalyst for the esterification of oleic acid with methanol, and obtained a conversion of 60.6% (0.2 g, catalyst, 75 °C, 10 h), which was found to be higher than commercial catalysts such as Nafion (53%) and Amberlite IR-120 (37.4%).[99] Further, Lee employed a sulfonated carbon catalyst in the esterification of cyclohexanecarboxylic acid with ethanol. The SC displayed better catalytic performance than Amberlyst-15, despite a lower density of SO_3H groups (1.24 mmol/g in comparison to 4.6 mmol/g in Amberlyst). They explained the difference in catalytic activity based on accessibility of reactants to the active sites.[100]

Few studies have also investigated the applications of SC in the esterification of fermentation-derived/aqueous solutions of organic acids. The aqueous environment of the fermentation broth can present challenges for esterification catalysts, as the presence of water can affect catalytic activity by blocking the active sites. Further, fermentation broth impurities including amino acids, proteins, and salts (e.g., sulfates and phosphates) can be inhibitory to the catalyst.[101] While studying the esterification of aqueous lactic acid solutions (water content of 15-80 wt%) with ethanol using sulfonated carbon and sulfonated graphene oxide catalysts, Nguyen and co-workers observed a decrease in lactic acid conversion and ethyl lactate yield on increasing the

amount of water in the reaction, indicating poisoning of active sites by water.[102] Luque and co-workers studied the esterification of fermentation-derived succinic acid (SA) crystals with ethanol using Starbon-400 (a sulfonated mesoporous carbon), (1 mmol SA, 30 mmol EtOH, 50 mmol H_2O, 0.1 g catalyst, 80 °C, 12 h residence time). They observed a conversion of 99% with pure SA and 80% with the fermentation-derived SA. The lower conversion with the fermentation-derived SA was attributed to adsorption/ deposition of organic compounds (acetic, pyruvic, formic acids) on the catalyst surface.[103] Further, Delhomme and coworkers noted catalyst deactivation of the ion exchange resin Nafion NR-50, due to the high concentration of phosphates in the fermentation medium.[104]

Various authors have also studied the applications of sulfonated carbon-based monoliths for esterification reactions in batch reactors. Nakhate and Yadav employed a sulfonated carbon-based graphene oxide monolith for the esterification of levulinic acid and benzyl alcohol. They obtained 97% conversion (110 °C, 90 min) and the catalyst retained approximately 92% of its activity after 5 reuse cycles.[105] In the esterification of palm fatty acid distillate (PFAD) with methanol over a sulfonated carbon-coated monolith, Hosseini and co-workers observed 97% conversion (80 °C, 300 min, 25:1 methanol/PFAD molar ratio, 1.25 wt% catalyst). However, their catalyst reusability studies indicated a 28% decrease in free fatty acid conversion after four reuse cycles.[106]

2.9.2 Solid Acid Monoliths for Continuous Esterification

Few studies have investigated the applications of solid acid monolith catalysts for continuous esterification reactions. Nijhuis and coworkers investigated the esterification of 1-octanol with hexanoic acid using internally finned BEA zeolite and Nafion coated monoliths. They employed

counter-current reactive stripping using nitrogen to eliminate water generated as a byproduct, thereby obtaining high conversions and selectivity with the BEA catalyst (99.4%, 92.8%) and Nafion (95%, 98.6%).[107] Wakayama and coworkers employed a monolithic resin catalyst bearing sulfonic acid groups in the continuous flow esterification of methacrylic acid and methanol (80 °C, liquid flow rate: 0.02 mL/min) and obtained 95% yield of methyl methacrylate.[108] In the continuous flow esterification of lactic acid and n-butanol using a monolithic silica microreactor, Koreniuk and co-workers observed 99% acid conversion (140 °C, lactic acid/ n-butanol molar ratio was 1:12).[83]

2.10 Solid-Base Hydrotalcites: Condensation Reactions

There is a growing interest in producing sustainable aviation fuels (SAF) using biomass platform chemicals. The aldol condensation of furfural, a platform molecule derived from hemicellulose in lignocellulosic biomass (by fast pyrolysis), and ketones is a promising route to produce biomass-derived SAF.[109] Various authors have studied the cross-condensation of furfural and ketones such as acetone,[110] cyclopentanone[111] and cyclohexanone.[112] Although furfural is a valuable aldehyde used in the synthesis of many valuable chemicals, it is unstable and prone to coke formation, which results in catalyst deactivation during upgrading. However, furfural is a suitable feedstock for a more stable intermediate, cyclopentanone (CP).[113] Furfural can be converted into CP through a hydrogenation reaction, using metal/bi-metal/metal-supported catalysts (e.g., Pt/C, Ru/ C).[16] CP can further be catalytically converted to 2-cyclopentylidene cyclopentanone (2-CP, dimer) and 2,5-dicyclopentylidene cyclopentanone (3-CP, trimer) followed by subsequent hydrodeoxygenation to yield cyclic/bi-cyclic pentane which can be used as a bio-jet fuel.[114] This conversion occurs through an aldol self-condensation reaction, which

plays a vital role in fuel synthesis, by increasing the carbon-chain length of the platform molecules.

Aldol condensation can be catalyzed by both basic and acidic catalysts. Various authors have employed solid base and acid catalysts for the self-condensation of cyclopentanone. Solid bases including MgO, CaO, potassium fluoride-impregnated alumina (KF/γ-Al_2O_3), Li-Al hydrotalcite, CaO-CeO_2, and Mg-Al hydrotalcites, and solid acids such as MCM-41 silica,[115] have been investigated for the self-condensation of CP.[114] More recently, CP self-condensation has been studied using solid acid - base bifunctional catalysts including attapulgite (clay mineral) grafted with -SO_3H groups,[116] KOH/diatomite [117] and TiO_2-ZrO_2.[118] The synergistic effect of acid and basic sites has been found to favor the condensation reaction.[117]

Mg-Al hydrotalcites (HT) have attracted a lot of attention for aldol condensation reactions as they are environmentally benign solid bases, possess strong alkalinity, and are low in cost.[119] HT's have been shown to have higher catalytic activity in comparison to other solid bases including MgO, KF/Al_2O_3, CaO-CeO_2, for the self-condensation of CP. Yang and co-workers observed 86% yield of 2-CP with Mg-Al HT (423 K, 8 h).[114] The high catalytic efficiency of HT's was attributed to the strong basicity as well as synergistic effect of acid and base sites on this catalyst. Further, supported HTs can increase the amount of accessible hydrotalcite crystallites, improve the mechanical properties of the catalyst and facilitate easier catalyst separation. Carbon, as a support for HT, is gaining attention due to its large surface area, extensive porous structure, and high adsorption capacity. Winter and co-workers employed Mg-Al HT supported on carbon-nanofibers in the self-condensation of acetone and observed a high specific activity, almost 4 times that of unsupported HT. This increase in activity was attributed to the increase in amount of accessible active sites.[63] There is limited knowledge on the

applications of supported/carbon-supported hydrotalcites for the self-condensation of CP. A plasma activated granular carbon supported catalyst displayed 61% CP conversion.[120]

These studies were performed in batch reactors. Performing the reactions under continuous operation enables accurate determination of the reaction rate, selectivity, and space-time-yield. Liu and co-workers investigated the cross-condensation of cyclopentanone and furfural using a calcined sodium-promoted Mg-Al hydrotalcite and obtained furfural conversion over 99%, and 100% selectivity to the condensation products 2-(2-furylmethylidene) cyclopentanone and 2,5-bis(2-furylmethylidene) cyclopentanone.[121] Very few studies have investigated the continuous aldol condensation of CP, particularly using hydrotalcite catalysts. While investigating the self-aldol condensation of CP in a fixed-bed continuous flow reactor using Mg-Al HT, Sheng and coworkers observed a maximum CP conversion of 73.2% and selectivity of 70% towards the condensation product 2,5-dicyclopentylidenecyclopentanone (3-CP).[122]

2.11 Pressure Drop and Mass Transfer in Granular and Monolithic Catalysts

2.11.1 Pressure Drop

Pressure drop represents energy dissipation caused by fluid flow through the reactor bed. During fluid flow over a packed bed, friction results in pressure loss, which results in energy loss and decreasing flow velocities. High pressure drop through the reactor system requires high energy input and prevents the reactor from being operated at high liquid and gas velocities, limiting throughput.[123] Low pressure drop is desired to improve the yield and selectivity for certain reactions, as well as reduce the capital and operating costs, as smaller reactors can be employed. However, large catalyst particle sizes are required to minimize pressure drop, which can cause intraparticle mass transfer limitations, channeling, and bypassing. Further, incomplete wetting of

the catalyst surface could lead to low reaction rates. Therefore, optimizing pressure drop and mass transfer is a challenge in the design of fixed bed/ trickle bed catalytic reactors.[124]

These concerns can be addressed by the application of structured catalysts such as monoliths. The open channel structure of monoliths offers minimum obstruction to fluid flow, resulting in low pressure drop, and therefore low energy requirements.[125] In monoliths, pressure drop is mainly caused by wall friction, along with other factors such as acceleration of the gas phase, orifice effects at the entrance region and between the individual monoliths, and by the gas-liquid distributor.[123]

Pressure drop for granular catalysts in packed beds can be determined from the Ergun equation (1952) as given below,

$$\frac{dP}{dZ} = -\frac{G}{\rho g_c D_p}\left(\frac{1-\emptyset}{\emptyset^3}\right)\left[\frac{150(1-\emptyset)\mu}{D_p} + 1.75G\right] \qquad \text{Equation 2.1}$$

Where $\emptyset$ is porosity, G is superficial mass velocity (ρu), ρ is density, D_p is particle size, μ is superficial velocity, P is pressure, Z is bed length and g_c is conversion factor for gravitational acceleration.

The pressure drop Δp across a monolithic bed can be determined from the equation.[124]

$$\frac{\Delta p}{L} = \frac{f_0}{2}\frac{\eta_g}{\epsilon_B d_h^2} u_0 + \frac{\zeta}{2}\rho_g {u_0}^2 \qquad \text{Equation 2.2}$$

Where f_0 is the friction factor (f_0= 16/Re for monoliths with circular channels), n_g is the viscosity of the fluid (Pa.s), ε_B is the void fraction, d_h is the hydraulic diameter of the monolith channel (m) and u_0 is the superficial velocity (m/s). The second term in the above equation is usually negligible for laminar flow conditions. [124]

2.11.2 Hydrodynamics and Mass Transfer in Monoliths

Reactors with monolithic catalysts (structured packing) have been found to exhibit superior hydrodynamics in comparison to current industrial reactors (random packing). The choice of a flow regime for industrial applications depends on the nature of the reaction and process conditions and is influenced by the gas and liquid properties and superficial velocities, and diameter of the capillary and monolith channel.[126] With multiphase flow, a monolithic reactor can be operated in either co-current (gas and liquid are introduced from the inlet (down-flow), or base of the reactor (up-flow) and flow in the same direction) or counter-current (gas and liquid flow in opposite directions) modes. The common flow regimes encountered in the channels of structured catalysts include bubbly flow, slug/laminar/Taylor flow, churn flow and annular flow. Taylor flow, which is achieved at high gas and low liquid flow rates, is mostly commonly employed to achieve high mass transfer from the bulk fluid to the monolith wall surface.[127]

External Mass Transfer

Enhanced mass transfer in monoliths, particularly under the Taylor flow regime, has been attributed to recirculation within the liquid slugs and the thin liquid film separating the gas slugs from the catalytic washcoat.[123] The combined advantages of high liquid radial mass transfer and low axial mass transfer during Taylor flow, makes it suitable to use monolithic catalysts for single phase liquid applications that are limited by back-mixing or two-phase applications that involve mass transfer.[127] External mass transfer in monoliths accounts for diffusion of reactants from the bulk gas/liquid phase to the surface of the catalytically active layer/washcoat (Figure 2.7).

The presence of external mass transfer effects for monolithic/granular catalysts can be assessed by calculating the Mear's criterion, which uses the measured rate of reaction, $-r_A'$ to determine if

mass transfer from the bulk phase to the catalyst surface can be neglected. Mear's criterion is evaluated using the relation,[128]

$$\frac{-r_A'\rho_b Rn}{k_c C_{Ab}} < 0.15$$

Equation 2.3

where $-r_A$ is the reaction rate for reactant A (kmol/kgcat.s), ρ_b is the bulk density(kg/m^3) , R is the catalyst particle radius (m), n, the reaction order, k_c is the mass transfer coefficient (m/s) and $C_{A,b}$, the concentration of the organic acid (mol/dm^3) in the bulk phase. A Mear's criterion value less than 0.15 indicates the reaction is not externally mass transfer limited.

Internal mass transfer

In heterogeneous catalytic systems, resistance to internal mass transfer stems from the diffusion of molecules within porous materials. Internal mass transfer limitations in monoliths account for internal diffusion within the porous washcoat, where reactants diffuse to and from the active sites, where the reaction occurs (Figure 2.7). The Weisz-Prater criterion is generally used to determine the presence of internal diffusion limitations. This criterion uses the observed value of reaction rate to determine if internal diffusion is limiting the reaction according to the equation, [128]

$$C_{WP} = \eta\phi_1^2 = \frac{-r_A'(obs)\rho_c R^2}{D_e C_{As}}$$

Equation 2.4

where $-r_{A\,(obs)}$ is the observed rate of reaction (kmol/kgcat.s), ρ_c is the catalyst density (kg/m^3) , R is the catalyst particle radius (m), D_e is the effective diffusivity (m^2/s) , C_{As} is the concentration of reactant A at the catalyst surface (mol/m^3), η is the internal effectiveness factor and ϕ is the

Thiele modulus. If $C_{WP} << 1$, then there are no internal diffusion limitations in the catalyst pellet, however, if $C_{WP} >> 1$, then internal diffusion severely limits the reaction.

2.12 Kinetic Models: Esterification Reactions

Kinetic analysis is performed to find a model that describes the rate of reaction as a function of the system variables that govern the chemical reaction. An understanding of the reaction mechanism is essential to construct an accurate kinetic model that can predict changes in the amount of specific product obtained. [128] Some of the main parameters considered for studying esterification kinetics include molar ratio of the reactants, catalyst loading, and reaction temperature. To describe the chemical kinetics of the solid-acid catalyzed esterification of a carboxylic acid with an alcohol, the adsorption of reactant molecules on the catalytic sites, surface reaction, as well as product desorption need to be taken into consideration. Esterification reaction kinetics have been described by different kinetic models including the Pseudo-homogeneous model, single-site Eley-Rideal (ER) and the dual-site Langmuir Hinshelwood (LH).[129] In pseudo-homogeneous models, chemical reaction controls the kinetics. The ER model is applied when reaction occurs between an adsorbed species and a non-adsorbed reactant from the bulk liquid, and esterification occurs on the surface of the catalyst. On the other hand, LH model proposes that both reactants are adsorbed on the catalyst surface, followed by a bimolecular reaction on the surface.[2] Several research groups have investigated the reaction mechanism for liquid and gas-phase esterification reactions and proposed different models, particularly ER and LH mechanisms (Figure 2.8).

The liquid-phase esterification of acetic acid with methanol/ethanol using Amberlyst-16 and sulfonated mesoporous silica (propylsulfonic acid-functionalized SBA-15) has been found to follow an LH mechanism through a protonated acetic acid intermediate, with the overall process

controlled by surface reaction.[130,131] The esterification of hexanoic acid with 1-octanol using a BEA zeolite monolithic catalyst, has also been described by an LH mechanism.[132] In contrast, Akyalcin and co-workers studied the kinetics of acetic acid esterification with 1-octanol using Amberlyst-36 and found that the reaction followed an ER mechanism with surface reaction as the rate-limiting step.[133] The above-mentioned kinetic studies for liquid-phase esterification reactions were performed in batch reactors, which, due to the inherent non-steady state, poses difficulties in accurate measurement of reaction rates. These limitations can be overcome by performing kinetic studies in continuous flow reactor systems.[134] Studies have also proposed similar mechanisms for vapor-phase esterification reactions. Chu and coworkers investigated the gas-phase esterification of acetic acid with ethanol and butanol respectively, using dodecatungstosilicic (SiW_{12}) acid supported on activated carbon. They observed a change in reaction mechanism from a dual-site LH mechanism for ethanol to a single-site ER mechanism for n-butanol, indicating the effect of the alcohol structure on the reaction mechanism.[135] The esterification mechanism has been found to vary for different catalysts, substrates and liquid/gas-phase operation, and there is no agreement in the literature on a generic mechanism for solid acid catalysts. Esterification kinetics can be studied to obtain the rate constant, and activation energy can be determined using the Arrhenius equation, to evaluate the energy consumption of the reaction.[136,137]

2.13 Catalyst deactivation

2.13.1 Deactivation Mechanisms

Catalyst deactivation, i.e., loss of catalytic activity and selectivity, limits the industrial applications of heterogeneous catalysts, as a significant quantity of resources and time are

invested in regeneration/replacement of the catalyst. The different modes of deactivation include poisoning, sintering, fouling, coke formation, attrition, and leaching of active components.[138] Poisoning causes blocking of active sites and may reduce catalytic activity during reuse due to lower accessibility of the reactants to the active sites. Sintering occurs by agglomeration of the active sites by particle migration and coalescence, while fouling occurs due to the deposition of insoluble feed components, that arise from degradation of the feed/intermediates.[139] Coke-forming processes involve chemisorption of carbon or condensed hydrocarbons on the catalyst surface, and leaching refers to the dissolution/solvation of active sites in the reaction medium. [140]

The main drawback with solid acids is their weak stability, correlated to the leaching of acid groups. Sulfonated carbons have been found to undergo deactivation by leaching of polycyclic aromatic hydrocarbons comprising sulfonic acid groups, or formation of sulfonic esters.[141,142] In reactions where water is produced as a second product (e.g., esterification), water can adsorb on the surface of the solid acid, inhibiting the acid sites for reaction.[19] Further, in the catalytic upgrading of fermentation-derived organic acids, fermentation-broth impurities including media components (e.g., amino acids, phosphates, sulfates) can deactivate the catalyst. For instance, amino acids such as tryptophan were found to be inhibitory to the activity of Amberlyst-36.[143] Further, by-products of succinic acid fermentation (acetic acid, formic acid, and pyruvic acid) caused the deactivation of a sulfonated mesoporous carbon catalyst.[103] Catalyst deactivation has also limited the potential of solid bases to replace their homogeneous counterparts. Deactivation of solid base catalysts such as Mg-Al mixed oxides can occur due to blockage of active sites (Mg-O) by a carbonaceous residue (coke) formed by secondary reactions.[144] Further, metal oxides are sensitive to deactivation by water due to active site quenching and dissolution.

2.13.2 Mitigating Deactivation

Deactivation mechanisms such as coking can be reversed by calcining the catalyst in air/oxygen (to burn off the carbonaceous deposit), while poisoning can be minimized by purification of the feed. Further, deactivation by attrition can be avoided by using structured catalysts such as monoliths. However, processes such as sintering and leaching can cause irreversible catalyst deactivation.[138] Different strategies have been proposed to address these deactivation phenomena in solid acid and base catalysts. To minimize deactivation due to water adsorption and acid group leaching, the stability of solid acids has been enhanced by introducing hydrophobic groups and overcoating with organic polymers. Grafting octyl groups onto a propyl sulfonic acid silica catalyst (SBA-15) enhanced its turnover frequency in the esterification of acetic acid with methanol, while displaying excellent water tolerance.[145] In addition, the application of polyvinylpyrrolidone coatings to SBA-15 has been found to minimize deactivation due to biogenic impurities and leaching of acidic groups.[146] Plasma processes have also been found to generate stable solid acid catalysts.[78] Further, carbon coatings have been found to enhance catalyst stability of solid bases by retaining key active sites and have been applied to catalysts such as MgO and hydrotalcite.[147] Atomic Layer Deposition (ALD), a thin-film deposition technique, has been used to control deactivation in metal-based catalysts by creating an overcoat on the catalyst surface. Overcoating by ALD (e.g., Al_2O_3 overcoat on Pd catalyst permits access to the active sites, while inhibiting sintering and coke formation in metal-based catalysts.[148] Further, deactivation caused by water adsorption can be minimized by using structured catalysts and *in-situ* water stripping. *In-situ* water removal (reactive stripping) with a dry inert gas in co-current/counter-current modes can eliminate water competitively adsorbed on the catalyst surface, improving the performance of solid acid catalyzed reactions.[19]

References

1. A.Z. Fadhel, P. Pollet, C.L. Liotta, C.A. Eckert, Combining the benefits of homogeneous and heterogeneous catalysis with tunable solvents and near critical water, Molecules 15 (2010) 8400-8424.
2. G. Rothenberg, Catalysis: Concepts and Green Applications. Weinheim [Germany]: Wiley-VCH, 2008.
3. F. Schuth, K. Unger, Precipitation and Coprecipitation. Preparation of Solid Catalysts. Ed. Ertl G., Knozinger H., Weitkamp J., Wiley-VCH Verlag GmbH, 1999.
4. B. Wiyantoko, P. Kurniawati, T.E. Purbaningtias, I. Fatimah, Synthesis and characterization of hydrotalcite at different Mg/Al molar ratios, Procedia Chem. 17 (2015) 21-26.
5. W. Mateo, H. Lei, E. Villota, M. Qian, Y. Zhao, E. Huo, Q. Zhang, X. Lin, C. Wang, Z. Huang, Synthesis and characterization of sulfonated activated carbon as a catalyst for bio-jet fuel production from biomass and waste plastics, Bioresour. Technol. 297 (2020) 122411.
6. P. Munnik, P.E. de Jongh, K.P. de Jong, Recent developments in the synthesis of supported catalysts. Chem. Rev., 115 (2015) 6687-6718.
7. S. Govender, H.B. Friedrich, Monoliths: A Review of the basics, preparation methods and their relevance to oxidation, Catalysts 7 (2017) 1-29.

8. Z. Wang, K. Zhao, B. Xiao, P. Gao, D. He, T. Cai, J. Yuan, Fabrication of monolithic catalysts: Comparison of the traditional and the novel green methods, Catalysts, 9 (2019) 981.

9. E.Lam, J.H.T. Luong, Carbon materials as catalyst supports and catalysts in the transformation of biomass to fuels and chemicals, ACS Catal. 4 (2014) 3393-3410.

10. M. Iwanow, T. Gärtner, V. Sieber, B. König, Activated carbon as catalyst support: precursors, preparation, modification, and characterization, Beilstein J. Org. Chem., 16 16 (2020) 1188-1202.

11. S. Suganuma, K. Nakajima, M. Kitano, D. Yamaguchi, H. Kato, S. Hayashi, M. Hara, Hydrolysis of Cellulose by Amorphous Carbon Bearing SO_3H, COOH and OH Groups. J. Am. Chem. Soc., 130 (2008) 12787-12793.

12. J. Jiagwe, P.W. Olupot, E. Menya, H.M. Kalibbala, Synthesis and application of granular activated carbon from biomass waste materials for water treatment: A review. J. Bioresour. Bioprod., 6 (2021) 292-322.

13. Y. Gao, Q. Yue, B. Gao, A. Li, Insight into activated carbon from different kinds of chemical activating agents: A review. Sci. Total Environ. 746 (2020) 141094.

14. M.B.Vazquez-Santos, F. Suarez-Garcia, A. Martinez-Alonso, J.M.D. Tascon, Activated carbon fibers with a high heteroatom content by chemical activation of PBO with phosphoric acid, Langmuir 28 (2012) 5850-5860.

15. S.M. Yakout, G.S. El-Deen, Characterization of activated carbon prepared by phosphoric acid activation of olive stones, Arab. J. Chem. 9 (2016) S1155-S1162.

16. M. Pirmoradi, N. Janulaitis, R.J.Jr Gulotty, J.R. Kastner, Bi-Metal-Supported Activated Carbon Monolith Catalysts for Selective Hydrogenation of Furfural. Ind. Eng. Chem. Res., 59 (2020) 17748-17761.

17. M. Nyström, C. Järnvik, H. Thor, S. Saari, Process for producing hydrogen peroxide and composition thereof. Patent Application. US006524547B1, Feb 25, 2003.

18. M.T. Kreutzer, P.D Johan, J. Heiszwolf, F. Kapteijn, J.A. Moulijn, Mass transfer characteristics of three- phase monolith reactors. Chem. Eng. Sci. 56 (2001) 6015-6023.

19. A.E.W. Beers Monolithic catalysts for acylation and esterification, TU Delft Repositories,2001.

20. T. Vergunst, M.J.G. Linders, F. Kapteijn, J.A Moulijn, Carbon- based monolithic structures, Catal. Rev.-Sci.Eng., 43 (2001) 291-314.

21. J.A. Moulijn, M.T. Kreutzer, T.A. Nijhuis, F. Kapteijn, Chapter 5 -Monolithic catalysts and reactors: High precision with low energy consumption. Adv. Catal. 2011, 54, 249-327.

22. C. Moreno-Castilla, A.F. Perez-Cadenas, Carbon-Based Honeycomb Monoliths for Environmental Gas-Phase Applications, Materials 3 (2010) 1203-1227.

23. K. Gadkaree, Carbon honeycomb structures for adsorption applications, Carbon, 36 (1998) 981-989.

24. M. Yates, J. Blanco, P. Avila, M.P. Martin, Honeycomb monoliths of activated carbons for effluent gas purification, Micropor. Mesopor. Mater. 37 (2000) 201-208.

25. K. Tanabe, W.F. Holderich, Industrial application of solid acid-base catalysts. Appl. Catal. A: Gen., 181 (1999) 399-434.

26. T. Okuhara, Water-Tolerant Solid Acid Catalysts. Chem. Rev., 102 (2002) 3641-3666.

27. V.M. Mello, G.P.A.G. Pousa, M.S.C, Pereira, I.M. Dias, P.A.Z. Suarez, Metal oxides as heterogeneous catalysts for esterification of fatty acids obtained from soybean oil. Fuel Process. Technol., 92 (2011) 53-57.

28. S. Shanmugam, B. Vishwanathan, T.K. Varadarajan, Esterification by solid acid catalysts-a comparison. J. Mol. Catal. A Chem. 223 (2004) 143-147.

29. K. Saravanan, B. Tyagi, H.C. Bajaj, Sulfated zirconia: an efficient solid acid catalyst for esterification of myristic acid with short chain alcohols, Catal. Sci. Technol., 2 (2012) 2512-2520.

30. O.B. Mya, M. Bita, I. Louafi, A. Djouadi, Esterification process catalyzed by ZSM-5 zeolite synthesized via modified hydrothermal method, MethodsX , 5 (2018) 277-282.

31. A. Hykkerud, J.M. Marchetti, Esterification of oleic acid with ethanol in the presence of Amberlyst 15, Biomass Bioenergy, 95 (2016) 340-343.

32. C. Tagusagawa, A. Takagaki, A. Iguchi, K. Takanabe J.N. Kondo K. Ebitani, S. Hayashi, T. Tatsumi, K. Domen, Highly active mesoporous Nb-W Oxide solid acid catalyst, Angew. Chem. Int. Ed. 49 (2010) 1128-1132.

33. A. Takagaki, Rational design of metal oxide solid acids for sugar conversion, Catalysts, 9 (2019) 907.

34. X. Qi, M. Watanabe, T.M. Aida, R.L. Smith Jr, Sulfated zirconia as a solid acid catalyst for the dehydration of fructose to 5-hydroxymethylfurfural, Catal. Commun., 10 (2009) 1771-1775.

35. M.L. Grecea, A.C. Dimian, S. Tanase, V. Subbiah, G. Rothenberg, Sulfated zirconia as a robust superacid catalyst for multiproduct fatty acid esterification, Catal. Sci. Technol. 2 (2012) 1500-1506.

36. J.C. Gee, Not all acid sites are created equal: Alkene isomerization and dimerization occur on separate sites on Amberlyst-15 catalyst, J. Phys.Org. Chem. 34 (2021) e4172.

37. M. Sharma, R.K. Wanchoo, A.P. Toor, Amberlyst 15 catalyzed esterification of nonanoic acid with 1-propanol: kinetics, modeling, and comparison of its reaction kinetics with lower alcohols, Ind. Eng.Chem.Res., 53 (2014) 2167-2174.

38. X. Li, K. Nagaoka, R. Olindo, J.A. Lercher, Synthesis of highly active sulfated zirconia by sulfation with SO_3, J. Catal., 238 (2006) 39-45.

39. J. Zhao, C. Zhou, C. He, Y. Dai, X. Jia, Y. Yang, Efficient dehydration of fructose to 5-hydroxymethylfurfural over sulfonated carbon sphere solid acid catalysts, Catal. Today, 264 (2016) 123-130.

40. K. Ngaosuwan, J.G. Goodwin Jr., P. A. Prasertdham, A green sulfonated carbon-based catalyst derived from coffee residue for esterification. Renew. Energy., 86 (2016) 262-269.

41. L.J. Konwar, P. Maki-Arvela, J-P. Mikkola, SO_3H- containing functional carbon materials: Synthesis, structure, and acid catalysis, Chem. Rev., 119 (2019) 11576-11630.

42. J.R. Kastner, J. Miller, D.P. Geller, J. Locklin, L.H. Keith, T. Johnson, Catalytic esterification of fatty acids using solid acid catalysts generated from biochar and activated carbon, Catal., 190 (2012) 122-132.

43. C.R. Khudsange, K.L. Wasewar, Process intensification of esterification reaction for the production of propyl butyrate by pervaporation, Resource-Efficient Technologies 3 (2017) 88-93.

44. S. Kang, J. Ye, J. Chang, Recent advances in carbon-based sulfonated catalyst: preparation and application, I.RE.CH.E.,5 (2013) 133-144.

45. T.S., Galhardo, N. Simone, M. Goncalves, F.C.A Figueiredo, D. Mandelli, W.A. Carvalho, Preparation of sulfonated carbons from rice husk and their application in catalytic conversion of glycerol, ACS Sustainable Chem. Eng., 1 (2013) 1381-1389.

46. U.I. Nda-Umar, I. Ramli, E.N. Muhamad, N. Azri, Y.H. Taufiq-Yap, Optimization and characterization of mesoporous sulfonated carbon catalyst and its application in modeling and optimization of acetin production. Molecules, 25 (2020) 5221.

47. N.T. Thanh, N.H. Long, L.Q. Dien, G.T. Phuong Ly, P.H. Hoang, N.T. Minh Phuong, N.T. Hue, Preparation of carbonaceous solid acid catalyst from *Acacia mangium* wood sawdust for conversion of same source into 5-hydroxymethylfurfural. Energy Sources A: Recovery Util. Environ. Eff. 42 (2020) 730-739.

48. S. Basumatary, B. Nath, P. Kalita, Application of agro-waste derived materials as heterogeneous base catalyst for biodiesel synthesis, J. Renew. Sustain. Energy. 10 (2018) 043105, 1-18.

49. Q. Li, Preparation of a sulfonated activated carbon fiber catalyst with γ-irradiation-induced grafting method. J. Mater. Res. Vol., 27 (2012) 3083- 3089.

50. L.H. Tamborini, M.P. Militello, J. Balach, J.M. Moyano, C.A. Barbero, D.F. Acevedo, Application of sulfonated nanoporous carbons as acid catalysts for Fischer esterification reactions. Arab. J. Chem. 12 (2019) 3172-3182.

51. M. Kitano, K. Arai, A. Kodama, T. Kousaka, K. Nakajima, S. Hayashi, M. Hara, Preparation of a sulfonated porous carbon catalyst with high specific surface area, Catal. Lett., 131 (2009) 242-249.

52. S. Adhikari, Z. Hood, N. Gallego, C. Contescu, Lignin-derived carbon fibers as efficient heterogeneous solid acid catalysts for esterification of oleic acid. MRS Adv. 3 (2018) 2865-2873.

53. P.O. Ibeh, F.J. Garcia-Mateos, J.M. Rosas, J. Rodriguez-Mirasol, T. Cordero, Activated carbon monoliths from lignocellulosic biomass waste for electrochemical applications. J. Taiwan. Inst. Chem. Eng., 97 (2019) 480-488.

54. A. V. Nakhate, G. D. Yadav, Synthesis and Characterization of Sulfonated Carbon-Based Graphene Oxide Monolith by Solvothermal Carbonization for Esterification and Unsymmetrical Ether Formation, ACS Sustainable Chem. Eng., 4 (2016) 1963-1973.

55. Y. Ono Solid base catalysts for the synthesis of fine chemicals. J. Catal. 216 (2003) 406-415.

56. O. Kikhtyanin, D. Kadlec, R. Velvarská, D. Kubička, Using Mg-Al mixed oxide and reconstructed hydrotalcite as basic catalysts for aldol condensation of furfural and cyclohexanone, ChemCatChem., 10 (2018) 1464-1475.

57. Z. Zhang, M. Hu, B. Lv, J. Kang, J. Tang, Z. Fei, X. Chen, Q. Liu, M. Cui, X. Qiao, Solvent-assisted stepwise redox approach to generate zeolite NaA-supported K_2O as strong base catalyst for Michael addition of ethyl acrylate with ethanol, ACS Omega, 3 (2018) 10188-10197.

58. Z. Zhao, W. Wu, L. Jia, X. Guo, Sodium phosphate solid base catalysts for production of novel biodiesel by transesterification reaction, RSC Adv., 13 (2023) 26700.

59. B. Sakthivel, A. Dhakshinamoorthy, Chitosan as a reusable solid base catalyst for Knoevenagel condensation reaction, J. Colloid Interface Sci., 485 (2017) 75-80.

60. P. Hajkova, Z. Tisler, Atmospheric Plasma Treated Hydrotalcite-Type Catalyst. Catal Letter 147 (2017) 374-38.

61. D.P. Debecker, E.M. Gaigneaux Prof., G. Busca Prof., Exploring, tuning, and exploiting the basicity of hydrotalcites for applications in heterogeneous catalysis, Chem. Eur. J. 15 (2009) 3920-3935.

62. M. Flores-Flores, E. Luevano-Hipolito, L.M. Torres Martinez, G. Morales-Mendoza, R. Gomez, Photocatalytic CO_2 conversion by MgAl layered double hydroxides: Effect of Mg^{2+} precursor and microwave irradiation time, J. Photochem. Photobiol., A, 363 (2018) 68-73.

63. F. Winter, V. Koot, A.J. van Dillen, J.W. Geus, K.P. de Jong, Hydrotalcites supported on carbon nanofibers as solid base catalysts for the synthesis of MIBK, J. Catal., 236 (2005) 91-100.

64. M. Mokhtar, T.S. Saleh, S. N. Basahel, Mg-Al hydrotalcites as efficient catalysts for aza-Michael addition reaction: A green protocol, J. Mol. Catal. A Chem. 353-354 (2012) 122-131.

65. E. Angelescu, O.D. Pavel, R. Bîrjega, R. Zăvoianu, G. Costentin, M. Che, Solid base catalysts obtained from hydrotalcite precursors, for Knoevenagel synthesis of cinamic acid and coumarin derivatives, Appl. Catal. A-Gen., 308 (2006) 13-18.

66. M.J. Climent, A. Corma, S. Iborra, J. Primo, Base catalysis for fine chemicals production: Claisen Schmidt condensation on zeolites and hydrotalcites for the production of chalcones and flavonones of pharmaceutical interest, J. Catal., 151 (1995) 60-66.

67. D. Tichit, M. N. Bennani, F. Figueras, R. Ruiz, Decomposition processes and characterization of the surface basicity of Cl^- and CO_3^{2-} hydrotalcites, Langmuir, 14 (1998) 2086-2091.

68. G.D. Yadav, P. Aduri, Aldol condensation of benzaldehyde with heptanal to jasminaldehyde over novel Mg-Al mixed oxide on hexagonal mesoporous silica, J. Mol. Catal A Chem., 355 (2012) 142-154.

69. L.K.G. Bhatta, S. Subramanyam, M.D. Chengala, S. Olivera, K. Venkatesh, Progress in hydrotalcite like compounds and metal-based oxides for CO_2 capture: a review. J. Clean. Prod., 103 (2015) 171-196.

70. Y. Miao, Y. Ma, Q. Wang, Plasma-assisted simultaneous reduction and nitrogen/sulfur codoping of graphene oxide for high-performance supercapacitors. ACS Sustainable Chem. Eng. 7 (2019) 7597-7608.

71. Z. Wang, Y. Zhang, E.C Neyts, X. Cao, X. Zhang, B. W.-L. Jang, C-j Liu, Catalyst preparation with plasmas: How does it work? ACS Catal., 8 (2018) 2093-2110.

72. A. Bogaerts, E.C. Neyts, Plasma technology: An emerging technology for energy storage. ACS Energy Lett., 3 (2018) 1013-1027.

73. C. Chen, B. Liang, A. Ogino, X. Wang, M. Nagatsu, Oxygen functionalization of multiwall carbon nanotubes by microwave-excited surface-wave plasma treatment, J. Phys. Chem. C., 113 (2009) 7659-7665.

74. K.C.Sabat, R.K. Paramguru, S. Pradhan, B.K. Mishra, Reduction of cobalt oxide (Co_3O_4) by low temperature hydrogen plasma, Plasma. Chem. Plasma Process, 35 (2015) 387-399.

75. H. Srour, N. Guignard, M. Tarighi, E. Devers, A. Mekki-Berrada, J. Toufaily, T. Hamieh, C. Batiot-Dupeyrat, L. Pinard, Regeneration of an aged hydrodesulfurization catalyst by non-thermal plasma: characterization of refractory coke molecules, Catalysts, 11 (2021) 1153.

76. A.M dos Santos, R.C. Catapan, D.A. Duarte, The potential of non-thermal plasmas in the preparation of supported metal catalysts for fuel conversion in automotive systems: A literature overview. Front. Mech. Eng., 6 (2020) 1-12.

77. O. L. Li, R. Ikura, T. Ishizaki, Hydrolysis of cellulose to glucose over carbon catalysts sulfonated *via* a plasma process in dilute acids. Green Chem. 19 (2017) 4774-4777.

78. L. Qin, N. Takeuchi, K. Takahashi, J. Kang, K.H. Kim, O.L. Li, N_2/Ar plasma-induced surface sulfonation on graphene nanoplatelets for catalytic hydrolysis of cellulose to glucose. Appl. Surf. Sci. 545 (2021) 149051.

79. Z. Luo, S. Tian, Z. Wang, Enhanced activity of Cu/ZnO/C catalysts prepared by cold plasma for CO_2 hydrogenation to methanol, Ind. Eng. Chem. Res., 59 (2020) 5657-5663.

80. Yang J.C., Small M.W., Grieshaber R.V., Nuzzo R.G. Recent developments and applications of electron microscopy to heterogeneous catalysis. *Chem. Soc. Rev*., 2012, 41, 8179-8194.

81. M. Senila, O. Cadar, L. Senila, S. Böringer, K. Seaudeau-Pirouley, A. Ruiu, P. Lacroix-Desmazes, Performance parameters of inductively coupled plasma optical emission spectrometry and graphite furnace atomic absorption spectrometry techniques for Pd and Pt determination in automotive catalysts, Materials, 13 (2020) 5136.

82. M. Manzoli, Boosting the characterization of heterogeneous catalysts for H_2O_2 direct synthesis by infrared spectroscopy, Catalysts., 9 (2019) 30.

83. A. Koreniuk, K. Maresz, K. Odrozek, A.B. Jarzebski, J. Mrowiec-Bialoń, Highly effective continuous-flow monolithic silica microreactors for acid catalyzed processes, Appl.Catal. A- Gen, 489 (2015) 203-208.

84. M. Baumann, T.S. Moody, M. Smyth, S. Wharry, A perspective on continuous flow chemistry in the pharmaceutical industry, Org. Process. Res. Dev., 24 (2020) 1802-1813.

85. J. A. Bennett, Z. S. Campbell, M. Abolhasani, Role of continuous flow processes in green manufacturing of pharmaceuticals and specialty chemicals, Curr. Opin. Chem. Eng. 26 **(**2019) 9-19.

86. M. Pagliaro, C.D. Pina, R. Ciriminna, Continuous flow single-atom catalysis: A viable organic process technology? ChemCatChem., 14 (2022) e202200768.

87. A. Kirschning, W. Solodenko, K. Mennecke, Combining enabling techniques in organic synthesis: Continuous flow processes with heterogenized catalysts, Chem. Eur. J., 12 (2006) 5972-5990.

88. A. Sachse, A. Galarneau, F. Fajula, F. Di Renzo, P. Creux, B. Coq, Functional silica monoliths with hierarchical uniform porosity as continuous flow catalytic reactors. Micropor. Mesopor. Mat., 140 (2011) 58-68.

89. Z. Khan, F. Javed, Z. Shamair, A. Hafeez, T. Fazal, A. Aslam, W.B. Zimmerman, F. Rehman, Current developments in esterification reaction: A review on process and parameters. J. Ind. Eng. Chem., 103 (2021) 80-101.

90. A. Palani, M. Palanichamy, P. Arumugam, Vapour phase esterification of butyric acid with 1-pentanol over Al-MCM-41 mesoporous molecular sieves, Catal. Lett., 115 (2007) 40-45.

91. A.A. Kiss, Novel catalytic reactive distillation processes for a sustainable chemical industry, Top. Catal., 62 (2019)1132-1148.

92. Shagufta, I. Ahmad, R. Dhar, Sulfonic acid-functionalized solid acid catalyst in esterification and transesterification reactions, Catal. Surv. Asia, 21 (2017) 53-69.

93. N. Singh, R. Kumar, P.K. Sachan, Kinetic study of catalytic esterification of butyric acid and ethanol over Amberlyst 15, ISRN Chem. Eng., 2013 (2013) 1-7.

94. U. Wollina, Fumaric acid esters in dermatology, Indian Dermatol. Online J., 2 (2011) 111- 119.

95. T.C. Bhalla, V. Kumar, S.K. Bhatia, Hydroxy acids: Production and applications. In Advances in Industrial Biotechnology; R.S. Singh, A. Pandey, C. Larroche, (Eds.), IK International Publishing House PVT. Ltd.: New Delhi, India, 2014; pp. 56–76.

96. G.K. Weakley, Kelly, C.E. Method for producing an alkyl 3-hydroxybutyrate. Patent Application. US 2015/0038734 A1, Feb. 5, 2015.

97. T. Rohwerder, R. H. Müller, Biosynthesis of 2-hydroxyisobutyric acid (2-HIBA) from renewable carbon, Microb. Cell Factories, 9 (2010) 13.

98. M. Nobuyuki, A. Takafumi, H. Hirofumi, Process for Producing Methyl α-Hydroxyisobutyrate. Patent Application. US005391813A, Oct 12, 1993.

99. L.H. Tamborini, M.P. Militello, J. Balach, J.M. Moyano, C.A. Barbero, D.F. Acevedo, Application of sulfonated nanoporous carbons as acid catalysts for Fischer esterification reactions, Arab. J. Chem., 12 (2019) 3172-3182.

100. D. Lee, Preparation of a sulfonated carbonaceous material from lignosulfonate and its usefulness as an esterification catalyst, Molecules, 18 (2013) 8168-8180.

101. F.J. Holzhäuser, J. Artz, S. Palkovits, D. Kreyenschulte, J. Büchs, R. Palkovits, Electrocatalytic upgrading of itaconic acid to methylsuccinic acid using fermentation broth as a substrate solution. Green Chem. 19 (2017) 2390-2397.

102. V.C. Nguyen, N.Q. Bui, P. Mascunan, T.T. Ha Vu, P. Fongarland, N. Essayem, Esterification of aqueous lactic acid solutions with ethanol using carbon solid acid catalysts: Amberlyst 15, sulfonated pyrolyzed wood and graphene oxide. Appl. Catal. A- Gen., 552 (2018) 184-191.

103. R. Luque, C.S.K. Lin, C. Du, D.J. Macquarrie, A. Koutinas, R. Wang, C. Wedd, J.H. Clark, Chemical transformations of succinic acid recovered from fermentation broths by a novel direct vacuum distillation-crystallisation method. Green Chem., 11 (2009) 193-200.

104. C. Delhomme, S.L.M. Goh, F.E. Kühn, D. Weuster-Botz. Esterification of bio-based succinic acid in biphasic systems: Comparison of chemical and biological catalysts. J.Mol.Catal. B Enzym., 80 (2012) 39-47.

105. A. V. Nakhate, G. D. Yadav, Synthesis and Characterization of Sulfonated Carbon-Based Graphene Oxide Monolith by Solvothermal Carbonization for Esterification and Unsymmetrical Ether Formation, ACS Sustainable Chem. Eng., 4 (2016) 1963-1973.

106. S. Hosseini, J. Janaun, T. S.Y. Choong, Feasability of honeycomb monolith supported sugar catalyst to produce biodiesel from palm fatty acid distillate (PFAD), Process Saf. Environ. Prot., 98 (2015) 285-295.

107. T.A. Nijhuis, A.E.W. Beers, F. Kapteijn, J.A. Moulijn, Water removal by reactive stripping for a solid-acid catalyzed esterification in a monolithic reactor, Chem. Eng. Sci. 57 (2002) 1627-1632.

108. F. Wakayama, R. Ito, K. Park, M. Ishida, Y. Yamada, S. Ichihara, H. Takada, S. Nakamura, A. Kato, T. Yamada, H. Sajiki, Y. Monguchi, Esterification or

thioesterification of carboxylic acids with alcohols or thiols using amphipathic monolith-SO_3H resin, Bull. Chem. Soc. Jpn., 94 **(**2021) 2702-2710.

109. G. Morales, M. Paniagua, D. de la Flor, M. Sanz, P. Leo, C. López-Aguado, H. Hernando, S.A. Orr, K. Wilson, A. F. Lee, J. A. Melero, Aldol condensation of furfural and methyl isobutyl ketone over Zr-MOF-808/silica hybrid catalysts, Fuel, 339 (2023) 127465.
110. M. Su, W. Li, T. Zhang, H. Xin, S. Li, W. Fan, L. Ma, Production of liquid fuel intermediates from furfural via aldol condensation over Lewis acid zeolite catalysts, Catal. Sci. Tech., 7 (2017) 3555-3561.
111. J. Cuteo, L. Faba, E. Diaz, S. Ordonez, Optimization of the process conditions for minimizing the deactivation in the furfural-cyclopentanone aldol condensation in a continuous reactor, Appl. Catal. B: Environ., 263 (2020) 118341.
112. Z.Tisler, P. Vondrova, K. Hrachovcova, K. Stepanek, R. Velvarska, J. Kocik, E. Svobodova, Aldol condensation of cyclohexanone and furfural in fixed-bed reactor, Catalysts, 9 (2019) 1068.
113. D.T. Ngo, T. Sooknoi, D. E. Resasco, Improving stability of cyclopentanone aldol condensation MgO-based catalysts by surface hydrophobization with organosilanes, Appl. Catal. B: Environ, 237 (2018) 835-843.
114. J. Yang, S. Li, N. Li, W. Wang, A. Wang, T. Zhang, Y. Cong, X. Wang, G.W. Huber, Synthesis of jet-fuel range cycloalkanes from the mixtures of cyclopentanone and butanal, Ind. Eng. Chem. Res., 54 (2015) 11825-11837.

115. G. Li, B. Wang, B. Chen, D. E. Resasco, Role of water in cyclopentanone self-condensation reaction catalyzed by MCM-41 functionalized with sulfonic acid groups, Journal of Catalysis, 377 (2019) 245-254.

116. X. Meng, H. Su, R. Song, J. Su, J. Bian, Solvent-free aldol condensation of cyclopentanone with natural clay-based catalysts : Origin of activity & selectivity., Catalysts, 13 (2023)530.

117. L. Ti, X. Sheng, H. Jia, W. Han, Q. Ping, J. Yang, N. Li, Process integration of KOH/diatomite preparation and cyclopentanone self-condensation via ball-milling method, Mol. Catal., 535 (2023) 112869.

118. J. Wan, L. Fu, H. Yang, K. Wang, F. Xi, L. Pan, Y. Li, Y. Liu, TiO_2-ZrO_2 composite oxide as an acid-base bifunctional catalyst for self-condensation of cyclopentanone, Ind. Eng. Chem. Res., 59 (2020) 19918-19928.

119. X. Zhou, C. Zhang, Effect of preparation method on the catalytic property of calcined Ca-Al hydrotalcite for the synthesis of ethyl methyl carbonate, ACS Omega, 6 (2021) 5056-5060.

120. S. Vasefi, Development of sustainable solid base hydrotalcite catalyst support by granular activated carbon, [Master Dissertation, University of Georgia], 2021.

121. Q. Liu, X. Zhang, Q. Zhang, Q. Liu, C. Wang, L. Ma, Synthesis of jet fuel range cycloalkanes with cyclopentanone and furfural, Energy Fuels, 34 (2020) 7149-7159.

122. X. Sheng, G. Li, W. Wang, Y. Cong, X. Wang, G.W. Huber, N. Li, A. Wang, T. Zhang, Dual-bed catalyst system for the direct synthesis of high-density aviation fuel with cyclopentanone from lignocellulose. AIChE J., 62 (2016) 2754-2761.

123. S. Roy, T. Bauer, M. Al-Dahhan, P. Lehner, T. Turek, Monoliths as multiphase reactors: A review, AIChE J., 50 (2004) 2918- 2938.

124. W. Liu, W. P. Addiego, C. M. Sorensen, T. Boger, Monolith reactor for the dehydrogenation of ethylbenzene to styrene, Ind. Eng. Chem. Res., 41 (2002) 3131-3138.

125. M.T. Kreutzer, P. Du, J.J. Heiszwolf, F. Kapteijn, J.A. Moulijn, Mass transfer characteristics of three-phase monolith reactors, Chem. Eng. Sci., 56 (2001) 6015-6023.

126. R. Gupta, D.F. Fletcher, B.S. Haynes, Taylor Flow in Microchannels : A review of experimental and computational work, J. Comput. Multiph. Flows, 2 (2010) 1-31.

127. P. Angeli, A. Gavriilidis, Hydrodynamics of Taylor flow in small channels : A review. Proc. Inst. Mech. Eng. C J. Mech. Eng. Sci. 222 (2008) 737-751.

128. H.S. Fogler, Elements of cgemical reaction engineering, Prentice-Hall, 5th ed.; Englewood Cliffs: New Jersey, 1986; pp 600-650.

129. A.A. Bhusari, B. Mazmudar, A.P. Rathod, R.D. Khonde, Kinetics of catalyzed esterification of acetic acid with n-butanol using carbonized agro-waste, Int. J. Chem. Kinet., 52 (2020) 450-462.

130. M.R., Avhad, M.V. Osborg, J.M. Marchetti, Reusable Amberlyst 16 catalyst for acetic acid esterification relevant for pyrolysis bio-oil upgrading process, React. Kinet. Mech.Catal., 126 (2019) 181-197.

131. S. Miao, B.H. Shanks, Mechanism of acetic acid esterification over sulfonic acid-functionalized mesoporous silica, J. Catal., 279 (2011) 136-143.

132. T.J. Schildhauer, I. Hoek, F. Kaptejin, J. Moulijn, Zeolite BEA catalyzed esterification of hexanoic acid with 1- octanol: Kinetics, side reactions and role of water, Appl.Catal. A: Gen., 358 (2009) 141-145.

133. S. Akyalcin, M.R. Altiokka, Kinetics of esterification of acetic acid with 1-octanol in the presence of Amberlyst 36, Appl. Catal. A-Gen. 429-430 (2012) 79-84.

134. R. Hilten, J. Weber, J.R. Kastner, Continuous catalytic esterification and hydrogenation of a levoglucosan/acetic acid mixture for production of ethyl levulinate/acetate and valeric biofuels, Energy Fuels, 30 (2016) 9480-9489.

135. W. Chu, X. Yang, X. Ye, Y. Wu, Vapor phase esterification catalyzed by immobilized dodecatungstosilicic acid (Si W_{12}) on activated carbon, Appl.Catal. A: Gen., 145 (1996) 125-140.

136. S. H. Ali, Kinetics of catalytic esterification of propionic acid with different alcohols over Amberlyst 15, International Journal of Chemical Kinetics 41 (2009) 377-448.

137. Y-T. Tsai, H-m. Lin, M-J Lee, Kinetics behavior of esterification of acetic acid with methanol over Amberlyst 36, Chem. Eng. J., 171 (2011) 1367-1372.

138. H.O. Otor, J.B. Steiner, C. García-Sancho, A.C. Alba-Rubio, Encapsulation methods for control of catalyst deactivation: A review. ACS Catal., 10 (2020) 7630-7656.

139. J-P. Lange. Renewable feedstocks: The problem of catalyst deactivation and its mitigation, Angew. Chem. Int. Ed. 54 (2015) 13186-13197.

140. M.D. Argyle, C.H. Bartholomew, Heterogeneous Catalyst Deactivation and Regeneration: A Review, Catalysts 5 (2015)145-269.

141. X. Mo, D. Lopez, K. Suwannakarn, Y. Liu, Activation and deactivation characteristics of sulfonated carbon catalysts, J. Catal., 254 (2008) 332-338.

142. B. Zhang, M. Gao, J. Geng, Y. Cheng, X. Wang, C. Wu, Q. Wang, S. Liu, S.M. Cheung, Catalytic performance and deactivation mechanism of a one-step sulfonated carbon-based solid -acid catalyst in an esterification reaction, Renew. Energy, 164 (2021) 824-832.

143. P. Kasinathan, D.W. Hwang, U. Lee, Y.K. Hwang, J.S. Change, Effect of solvent and impurity on synthesis of ethyl lactate from fermentation-derived ammonium lactate, Chem. Eng. Sci. 66 (2011) 4549-4554.

144. V.K. Diez, C.R. Apesteguia, J.I. Di Cosimo, Effect of acid-base properties of Mg-Al mixed oxides on the catalyst deactivation during aldol condensation reactions, Lat. Am. Appl. Res., 33 (2003) 79-86.

145. J.C. Manayil, V.C. dos Santos, F.C. Jentoft, M.G. Mesa, A.F. Lee, K. Wilson, Octyl Cografted PrSO3H/SBA-15: Tunable Hydrophobic Solid Acid Catalysts for Acetic Acid Esterification, ChemCatChem., 9 (2016) 2231-2238.

146. R. Alamillo, A.J. Crisci, J.M.R. Gallo, S.L. Scott, J.A. Dumesic, A tailored microenvironment for catalytic biomass conversion in inorganic-organic nanoreactors. Angew. Chem. Int. Ed., 52 (2013) 10349-10351.

147. R.I. Balderas, A.E. Settle, A. York, D.R. Conklin, H.N. Pham, P.C. Metz, K. Page, A.K. Datye, B.G. Trewyn, D.R. Vardon, R.M. Richards, MgO (111) nanocatalyst for biomass conversion: A study of carbon coating effects on catalyst faceting and performance. Catal.Lett., 152 (2022) 1-11.

148. J. Lu, B. Fu, M.C. Kung, G. Xiao, J.W. Elam, H.H. Kung, P.C. Stair, Coking- and sintering-resistant palladium catalysts achieved through atomic layer deposition. Science, 335 (2012) 1205-1208.

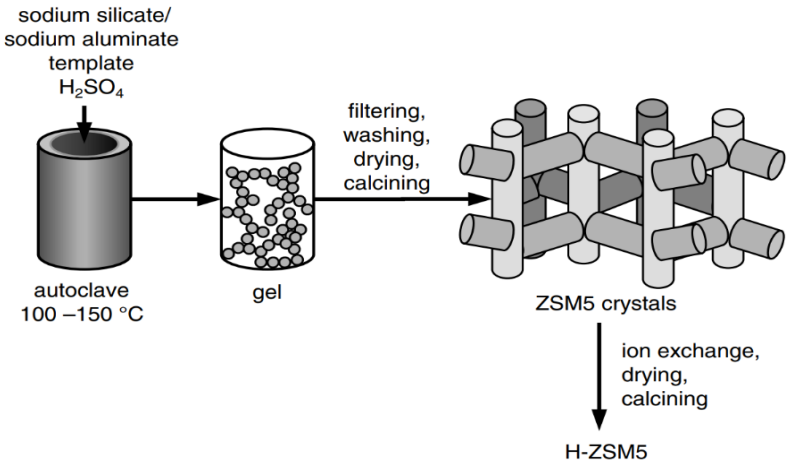

Figure 2.1. Hydrothermal synthesis of HZSM-5 zeolite.[2]

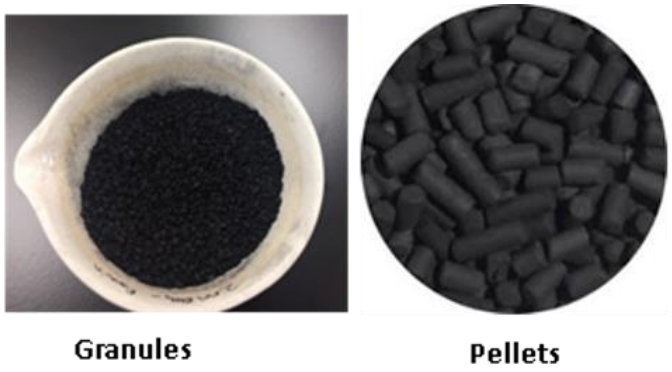

Figure 2.2. Activated carbon in the form of granules and pellets.

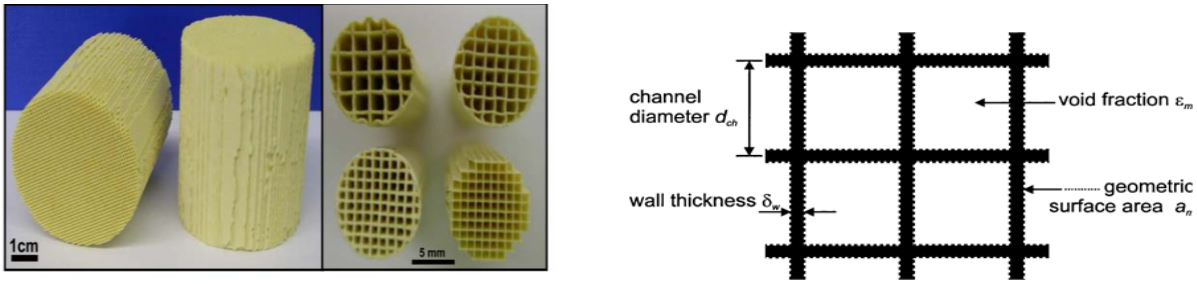

Figure 2.3. (a) Ceramic monoliths of different cell densities/sizes (side view and top view), (b) Geometric parameters for a monolith with square channels. [21]

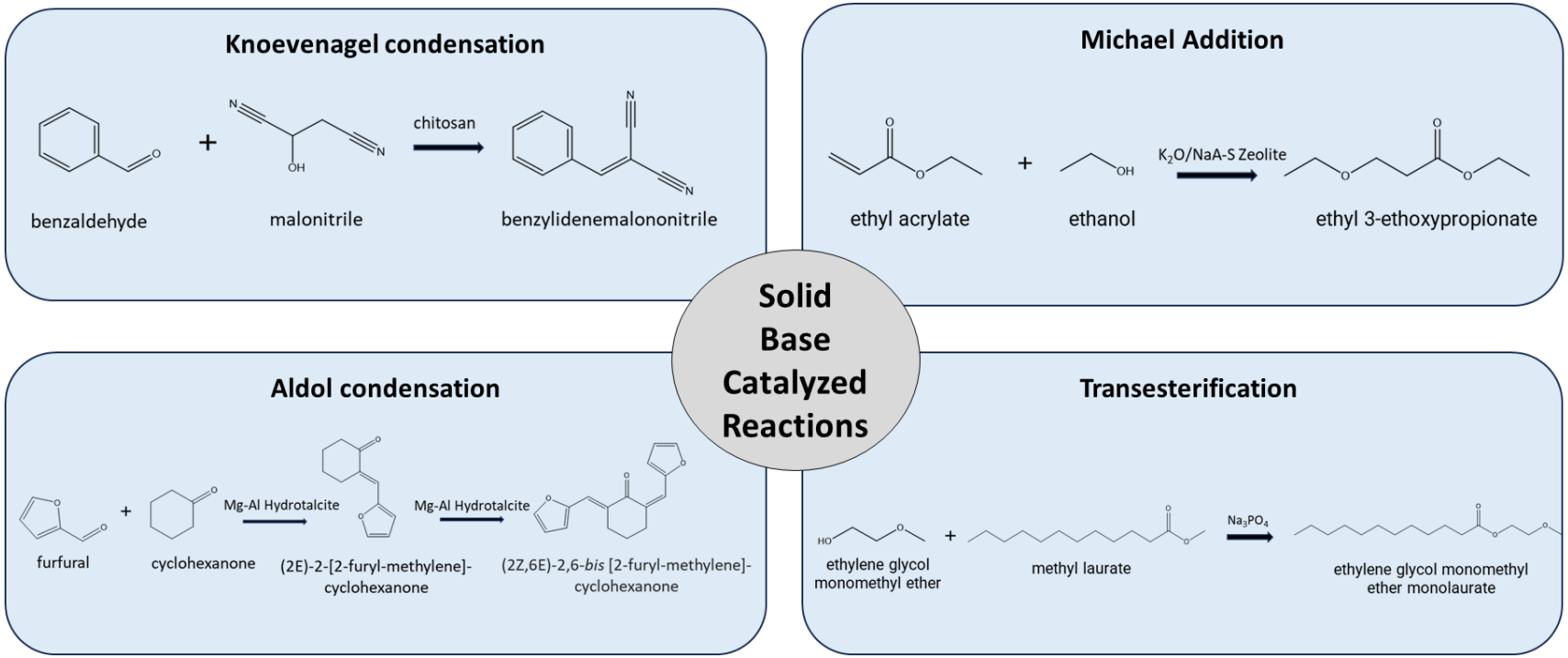

Figure 2.4. Types of solid base-catalyzed reactions.[56,57,58,59]

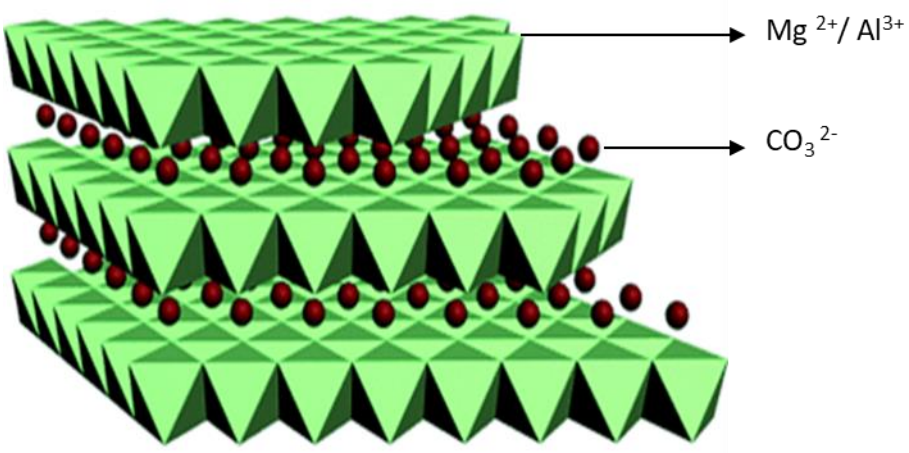

Figure 2.5. Schematic view of the structure of hydrotalcites.[60]

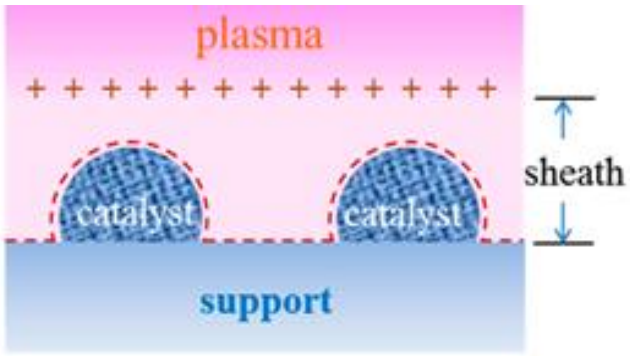

Figure 2.6. Plasma-Catalyst Interaction.[71]

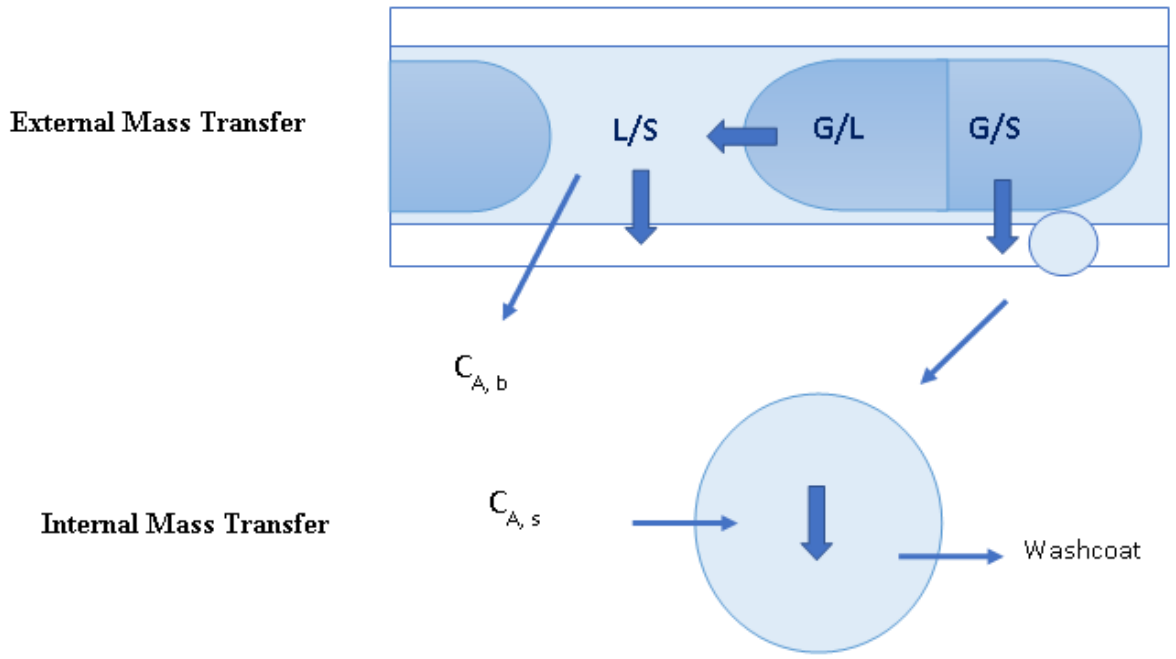

Figure 2.7. External and internal mass transfer in monolithic catalysts[123,127] (L/S: liquid-solid mass transfer, G/L: gas-liquid mass transfer, G/S: gas-solid mass transfer, C_{Ab} and C_{As} are the bulk and surface concentrations of substrate A).

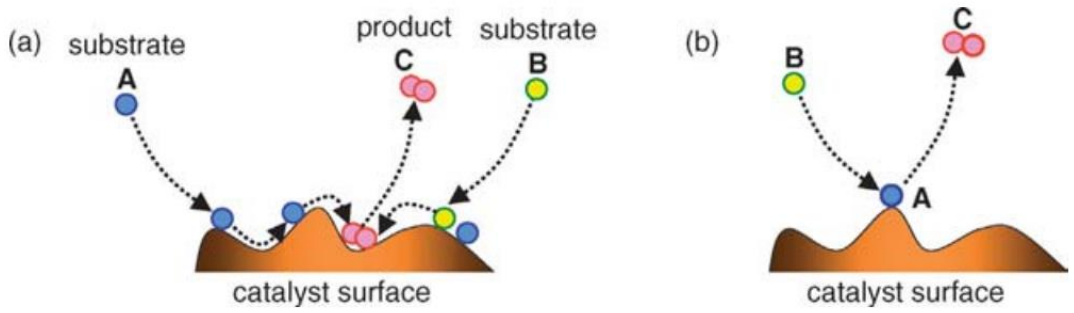

Figure 2.8. The two main mechanisms in heterogeneous catalysis (a) Langmuir-Hinshelwood and (b) Eley-Rideal.

CHAPTER 3

CATALYTIC ESTERIFICATION USING SOLID ACID CARBON CATALYSTS SYNTHESIZED BY SUSTAINABLE HYDROTHERMAL AND PLASMA SULFONATION TECHNIQUES

[1] S. Sripada, J.R. Kastner, Catalytic esterification using solid acid carbon catalysts synthesized by sustainable hydrothermal and plasma sulfonation techniques, Ind. Eng. Chem. Res., 61 (2022) 3928-3940. Reprinted here with permission of publisher.

Catalytic Esterification Using Solid Acid Carbon Catalysts Synthesized by Sustainable Hydrothermal and Plasma Sulfonation Techniques

Author: Sarada Sripada, James R. Kastner

Publication: Industrial & Engineering Chemistry Research
Publisher: American Chemical Society

Date: Mar 1, 2022

Abstract

Solid acid carbon catalysts were synthesized from wood activated carbon in granular (GAC) and monolith (ACM) forms using incipient wetness and plasma or hydrothermal methods at sulfonation agent:carbon ratios of 0.62:1 to 1.75:1 [v/w, mL/g], significantly lower than a commonly used ratio of 10:1 (6-16 × lower). Yet, esterification rates and yields were comparable to those of catalysts generated with excess concentrated sulfuric acid and commercial acid resins. Acid sites were confirmed by multiple methods, and catalytic activity was investigated by batch esterification of 2-hydroxyisobutyric acid. Hydrothermally sulfonated GAC and ACM generated reaction rates and ester yields comparable to commercial Amberlyst-15 (150 °C, 1 h). Room temperature plasma (Ar/H_2O vapor, 10-15 min) successfully sulfonated GAC and ACM, but generated lower ester yields, due to lower acid site density. Reaction and reuse studies suggest the hydrothermal incipient wetness and plasma sulfonation methods can sustainably generate solid acid carbon catalysts from renewable biomass for catalytic upgrading biobased organic acids.

Key Words: Sulfonated carbon; activated carbon monolith (ACM); incipient wetness; plasma; 2-hydroxyisobutyric acid; esterification

3.1 Introduction

Homogeneous acids, such as H_2SO_4, have been widely employed for industrial esterification reactions, yet have several limitations including equipment corrosion, lack of reuse, and required treatment of the spent effluent.[1] Heterogeneous solid acid catalysts facilitate product separation, ensure catalyst recyclability, and generate little waste, circumventing the environmental impacts associated with their homogeneous counterparts.[2] Solid acids used in esterification reactions include metal oxides, heteropoly acids, zeolites, and acidic ion exchange resins such as Amberlyst-15.[3] Their drawbacks include low porosity and surface area, low acid site density in some materials, poor stability, low water tolerance and high preparation cost.[4] Although acid resins (e.g., Amberlyst-15) have been employed for catalytic esterification, they can be limited by low thermal stability and are synthesized from petroleum resources.[5] Sulfonated carbon catalysts have received much attention as esterification catalysts, since they have Bronsted acid sites,[6] large surface area, are stable under acidic and basic conditions, and can be prepared from renewable lignocellulosics. Carbon supported catalysts are also stable in aqueous environments, which is a prerequisite for equilibrium-limiting esterification reactions that generate water.[7]

In conventional post-grafting methods (after pyrolysis and activation), sulfonated carbons are typically synthesized by wet impregnation of concentrated or fuming sulfuric acid at elevated temperatures (100-200 °C) for long durations (10-24 h). For instance, activated carbon has been sulfonated using concentrated sulfuric acid (20 mL H_2SO_4/g catalyst) at 150 °C for 16 h.[8] Similarly, carbon fibers have been refluxed in concentrated H_2SO_4 (50 mL H_2SO_4/g catalyst) for 12 h at 150 °C.[9] A review of the post-grafting literature indicates sulfonation agent to carbon ratios (v/w, mL/g) from 7:1 to 50:1, with 10:1 suggested as optimum, and increasing the temperature to 250 °C was shown to increase acid site density in activated carbon.[10,11] These

techniques utilize large quantities of acid, necessitating a more environmentally friendly preparation method for scale-up. Modifications to existing hydrothermal methods are essential to minimize activating agent consumption, reduce acidic waste, and ensure optimal sulfonation conditions.

Sustainable strategies for catalyst fabrication have led to the emergence of plasma technology as a design tool for surface modification.[12] Non-thermal plasmas (NTP), characterized by a thermodynamic non-equilibrium, permits catalyst synthesis in shorter durations, does not affect the bulk structure, and limits the use of hazardous reagents, thereby minimizing waste.[13] This makes NTP an attractive alternative to the conventional high temperature, longer treatment duration hydrothermal methods. Recently, plasma sulfonation of carbon black (ambient air and N_2/Ar) in dilute sulfuric acid was reported (0.1-1 M, 30 min) resulting in a solid acid catalyst active for decrystallized cellulose hydrolysis.[14,15] Plasma treatment was performed in solution with powdered carbon, using carrier gases such as air, N_2, and argon. Although effective in sulfonating the catalyst surface, continuous generation of plasma in a liquid requires large electrical power compared to vacuum or atmospheric pressure, which increases thermal load on the electrodes and deterioration of the electrode surface.[16] Further, large volumes of dilute acid solution are required for catalyst preparation, reducing process scale-up viability, and the process does not seem applicable to structured carbon. Alternatively, we propose the catalyst can be pre-treated with dilute sulfuric acid and subjected to plasma treatment under a vacuum, with hydrogen radical generating carrier gas mixtures such as hydrogen-argon or argon-water vapor. Such a method could be applied to structured catalysts (e.g., pellets and monoliths) used in continuous processing. Activated carbon monoliths combine the advantages of activated carbon and monolithic structure into a single catalyst,[17] because they have high external surface area and

interfacial mass transfer rates, and low pressure drop, which facilitates continuous processing. Studies pertaining to activated carbon monoliths as acid catalysts have been scarce.[18]

Esters of hydroxyacids have valuable industrial and medical applications.[19] Eastman Chemical developed an organic cleaning solvent butyl 3-hydroxybutyrate, marketed under the trade name Omnia™, by esterifying a diketene with butanol and hydrogenation.[20] Recently, highly crosslinked strong acid resins have been used to directly esterify 3-hydroxybutyric acid (3-HBA) for butyl 3-HBA synthesis (91% conversion, 2 h, 70 °C).[21] 2-Hydroxyisobutyric acid (2-HIBA) is gaining significance as a platform chemical[22] and has been identified as a building block for polymer synthesis. The methyl ester of 2-HIBA is produced from 2-hydroxyisobutyramide and methyl formate, and used for electronic materials, ink cleaning and an intermediate for agrochemicals and medicine.[23] Ethyl 2-hydroxyisobutyrate (E-2HIBA), which has applications as a solvent for nitrocellulose and cellulose acetate, pharmaceuticals and organic synthesis has been less explored.[24] Fermentative production of 2-HIBA has been reported from several recombinant microbial strains[25] and ethanol is a renewable, biobased platform chemical. Developing a stable solid acid catalyst for 2-HIBA esterification with ethanol would create sustainable avenues for renewable 2-HIBA in fine chemical synthesis, and catalytic upgrading of other biobased organic acids.

To reduce the sulfonating agent to carbon ratio, reduce contact time, and lower energy inputs, novel, modified hydrothermal and plasma sulfonation methods were developed. Hydrothermal and plasma sulfonation methods employed the rarely used incipient wetness impregnation (GAC) and sonication (ACM) of wood-based activated carbons using dilute H_2SO_4 (2 M) as the sulfonating agent. This is one of the first reports on the hydrothermal synthesis of sulfonated carbon (GAC) through incipient wetness impregnation with dilute H_2SO_4 and plasma sulfonation

by introducing water vapor or hydrogen into a low-pressure plasma reactor. Carrier gases of argon/water vapor and 3% hydrogen/ argon were used for plasma treatment. Catalytic efficiency of the hydrothermal and plasma sulfonated GAC and ACM catalysts was assessed in the esterification of 2-HIBA with ethanol as a model reaction and compared to a benchmark catalyst, Amberlyst-15. Our objectives were to develop more sustainable and reusable esterification catalysts from activated carbon, investigate the possibility of modifying the current hydrothermal methods, as well as replacing the hydrothermal steps by plasma methods.

3.2 Materials and Methods

3.2.1 Chemicals

2-hydroxyisobutyric acid ($C_4H_8O_3$, purity > 98%) and ethyl 2-hydroxyisobutyrate ($C_6H_{12}O_3$, purity > 98%) were purchased from TCI chemicals. 200 proof ethanol (purity >99.5%) was procured from Sigma Aldrich. Sulfuric acid used for carbon sulfonation was purchased from J.T. Baker. Amberlyst-15 (hydrogen form) was obtained from Sigma Aldrich.

3.2.2 Specifications of Activated Carbon Materials

A granular activated carbon (Nuchar WV-B 20 GAC) was obtained from Ingevity and used to synthesize the sulfonated carbon catalysts.[7] Nuchar WV-B 20 has a surface area of 1490 m^2/g (Brunauer-Emmett-Teller, BET), pore diameter of 26.9 Å, pore volume of 1.23 cc/g (Barrett-Joyner-Halenda, BJH) and particle size of $1 < d_p < 3$ mm. The wood-based activated carbon monolith (ACM 101-H) was provided by Applied Catalysts (Laurens, SC) and manufactured by coextrusion of 50% activated carbon and 50% of a ceramic binder. Each monolith core has a diameter and length of 1 inch (2.54 cm), 400 cells/in^2 (62 cells/cm^2), wall thickness of 0.01 in. (0.25 mm), cell spacing of 0.044 in. (1.11 mm), geometric surface area of 70.8 in^2/in^3 (27.9

cm^2/cm^3), open frontal area of 0.6 in^2 (3.8 cm^2), density of 350 kg/m^3, surface area of 598 m^2/g (BET), pore diameter of 29.8 Å, and pore volume of 0.5 cc/g (BJH). The monolith structure was crushed (cACM) and sieved to a particle size of $1 < d_p < 3$ mm prior to the catalytic reactions.

3.2.3 Catalyst Preparation

The base granular activated carbon (Base-GAC) was washed until neutral pH (3 ×) to eliminate any contaminants (initial pH was ~5.8). Sulfuric acid (18 or 2 M) was introduced into the GAC by incipient wetness impregnation at 1.75 mL/g catalyst (1.75:1 [v/w] sulfonating agent: carbon ratio), a little excess than the pore volume of 1.23 mL/g, to ensure all particles were sufficiently wetted. The monolith cores (Base-ACM) were immersed into 2 M H_2SO_4 (100 mL) and sonicated at 30 °C for 30 min. After sonication, the cores were removed (excess liquid was removed by blotting) and weighed to determine the volume of impregnated sulfonating solution. A sulfonating agent to carbon ratio of 0.62:1 [v/w] was calculated for the ACM process. A schematic depicting the catalyst preparation methods is presented in Figure 3.1.

Hydrothermal Synthesis (HT)

The GAC and ACM catalysts subjected to incipient wetness or wetness impregnation with sonication respectively, were treated hydrothermally at 250 °C in a muffle furnace (Fisher Scientific) for 12-16 h. These catalysts are named GAC-HT-18M, GAC-HT-2M, and cACM-HT-2M. Hydrothermal treatment of the monolith using 18M H_2SO_4 was avoided.

Plasma Treatment (PT)

For plasma sulfonation, the GAC and ACM catalysts treated with dilute H_2SO_4 by incipient wetness or sonication respectively, were air-dried overnight. Plasma treatment was performed in a Harrick expanded plasma cleaner (PDC-001, 115 V, chamber size 150 × 170 mm, maximum

radiofrequency power 30 W), connected to a vacuum pump (Edwards XDS 5). Plasma treatment was investigated with a mixture of argon and water vapor and 3% hydrogen balance argon (inflammable) at three different time points of 5, 10 and 15 min (details in supporting information and Figure S3.1). These catalysts are named GAC-PT-Ar/H_2O-5,10,15 min; GAC-PT-H_2/Ar-5,10,15 min; cACM-PT-Ar/H_2O-5,10,15 min; and cACM-PT-H_2/Ar-5,10,15 min. A comparison of the two plasma treatments is provided in the supporting information.

3.2.4 Washing

Post treatments, all sulfonated catalysts were washed (the ACM cores were crushed prior to washing) with deionized water (25-50 mL/g catalyst) at room temperature to remove traces of excess acid (H_2SO_4), and to ensure the catalytic activity was solely due to the sulfonated carbon. Washing (8-12 ×, 1 h washes) was carried out until the filtrate displayed a constant pH, (approximately 5.2-5.5 for the GAC and 4.0 for the ACM catalysts). Care was exercised to minimize particle attrition. Post-washing, all catalysts were dried in a hot air oven at 105 °C overnight and stored for further experiments.

3.2.5 Catalyst Characterization

The surface area of the hydrothermal and plasma sulfonated carbons was measured by N_2 adsorption (Nova LX4, Anton Parr, U.S.A) and a 3-point BET analysis. Scanning transmission electron microscopy (STEM) imaging was performed on a Hitachi SU-9000. Subsequent Energy-dispersive X-ray spectroscopy (EDS) analysis was conducted on a ThermoFisher Teneo with an Oxford Xmax EDS detector. The sulfur (S) and phosphorus (P) content on the catalysts was quantified by microwave digestions followed by inductively coupled plasma - optical emission spectroscopy (ICP-OES) analysis. The samples were digested following EPA Method

3052, and the final solutions were analyzed for S and P following EPA Method 200.8 by ICP-OES (Spectro Arcos FHS16, Germany). Sulfonic acid density was estimated from the sulfur content, assuming all S atoms were in the $-SO_3H$ form. Fourier transform infrared (FTIR) analysis (1 mg of catalyst with 300 mg of KBr) was performed to qualitatively assess the formation of sulfonic acid groups on the carbon catalysts using a Thermo Scientific Nicolet 6700 FTIR (4000-399 cm^{-1}). X-ray photoelectron spectroscopy (XPS) analysis was performed on a Thermo Scientific K-Alpha XPS system with a monochromatic Al-K_α (1486.6 eV) X-ray source (details for all methods are in supporting information).

3.2.6 Analytical Methods

Standard solutions of 2-hydroxyisobutyric acid (2-HIBA) and ethyl-2-hydroxyisobutyrate (E-2HIBA) were prepared in ethanol. Each standard was analyzed in triplicate to determine the standard deviations (SD). Liquid sample collected from the reactor was analyzed using HP 5890 Series II gas chromatography equipped with a flame ionization detector (GC-FID) and a HP Innowax column (30 m × 0.25 mm × 0.25mm). The GC-FID was operated with the method of inlet temperature 240 °C, detector temperature 250 °C, initial oven temperature of 45 °C for 2.5 minutes followed by a ramp of 10 °C/min for 21 minutes and then held at 230 °C for 4 minutes. One microliter of each sample was injected on the GC-FID in triplicate.

3.2.7 Catalytic Reactions

Catalytic esterification of 2-hydroxyisobutyric acid was performed in 75 mL autoclave batch reactors (Parr Series 5000 Multiple Reactor System). A working volume of 20 mL (40 ± 2 g L^{-1} 2-HIBA in ethanol) and catalyst was mixed using a magnetic stir bar (725 rpm). Details on reaction conditions can be found in the supporting information. All experiments were performed

in duplicate. Scheme 1 shows the main reaction and possible byproducts, diethyl ether and ethylene. Esterification reaction rates (mmolg-cat^{-1}h^{-1}), 2-HIBA conversion (mol converted/mol initial 2-HIBA), E-2HIBA yield (mol produced/mol initial 2-HIBA) and selectivity (mol produced/mol 2-HIBA remaining and E-2HIBA) were calculated using the batch data as previously reported.[7] The turnover frequency (TOF, min^{-1}) was estimated from the reaction rate (mmolg^{-1}min^{-1}) and acid site density (mmolg^{-1}). In calculating the reaction rates and TOF, the heat-up time (15 min) was included in the contact time (Table 3.1).

3.2.8 Statistical Analysis

All 2-HIBA esterification reactions were performed in duplicate, while ICP-OES and GC-FID analyses were performed in triplicate and reported as the mean and sample standard deviation. Sample standard deviation was calculated from the range (R) for small sample size (n) for reaction rate, TOF, yield, and conversion (for $n \leq 5$, R/d_2, where d_2=1.128).[26] In the analysis between two means for the TOF, E-2HIBA yield and 2-HIBA conversion, a student t-test was performed, assuming the null hypothesis, and the level of significance (α) is reported.

3.3 Results and Discussion

In the following sections, catalyst characterization is correlated with structural and physical properties, and catalytic activity. 2-HIBA batch esterification results are compared between the untreated base materials, and the hydrothermal and plasma sulfonated carbons. Catalyst reusability as well as reaction studies are also analyzed.

3.3.1 Catalyst Structure

Untreated GAC and cACM had surface areas of 1490 and 598 m^2/g, respectively, with limited reduction in surface area for plasma treatment and dilute H_2SO_4 impregnation (Table 3.1). Like previous work, a surface area reduction of 31.9% in GAC-HT-2M and 69.6% in the GAC-HT-18M was observed, due to sulfonation and oxidation reactions on the carbon catalysts.[15, 27-29] Plasma sulfonation of GAC caused a small decrease (7.0%) in surface area, providing a larger surface area for catalytic reactions, indicating plasma treatment did not significantly affect the bulk structure. A lower reduction in surface area for ACM versus GAC was observed (8% for HT). Plasma treatment of ACM did generate larger surface area reduction than GAC (~23%), potentially due to its open structure and better plasma exposure. Amberlyst-15 has a much lower surface area (38 m^2/g) and limited porosity.[30]

Elemental mapping by STEM-EDS revealed base-GAC had a phosphorus (P) content of 1.5%, indicating chemical activation by phosphoric acid (Figure S3.2, Table 3.1).[31] Phosphate sites were also displayed on the hydrothermally sulfonated GAC catalysts (GAC-HT-18M and GAC-HT-2M) (Figures 3.2 and 3.3). EDS analysis indicated a sulfur (S) content of 0.3% and 1% on the GAC-HT-2M and the GAC-HT-18M respectively, uniformly distributed on the catalyst surface. The P content decreased to 1.3% and 0.5% in GAC-HT-2M and GAC-HT-18M respectively. STEM images of base-cACM (Figure S3.3) indicate a porous network, with silica and aluminum surrounding the carbon, attributed to the ceramic binder used to manufacture the ACM. A sulfur content of 0.4% was detected on the cACM-HT-2M (Figure 3.4), evenly distributed on the catalyst surface. EDS analysis of GAC-PT-Ar/H_2O-15min and cACM-PT-Ar/H_2O-10min could not detect any sulfur, indicating its concentration was below the detection limit of the EDS (< 0.1%).

ICP-OES analysis was performed to quantify sulfur and sulfonic acid densities were estimated assuming all S corresponded to -SO_3H groups (Table 3.1). The Base-GAC and cACM did not contain any S/-SO_3H acid groups prior to sulfonation. Sulfonic acid densities of 0.16 mmol/g and 0.09 mmol/g were obtained for GAC-HT-18M and GAC-HT-2M respectively, which indicate the incipient wetness impregnation method results in lower acid densities compared to traditional methods. An H_3PO_4-activated carbon sulfonated with concentrated H_2SO_4 (15 mL/g catalyst) under reflux generated a sulfonic acid density of 0.24 mmol/g (92 °C, 7 h).[32] Carbon refluxed in 6 M H_2SO_4 generated an -SO_3H density lower than 0.1 mmol/g, similar to our results.[33] Hydrothermal sulfonation of ACM (cACM-HT-2M) resulted in a sulfonic acid density of 0.12 mmol/g, again similar to the literature.[29] The sulfur content of the plasma sulfonated GAC (GAC-PT-Ar/H_2O-15min) and cACM (cACM-PT-Ar/H_2O-10min) were found to be 0.02% and 0.05% respectively, corresponding to sulfonic acid densities below 0.1 mmol/g.

FTIR spectra indicated a peak at 1047 - 1049 cm^{-1} and a broad band between 1254 and 1174 cm^{-1} in all the GAC catalysts (Figures S3.5 and S3.6, Table S3.1). The band between 1000 and 1300 cm^{-1} is characteristic of phosphorylated carbons and attributed to stretching vibrations of hydrogen bonded P=O, O-C stretching in P-O-C linkage, and to P=OOH.[31, 34] The hydrothermal (cACM-HT-2M) and plasma treated ACM (cACM-PT-Ar/H_2O-10min) show a distinct peak at 1059 cm^{-1} attributed to S=O stretching vibrations of -SO_3H groups; O=S stretching at 1042 cm^{-1} is reported in a sulfonated graphene oxide monolith.[35] Peaks at 1030 and 1210 cm^{-1} are attributed to symmetric and asymmetric stretching vibrations of the SO_3^{-1} group respectively.[36] The peak at 1188 cm^{-1} has also been assigned to S=O symmetric stretching vibration and the peaks at 1036 cm^{-1} assigned to S=O and SO_3^{2-} stretching vibrations respectively.[37,38]

Since -SO_3H signatures, especially in the sulfonated GAC catalysts, were not clear, XPS analysis was performed (Figures 3.5, 3.6, Table S3.2). Prominent peaks for oxygen and carbon, and weak peaks for sulfur were observed at binding energies of 284.5, 532 and 168 eV respectively in all treated catalysts.[38] The C1s peak at 284.5 eV corresponds to polycyclic aromatics (C=C), and the peaks at 285.2 eV and 286.0 eV can be assigned to aliphatic hydrocarbons (C-C) and C-O-C respectively. Peaks for carbonyl C=O and carboxyl O-C=O groups appear at 287.2 eV and 288.7 eV respectively. The peak at 532.9 eV is assigned to O-H, C=O at 531.7 eV and bridging C-O-C at 533.7 eV.[37] The sulfur peaks at 164.0 eV and 165.2 eV corresponds to S $2p_{3/2}$ and S $2p_{1/2}$ of thiophenic sulfur respectively (-C-S-C-) and the peak at 168.0 eV can be assigned to the SO_3H group. These sulfur peaks have also been observed in XPS analyses of sulfonated carbon materials.[38] The two peaks for sulfur were prominent in the hydrothermal and plasma sulfonated GAC catalysts (relative to Base-GAC) and Amberlyst-15 but were not as evident in the ACM catalysts (Figure S3.5). Additionally, the base GAC had one broad P 2p peak at 133 eV. Two peaks at 132.7 eV and 134.8 eV, were apparent in the hydrothermal and plasma sulfonated GAC catalysts and can be assigned to P-O-C and P-O (phosphate).[39]

Argon-water vapor plasma has been shown to alter C 1s binding energy in carbon materials. It is reported that a small decrease in the C 1s peak at 285.0 eV, and increase in the peaks at 286.5, 287.7 and 289.1 eV, indicate a decrease in concentration of C-C/C-H bonds and increase in oxygen containing groups (C-O, C=O, O-C-O and O-C=O) with increasing water vapor concentration.[40] It is theorized that argon-water vapor plasma promotes surface hydrogen abstraction by OH radicals and O atoms.[40] We observed similar results with our Ar/H_2O vapor treated GAC and ACM catalysts. With GAC-PT-Ar/H_2O-15min, we noted a clear shift in the C 1s peak at 284 eV (C=C) to 285 eV (oxygenated carbon). This shift was prominently noted in the

GAC-HT-2M and GAC-HT-18M catalysts (Figure 3.5). The cACM-PT-Ar/H_2O-10 min catalyst had a shoulder at 285 eV indicative of partial surface oxidation and incorporation of oxygen groups, compared to the cACM-HT-2M which had a prominent peak at 285 eV (Figure 3.6).

3.3.2 Catalytic Esterification

Esterification studies were performed to compare the catalytic performance of the plasma and hydrothermally sulfonated carbons (GAC and ACM) with Amberlyst-15 (150 °C, 1 h, 1 g of catalyst). Reaction conditions were chosen based on preliminary experiments at conditions ranging from 100-150 °C, 0.5-3 h, and catalyst loadings of 0.25 and 1 g, and with both 1 and 2 M H_2SO_4 treated GAC (plasma and hydrothermal). Preliminary esterification reactions indicated higher conversions with 2 M H_2SO_4 treated carbons, and these catalysts were selected for further studies (data not shown) at 40 g/L of 2-HIBA in excess ethanol (~44:1 ethanol to 2-HIBA molar ratio).

In the absence of catalyst, E-2HIBA yield and 2-HIBA conversion were 6.2% and 17.4% respectively, indicating that at 150 °C heat alone can drive the reaction (Figure 3.7). With both base GAC and cACM, the E-2HIBA yields were about 10%, while the 2-HIBA conversions were 20.5% and 16.5% respectively. Weak acid sites (-COOH) and -PO_4 sites in GAC may have contributed to esterification activity and a larger catalyst surface area may have generated higher conversion with the Base-GAC. The hydrothermally sulfonated ACM (cACM-HT-2M) displayed the maximum ester yield of 68.5% among all catalysts, and a 2-HIBA conversion of 81.5% in comparison to an E-2HIBA yield of 64.7% (α = 0.05-0.1) and 2-HIBA conversion of 80% with Amberlyst-15. These results suggest wet impregnation with dilute H_2SO_4 coupled with sonication and thermal activation can generate solid acid carbon monolith catalysts. Our results

compare with a report using graphene oxide (the hazardous and potentially explosive Hummer's method is typically used to synthesize graphene).[41] Esterification of levulinic acid with benzyl alcohol using a sulfonated graphene oxide monolith generated a conversion of 97% at 110 °C and 90 min. [35]

The two hydrothermally treated GAC catalysts, GAC-HT-18M and GAC-HT-2M, gave similar ester yields of 63.7% and 64.7%, with 2-HIBA conversions of 87% and 71% respectively. These results indicate that the catalytic performance of the GAC-HT-2M and cACM-HT-2M was similar to Amberlyst-15 (150 °C, 1 h) and reports in the literature. Esterification of glycerol with acetic acid using a sulfonated carbon generated a maximum glycerol conversion of 80% at 150 °C after 5 h.[33]

Among the 3% H_2/Ar plasma treated GAC catalysts, a maximum E-2HIBA yield of 18.5% was observed at the 10 min treatment time, (2-HIBA conversion was 25.1%), although varying the plasma treatment duration did not significantly impact the ester yield. With the Ar/H_2O vapor treated GAC catalysts, the E-2HIBA yield increased from 18.6% to 23.2% on increasing the exposure time to 15 min. (2-HIBA conversion and E-2HIBA selectivity were 35.3% and 26.8% respectively). Of the 3% H_2/Ar treated ACM catalysts, a maximum E-2HIBA yield of 19.3% and selectivity of 20.2% were obtained at the 10 min treatment time (2-HIBA conversion was 23.5%). Although prolonged plasma exposure (15 min) led to an increase in 2-HIBA conversion, a decrease in E-2HIBA yield and selectivity were observed, with byproduct formation. With the Ar/H_2O vapor plasma, at the 10 min treatment time, a maximum 2-HIBA conversion, E-2HIBA yield and selectivity of 34.5%, 22.6%, and 25.6% respectively, were obtained.

For all sulfonated ACM catalysts, with both plasma treatments, an increase in E-2HIBA yield and selectivity, as well as 2-HIBA conversion were observed on increasing the plasma duration from 5 to 10 min. Similar results were obtained with the sulfonated GAC catalysts, although the difference was more evident on increasing the exposure time to 15 min. It has been found that nonhomogeneous plasma modification is likely for shorter treatment durations or low ion doses, as the ion dose may not be uniform on the catalyst surface.[42] Increasing the plasma exposure time to 10 and 15 min were found to be optimal for the ACM and GAC catalysts, respectively. Increasing the treatment time to 15 min for the sulfonated ACM catalysts, resulted in a decrease in ester yield, selectivity, and substrate conversion, which could be attributed to byproduct formation.

Similar E-2HIBA yields and 2-HIBA conversions were obtained with both the GAC and ACM using Ar/H_2O vapor as carrier gas, at different treatment times of 15 and 10 min, respectively. The monolith core was treated intact during the plasma exposure and crushed prior to the catalytic reactions, which could be the reason for the shorter exposure time requirement. Since the monolith is a uniform block (2.54 × 2.54 cm) with open channels, it may have experienced better catalyst-gas-plasma interaction in comparison to the GAC during the plasma treatment.[43] Since the GAC-PT-Ar/H_2O-15min and cACM-PT-Ar/H_2O-10min were the most catalytically active plasma sulfonated catalysts, reaction analysis and catalyst reuse studies were performed with these catalysts and the hydrothermal GAC and ACM catalysts (GAC-HT-18M, GAC-HT-2M, cACM-HT-2M).

3.3.3 Catalyst Reuse

Catalyst reuse studies were carried out for 4 cycles (5 h, Figure 3.8). Both GAC-HT-18M and Amberlyst-15 retained 100% of their catalytic activity, and an increase in E-2HIBA yield from the first to fourth spent run was noted. Analysis of the carbon balance resulted in over 100% carbon recovery, indicating carry over from the previous spent run. This could be because the catalysts were recovered and reused as is, without washing, causing any ester bound to the catalyst to leach out in the subsequent run. The GAC-HT-2M retained 85% of its catalytic activity with a 35.6% loss in ester yield (41.6 vs 64.6 g/L). However, cACM-HT-2M depicted a decrease in catalytic activity with 2-HIBA conversion decreasing from 81.5% to 24.5% in the fourth spent run (~70% decrease). To understand the loss in catalytic activity, we performed STEM-EDS on the spent (4^{th} run) hydrothermal GAC and cACM catalysts. EDS analysis of the spent GAC-HT-2M indicated stability of SO_3H groups in the hydrothermal GAC catalysts as the sulfur content remained constant at 0.3%. However, a decrease in sulfur content from 0.4% to 0.2% was observed in the cACM-HT-2M, confirming loss of SO_3H groups and reduction in activity (Figure S3.4). Similar results were observed using a hydrothermally synthesized sulfonated carbonaceous monolith in the acetalization of benzaldehyde.[44] In this work a significant loss in catalytic activity with each reaction cycle was reported, and one carbon catalyst only retained 31% of its initial catalytic activity (conversion decreased from 87.1% with the fresh catalyst to 27.3% in the fourth spent run).[44] ICP-OES analysis on the spent catalysts confirmed that catalyst deactivation was due to sulfur leaching.[47] Plasma sulfonated GAC (GAC-PT-Ar/H_2O-15min) retained 75% of its catalytic activity, and 81.8% of the E-2HIBA yield obtained with the fresh catalyst, similar to previous work with in-solution (1 M H_2SO_4) plasma sulfonated carbon black (98% catalytic activity after 3 spent cycles).[14] The surface area of this

catalyst was much lower (40 m^2/g)[14] in comparison to our plasma sulfonated GAC, GAC-PT-Ar/H_2O-15min (1385 m^2/g). Our results indicate that the plasma process imparted good stability and reusability to the GAC, and since the catalyst has a high surface area, its performance can be enhanced by modifying the plasma parameters, to obtain higher acid site densities. Similar to the hydrothermal cACM catalyst, the plasma sulfonated cACM also showed a decline in catalytic activity, with a 59.3% and 30.4% decrease in E-2HIBA yield and 2-HIBA conversion respectively. Despite the lower ester yield and 2-HIBA conversion, the plasma sulfonated cACM performed better in comparison to the hydrothermally sulfonated ACM in terms of catalyst stability, indicating stability conferred by the plasma. The sulfonated GAC catalysts also displayed greater catalyst stability in comparison to the monolithic catalysts, which may be attributed to phosphoric acid chemical activation of the carbon. Phosphorylated activated carbon fiber catalysts are reportedly thermally stable for 12 h at 350 °C in air.[45] Catalytic esterification of oleic acid with methanol has recently been reported using phosphorylated carbon.[1] The thermally stable -PO_4 groups noted in the GAC catalysts may have promoted adsorption of 2-HIBA and synergistically enhanced esterification at the -SO_3 sites.

3.3.4 Reaction Studies

From the catalyst reuse studies, four sulfonated carbon catalysts including the GAC-HT-18M, GAC-HT-2M, GAC-PT-Ar/H_2O-15min and Amberlyst-15 were found to be the most stable, retaining over 80% catalytic activity. Additional reaction studies were performed with these catalysts to determine the effect of temperature (100, 120, 150 °C) and residence time (0.5, 1, 3 h) on E-2HIBA yield and 2-HIBA conversion (Figures 3.9 and 3.10). Some product was formed at time zero, with the GAC-HT-18M and Amberlyst-15 displaying an increase in 2-HIBA conversion from 23.5% to 56.6%, and 33.1% to 65.7% on increasing the temperature from 100

°C to 150 °C. The 2-HIBA conversions for the GAC-HT-2M and GAC-PT-Ar/H_2O-15min at time zero were less than 10% (reported conversions are after the time required to reach operating temperature, 15 min).

With all the four catalysts, increasing both the temperature and residence time increased 2-HIBA conversion and E-2HIBA yield, indicating 2-HIBA reaction rates were lower at 100 °C and increased with temperature up to 150 °C. With both GAC-HT-18M (Figure 3.9) and Amberlyst-15 (Figure 3.10), maximum E-2HIBA yields of 64-65% were obtained at 120 °C and 1 h residence time. Increasing the temperature to 150 °C, led to an increase in the 2-HIBA conversion and E-2HIBA selectivity (87% and 83% with GAC-HT-18M and 82.6% and 78.8% with Amberlyst-15). However, increasing the residence time to 3 h at 150 °C did not affect the ester yield or 2-HIBA conversion. Similar results have been reported for the esterification of oleic acid and methanol using a sulfonated carbon catalyst (oleic acid conversion of 97.9% at 1.5 h, and > 2.5 h did not significantly affect conversion). [46]

With GAC-HT-2M, a maximum E-2HIBA yield of 64.7% was obtained at 150 °C and 1 h reaction time (2-HIBA conversion and E-2HIBA selectivity were 71% and 68.8%, (Figure 3.9)). The 2-HIBA conversion and E-2HIBA selectivity increased to 81% and 76.4% respectively, after 3 h (E-2HIBA yield was 61.7%). These results indicate that the GAC-HT-18M and Amberlyst-15 attained equilibrium around 120 °C, while the GAC-HT-2M attained equilibrium at 150 °C, at approximately 1 h of reaction time. Similar results were observed with a carbon catalyst synthesized using concentrated sulfuric acid under reflux (150 °C, glycerol conversion of 76% after 5 h). [36]

For all reactions, the carbon recovery was above 90%. About 5-10% of the recovered carbon in terms of percent peak area were two unknowns (retention times of 1.76 min and 7.1 min). As reaction temperature increased and time progressed, the peak at 1.76 min increased, particularly with the hydrothermal GAC catalysts and Amberlyst-15. Sulfonated and phosphorylated carbons can catalytically dehydrate ethanol forming diethyl ether and ethylene, suggesting these compounds as possible byproducts.[47] The increase in 2-HIBA conversion with the GAC-HT-18M and Amberlyst-15 on increasing the temperature from 120 °C to 150 °C (1 h of residence time), and with the GAC-HT-2M on increasing the residence time to 3 h at 150 °C, did not affect the ester yield, yet led to an increase in the formation of byproducts. We therefore concluded that reaction temperatures of 120 °C for the GAC-HT-18M and Amberlyst-15, and 150° C for the GAC-HT-2M at 1 h of residence time were optimal for 2-HIBA esterification. With the GAC-PT-Ar/H_2O-15min, the ester yield and hydroxyacid conversion increased with both temperature and residence time, and a maximum E-2HIBA yield of 39.3% and 2-HIBA conversion of 48.3% were observed at reaction conditions of 150 °C and 3 h (E-2HIBA selectivity 43.2%). The slower esterification rate with the plasma sulfonated GAC catalyst can be attributed to the low sulfonic acid site density. Low sulfonic acid site density on the catalyst may indicate lower availability of H^+ ions in the solution, resulting in a decrease in both 2-HIBA conversion and esterification rate.[48]

Although the plasma treated carbons had lower reaction rates on a per mass basis (mmol/g-cat/min), TOF based on strong acid sites (-SO_3H) was significantly higher (Table 3.1). For example, the TOF for GAC-PT-Ar/H_2O-15min was 86-150 × higher than Amberlyst-15 (α = 0.02-0.05) and 6-10 × higher than GAC-HT-18M (α = 0.02-0.05). Notably, the TOFs for the GAC-HT-2M/18M and cACM-HT-2M are significantly larger than Amberlyst-15 (Table 3.1, α =

0.001). There are two possible reasons; many of the Amberlyst-15 acid sites may not be accessible and its non-polar surface may inhibit 2-HIBA adsorption. The low surface area of Amberlyst-15 limits access to acid sites and the polar nature (-COOH, -C=O, -OH, -PO_4 sites) on the treated GAC and ACM probably promoted 2-HIBA adsorption, relative to Amberlyst-15. Similar results have been observed in the esterification of oleic acid.[49] Mesoporous carbons grafted with benzenesulfonic acid had TOF's 5-7 × greater than that of Amberlyst-15, yet lower strong acid density. These carbons also had greater total acid site densities than strong acid densities, suggesting additional weak acid sites on the carbon (e.g., -COOH). The increased TOF was due to better dispersion of carbons in methanol via the weak acid sites, and limited oleic acid access in Amberlyst-15 due to a poor swelling network.[49]

3.4 Conclusions

Sustainable routes for granular (GAC) and carbon monolith sulfonation have been developed using the incipient wetness method and sonication with hydrothermal or plasma activation. Significantly lower activating agent to catalyst mass ratios were used to synthesize the materials, yet activity and stability were similar to a commercial catalyst (Amberlyst-15) derived from petroleum resources. For example, 0.62 to 1.75 mL/g was used in this work compared to 7-50 mL/g in the literature [8-10] and TOF's greater than Amberlyst-15. If all activating agent ends up as waste, an *E*-factor (kg waste/kg product) 11-46 × lower than the literature is estimated (e.g., E = 2 for GAC-HT-2M vs E = 91.5).[9] Although the plasma treatments generated lower acid site density and esterification reaction rates (mmol/g-cat/min), the plasma method was validated for synthesis of acid functionalized carbon monoliths. Further improvements in the plasma technique could generate an optimum ratio of strong and weak acid sites which can be scaled more easily

to larger sized monoliths, pellets, or granules. The carbon catalysts were also stable; GAC-HT-18M retained 98.9% catalytic activity, comparable to Amberlyst-15 and GAC-HT-2M retained over 85% of its catalytic activity after 4 runs. However, both the sulfonated ACM catalysts showed a decline in E-2HIBA yield and catalytic activity. Since ACM was crushed to use in the agitated batch reactions, attrition (loss of carbon support with $C\text{-}SO_3\text{-}H^+$ sites) may have contributed to the activity decline; future testing in monolith form is required to confirm this theory. Further plasma optimization, by increasing power and H_2 concentration may generate higher $\text{-}C\text{-}SO_3^-H^+$ densities and results comparable to the hydrothermal treatment. This work provides two sustainable sulfonation methods, both hydrothermal and plasma, for the synthesis of sulfonated carbon catalysts, which may have widespread applications in the synthesis of various esters from biobased organic acids. The acid carbon monolith could provide a more efficient and sustainable platform for continuous esterification processes in fine and specialty chemical industries.

Associated Content

Supporting Information

The following results are presented, 1) Apparatus for plasma treatment, 2) methods for batch reactions, FTIR and XPS analyses, comparison of plasma treatments, 3) STEM-EDS for Base GAC (untreated), 4) STEM-EDS for Base cACM (untreated activated carbon monolith), 5) EDS images for fresh and spent GAC and cACM catalysts, 6) FTIR peak assignments, 7) XPS peak assignments, 8) FTIR figures, 9) plot of TOF versus carbon catalyst and strong acid site density.

Acknowledgements

Support for this research was provided by the USDA-NIFA Grant (Carbon Monolith Catalysts from Wood for Biobased Platform Chemicals: 2017-67021-26136). The authors thank Myranda Jackson, Applied Catalysts, for her contribution in performing the BET surface area analysis, and Dr. Kun Yao and Seyedehsan Vasefi for assistance with the plasma work. The XPS analysis was performed at the Georgia Tech Institute for Electronics and Nanotechnology or Joint School of Nanoscience and Nanotechnology, a member of the National Nanotechnology Coordinated Infrastructure (NNCI), which is supported by the National Science Foundation (Grant ECCS-1542174).

References

1) C. Wang, X. Gui, Z. Yun, Esterification of lauric and oleic acids with methanol over oxidized and sulfonated activated carbon catalyst, Reac. Kinet. Mech. Cat., 113 (2014) 211-223.

2) P. Sudarsanam, R. Zhong, S.V. den Bosch, S.M. Coman, V.I. Parvulescu, B.F. Sels, Functionalized heterogeneous catalysts for sustainable biomass valorization. Chem. Soc. Rev., 47 (2018) 8349-8402.

3) A. Kokel, C. Schäfer, B. Török, Organic Synthesis Using Environmentally Benign Acid Catalysis. Curr. Org. Synth., 16 (2019) 615-649.

4) W-Y. Lou, Q. Guo, W-J. Chen, M-H. Zong, H. Wu, T.J. Smith, A highly active bagasse-derived solid acid catalyst with properties suitable for production of biodiesel. ChemSusChem., 5 (2012)1533-1541.

5) P.F Siril, H.E. Cross, D.R. Brown, New polystyrene sulfonic acid resin catalysts with enhanced acidic and catalytic properties. J. Mol. Catal. A- Chem., 279 (2008) 63-68.

6) L.J. Konwar, P. Maki-Arvela, J-P. Mikkola, SO_3H- containing functional carbon materials: Synthesis, structure, and acid catalysis, Chem. Rev., 119 (2019) 11576-11630.

7) J.R. Kastner, J. Miller, D.P. Geller, J. Locklin, L.H. Keith, T. Johnson, Catalytic esterification of fatty acids using solid acid catalysts generated from biochar and activated carbon, Catal., 190 (2012) 122-132.

8) J.M. Fraile, E. García-Bordejé, L. Roldán, Deactivation of sulfonated hydrothermal carbons in the presence of alcohols: Evidences for sulfonic esters formation, J. Catal. 289 (2012) 73-79.

9) S. Adhikari, Z. Hood, N. Gallego, C. Contescu, Lignin-derived carbon fibers as efficient heterogeneous solid acid catalysts for esterification of oleic acid. MRS Adv. 3 (2018) 2865-2873.

10) C.C. Chong, Y.W. Cheng, M.K. Lam, H.D. Setiabudi, D-V. N. Vo, Stae-of-the-art of the synthesis and applications of sulfonated carbon-based catalysts for biodiesel production: a review, Energy Technol., 9 (2021) 2100303.

11) J. Pang, A. Wang, M. Zheng, T. Zhang, Hydrolysis of cellulose into glucose over carbons sulfonated at elevated temperatures. Chem. Comm. 46 (2010) 6935-6937.

12) Y. Miao, Y. Ma, Q. Wang, Plasma-assisted simultaneous reduction and nitrogen/sulfur codoping of graphene oxide for high-performance supercapacitors. ACS Sustainable Chem. Eng. 7 (2019) 7597-7608.

13) Z. Wang, Y. Zhang, E.C Neyts, X. Cao, X. Zhang, B. W.-L. Jang, C-j Liu, Catalyst preparation with plasmas: How does it work? ACS Catal., 8 (2018) 2093-2110.

14) O. L. Li, R. Ikura, T. Ishizaki, Hydrolysis of cellulose to glucose over carbon catalysts sulfonated *via* a plasma process in dilute acids. Green Chem. 19 (2017) 4774-4777.

15) L. Qin, N. Takeuchi, K. Takahashi, J. Kang, K.H. Kim, O.L. Li, N_2/Ar plasma-induced surface sulfonation on graphene nanoplatelets for catalytic hydrolysis of cellulose to glucose. Appl. Surf. Sci. 545 (2021) 149051.

16) S. Horikoshi, N. Serpone, In-liquid plasma: a novel tool in the fabrication of nanomaterials and in the treatment of wastewaters, RSC Adv., 7 (2017) 47196.

17) M. Pirmoradi, N. Janulaitis, R.J. Gulotty, Jr., J.R. Kastner, Bi-Metal-Supported Activated Carbon Monolith Catalysts for Selective Hydrogenation of Furfural, Ind. Eng. Chem. Res., 59 (2020) 17748-17761.

18) A. Sachse, A. Galarneau, B. Coq, F. Fajula, Monolithic flow microreactors improve fine chemical synthesis, New J. Chem., 35 (2011) 259-264.

19) T.C. Bhalla, V. Kumar, S.K. Bhatia, Hydroxy acids: Production and applications. In Advances in Industrial Biotechnology; R.S. Singh, A. Pandey, C. Larroche, (Eds.), IK International Publishing House PVT. Ltd.: New Delhi, India, 2014; pp. 56–76.

20) G.K. Weakley, Kelly, C.E. Method for Producing An Alkyl 3-Hydroxybutyrate, Patent Application. US 2015/0038734 A1, Feb. 5, 2015.

21) V. Trombettoni, D. Sciosci, M.P. Bracciale, F. Campana, M.L. Santarelli, A. Marrocchi, L. Vaccaro, Boosting biomass valorisation. Synergistic design of continuous flow reactors and water-tolerant polystyrene acid catalysts for a non-stop production of esters, Green Chem., 20 (2018) 3222.

22) T. Rohwerder, R. H. Müller, Biosynthesis of 2-hydroxyisobutyric acid (2-HIBA) from renewable carbon, Microb. Cell Factories, 9 (2010) 13.

23) M. Nobuyuki, A. Takafumi, H. Hirofumi, Process for Producing Methyl α-Hydroxyisobutyrate. Patent Application. US005391813A, Oct 12, 1993.

24) Ethyl 2-hydroxyisobutyrate, ChemicalBook,

https://www.chemicalbook.com/ChemicalProductProperty_EN_CB8376602.htm, 2017 (accessed November 2021).

25) M-T. Rohde, S.Tischer, H. Harms, T. Rohwerder, Production of 2-hydroxyisobutyric acid from methanol by *Methylobacterium extorquens* AM1 expressing (R)-3- hydroxybutyryl coenzyme A-isomerizing enzymes. Appl. Environ. Microbiol. 83 (2016) 1-16.

26) I. Miller, J.E. Freund, Probability and statistics for engineers, Prentice-Hall, Inc.: Englewood Cliffs, NJ, 1985.

27) Z.D. Hood, S.P. Adhikari, S.F. Evans, H. Wang, Y. Li, A.K. Naskar, M. Chi, A. Lachgar, M.P. Paranthaman, Tire-derived carbon for catalytic preparation of biofuels from feedstocks, Carbon Resour. Convers., 1 (2018) 165-173.

28) X. Wang, R. Liu, M.M. Waje, Z. Chen, Y. Yan, K.N. Bozhilov, P. Feng, Sulfonated ordered mesoporous carbon as a stable and highly active protonic acid catalyst, Chem. Mater., 19 (2007) 2395-2397.

29) F. Liguori, P. Barbaro, B. Said, A. Galarneau, V. Dal Santo, E. Passaglia, A. Feis, Unconventional Pd@sulfonated silica monoliths catalysts for selective partial hydrogenation reactions under continuous flow, ChemCatChem. 9 (2017) 3245-3258.

30) R. Ormsby, J.R. Kastner, J. Miller, Hemicellulose hydrolysis using solid acid catalysts generated from biochar, Catal.190 (2012) 89– 97.

31) S.M. Yakout, G.S. El-Deen, Characterization of activated carbon prepared by phosphoric acid activation of olive stones, Arab. J. Chem. 9 (2016) S1155-S1162.

32) W. Mateo, H. Lei, E. Villota, M. Qian, Y. Zhao, E. Huo, Q. Zhang, X. Lin, C. Wang, Z. Huang, Synthesis and characterization of sulfonated activated carbon as a catalyst for bio-jet fuel production from biomass and waste plastics, Bioresour Technol., 297(2020) 122411.

33) T.S. Galhardo, N. Simone, M. Goncalves, F.C.A. Figueiredo, D. Mandelli, W.A. Carvalho, Preparation of Sulfonated Carbons from Rice Husk and Their Application in Catalytic Conversion of Glycerol, ACS Sustainable Chem. Eng., 1 (2013) 1381-1389.

34) A.M. Puziy, O.I. Poddubnaya, A. Martínez-Alonso, F. Suárez-García, J.M.D. Tascón, Characterization of synthetic carbons activated with phosphoric acid. Appl. Surf. Sci., 200 (2002) 196-202.

35) A. V. Nakhate, G. D. Yadav, Synthesis and Characterization of Sulfonated Carbon-Based Graphene Oxide Monolith by Solvothermal Carbonization for Esterification and Unsymmetrical Ether Formation, ACS Sustainable Chem. Eng., 4 (2016) 1963-1973.

36) H. Galindo, Y. Carvajal, S.L. Suib, Sulfonation of the surface of cordierite monoliths through a novel multi-step wet chemical process. Micropor. Mesopor. Mat., 135 (2010) 37-44.

37) X. Peng, S. Shen, C. Wang, T. Li, Y. Li, S. Yuan, X. Wen, Influence of relative proportions of cellulose and lignin on carbon-based solid acid for cellulose hydrolysis, Mol. Catal., 442 (2017) 133–139.

38) Z. Liu, Y. Qi, M. Gui, C. Feng, X. Wang, Y. Lei, Sulfonated carbon derived from the residue obtained after recovery of essential oil from the leaves of Cinnamomum longepaniculatum using Brønsted acid ionic liquid, and its use in the preparation of ellagic acid and gallic acid, RSC Adv., 9 (2019) 5142-5150.

39) H. Hou, L. Shao, Y. Zhang, G. Zou, J. Chen, X. Ji, Large- area carbon nanosheets doped with phosphorus: A high-performance anode material for sodium-ion batteries. Adv. Sci., 4 (2017) 1600243.

40) A.V. Deynse, N. De Geyter, C. Leys, R. Morent, Influence of water vapor addition on the surface modification of polyethylene in an Argon dielectric barrier discharge, Plasma Process. Polym., 11 (2014) 117-125.

41) L. Peng, Z. Xu, Z. Liu, Y. Wei, H. Sun, Z. Li, X. Zhao, C. Gao, An iron-based green approach to 1-h production of single-layer graphene oxide, Nat. Commun., 6 (2015) 5716.

42) V. Martirosyan, Atomistic simulations of H_2 and He plasmas modification of thin-films materials for advanced etch processes, 2017. Micro and nanotechnologies/Microelectronics. Université Grenoble Alpes, 2017. English. NNT: 2017GREAT101.

43) P. Hinde, V. Demidyuk, A. Gkelios, C. Tipton, Plasma catalysis: A review of the interdisciplinary challenges faced, Johnson Matthey Technol. Rev., 64 (2020) 138-147.

44) W. Zhang, H. Tao, B. Zhang, J. Ren, G. Lu, Y. Wang, One-pot synthesis of carbonaceous monolith with surface sulfonic groups and its carbonization/ activation, Carbon, 49 (2011) 1811-1820.

45) F.J. García-Mateos, R. Ruiz-Rosas, J.M. Rosas, J. Rodríguez-Mirasol, T. Cordero, Phosphorus containing carbon (submicron) fibers as efficient acid catalysts. Catal. Today, 383 (2020) 308-319.

46) A.P. da Luz Corrêa, R.R.C. Bastos, G.N. da Rocha Filho, J.R. Zamian, L.R.V. da Conceicão, Preparation of sulfonated carbon-based catalysts from murmuru kernel shell and their performance in the esterification reaction, RSC Adv., 10 (2020) 20245-20256.

47) E. Chaichana, W. Wiwatthanodom, B. Jongsomjit, Carbon-based catalyst from pyrolysis of waste tire for catalytic ethanol dehydration to ethylene and diethyl ether. Int.J. Chem.Eng. 2019, (2019) 1-10.

48) C.R. Khudsange, K.L. Wasewar, Process intensification of esterification reaction for the production of propyl butyrate by pervaporation, Resource-Efficient Technologies 3 (2017) 88-93.

49) L. Geng, Y. Wang, G. Yu, Y. Zhu, Efficient carbon-based solid acid catalysts for the esterification of oleic acid, Catal. Commun., 13 (2011) 26-30.

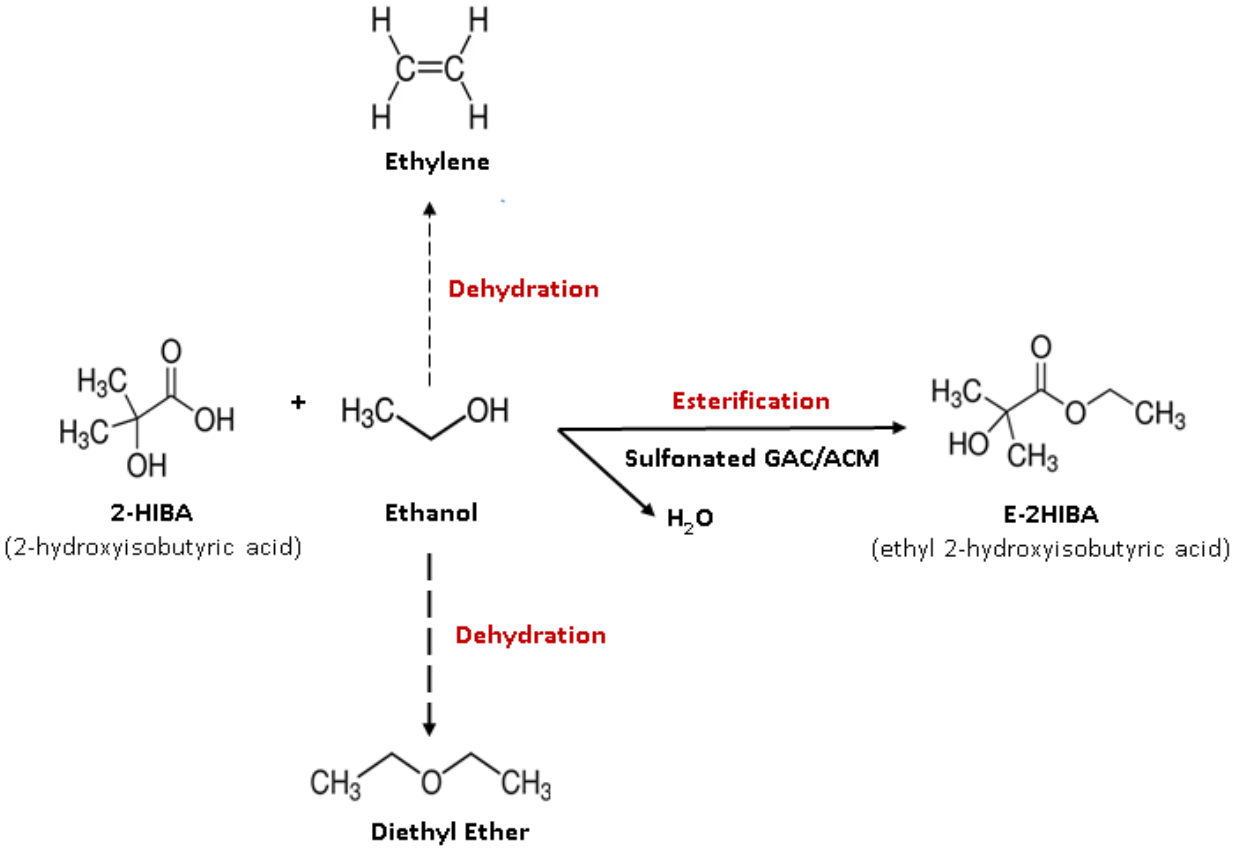

Scheme 1. Reaction scheme depicting the esterification of 2-hydroxyisobutyric acid (2-HIBA) to ethyl 2-hydroxyisobutyric acid (E-2HIBA) over a sulfonated GAC/ACM catalyst, and the possible formation of diethyl ether and ethylene as byproducts of ethanol.

Table 3.1. Physical and Kinetic Characteristics of the Sulfonated Carbons and Amberlyst-15.

Catalyst	Surface area (m^2/g)	Phosphorous (%)	SO_3H density[g] (mmol/g)	Reaction rate (0.25 h) (mmol/g/min)	TOF (0.25 h) (min^{-1})	TOF (0.75 h) (min^{-1})
Base-GAC	1490	1.5	_	_	_	_
GAC-HT-18M [a]	453	0.5	0.16 ± 0.00	0.33 ± 0.04	1.99 ± 0.23	0.93 ± 0.01
GAC-HT-2M [b]	1015	1.3	0.09 ± 0.03	0.09 ± 0.07	1.00 ± 0.80	1.28 ± 0.11
GAC-PT-Ar/ H_2O-15min [c]	1385	0.9	0.006 ± 0.001	0.07 ± 0.01	11.90 ± 2.90	9.24 ± 2.08
Base-cACM	598	0	_	_	_	_
cACM-HT-2M [d,e]	550	0.04	0.12 ± 0.00	0.09 ± 0.00[e]	_	0.73 ± 0.03[e]
cACM-PT-Ar/ H_2O-10min[f,e]	462	0.04	0.02 ± 0.00	0.03 ± 0.01[e]	_	2.02 ± 0.84[e]
Amberlyst-15	38	0.00	2.36 ± 0.45	0.33 ± 0.00	0.14 ± 0.00	0.06 ± 0.00

Reaction conditions: temperature 150 °C, residence time includes heat-up time, catalyst loading 1g, reaction volume 20 mL, and 2-HIBA concentration 40g/L.

Base-GAC and Base-cACM are the untreated GAC and cACM (crushed monolith).

Except where noted, the value in the parentheses for reaction rate and TOF are the contact times.

TOF, turnover frequency based on the 2-HIBA reaction rate and SO_3H density.

[a] GAC treated with 18M H_2SO_4 by incipient wetness impregnation, followed by hydrothermal treatment at 250 °C.

[b] GAC treated with 2M H_2SO_4 by incipient wetness impregnation, followed by hydrothermal treatment at 250 °C.

[c] GAC treated with 2M H_2SO_4 by incipient wetness impregnation, followed by plasma treatment with argon-H_2O vapor for 15 min.

[d] crushed ACM treated with 2M H_2SO_4 by sonication, followed by hydrothermal treatment at 250 °C.

[e], 1.25 h including heat-up time.

[f], crushed ACM treated with 2M H_2SO_4 by sonication, followed by plasma treatment with argon-H_2O vapor for 10 min.

[g], based on elemental analysis.

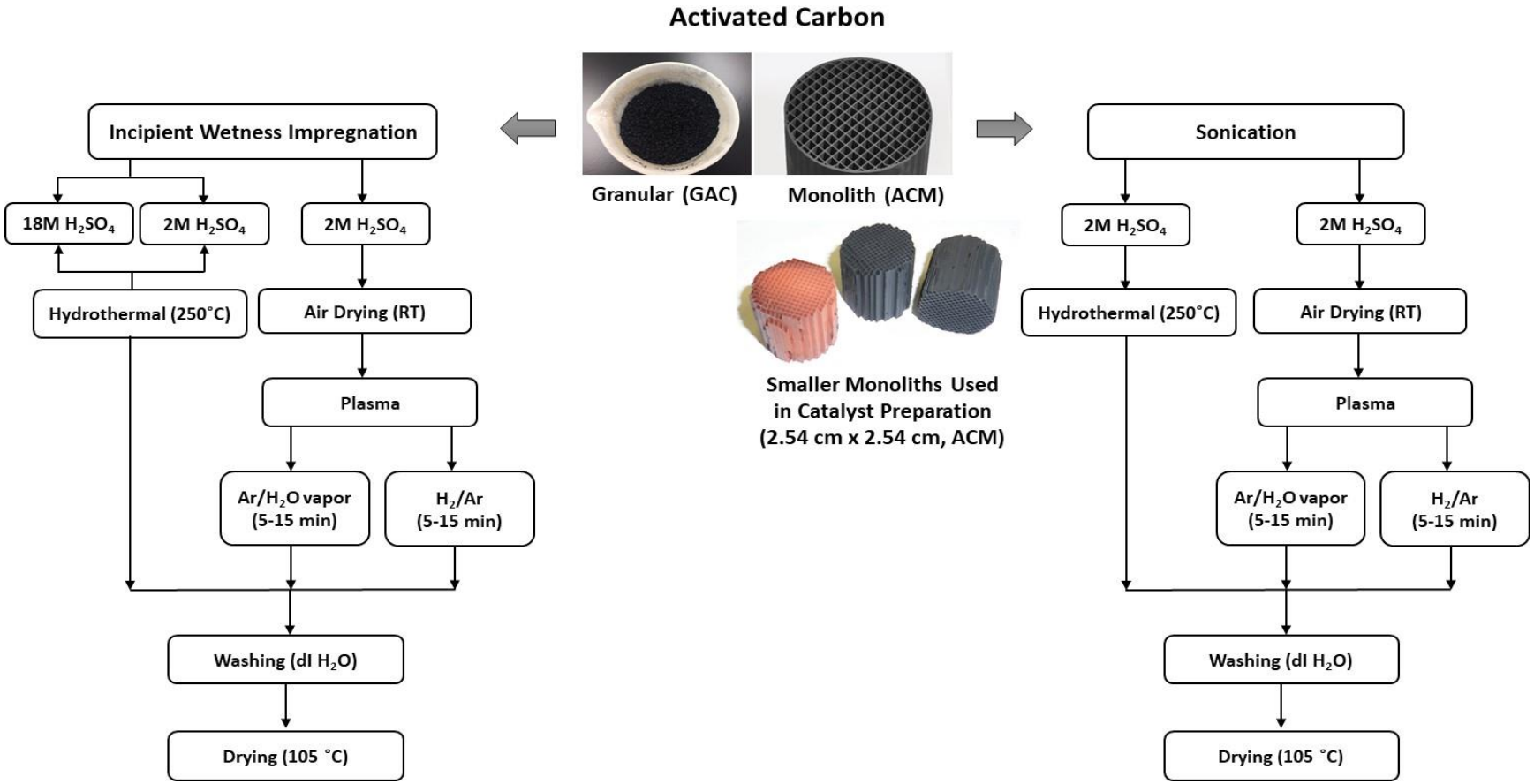

Figure 3.1. Schematic depicting the catalyst preparation methods of the hydrothermal and plasma sulfonated granular activated carbon (GAC) and activated carbon monolith (ACM: 2.54 × 2.54 cm cores) catalysts. (RT: room temperature, dI H_2O: deionized water). Iron oxide impregnated ACM (red to orange ACM) was not used but is shown to demonstrate ability to deposit active metal oxides. The larger monolith (5.1 cm diameter) was not used in the work and shown as example of monolith scale-up.

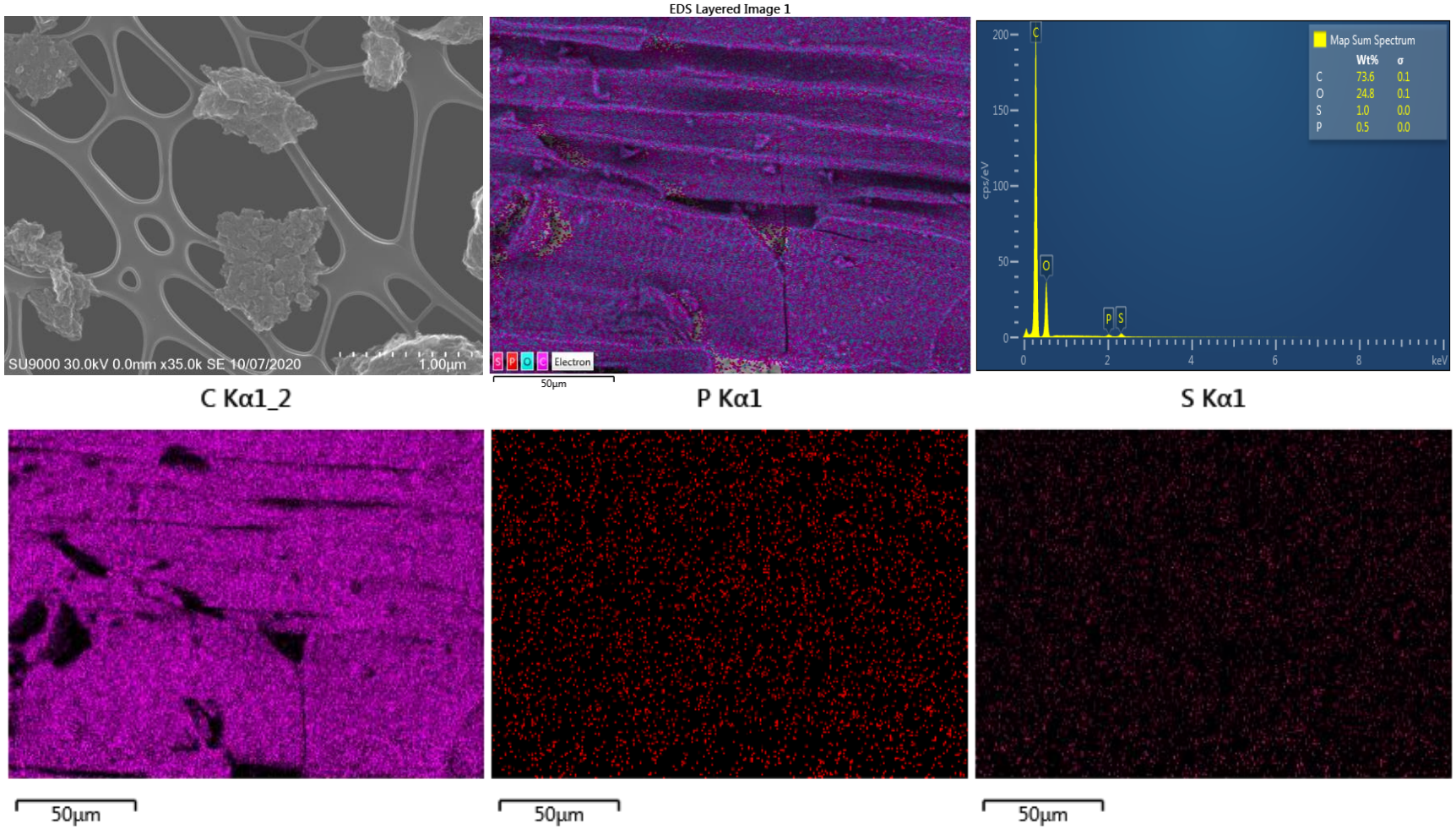

Figure 3.2. STEM-EDS images of GAC-HT-18M catalyst.

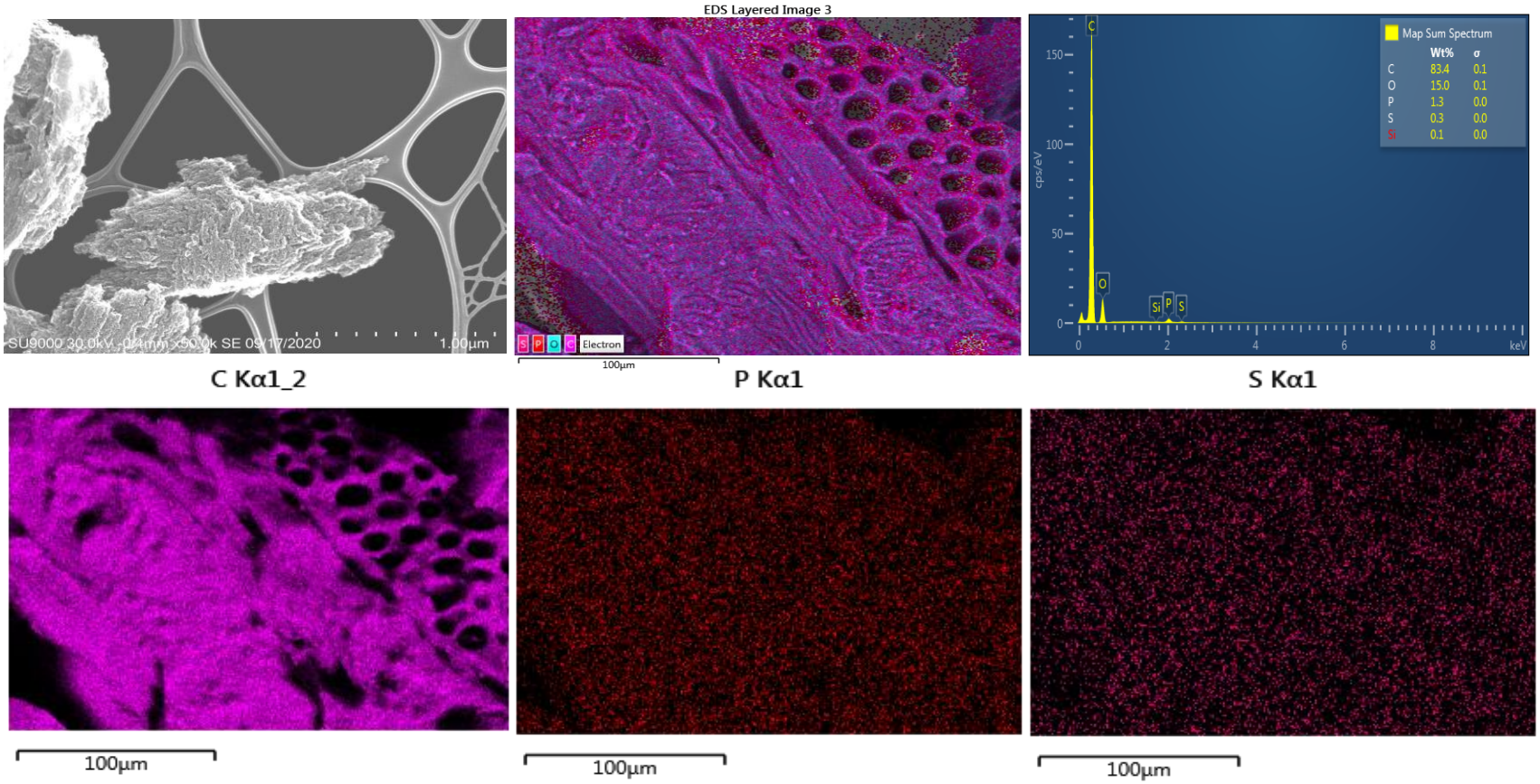

Figure 3.3. STEM-EDS images of GAC-HT-2M catalyst.

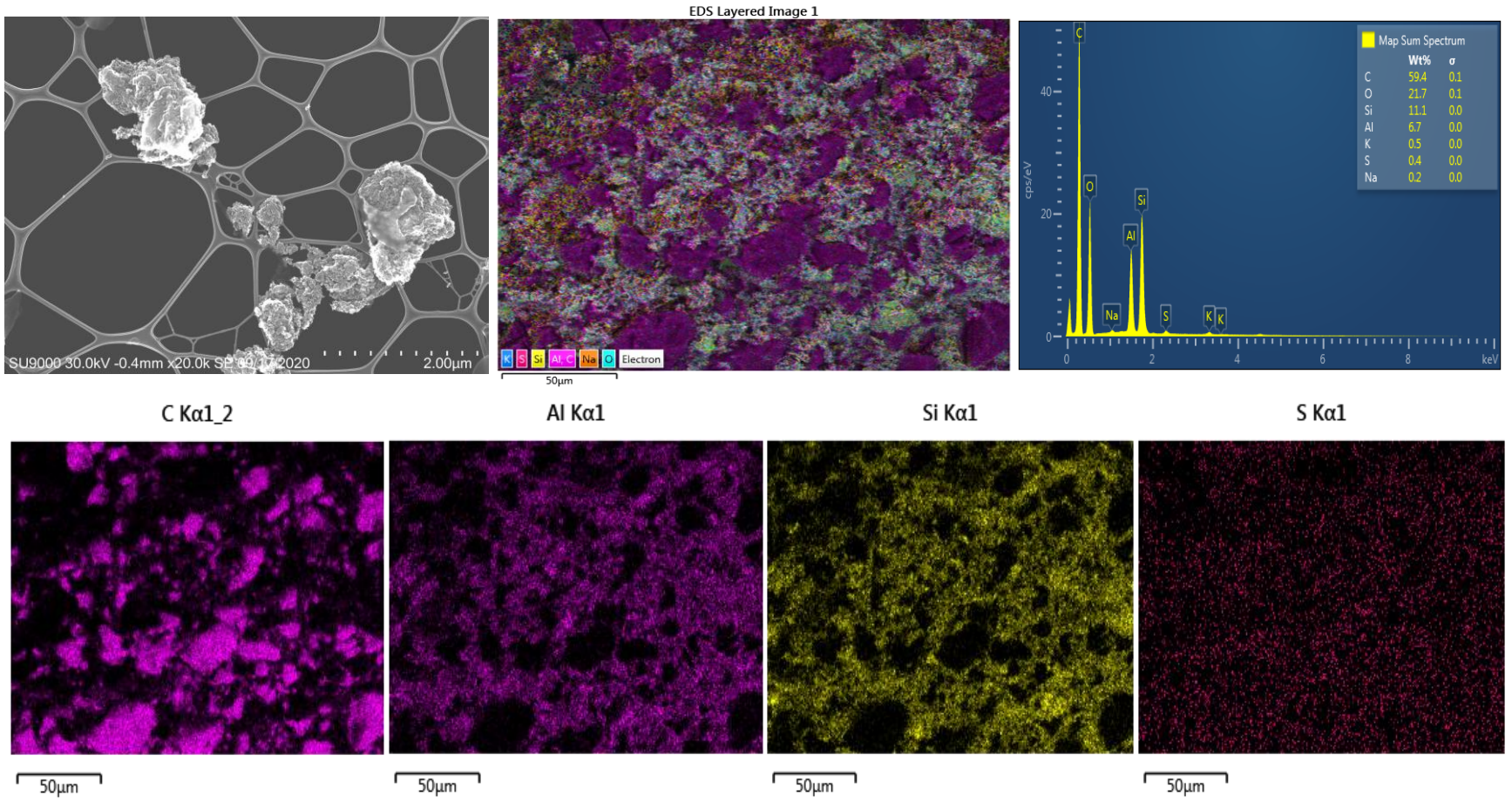

Figure 3.4. STEM-EDS images of cACM-HT-2M catalyst.

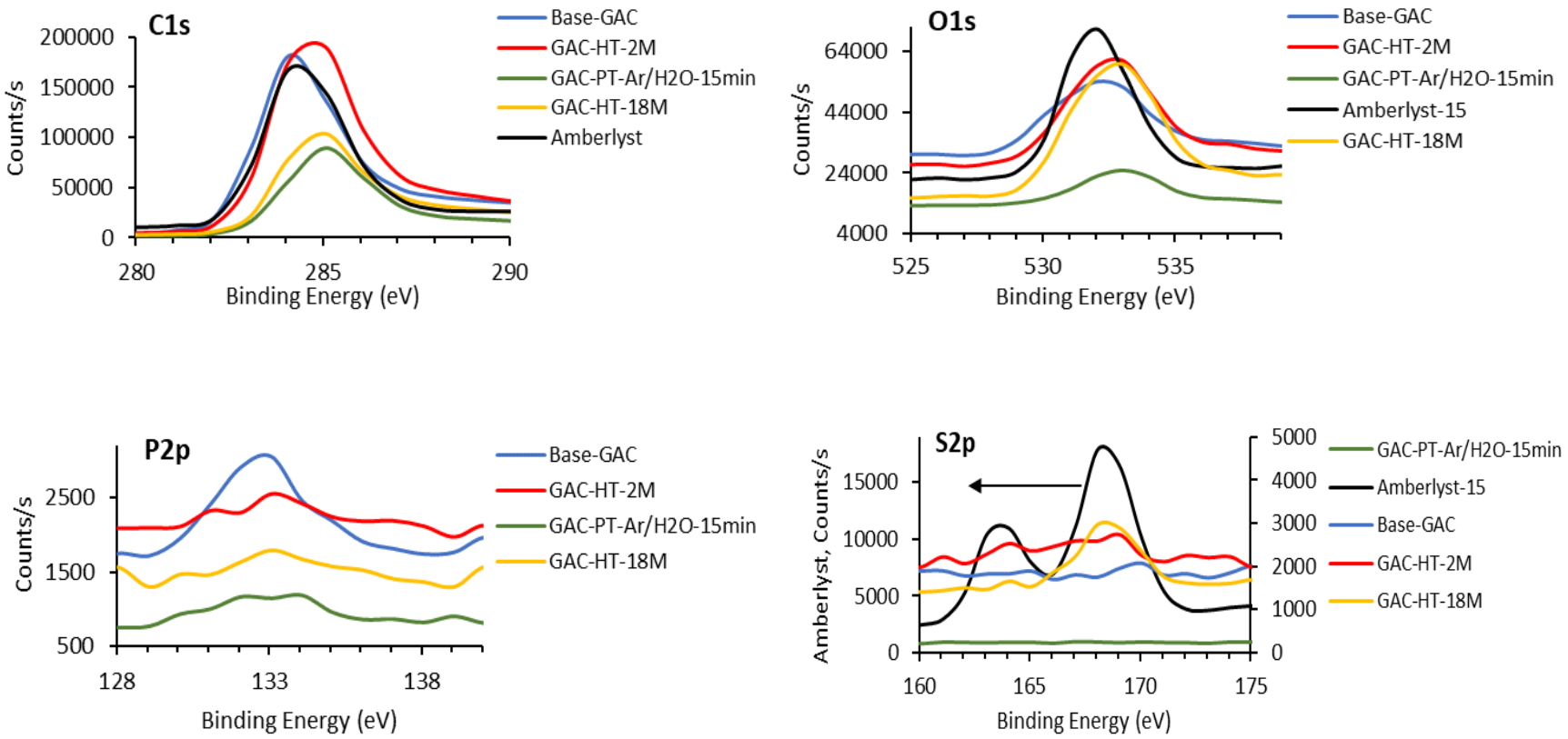

Figure 3.5. XPS analysis of Base-GAC, GAC-HT-2M, GAC-PT-Ar/H_2O-15min and Amberlyst-15.

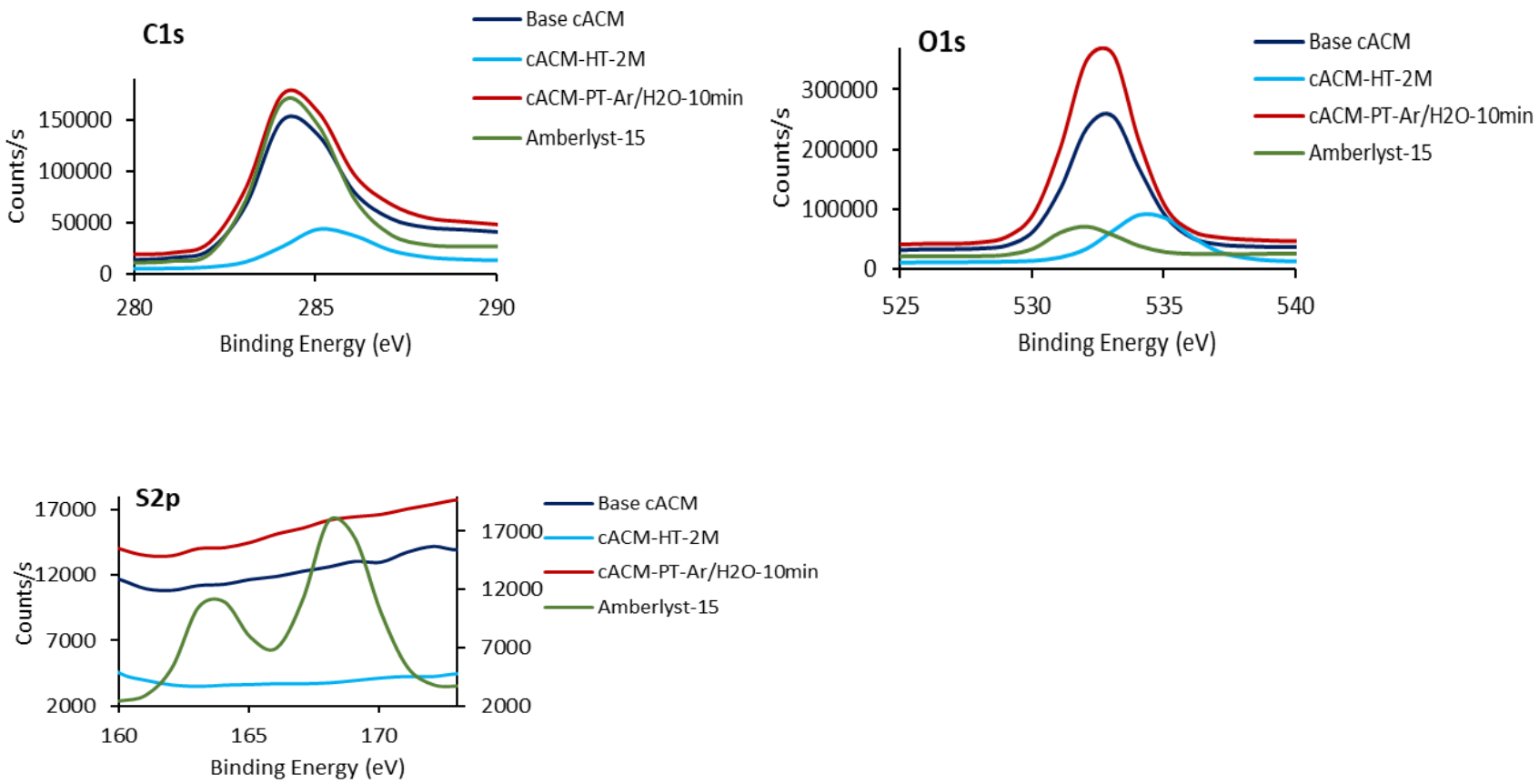

Figure 3.6. XPS analysis of Base-cACM, cACM-HT-2M, cACM -PT-Ar/H_2O-10min and Amberlyst-15.

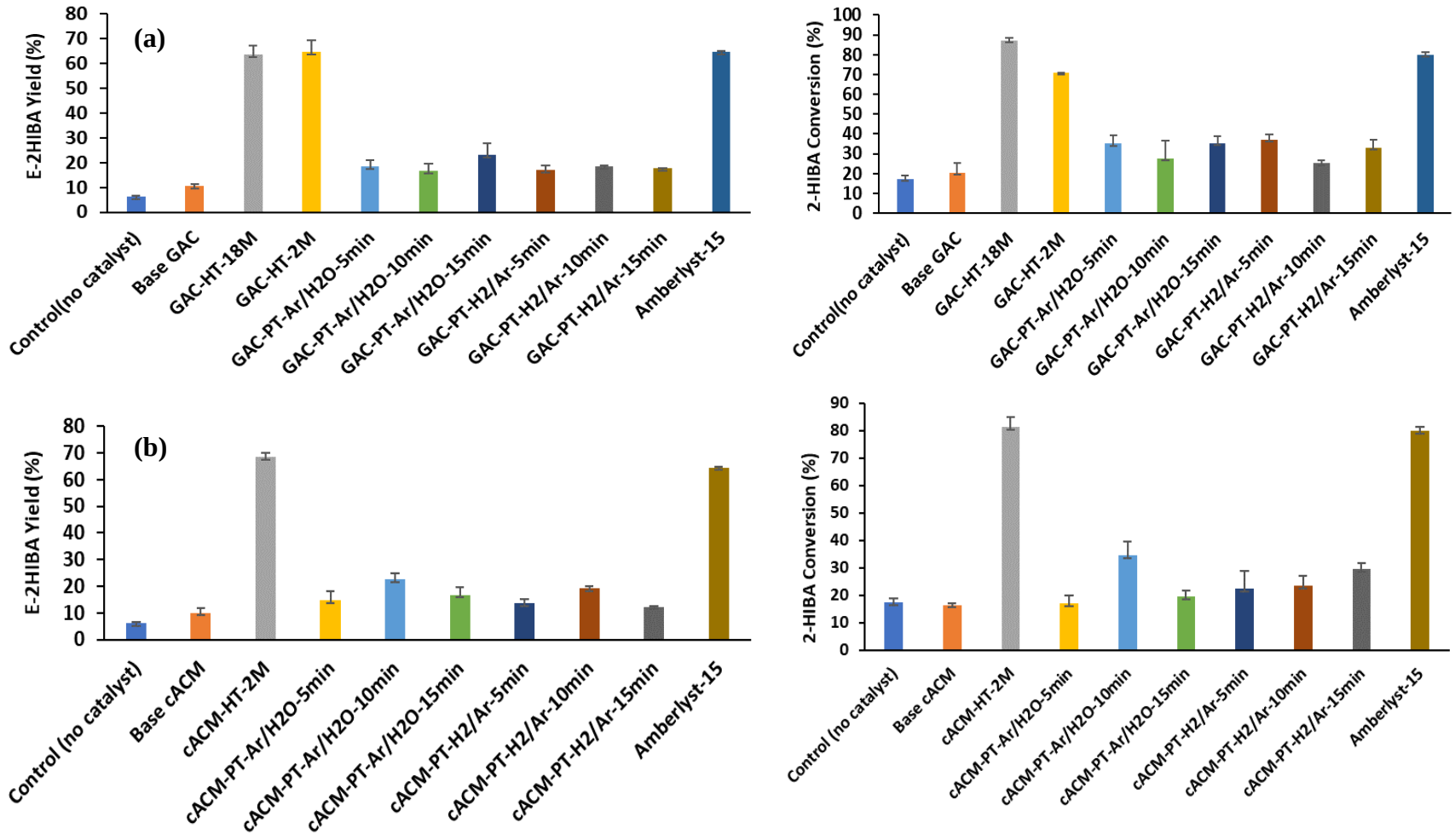

Figure 3.7. E-2HIBA yield and 2-HIBA conversion for the hydrothermal and plasma sulfonated (a) GAC and (b) cACM catalysts vs Amberlyst-15 in the batch esterification of 2-HIBA with ethanol. Reaction conditions: temperature 150 °C, residence time 1 h, catalyst loading 1 g, reaction volume 20 mL and 2-HIBA concentration 40 g/L.

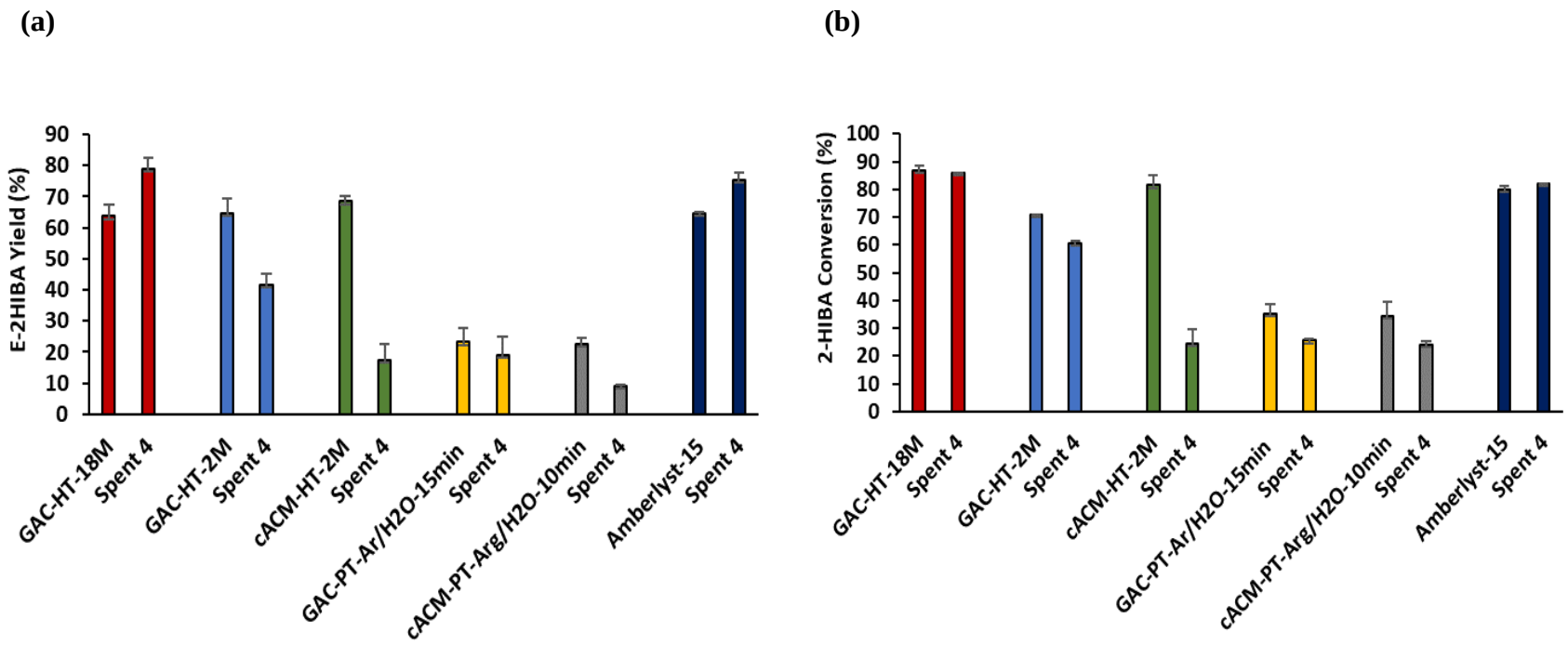

Figure 3.8. (a) E-2HIBA yield and (b) 2-HIBA conversion in catalyst reuse studies with the hydrothermal and plasma sulfonated GAC and cACM catalysts compared to Amberlyst-15.

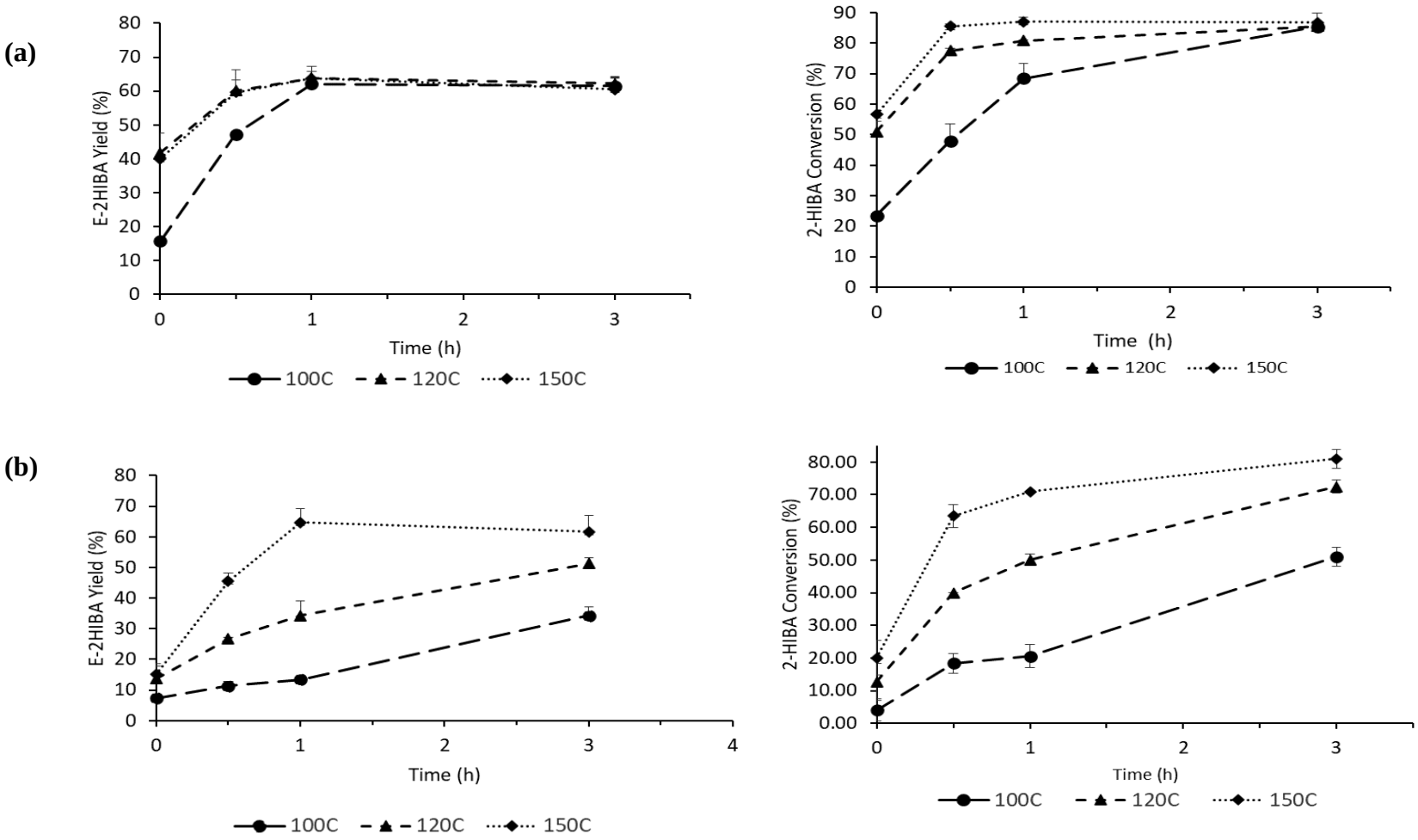

Figure 3.9. Kinetic studies depicting the E-2HIBA yield and 2-HIBA conversion for the (a) GAC-HT-18M and (b) GAC-HT-2M at temperatures of 100 °C-150 °C and residence times ranging from 0.5-3 h.

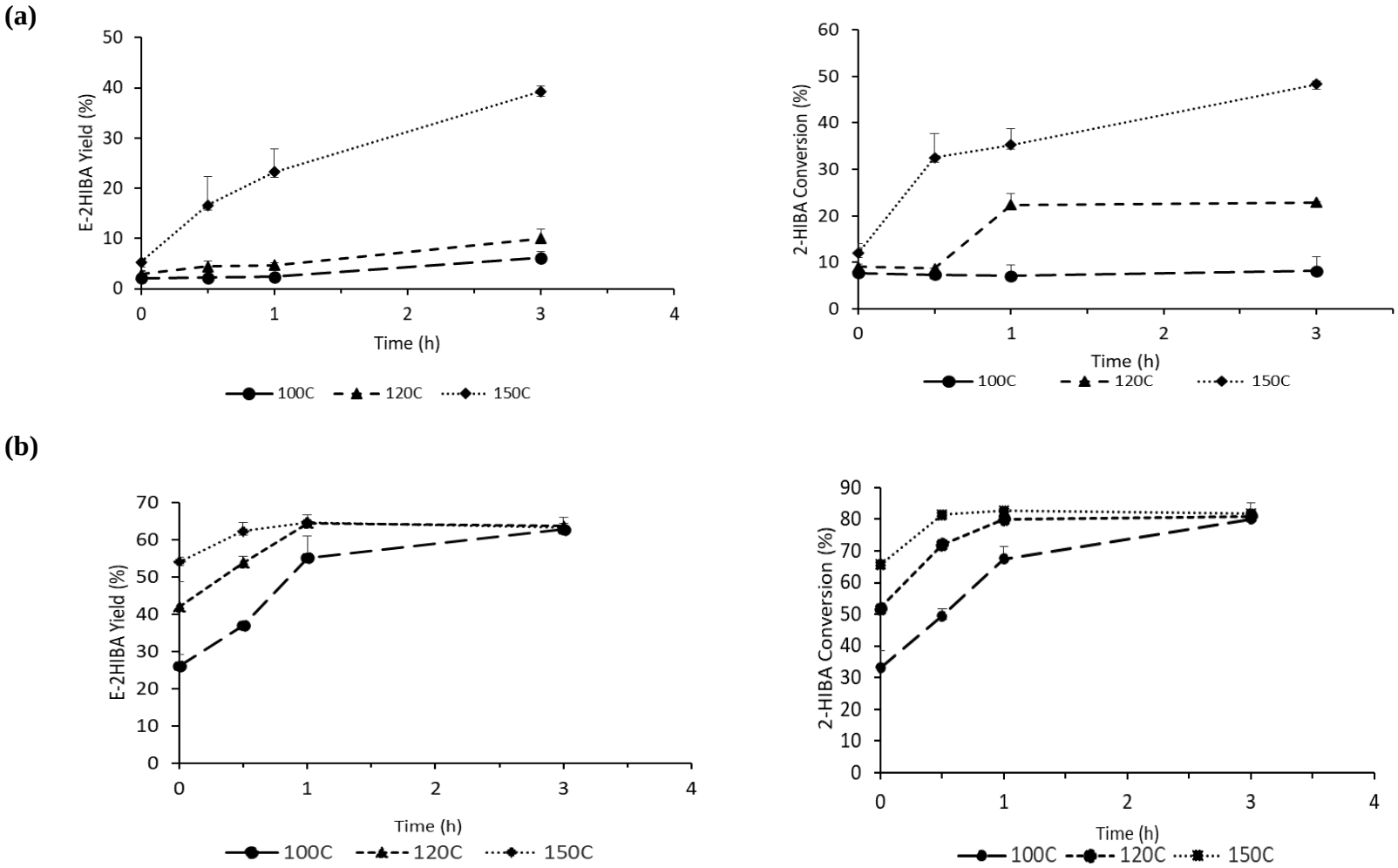

Figure 3.10. Kinetic studies depicting the E-2HIBA yield and 2-HIBA conversion for (a) GAC-PT-Ar/H_2O-15min and (b) Amberlyst-15 at temperatures of 100 °C-150 °C and residence times ranging from 0.5-3 h.

CHAPTER 4

CONTINUOUS CATALYTIC ESTERIFICATION USING A SOLID ACID ACTIVATED CARBON MONOLITH: COMPARISON OF GRANULAR AND MONOLITH FORMS WITH A COMMERCIAL CATALYST

[1] S. Sripada, J.R. Kastner, Continuous catalytic esterification using a solid acid activated carbon monolith: Comparison of granular and monolith forms with a commercial catalyst, Chem. Eng. J., 476 (2023) 146586.

Reprinted here with permission of publisher.

Continuous catalytic esterification using a solid acid activated carbon monolith: Comparison of granular and monolith forms with a commercial catalyst

Author: Sarada Sripada,James R. Kastner Publication: Chemical Engineering Journal Publisher: Elsevier

Date: 15 November 2023

Abstract

2-hydroxyisobutyric acid (2-HIBA) is a significant platform chemical for the synthesis of various products and has been produced fermentatively. Recently, the esters of 2-HIBA have gained interest for applications in fragrances and as low-toxic solvents. In this study, solid acid (sulfonated) wood-based activated carbon granular (sGAC) and monolith (sACM) catalysts were employed for the continuous esterification of 2-hydroxyisobuytric acid with ethanol. The effect of reaction conditions, including pressure and feed flow rate (Q_l) on ester (ethyl 2-hydroxyisobutyrate) space-time yield (STY), ester yield, and selectivity, were determined. A higher STY of 96 g $Lcat^{-1}$ h^{-1} (341 g kg cat^{-1} h^{-1}) and selectivity of 76% was achieved with the sACM compared to the sGAC (87 g $Lcat^{-1}$ h^{-1}, 60 %) at 150 °C, 300 psig, and 3 mL min^{-1} (18.5-20 min contact time). At optimum pressure (300 psig) and temperature (150 °C for sGAC and sACM; maximum of 120 °C for Amberlyst-15), and in time-on-stream studies, 2-HIBA turnover frequency and ester selectivity were higher for sGAC and sACM over Amberlyst-15. The solid acid carbon monolith is a promising catalyst for the continuous catalytic upgrading of biobased organic acids.

Key Words: Sulfonated carbon, activated carbon monolith, continuous, esterification, 2-hydroxyisobutyric acid, ethyl 2-hydroxyisobutyrate.

Abbreviations:

2-HIBA: 2-hydroxyisobutyric acid, E-2HIBA: Ethyl-2-hydroxyisobutyrate, sGAC: sulfonated granular activated carbon, sACM: sulfonated activated carbon monolith, STY: Space-time-yield, TOS: time-on-stream.

4.1 Introduction

The growing demand for sustainable production of specialty chemicals such as esters and pharmaceuticals has resulted in a transition from batch to continuous processing.[1,2] Continuous flow technology offers many advantages over its batch counterpart including smaller reactors,[3] absence of separation requirements for heterogeneous catalysts,[4] easier scale-up (for monolithic systems)[5,6] and safer operation at higher temperatures and pressures.[7] Precise temperature control enables greater reaction efficiency and productivity.[8] Continuous flow enables a reduction in the use of reagents and solvents, and power consumption, which contributes to lowering the carbon footprint of chemical manufacturing processes.[9]

Catalyst morphology plays a vital role in continuous processes using packed bed reactors, as the pores of the catalyst must be easily accessible for the substrate molecules, to ensure small residence time distributions and rapid flow of the liquid reaction mixture without causing a large pressure-build up. Recent studies on continuous flow esterification processes have employed enzymes such as lipases,[10] and solid acid catalysts including zeolites, ion exchange resins, and sulfonated carbon in powder/granular forms in slurry and trickle-bed reactors.[11,12,13] Although enzymes function at moderate temperatures, their applications are mostly limited to aqueous media, which hinders the possibility of using them for hydrophobic substrates.[14] The solid acids mentioned above are limited by their low surface area, and acidic resins like Amberlyst-15 have low thermal stability, which limits their ability to be used in continuous reactions at high temperatures.[13] Amberlyst-15 also tends to swell in organic solvents, thereby clogging flow through the catalyst bed. Moreover, polystyrene-based resins such as Amberlyst-15 present a risk of leaching styrene monomers, potential human carcinogens, and are avoided in manufacturing active pharmaceutical ingredients.[6] Further, a disadvantage with slurry catalysts is the difficulty

of separating product from the catalyst and attrition. This limitation can be overcome with a trickle bed reactor using larger particles to ensure lower pressure drop but can result in intraparticle mass transfer limitations. Low gas-liquid velocities are required to avoid excessive pressure-drop, resulting in low productivity and high operating costs.[15]

To overcome the challenges with granular/powdered catalysts, there is interest in continuous flow processing with structured monolith catalysts to increase process efficiency.[16] A monolith is a large uniform block of material with straight parallel channels used mostly as a support for a catalytically active phase. Monolithic catalysts such as ceramic and metallic monoliths have been extensively applied in gas-solid systems.[17,18] However, their use in multiphase reactions is limited, one of the few commercial scale applications being the production of hydrogen peroxide.[19] Monoliths can serve as good alternatives to slurry and trickle bed reactors for continuous gas-liquid-solid processes due to their large open frontal area that enables a low pressure-drop at high flow rates, short diffusion paths enabling high mass transfer rates, good thermal and mechanical properties, combining reaction and separation processes, and easier scalability.[20] Other advantages of monolith catalysts include the large surface to volume ratio that improves space time yields, high selectivity and productivity, and process safety.[21] In multiphase reactions, two flow patterns of interest in monoliths are the Taylor and film flow regimes. High mass transfer rates attainable under Taylor flow is a key advantage of monolithic catalysts for multi-phase applications.[22] Higher solid-liquid and gas-liquid volumetric mass transfer coefficients have been reported in a monolith reactor operated under Taylor flow in comparison to a stirred tank and trickle bed reactor in the hydrogenation of 2-butyne-1,4-diol.[23] However, film flow regime is of interest when long residence times and high gas to liquid ratios

are required to achieve the desired conversion. Very few studies have investigated the multi/liquid-phase applications of monoliths for continuous esterification processes.

Solid acid monoliths are promising catalysts for the continuous manufacturing of esters. In continuous-flow esterification of lactic acid with n-butanol using a sulfonated monolithic silica microreactor, Koreniuk and co-workers observed high catalytic activity (99% conversion), productivity (1.25 mmol/g min) and stability (4 h).[24] Similarly, a sulfonated monolithic silica catalyst displayed higher conversions and productivity (79%, 49.2 mmol/h/g) in comparison to a randomly packed bed with crushed monolith (22%, 16.7 mmol/h/g) in the continuous transesterification of triacetine with methanol. The high conversions and productivity of the monolith catalyst were attributed to a higher permeability of the intact monolith.[25] In addition, resin-based monoliths have been employed in the continuous synthesis of various esters and thioesters.[26] However, there has been very limited research on continuous catalytic esterification with solid acid carbon monoliths.

Activated carbon in monolith form offers advantages over its powdered/granular forms, including a large surface area to volume ratio, lower pressure-drop, and higher space time yields.[27] Carbon monoliths prepared from petroleum residues have been studied as esterification catalysts. Murakami and co-workers synthesized a carbon-based solid acid monolith by carbonizing a resorcinol-formaldehyde resin and subsequently sulfonating the resin with sulfuric acid. They reported stable catalytic activity in the esterification of acetic acid with ethanol at 60 °C for 50 h continuous flow operation.[28] However, monoliths are currently limited by their high cost compared to particle-based catalysts.[29] To be more cost competitive compared to particle catalysts in fixed bed reactors, monolithic catalysts need to be sourced from economical and

renewable raw materials. Recently, there has been an interest in carbon monoliths derived from wood owing to abundance, renewability, low cost, and ease of processing.[30]

2-Hydroxyisobutyric acid (2-HIBA), a C_4 hydroxycarboxylic acid, is a specialty chemical used as a complex-forming agent for lanthanide and actinide heavy metals, as well as a pharmaceutical intermediate. 2-HIBA is gaining significance as a building block for various polymers with the isobutane structure (e.g., methacrylic acid, tetramethylglycolide).[31] 2-HIBA has been synthesized chemically by the oxidation of isobutylene, dehydrogenation of isobutylene glycol,[32] the hydrolysis of acetone cyanohydrin[33] and the hydrolysis of methyl α-hydroxyisobutyrate.[34] The fermentative production of 2-HIBA has also been reported from various microbial strains.[35,36] Esters of 2-HIBA have received attention as sustainable, environmentally benign fragrance compositions displaying excellent biodegradability and a low degree of bioaccumulation. The ethyl ester of 2-HIBA, ethyl 2-hydroxyisobutyrate (E-2HIBA), finds a wide range of applications in flavor and fragrance ingredients, green solvents, and pharmaceuticals.[37] 2-HIBA esters can be synthesized by a Grignard reaction of a pyruvic ester and methyl halogenated magnesium, by the esterification of 2-HIBA with an alcohol or by the transesterification of the 2-hydroxyisobutyrate ester with an alcohol. E-2HIBA has been synthesized by the batch transesterification of methyl 2-hydroxyisobutyrate with ethanol in the presence of titanium tetraethoxide (reaction conditions: 96 h, yield: 97%) and the esterification of 2-HIBA with an acid catalyst.[37] The direct esterification of 2-HIBA with ethanol using an acid catalyst appears to be a commercially viable approach to produce E-2HIBA.

Although solid acid catalysts have been widely applied in esterification reactions, catalyst deactivation remains a major concern. Several authors have observed partial deactivation of solid acids in batch esterification studies, which has been attributed to the formation of sulfonic

esters,[38] leaching of sulfonic acid groups or pore blocking by carboxylic acid substrates,[39] limiting the reusability of these catalysts. However, there is limited knowledge in the literature on the longevity of solid acids, particularly structured solid acid catalysts in continuous flow-synthesis.

Previously, we devised a more sustainable approach to synthesizing wood-based solid acid carbon catalysts in granular and monolith form using dilute sulfuric acid (2M) and studied their catalytic activity in the batch esterification of 2-hydroxyisobutyric acid (2-HIBA).[40] Our objectives in this work were to compare catalyst performance of a sulfonated carbon monolith (sACM) with a sulfonated granular activated carbon (sGAC) and the commercial ion exchange resin Amberlyst-15 in continuous flow esterification. While several research groups have investigated continuous esterification using ion exchange resins such as Amberlyst-15, [5, 41] there is limited to no information on continuous esterification processes using solid acid carbon monoliths and E-2HIBA synthesis, thus providing the novelty of this work. Additional objectives were to understand 1) mass transfer effects on the reaction in the monolith relative to the granular and Amberlyst-15 catalyst and 2) catalyst deactivation via time-on-stream studies. The overall goal is to develop continuous esterification processes based on renewable and inexpensive, wood-based structured solid acid carbon catalysts that could be applied for the synthesis of valuable specialty/fine chemicals and integrated with fermentation. 2-HIBA and other carboxylic acids are produced fermentatively from several recombinant microbial strains allowing the possibility of creating a sustainable platform for catalytic upgrading a range of bio-based carboxylic acids.

4.2 Experimental Section

4.2.1 Materials

2-hydroxyisobutyric acid ($C_4H_8O_3$, purity > 98%) and ethyl 2-hydroxyisobutyrate ($C_6H_{12}O_3$, purity > 98%) were purchased from TCI chemicals. 200 proof ethanol (purity >99.5%), sulfuric acid used for carbon sulfonation, and Amberlyst-15 (hydrogen form) were procured from Sigma Aldrich. Three catalysts were used in this study, a sulfonated granular activated carbon catalyst (sGAC), a sulfonated activated carbon monolith (sACM) and a commercial petroleum-derived sulfonated styrene-divinyl benzene acidic resin, Amberlyst-15. Details of the carbon materials are provided in the supporting information.

4.2.2 Catalyst Preparation

The base granular activated carbon (GAC) was crushed and sieved to a particle size of 0.5-1 mm, washed until constant pH (3 ×) to eliminate any contaminants (initial pH was ~9.0) and dried at 105 °C. Sulfuric acid (2M) was introduced into the GAC by incipient wetness impregnation at 1.2 mL/g catalyst (1.2:1 [v/w] sulfonating agent: carbon ratio), according to the pore volume of the GAC (1.2 mL/g), to ensure all particles were sufficiently wetted. The monolith cores (ACM) were immersed into 2M H_2SO_4 (100 mL) and sonicated at 30 °C for 30 minutes as reported previously.[40] Preliminary studies were carried out to determine the optimum sulfonation temperature and time by treating the GAC and ACM hydrothermally in a muffle furnace (Fisher Scientific) at temperatures ranging between 100-250 °C for the GAC and 180-280 °C for the ACM for 12 h, and subsequently at the optimum temperature for each material for 3-12 h. Based on the results of these studies (Figure S4.1), the GAC and ACM were treated hydrothermally at 180 °C and 250 °C respectively for 12 h. Post treatment, the sulfonated GAC and ACM cores

were washed with deionized water (25-50 mL/g catalyst) at room temperature to remove traces of excess acid (H_2SO_4), to ensure the catalytic activity was solely due to the sulfonated carbon. The sulfonated ACM cores were washed by sonication in deionized water. Washing (8-12 ×, 1 h washes) was carried out until the filtrate displayed a constant pH, (approximately 4.0 for the GAC and ACM catalysts). Post-washing, all catalysts were dried in a hot air oven at 105 °C overnight and stored for further experiments.

4.2.3 Catalyst Characterization

Brunauer-Emmett-Teller (BET) surface area analysis was performed using a Micromeritics ASAP 2020. For each sample, approximately 0.4 grams of material was degassed at 150 °C until no significant change in pressure was detected. Samples were then reweighed before performing a 3-point BET analysis between relative pressures (P/Po) of 0.1 and 0.28. Scanning Transmission Electron Microscopy (STEM) Imaging was performed on a Hitachi SU-9000 STEM. Subsequent Energy-dispersive X-ray spectroscopy analysis was conducted on an Oxford Xmax EDS detector. The total acid site density of the catalysts was determined by the Boehm titration method. 0.1g of each catalyst was dispersed in 20 mL of 0.1 N NaOH and was kept under stirring for 1 h. The mixture was filtered, and the filtrate was titrated with a 0.1 N HCl solution using a phenolphthalein indicator.[42] The sulfur (S) content on the fresh and spent Amberlyst-15 was determined using a Thermo Scientific FLASH 2000 CHNS-O Analyzer. The S content on the fresh and spent sulfonated carbon catalysts was quantified by Microwave Digestions followed by Inductively Coupled Plasma - Optical Emission Spectroscopy (ICP-OES) analysis. The samples were digested following EPA Method 3052 and the final solutions were analyzed for S according to EPA Method 200.8 by Inductively ICP-OES (Spectro Arcos FHS16, Germany). Sulfonic acid density was estimated from the sulfur content, assuming all S atoms

were in the -SO_3H form. Fourier transform infrared spectroscopy (KBr-FTIR) was performed on a Thermo Scientific Nicolet 6700 FTIR Spectrometer in the scanning range of 400 to 4000 cm^{-1}. Approximately 1 mg of the catalyst sample was finely powdered with 300 mg KBr and pressed into a disc in a hydraulic press (Carver. Inc). The disc was placed in the sample holder and the FTIR spectra were collected (resolution: 6, number of scans: 64). XPS analysis was performed on a Thermo Scientific K-Alpha XPS system with a monochromatic Al-K_α (1486.6 eV) X-ray source. X-ray diffraction (XRD) data were collected on a PANalytical X'Pert PRO using a Cu-Ka radiation source (l = 1.5418 Å) at a scanning speed of 0.5 sec/step, 2 theta scan range of 15-80° and a step size of 0.02°/step. Thermogravimetric analysis (TGA) was performed to study the hydrothermal stability of the sulfonated carbon catalysts (Discovery TGA, TA Instruments) in the temperature range of 35 to 600 °C at a ramping rate of 10 °C / min with nitrogen flow (10 mL/min) over the samples (5-10 mg, platinum pans).

4.2.4 Analytical

The liquid sample collected from the reactor was analyzed using HP 5890 Series II gas chromatography equipped with a flame ionization detector (GC-FID) and a HP Innowax column (30 m × 0.25 mm × 0.25 mm). The GC-FID was operated with the method of inlet temperature 240 °C, detector temperature 250 °C, initial oven temperature of 45 °C for 2.5 minutes followed by a ramp of 10 °C /min for 21 minutes and then held at 230 °C for 4 minutes. 1 μL of each sample was injected on the GC-FID in triplicate.[40]

4.2.5 Catalytic Esterification

2-HIBA esterification reactions were performed in a continuous flow reactor system designed by Parr Instrument Company. Figure 4.1 shows the experimental set-up for the continuous flow

esterification of 2-HIBA in a Parr packed-bed reactor system with Amberlyst-15, sulfonated GAC (sGAC) and sulfonated ACM (sACM). The system comprised a stainless-steel packed bed reactor (Parr, Moline, IL) (1-inch inner diameter). The catalyst (15 g sGAC, 17 g sACM (4 cores, packing height of 12.4 cm), or 5 g Amberlyst-15) was held in place by a stainless-steel screen and quartz wool above and below the bed. The reactor temperature was controlled by a Thermcraft Lab-Temp 1760-watt furnace powered by a Parr 4875 Power Controller and the pressure was regulated with a TESCOM back pressure regulator. The gas flow rate was controlled by a Brooks Delta II Smart Mass Flow Controller, while the liquid feedstock was pumped into the reactor using a Scientific Systems LD-Class HPLC pump.

The reactor was heated and pressurized with nitrogen to the desired temperature and pressure respectively. Once steady state regime was achieved, the liquid feed (40 g/L 2-HIBA in ethanol) and nitrogen (50 mL/min) were continuously passed through the reactor concurrently downwards through a T-junction. Since the reactions were performed in an excess of ethanol (ethanol to 2-HIBA molar ratio 44:1), they were not thermodynamically limited. The liquid product was continuously collected in a condenser (stainless steel vessel with a cooling jacket) connected to a Brookfield TC-602 water bath maintained at 6 °C. Post reaction (t =39-41 min), the reactor was cooled and depressurized, and the condensed product was collected and analyzed. Since the optimum temperatures for Amberlyst-15 and the sulfonated GAC and ACM were previously determined to be 120 °C and 150 °C respectively in batch esterification experiments,[40] continuous reactions were performed at these temperatures. To determine the effect of pressure on 2-HIBA esterification, a series of experiments were performed at pressures ranging from atmospheric pressure to 450 psig (feed flow rate = 2 mL/min, volume feed processed = 78-80 mL, processing times = 39-41 min). To determine the effect of feed flow rate on 2-HIBA

esterification, a series of experiments were performed at liquid flow rates ranging from 2-5 mL/min, corresponding to liquid hourly space velocities (LHSV) of 2.2 - 5.4 /h for sGAC, 2 - 5 /h for sACM and 16.6 - 41.4 /h for Amberlyst-15 (pressure = 300 psig, volume feed processed = 80-200 mL, processing times = 39-41 min). The order of performing the optimization experiments to determine the effect of reaction parameters on ester selectivity and space time yield were as follows, (i) testing the effect of varying pressure (P) and (ii) varying liquid flow rates (Q_l). For each catalyst, the effect of pressure and feed flow rate were studied as consecutive experiments using the same batch of catalyst, corresponding to an accumulated time on stream of approximately 4 h.

For all continuous reactions, the main kinetic parameters including conversion (X = mol 2-HIBA converted/mol 2-HIBA fed), yield (Y= mol E-2HIBA produced/mol 2-HIBA fed), and selectivity (S = mol E-2HIBA produced/mol feed converted) were determined. Liquid hourly space velocity (LHSV, 1/h) was calculated from $[Q_{in} * \rho_{cat}]/W$, and ester space time yield (STY, g/L-cat/h) as $[F_{out} * \rho_{cat} * MW]/W$ where Q_{in} is the inlet volumetric molar flow rate (mL/min), ρ_{cat} is the bulk density of the catalyst, F_{out} is the outlet molar flow rate, W is the catalyst mass, and MW is the molecular weight. A description of the external and internal mass transfer, and pressure drop calculations are provided in the supporting information. Turnover frequency for 2-HIBA (TOF, 1/h) was estimated from the reaction rate (mmol/g/h) and sulfonic acid ($-SO_3H$) density (mmol/g). We also compared the conversion obtained with the sulfonated carbon catalysts and Amberlyst-15 to the equilibrium conversion previously observed in our 2-HIBA batch esterification work.[40] The details of the equilibrium conversion and constants obtained in our batch experiments are included in the supporting information (Table S4.3).

4.2.6 Catalyst Longevity Studies

Catalyst longevity (time-on-stream) studies were performed for the sulfonated carbons and Amberlyst-15 under the reaction conditions optimized for each catalyst. These studies were conducted to assess any changes in catalytic activity, ester yield/selectivity and STY. The durability of the sACM relative to the sGAC and Amberlyst-15 was studied by performing time-on-stream studies for 3.33 h. Liquid product from the reactor i.e., E-2HIBA was sampled after every 40 min (120 mL) and analyzed by GC-FID. After 3.33 h TOS, the spent catalysts were recovered and characterized by elemental analysis, acid-base titrations, STEM-EDS and XPS.

4.2.7 Statistical Analysis

The CHNS, ICP-OES, and GC-FID analyses were performed in triplicate and reported as the mean and sample standard deviation. The sample standard deviation was calculated from the range (R) for small sample size (n) (for $n \leq 5$, R/d_2, where $d_2 = 1.128$). [43] A Student's t-test was performed in the analysis between two means (i.e., catalysts) for the E-2HIBA STY, yield, 2-HIBA conversion and TOF, assuming the null hypothesis with the reported level of significance (α).

4.3 Results and Discussion

4.3.1 Catalyst Characterization

The untreated base GAC and ACM displayed surface areas of 1350 and 598 m^2/g respectively. The reduction in surface area observed in the sGAC (867 m^2/g) and sACM (550 m^2/g) can be attributed to sulfonation and oxidation reactions on the carbon catalysts (Table 4.1). STEM-EDS images of the sGAC and sACM (Figure 4.2) indicate a porous network, and the sACM displayed silica and alumina distributed around the carbon, due to the use of a ceramic binder used to

manufacture the ACM. The total acid density (i.e., total density of SO_3H, COOH and OH groups) values estimated by titration and the sulfonic acid ($-SO_3H$) density obtained from CHNS and ICP-OES analyses are summarized in Table 4.1. The SO_3H density was estimated by assuming all S atoms corresponded to $-SO_3H$ groups. The total acidity of the Base-GAC increased from 3.13 to 3.80 mmol/g and the Base-ACM from 3.33 to 5 mmol/g on sulfonation, confirming sulfonation and incorporation of weak acidic oxygenated functional groups (-COOH, -OH groups).[44] A sulfonated carbon coated monolith, treated with concentrated sulfuric acid at 300 °C displayed a similar total acidity of 4.6 mmol/g.[45] The base GAC and ACM did not display any sulfur, and post sulfonation, the sGAC and sACM showed $-SO_3H$ densities of 0.04 and 0.12 mmol/g. The $-SO_3H$ densities of our sulfonated carbons are lower compared to sulfonated carbons synthesized using concentrated sulfuric acid. [28]

The FTIR spectra of the sulfonated carbons (sGAC and sACM) and Amberlyst-15 (Figure S4.2) display a broad peak at approximately 3400 cm^{-1} and weak vibration bands at 2916 cm^{-1}, 1700 cm^{-1} and 1630 cm^{-1}, which can be assigned to -OH, -C-H, -COOH, and C=C respectively.[46] A significant peak observed at 1420 cm^{-1} in the base (untreated) and sulfonated carbon materials can be assigned to CH_2 stretching vibrations. The sACM displayed a distinct peak at 1059 cm^{-1} corresponding to S=O stretching vibrations of sulfonic acid groups.[40] Stretching vibrations for $-SO_3H$ groups have previously been reported at 1032 cm^{-1} in a honeycomb type sulfonated monolith[28] and 1045 cm^{-1} in a sulfonated carbon coated monolith.[45] Stretching vibrations at 1038 and 1128 in Amberlyst-15 cm^{-1} can be ascribed to the asymmetric and symmetric vibrations of $-SO_3H$ groups respectively.[47] Vibration bands at approximately 1155 cm^{-1} and 1032 cm^{-1} corresponding to O=S=O and SO_3H stretching vibrations have been previously reported in sulfonated carbon catalysts.[46] However, in the FTIR spectra of the sGAC, distinct $-SO_3H$

signatures were not visible, possibly due to the low sulfur content as confirmed by the ICP-OES analysis. Therefore, the catalysts were further characterized by XPS analysis.

The XPS spectra of the carbon catalysts and Amberlyst-15 are depicted in Figures 4.3 and S4.3. Figure S4.3 depicts overlays of the C1s and O1s spectra for the base and sulfonated GAC and base and sulfonated ACM. The C1s peaks at 284.5, 285.6, and 287 eV can be ascribed to C-C/C=C, C-O/C-S, and O=C. The O1s peaks at 531.7, 533 and 533.7, eV can be assigned to C=O, O-H and C-O-C groups. In addition, the O1s peak at 532.6 eV can be attributed to oxygen atoms in the -SO_3H groups.[48] From the XPS, no significant change in the O1s signal was observed in the sGAC in comparison to the base material (oxygen atomic percentage was 5.3 % in sGAC and 6.1% in the base GAC). However, the O1s spectra of the sulfonated ACM indicates that sulfonation induces a shift to a higher binding energy (O% was 36.9 % in sACM vs 32.2 % in the base ACM), which can be ascribed to sulfonation and partial oxidation of the carbon materials. Further, the higher intensity of the O1s peak in the sACM compared to the sGAC can be attributed to the higher concentration of sulfonic acid groups, corresponding to a more oxidized carbon surface, and oxygen atoms in silica and alumina in the ceramic binder of the ACM. The S2p spectra of the sGAC, sACM and Amberlyst-15 (Figure 4.3) indicate two types of sulfur, thiophenic sulfur (C-S-C) and sulfonic acid groups (-SO_3H). Thiophenic sulfur groups, observed between 161-164 eV in the sGAC, 162-164 eV in the sACM and as a broad peak (162-165 eV) in Amberlyst-15, have high thermal stability [49] and may contribute to the stability of the sulfonated carbon catalysts and Amberlyst-15. The S2p peaks at 168-169 eV can be attributed to the S $2p_{3/2}$ and S $2p_{½}$ in SO_3H groups.[48] The higher intensity of -SO_3H groups in the sACM in comparison to the sGAC corresponds to the higher sulfonic acid density of the monolithic catalyst.

Figure 4.4 depicts the XRD patterns of the carbon materials (GAC and ACM) before and after sulfonation. A broad diffraction peak observed between a 2θ of 15 ° to 30 ° in the Base GAC indicates an amorphous carbon structure comprising a random orientation of aromatic sheets with a C (002) plane.[46] This peak shifted to the right and was stronger in the sGAC, which illustrates an enhancement of the amorphousness degree of the carbon material post sulfonation, favoring grafting of sulfonic acid groups.[50] The weak 2θ peak between 40 ° to 50 ° in the base GAC indicates a graphite structure with C (101) plane. A higher intensity of this peak was observed in the sGAC, indicating a more graphene sheet structure in comparison to the base carbon, which could be due to shedding of certain disordered aromatic ring species.[51] The XRD pattern of the Base ACM shows a sharp diffraction peak at 2θ = 26.6 °, which corresponds to the (002) plane of graphite. Similar to the sGAC, there is a shift (2θ = 31 °), and this peak is more pronounced in the sACM. Other peaks at a 2θ of 43 ° and 77 ° can be assigned to the (100) and (110) planes of graphite.[52] XRD peaks observed at a 2θ of 39 °, 45.8 °, 59 ° and 68.4 ° could be attributed to γ-Al_2O_3.[53] Further, a diffraction peak for amorphous silica was noted at 2θ = 21.3 °. This peak shifted to about 19.5 ° in the sACM, suggesting sulfonation of silica in the binder, and a loss of crystallinity on sulfonation.[54]

From the TGA-MS analysis, all three catalysts exhibited two main weight losses (Figure 4.5). The first occurred below 100 °C (about 3% in the sACM, 11% in the sGAC and 15% in Amberlyst-15) and was attributed to the loss of moisture from the catalysts. The second weight loss (an additional 2%) between 250-350 °C in the sGAC and 225-400 °C in the sACM was attributed to the decomposition of sulfonic acid groups. Amberlyst-15 displayed an early onset

degradation temperature of 200 °C, and -SO_3H group decomposition occurred between 200-360 °C. The mass spectra confirmed the evolution of sulfur dioxide (m/z = 64) from the sGAC at a maximum of 285 °C and the sACM and Amberlyst-15 at a maximum of 300 °C (Figures 4.5a and 4.5b). Sulfonated carbon catalysts have been previously reported to have good thermal stability below 250 °C.[55,56] With Amberlyst-15, the TGA-MS detected a weight loss (an additional 25%) corresponding to evolution of SO_2 between 200-360 °C which can be attributed to the thermal decomposition of the sulfonic acid groups (Figure 4.5c). An additional peak corresponding to the evolution of SO_2 was observed between 360 - 470 °C in Amberlyst-15, and approximately 330-400 °C in the sGAC and 350-400 °C in the sACM. This peak can be ascribed to the degradation of thiophenic C-S bonds.[57] Mass loss in Amberlyst-15 in the temperature range of 200-400 °C and above 400 °C has previously been associated with the degradation of polystyrene chains and -SO_3H groups, and divinylbenzene respectively.[47] Our TGA-MS results indicate greater thermal stability of thiophenic sulfur bonds in comparison to the sulfonic acid groups. The results also suggest higher thermal stability of the sulfonated carbon catalysts in comparison to Amberlyst-15. The sGAC and sACM can be used at temperatures below 250 °C to avoid catalyst deactivation.

4.3.2 Effect of Pressure

A series of reactions were performed with the sGAC and sACM at a temperature of 150 °C and Amberlyst-15 at 120 °C at pressures ranging from atmospheric pressure to 450 psig (Q_l = 2mL/min) to determine the effect of pressure on E-2HIBA space-time yield and selectivity. All three catalysts depicted a similar trend where the ester STY and selectivity increased with an

increase in pressure up to 300 psig (Figure 4.6). At a temperature of 120 °C (Amberlyst-15) or 150 °C (sGAC and sACM) and ambient pressure, ethanol (normal boiling point 78 °C) and water are in the vapor state. As the pressure is increased, ethanol vaporization is more difficult, and the high boiling 2-HIBA (normal boiling point 212 °C) is in the liquid state, thus the more volatile ethanol and water product partition between gas and liquid phases. Thereby, contact between the reactants becomes more efficient on increasing the pressure. This is evident from the increase in 2-HIBA conversion observed with Amberlyst-15 from 28.3% to 58.6% on increasing the pressure from 15 psig to 450 psig. Performing a reaction under pressure also reduces mass transfer related issues between the catalyst and reactants and improves contact between the reactants. At atmospheric pressure, high 2-HIBA conversions were noted with the sGAC and sACM, with low ester yield and carbon recovery (sGAC: 51.7 ± 3.4%, sACM: 46.6 ± 7.5%). This trend in conversion noted with the sulfonated carbons can be explained by the poor contact between the vapor and liquid phases or poor distribution of the two phases in the monolith at atmospheric pressure (which may have affected the gas-liquid mass transfer coefficient). Since ethanol vaporized and separated into the gas phase while 2-HIBA was in the liquid phase possibly undergoing an unknown side reaction (e.g., dimerization or cyclic esters on acid sites), there was limited contact between the two reactants at the catalyst surface.

At a pressure of 300 psig, (Q_l = 2 mL/min), a STY and ester selectivity of 53.5 g/Lcat/h and 53.5 % were achieved with the sGAC. With the sACM, a higher E-2HIBA STY of 66.8 g/Lcat/h (α = 0.05, level of significance) and selectivity of 59.7% were obtained compared to the sGAC. Further increase in pressure to 450 psig resulted in a decrease in E-2HIBA STY with sGAC and sACM. We speculate that the decrease in STY, due to a reduction in conversion or yield on increasing the pressure to 450 psig with both the sulfonated carbon catalysts, could be due to

channeling or a 2HIBA side reaction at the higher pressure. Although a high STY of 226.9 g/Lcat/h was noted with Amberlyst-15, a lower ester yield of 26% and selectivity of 48.5% in comparison to the sulfonated carbons were observed (P=300 psig, Q_l = 2 mL/min). Compared to sGAC, the sACM displayed maximum E-2HIBA STY and selectivity and almost complete 2-HIBA conversion of 99.5% (150 °C, 300 psig, Q_l = 2 mL/min). Further, we compared the conversion obtained with the three catalysts to the equilibrium conversion (sACM: 82%, sGAC and Amberlyst-15: 81%) previously observed in our 2-HIBA batch esterification experiments (temperature: 150 °C, pressure: 9 bar, residence time: 3 h, 2-HIBA: ethanol molar ratio 1:44).[40] The conversion displayed by the sACM exceeded the equilibrium conversion of 81% noted in our batch studies. The nearly complete conversion observed with the sACM could be due to the removal of water from the reaction mixture by reactive stripping (co-current water removal by stripping with nitrogen), which shifts the equilibrium conversion towards ester formation. Previously, co-current and counter-current stripping operations in the esterification of 1-octanol and hexanoic acid in a monolithic reactor resulted in significant increase in conversion due to water removal.[58] The sGAC also displayed a slightly higher conversion of 88% compared to the batch equilibrium conversion. However, in comparison to the sulfonated carbon catalysts, Amberlyst-15 displayed a much lower conversion of 53% (150 °C, 300 psig, Q_l = 2 mL/min), due to the shorter contact time and the possibility that water produced during the reaction may have adsorbed on the sulfonic acid sites on the resin and affected the reaction equilibrium. An analysis of the catalysts' turnover frequency (TOF) indicated a significantly higher TOF of 1.06 min^{-1} with the sGAC, approximately 36 times that of Amberlyst-15. The sACM also displayed a much greater TOF (14 ×) compared to Amberlyst-15 (α = 0.05, level of significance). We further analyzed the variation in carbon closure of the three catalysts with pressure. With the sGAC, the

carbon closure increased with pressure from 51.5% at 15 psig to 94.1% at 450 psig (150 °C, Q_l = 2 mL/min). For the sACM, the carbon closure also increased with an increase in pressure from 46.1% at 14.7 psig to 90.9% at 300 psig (150 °C, Q_l = 2 mL/min). A further increase in pressure up to 450 psig led to a decrease in carbon recovery (66.7%). For Amberlyst-15, the carbon closure increased with pressure to 83.8% at 150 psig (120 °C, Q_l = 2 mL/min), and further increasing the pressure to 450 psig led to a decrease in carbon recovery (78.2%). Since higher ester STY, 2-HIBA conversion, and carbon closure were achieved at 300 psig with the sulfonated carbons and Amberlyst-15, further studies were performed at this pressure.

4.3.3 Effect of Feed Flow Rate

Figure 4.7 shows the effect of liquid flow rate on 2-HIBA conversion, ester yield, and selectivity, STY and TOF (2-5 mL/min, 150 °C, 300 psig). With the sulfonated carbon catalysts, we noted a decrease in 2-HIBA conversion on increasing the feed flow rate from 2 to 5 mL/min (or decreasing the liquid residence time from 3 to 1.2 h for the sGAC, 3.4 to 1.3 h for the sACM and 1 to 0.4 h for Amberlyst-15). Further, a more significant drop in conversion was observed on increasing the liquid flow rate to 5 mL/min. However, we observed an increase in TOF, E-2HIBA STY, yield (except sACM) and selectivity on increasing the feed flow rate to 3mL/min (LHSV is 3.2/h for sGAC, 3/h for sACM and 24.8/h for Amberlyst-15). An increase in feed flow rate lowers the residence time and the corresponding conversion yet improves the fluid-catalyst mass transfer characteristics of the system, suggesting the possibility of external mass transfer limitations at the lower flow rate (Q_l = 2 mL/min). Further, higher conversions and ester yields at the lower liquid flow rates are due to sufficient liquid residence time in the reaction zone. However, a different trend was noted with Amberlyst-15; the 2-HIBA conversion increased on

increasing the feed flow rate from 2 to 3 mL/min. We speculate there may have been competitive adsorption between ethanol and 2-HIBA and differential mass transfer of the two reactants to the internal active sites of the cation exchange resin, limiting 2-HIBA conversion at the lower flow rate. The high levels of diethyl ether (DEE) formed from ethanol dehydration on Amberlyst-15, yet not sGAC or sACM, support this concept (Figure S4.4).

At a liquid flow rate of 3 mL/min and pressure of 300 psig, the sACM displayed a higher E-2HIBA STY of 95.5 g/Lcat/h and selectivity of 75.7% in comparison to the sGAC (STY: 87.1 g/Lcat/h, S: 62.9%). The higher ester STY and selectivity observed with the sACM can be attributed to the greater surface area to volume ratio of the monolith, which enabled higher acid site density and enhanced mass transfer.[59] While we noted significantly higher STY's of 660 g/Lcat/h with Amberlyst-15 in comparison to the sulfonated monolith (α = 0.05, level of significance), we obtained a higher ester yield of 55.5% with the sACM compared to 48.1% with Amberlyst-15 under these reaction conditions (Q_l = 3 mL/min, P= 300 psig). With Amberlyst-15, a byproduct was observed, which we initially speculated to be the ethanol dehydration product diethyl ether, based on literature.[60] Further analysis by GC-FID confirmed that byproduct as diethyl ether, which was produced at high concentrations of approximately 35 g/L (Q_l = 3mL/min, P= 300 psig). Due to the macroreticular structure of Amberlyst-15 with the acid sites located within the porous structure, we believe that ethanol penetrates the structure more efficiently than 2-HIBA, resulting in etherification and a subsequent decrease in ester yield.[61] However, under the same reaction conditions, low concentrations of diethyl ether (1-2 g/L) were noted with the sulfonated GAC and ACM. Since these catalysts have acid sites located on the surface, accessible to both the alcohol and carboxylic acid, they enable rapid esterification and negligible etherification, presenting an advantage over Amberlyst-15. The diethyl ether

concentration trends on varying the pressure and feed flow rate for all three catalysts are depicted in Figure S4.4. On further increasing the liquid flow rate to 5 mL/min, for all three catalysts, the 2-HIBA conversion, as well as ester STY decreased. The carbon closure was above 80% for all the runs. Among the three catalysts, the sGAC displayed a significantly higher TOF of 1.55 min^{-1}, approximately 26 times that of Amberlyst-15 (Q_l = 3 mL/min, P= 300 psig) (α=0.05, level of significance). The high TOF of the sGAC, despite the low sulfonic acid density can be attributed to the high surface area of the catalyst (867 m^2/g). The sACM also displayed a higher TOF (8 ×) compared to Amberlyst-15 (α=0.05, level of significance). Geng and coworkers also observed high TOFs, seven times that of Amberlyst-15, in the batch esterification of oleic acid and methanol using a granular solid acid carbon catalyst.[62] The high catalytic efficiency of the sulfonated carbons can be attributed to the high density of weak acidic -COOH and -OH groups that facilitate enhanced access of the reactants to the active sites and promote catalytic activity.[63] Although Amberlyst-15 has a higher $-SO_3H$ density compared to the sulfonated carbons, its low BET surface area (38 m^2/g) indicates that most of the acid sites are located within the swelling network which is more easily penetrated by small ions such as H^+, limiting 2-HIBA access to the acid sites resulting in low turnover frequencies.[62]

4.3.4 Mass Transfer Analysis for 2-HIBA

For two-phase gas-liquid flows in monoliths, two flow regimes - i.e., Taylor flow and film flow are possible based on the gas and liquid superficial velocities. Film flow occurs at gas to liquid flow rate ratios (Q_g/Q_l) of 6-200, where the liquid flows as a film along the channel walls and the gas flows through the core of the channels.[27] On the other hand, Taylor flow, in which gas bubbles and liquid slugs move alternately in the monolith channels occurs at a Q_g/Q_l of 0.3-2.[64] In this work, the liquid superficial velocity ranged from 6.6 – 16.5 x 10^{-5} m s^{-1}, while the gas

superficial velocity was fixed at 16.4 x 10^{-4} m s^{-1}. Therefore, the Q_g/Q_l ratio ranged from 24.9 (Q_l= 2 mL/min) to 9.9 (Q_l= 5 mL/min), indicating that the reactions with the sACM were performed under film flow. Mass transfer in monoliths, occurs in three steps; gas to solid through the liquid film, gas-liquid, and liquid-solid mass transfer.[65] Based on the Q_g/Q_l ratios used in this study, film flow was assumed, and 2-HIBA transport was considered from the bulk liquid phase (ethanol) to the solid catalyst wall through a thin film. For the sulfonated monolith, vapor phase resistance can be neglected, and the liquid-solid mass transfer coefficient was estimated as described in the supporting information.[66] The Mears and Weisz-Prater criteria were used to estimate the external and internal mass transfer resistances respectively for all three catalysts, the details of which are also provided in the supporting information. The estimated Mears criteria for the three catalysts were lower than 0.15 and Weisz-Prater criteria were less than 1, suggesting negligible external and intraparticle mass-transfer-limitations (Tables S4.1 and S4.2).

4.3.5 Catalyst Longevity

The catalyst longevity of the sulfonated GAC and ACM was compared with Amberlyst-15 in the esterification of 2-HIBA and ethanol. Time on stream (TOS) studies for all the 3 catalysts were performed for 3.33 h at a liquid flow rate of 3 mL/min and a pressure of 300 psig at a temperature of 150 °C for the sGAC and sACM, and 120 °C for Amberlyst-15. The sGAC displayed high catalytic activity and stability and retained 89.7% of its initial activity at 3.33 h (Figure 4.8). In the continuous flow esterification of oleic acid using a granular sulfonated hydrothermal carbon catalyst (synthesized using concentrated sulfuric acid), Fraley and co-workers observed a conversion of over 90% and good stability up to 4.5 days of operation.[13] The sGAC also displayed a higher TOF in comparison to the sACM and Amberlyst-15 (4 × of the sACM and 23 × of Amberlyst-15) (α = 0.05, level of significance), with a slight decline in TOF

from 1.36 to 1.22 min^{-1} during time-on-stream (Figure S4.5). In addition, over 60% E-2HIBA yield and 80% E-2HIBA selectivity were observed with the sGAC in TOS runs. Similarly, the sACM displayed high catalytic stability, retaining 90.7% of its initial activity after 3.33 h TOS (X = 62-68%). Ciemega and co-workers also reported good catalytic stability for 6 h (X = 40-45%, Q_l = 0.06 mL/min) in the continuous flow esterification of acetic acid with n-butanol using a silica monolithic microreactor comprising arenesulfonic acid groups.[59] The sACM also showed a similar reaction rate (2.63 - 2.64 mmol/g/h) and TOF (0.35-0.36 min^{-1}) and displayed a TOF 10 times that of Amberlyst-15 in all reuse cycles (α=0.05, level of significance). Further, after 3.33 h, the sulfonated monolith retained 82.2%, 90.1% and 90.7% of its initial E-2HIBA yield, STY, and selectivity respectively. An analysis of the carbon balance of the spent runs indicated a carbon recovery of over 100%, suggesting carry over of ester from previous runs. Further, low yields (0.5-4 g/L) of the byproduct diethyl ether were observed during TOS with the sulfonated carbon catalysts. Overall, despite the low sulfonic acid density, high E-2HIBA STY, yield, and selectivity were achieved with the sulfonated carbons. Similar STYs were observed with the sGAC and sACM, with a 10% decline in STY for the sACM after 3.33 h. The sACM also displayed higher ester selectivity in comparison to the sGAC after 1.4 h (92.9% with the sACM vs 82.2% with the sGAC) with a 9.4% decrease in selectivity by 3.33 h. Although the STYs for both catalysts were comparable in the TOS studies, the sACM presents an advantage in terms of slightly higher selectivity, lower pressure-drop, high mass transport rates and better handling properties.

With Amberlyst-15, a reduction in 2HIBA conversion and ester yield was observed after 1.4 h, with a 59% decrease in 2-HIBA conversion and 50% decrease in TOF, after which the catalytic activity remained almost steady (Figure 4.8). Similar trends were observed in the ester STY and

yield; after 3.33 h the catalyst displayed only 55.7% of its initial activity. Similar decline in catalytic activity and TOF were reported in the esterification of stearic acid using sulfonated ion exchange resins, where among three acidic resins, two were inactive, while one retained only 30% of its initial activity after 4 spent cycles.[67] Further, diethyl ether yields of 29 – 33 g/L were observed with Amberlyst-15 throughout TOS. From the results obtained in the catalyst longevity studies, the decline in catalytic activity observed with Amberlyst-15 was hypothesized to be due to sulfonic acid leaching or pore blocking due to adsorption of reactants or products/byproducts (diethyl ether).[68] To determine if there were any changes in the morphology or physiochemical properties of the catalysts, the spent catalysts were collected and subjected to elemental analysis, acid-base titrations, STEM-EDS and XPS.

4.3.6 Characterization of Spent Catalysts

The STEM-EDS images of the spent and fresh catalysts (Figure S4.6 and Figure 4.2) appear similar, suggesting that all three catalysts maintained their surface morphology after the time-on-stream studies. However, the STEM-EDS image of the sGAC indicated a decline in sulfur content. To confirm this, we performed ICP-OES and measured total acid density of the spent catalysts. A decrease in sulfur content (85-87%) on the spent sGAC (0.02% vs 0.14% in the fresh catalyst) and sACM (0.05% vs 0.4% in the fresh catalyst) was observed, suggesting leaching of sulfonic acid groups from the carbon surface (Table S4.4). Leaching of -SO_3H groups is possibly due to acid-catalyzed hydrolysis or desulfonation of the C-S bond in the catalyst. Various authors have previously observed deactivation of sulfonated carbons by leaching of sulfonic acid groups.[56,69] Deactivation by exfoliation of carbon particles with sulfonic acid sites from the catalyst[70] and formation of sulfonate esters[71] have been reported. In addition, a decrease in total

acid site density was also observed (2.6 mmol/g with the spent sGAC and 2.5 mmol/g with the spent sACM), indicating leaching of weak acidic groups.

With Amberlyst-15, considering the change in catalytic activity after 1.4 h, we presumed catalyst deactivation may also have occurred due to leaching of acid sites. However, there was no decrease in the sulfur content of the spent catalyst, indicating leaching was not the cause of deactivation (Table S4.4). We speculate that accumulation of water generated during the reaction by absorption on the catalyst surface may have resulted in reduced Amberlyst-15 activity. Coverage of sulfonic acid groups by a hydrate shell could hinder access of the 2-HIBA molecules to the active sites, [67] causing a corresponding decline in conversion. This may have been promoted by ethanol dehydration, indicated by the high concentration of diethyl ether (approximately 30 g/L), Adsorption of diethyl ether may also be responsible for blocking the pores or active sites.[38,39] XPS analyses of the spent sGAC and Amberlyst-15 indicate an increase in C1s and O1s peak intensities compared to the fresh catalysts, suggesting the possibility of deposition of products/byproducts (Figure S4.7). XPS overlays of the S2p spectra of the fresh and spent sulfonated carbons and Amberlyst-15, indicate a decline in intensity of the thiophenic sulfur peak (162-164 eV) and a slight shift in the sulfonic acid group peak to a higher binding energy. The loss of electrons during the interaction of sulfur atoms on the catalyst surface with the reactants, may have caused this shift to higher binding energy values.[72] The elemental analyses and XPS results confirm the presence of sulfonic acid groups on the spent catalysts. Despite the high degree of leaching, the spent sGAC and sACM catalysts displayed significantly higher turnover frequencies (10-35 ×) in comparison to Amberlyst-15. Although the sulfonic acid densities of the spent sGAC and sACM were very low, the presence of weak acidic groups on the catalysts may have aided in catalytic activity.[63]

4.4 Conclusions

A continuous 2-HIBA esterification process with a structured and renewable solid acid carbon monolith catalyst was demonstrated. Significantly higher ester yields, and selectivity were observed on increasing the pressure to 300 psig and feed flow rate to 3 mL/min. The sulfonated ACM displayed higher E-2HIBA STY and selectivity (95.5 g/Lcat/h, 75%) compared to the sGAC (87.1 g/Lcat/h, 60.2%) (150 °C, 300 psig, 3 mL/min). Although Amberlyst-15 displayed higher E-2HIBA STY compared to the sulfonated carbons, lower ester yield, and selectivity in TOS was observed due to lack of acid site access to 2-HIBA (possibly due to preferential water and/or ethanol adsorption and low surface area). The sGAC and sACM displayed significantly higher TOF's, approximately 8-26 × that of Amberlyst-15 (300 psig, 3 mL/min). Further, the sGAC and sACM displayed good stability in the TOS studies, retaining 89-91% of the initial catalytic activity, indicating the potential of our sulfonated carbons as industrial esterification catalysts. Our results suggest the potential of employing solid acid carbon monolith catalysts as possible future replacements for petroleum derived commercial sulfonated resins for continuous liquid phase esterification and other acid catalyzed reactions. Future work would involve stabilizing the acid sites towards leaching, developing an esterification kinetic model with the solid acid monolith for scale-up, and testing the stability of the monolith towards vapor phase esterification reactions (e.g., methyl or ethyl acetate production).

Declaration of Competing Interest

The authors declare that there are no known competing financial or personal relationships that could influence the work reported in this manuscript.

Acknowledgements

Support for this research was provided by the USDA-NIFA Grant (Carbon Monolith Catalysts from Wood for Biobased Platform Chemicals: 2017-67021-26136). The authors thank Applied Catalysts for providing the GAC and ACM materials, and their contribution in performing the BET surface area analysis. The authors also thank Dr. Evan White for assistance with the TGA-MS analysis and Seyedehsaan Vasefi for his contribution to the CHNS analysis. The XPS analysis was performed at the Georgia Tech Institute for Electronics and Nanotechnology or Joint School of Nanoscience and Nanotechnology, a member of the National Nanotechnology Coordinated Infrastructure (NNCI), which is supported by the National Science Foundation (Grant ECCS-1542174).

References

1) J. A. Bennett, Z. S. Campbell, M. Abolhasani, Role of continuous flow processes in green manufacturing of pharmaceuticals and specialty chemicals, Curr. Opin. Chem. Eng. 26 **(**2019) 9-19.

2) V.Russo, R. Tesser, C. Rossano, T. Cogliano, R. Vitiello, S. Leveneur, M. Di Serio, Kinetic study of Amberlite IR120 catalyzed acid esterification of levulinic acid with ethanol: from batch to continuous operation, Chem. Eng. J., 401 (2020) 126126.

3) S.G. Newman, K.F. Jensen, The role of flow in green chemistry and engineering, Green Chem. 15 (2013), 1456-1472.

4) K. Masuda, T. Ichitsuka, N. Koumura, K. Sato, S. Kobayashi, Flow fine synthesis with heterogeneous catalysts, Tetrahedron, 74 (2018) 1705-1730.

5) A. I. Alfano, S. Pelliccia, G. Rossino, O. Chianese, V. Summa, S. Collina, M. Brindisi, Continuous-flow technology for chemical rearrangements: A powerful tool to generate pharmaceutically relevant compounds, ACS Med. Chem. Lett. 14 (2023) 326-337.

6) F. Dede, O. Piccolo, D. Vigo. Dimethyl fumaratae: Heterogeneous catalysis for the development of an innovative flow synthesis, Org. Process. Res. Dev., 25 (2021) 292-299.

7) Dr. B. Gutmann, Dr. D. Cantillo, Prof. Dr. C.O. Kappe, Continuous-flow technology-A tool for the safe manufacturing of active pharmaceutical ingredients, Angew. Chem. Int. Ed. 54 (2015) 6688-6728.

8) J. A. M. Lummiss, P.D. Morse, R. L. Beingessner, T. F. Jamison, Towards more efficient, greener synthesis through flow chemistry, Chem. Rec. 17 (2017) 667-680.

9) L. Rogers, K.F. Jensen, Continuous manufacturing-the Green Chemistry Promise? Green Chem. 21 (2019) 3481-3498.

10) A. Cordier, M. Klinksiek, C. Held, J. Legros, S. Leveneur, Biocatalyst and continuous microfluidic reactor for an intensified production of n-butyl levulinate: kinetic model assessment, Chem. Eng. J., 451 (2023) 13854.

11) Z.T. Alismaeel, A.S. Abbas, T.M. Albayati, A. Doyle, Biodiesel from batch and continuous oleic acid esterification using zeolite catalysts, Fuel, 234 **(**2018) 170-176.

12) S. Mo Son, H. Kimura, K. Kusakabe, Esterification of oleic acid in a three-phase, fixed-bed reactor packed with a cation exchange resin catalyst, Bioresour. Technol., 102 (2011) 2130-2132.

13) N. Fraley, M. Wright, A. Lachgar, Characterizing reaction space in the continuous-flow esterification of oleic acid using a sulfonated hydrothermal carbon catalyst, ChemistrySelect, 7 (2022**)** e202200287.

14) A. Z. Fadhel, P. Pollet, C. L. Liotta, C. A. Eckert, Combining the benefits of homogeneous and heterogeneous catalysis with tunable solvents and near critical water, Molecules, 15 (2010) 8400-8424.

15) R. Hilten, J. Weber, J.R. Kastner, Continuous upgrading of fast pyrolysis oil by simultaneous esterification and hydrogenation, Energy Fuels, 30 **(**2016) 8357-8368.

16) S. Roy, T. Bauer, M. Al-Dahhan, P. Lehner, T. Turek, Monoliths as multiphase reactors: A review, AIChE J., 50 (2004) 2918- 2938.

17) R. Porta, M. Benaglia, A. Puglisi, Flow chemistry: Recent developments in the synthesis of pharmaceutical products, Org. Process. Res. Dev., 20 (2016) 2-25.

18) W. Liu, W. P. Addiego, C. M. Sorensen, T. Boger, Monolith reactor for the dehydrogenation of ethylbenzene to styrene, Ind. Eng. Chem. Res., 41 (2002) 3131-3138.

19) R.E. Albers, M. Nyström, M. Siverström, A. Sellin, A.-C. Dellve, U. Andersson, W. Herrmann, Th. Berglin, Development of a monolith-based process for H_2O_2 production: from idea to large scale implementation, Catal. Today, 69 (2001) 247-252.

20) J.A. Moulijn, F. Kaptejin, Monolithic reactors in catalysis: excellent control, Curr. Opin. Chem. Eng., 2 (2013) 346-353.

21) K. Szymańska, A. Ciemiega, K. Maresz, W. Pudlo, J. Malinowski, J. Mrowiec-Bialon, A. B. Jarzebski, Catalytic functionalized structured monolithic micro-/mesoreactors: Engineering, properties, and performance in flow synthesis: An overview and guidelines, Front. Chem. Eng. 3 (2021) 789102.

22) F.L.D. Martínez, C. Julcour, A-M. Billet, F. Larachi, Modelling and simulations of a monolithic reactor for three-phase hydrogenation reactions-Rules and recommendations for mass transfer analysis, Catal. Today 273 (2016) 121-130.

23) R. P. Fishwick, R. Natividad, R. Kulkarni, P.A. McGuire, J. Wood, J. M. Winterbottom, E. H. Stitt, Selective hydrogenation reactions: A comparative study of monolith CDC, stirred tank and trickle bed reactors, Catal. Today, 128 (2007) 108-114.

24) A. Koreniuk, K. Maresz, K. Odrozek, A.B. Jarzebski, J. Mrowiec-Bialoń, Highly effective continuous-flow monolithic silica microreactors for acid catalyzed processes, Appl.Catal. A- Gen, 489 (2015) 203-208.

25) A. Sachse, A. Galarneau, F. Fajula, F. Di Renzo, P. Creux, B. Coq, Functional silica monoliths with hierarchical uniform porosity as continuous flow catalytic reactors. Micropor. Mesopor. Mat., 140 (2011) 58-68.

26) F. Wakayama, R. Ito, K. Park, M. Ishida, Y. Yamada, S. Ichihara, H. Takada, S. Nakamura, A. Kato, T. Yamada, H. Sajiki, Y. Monguchi, Esterification or thioesterification of carboxylic acids with alcohols or thiols using amphipathic monolith-SO_3H resin, Bull. Chem. Soc. Jpn., 94 **(**2021) 2702-2710.

27) M. Pirmoradi, N. Janulaitis, R.J. Gulotty, Jr., J.R. Kastner, Continuous hydrogenation of aqueous furfural using a metal-supported activated carbon monolith, ACS Omega, 5 (2020) 7836-7849.

28) K. Murakami, Y. Satoh, I. Ogino, S. R. Mukai, Synthesis of a monolithic carbon-based acid catalyst with a honeycomb structure for flow reaction systems, Ind. Eng. Chem. Res. 52 (2013) 15372-15376.

29) T. Boger, A.K. Heibel, C.M. Sorensen, Monolithic catalysts for the chemical industry. Ind. Eng. Chem. Res., 43 (2004) 4602-4611.

30) Y. Sun, Z. He, Y. Wei, G. Liu, R. Liu, J. Hu, H. Liu, X. Zhang, G. Yuan, Wood-derived monolithic carbon materials and their functional applications, Clean-Soil, Air, Water, 50 (2022) 2100420.

31) T. Rohwerder, R. H. Müller, Biosynthesis of 2-hydroxyisobutyric acid (2-HIBA) from renewable carbon, Microb. Cell Factories, 9 (2010) 13.

32) O. Vogl, Synthesis of α-Hydroxyisobutyric Acid from Isobutylene, J. Org. Chem. 23 (1958) 1488-1489.

33) C.L. Willis, L.H. Slaugh, Alpha-hydroxyisobutyric acid process. Patent Application. US4351955A, Sep. 28, 1982.

34) Y. Shima, T. Abe, H. Higuchi, Process for producing methacrylic acid. Patent Application. US5225594A, Jul. 6, 1991.

35) D. Przybylski, T. Rohwerder, C. Dilβner, T. Maskow, H. Harms, R.H. Mueller, Exploiting mixtures of H_2, CO_2 and O_2 for improved production of methacrylate precursor 2-hydroxyisobutyric acid by engineered Cupriviadus necator strains. Appl. Microbiol. Biotechnol. 99 (2015) 2131-2145.

36) M-T Rohde, S. Tischer, H. Harms, T. Rohwerder, Production of 2-Hydroxyisobutyric acid from methanol by *Methylobacterium extorquens* AM1 Expressing (*R*)-3-Hydroxybutyryl Coenzyme A-Isomerizing Enzymes. Appl. Environ. Microbiol. 83 (2017) 1-16.

37) A. Okamoto, E. Kushida, U. Yokobori, K. Kimura, α-hydroxyisobutyric acid ester compound, Fragrance material composition and use as fragrance material. Patent Application. EP 3816266A1, May 5, 2021.

38) J.M. Fraile, E. García-Bordejé, L. Roldán, Deactivation of sulfonated hydrothermal carbons in the presence of alcohols: Evidences for sulfonic esters formation, J. Catal. 289 (2012) 73-79.

39) A.C. Alba-Rubio, F. Vila, D. Martin Alonson, M. Ojeda, R. Mariscal, M. Lopez Granados, Deactivation of organosulfonic acid functionalized silica catalysts during biodiesel synthesis, Appl. Catal. B: Environ., 95 (2010) 279-287.

40) S. Sripada, J.R. Kastner, Catalytic esterification using solid acid carbon catalysts synthesized by sustainable hydrothermal and plasma sulfonation techniques, Ind. Eng. Chem. Res, 61 (2022) 3928-3940.

41) M. Rezayat, H.S. Ghaziaskar, Continuous synthesis of glycerol acetates in supercritical carbon dioxide using Amberlyst 15, Green Chem. 11 (2009) 710-715.

42) A.P. da Luz Corrêa, R.R.C. Bastos, G.N. da Rocha Filho, J.R. Zamian, L.R.V. da Conceicão, Preparation of sulfonated carbon-based catalysts from murmuru kernel shell and their performance in the esterification reaction, RSC Adv., 10 (2020) 20245-20256.

43) I. Miller, J.E. Freund, Probability and statistics for engineers, Prentice-Hall, Inc.: Englewood Cliffs, NJ, 1985.

44) P.Sangsiri, N. Laosiripojana, W. Laosiripojana, P. Daorattanachai, Activity of a sulfonated carbon-based catalyst derived from organosolv lignin towards esterification of stearic acid under near-critical alcohol conditions, ACS Omega, 7 (2022) 40025-40033.

45) S. Hosseini, J. Janaun, T. S.Y. Choong, Feasability of honeycomb monolith supported sugar catalyst to produce biodiesel from palm fatty acid distillate (PFAD), Process Saf. Environ. Prot., 98 (2015) 285-295.

46) Z. Liu, Y. Qi, M. Gui, C. Feng, X. Wang, Y. Lei, Sulfonated carbon derived from the residue obtained after recovery of essential oil from the leaves of *Cinnamomum longepaniculatum* using Bronsted acid ionic liquid, and its use in the preparation of ellagic acid and gallic acid, RSC Adv., 9 (2019) 5142-5150.

47) G. Fan, C Liao, T. Fang, S. Luo, G. Song, Amberlyst 15 as a new and reusable catalyst for the conversion of cellulose into cellulose acetate, Carbohydr Polym., 112 (2014) 203-209.

48) Z-Y. Wu, P. Yin, H-X. Ju, Z-Q. Chen, C. Li, S-C. Li, H-W. Liang, J-F. Zhu, S-H. Yu, Natural nanofibrous cellulose - derived solid acid catalyst, Research (Wash DC) 2019 (2019) 6262719.

49) T. Li, H. Zhang, Y. Li, J. Li, J. Wang, J. Xiao, Theoretical study on the unimolecular pyrolysis of thiophene and modeling, ACS Omega, 6 (2021) 20471-20482.

50) M. Cao, L. Peng, Q. Xie, K. Xing, M. Lu, J. Ji., Sulfonated *Sargassum horneri* carbon as solid acid catalyst to produce biodiesel via esterification, Bioresour. Technol. 324 (2021) 124614.

51) K. Ngaosuwan, J.G. Goodwin Jr., P. Prasertdham, A green sulfonated carbon-based catalyst derived from coffee residue for esterification, Renew. Energ., 86 (2016) 262-269.

52) W. Liu, G. Liu. Q. Kou, S. Xiao, Novel process for producing hierarchical carbide derived carbon monolith and low carbon ferromanganese from high carbon ferromanganese, RSC Adv., 7 (2017) 33875-33882.

53) F. Kanwal, A. Batool, M. Adnan, S. Naseem, The effect of molecular structure, band gap energy and morphology on the dc electrical conductivity of polyaniline/aluminum oxide composites, Mater. Res. Innov., 19 (2015) S8-354-S8-358.

54) J.B.A.J.H. Therese, R. Gayathri, K. Selvakumar, M. R. Prabhu, P. Sivakumar, Incorporation of sulfonated silica nano particles into polymer blend membrane for PEM fuel cell applications, Mater. Res. Express. 6 (2019) 115336.

55) H-Y. Chen, Z-W. Cui, A microwave- sensitive solid acid catalyst prepared from sweet potato via a simple method, Catalysts, 6 (2016) 211.

56) U.I. Nda-Umar, I. Ramli, E.N. Muhamad, N. Azri, Y. H. Taufiq-Yap, Optimization and characterization of mesoporous sulfonated carbon catalyst and its application in modeling and optimization of acetin production, Molecules, 25 (2020) 5221.

57) S.K. Kundu, A. Bhaumik, Novel nitrogen and sulfur rich hyper-cross-linked microporous poly-triazine-thiophene copolymer for superior CO_2 capture, ACS Sustainable Chem. Eng. 4 (2016) 3697-3703.

58) T.A. Nijhuis, A.E.W. Beers, F. Kapteijn, J.A. Moulijn, Water removal by reactive stripping for a solid-acid catalyzed esterification in a monolithic reactor, Chem. Eng. Sci. 57 (2002) 1627-1632.

59) A. Ciemiega, K. Maresz, J.J. Malinowski, J. Mrowiec-Bialon, Continuous-flow monolithic silica microreactors with arenesulphonic acid groups: structure-catalytic activity relationships, Catalysts, 7 (2017) 255.

60) A.K. Kolah, N.S. Asthana, D.T. Vu, C.T. Lira, D.J. Miller, Reaction kinetics of the catalytic esterification of citric acid with ethanol, Ind. Eng. Chem. Res., 46 (2007) 3180-3187.

61) M. A. Harmer, Q. Sun, Solid acid catalysis using ion-exchange resins, Appl. Catal. A-Gen, 221 (2001) 45-62.

62) L. Geng, Y. Wang, G. Yu, Y. Zhu, Efficient carbon-based solid acid catalysts for the esterification of oleic acid, Catal. Commun. 13 (2011) 26-30.

63) S. Suganuma, K. Nakajima, M. Kitano, D. Yamaguchi, H. Kato, S. Hayashi, M. Hara, Hydrolysis of cellulose by amorphous carbon bearing SO_3H, COOH, and OH groups, J. Am. Chem. Soc. 130 (2008) 12787-12793.

64) A.K. Mogalicherla, D. Kunzru, Effect of gas and liquid superficial velocities on the performance of monolithic reactors, Ind. Eng. Chem. Res., 49 (2010) 1631-1641.

65) M.T. Kreutzer, P. Du, J.J. Heiszwolf, F. Kapteijn, J.A. Moulijn, Mass transfer characteristics of three-phase monolith reactors, Chem. Eng. Sci., 56 (2001) 6015-6023.

66) I. Mueller, U. Brinkmann, E. Y. Kenig, Modeling of transport phenomena in two-phase film-flow systems: Application to monolith reactors, Chem. Eng. Commun. 198 (2011) 629-651.

67) B.M.E Russbueldt, W.F. Hoelderich, New sulfonic acid ion-exchange resins for the preesterification of different oils and fats with high content of free fatty acids, Appl. Catal. A- Gen, 362 (2009) 47-57.

68) P. Fernández, J.M. Fraile, E. García-Bordejé, E. Pires, Sulfonated hydrothermal carbons from cellulose and glucose as catalysts for glycerol ketalization, Catalysts, 9 (2019) 804.

69) X. Mo, D.E. López, K. Suwannakarn, Y. Liu, E. Lotero, J.G.Goodwin Jr., C. Lu, Activation and deactivation characteristics of sulfonated carbon catalysts, J. Catal., 254 (2008) 332-338.

70) G. Chen, X. Wang, Y. Jiang, X. Mu, H. Liu, Insights into deactivation mechanism of sulfonated carbonaceous solid acids probed by cellulose hydrolysis. Catal. Today, 319 (2019) 25-30.

71) D. Scholz, Prof. O. Kröcher, Prof. F. Vogel, Deactivation and regeneration of sulfonated carbon catalysts in hydrothermal reaction environments, ChemSusChem, 11 (2018) 2189-2201.

72) F. Jamil, A.H. Al-Muhtaseb, M. Naushad, M. Baawain, A. Al-Mamun, S. K. Saxena, N. Viswanadham, Evaluation of synthesized green carbon catalyst from waste date pits for tertiary butylation of phenol, Arab. J. Chem., 13 (2020) 298-307.

Table 4.1. Physical Properties of the Sulfonated Carbons and Amberlyst-15.

Catalyst	Surface Area ($m^2\ g^{-1}$)	Total acid density (mmol $H^+\ g^{-1}$)	SO_3H Density (mmol g^{-1})	Weak acid groups (COOH/OH) (mmol g^{-1})
Base-GAC	1350	3.13 ± 0.64	_	3.13 ± 0.64
Base-ACM	598	3.33 ± 0.50	_	3.33 ± 0.50
sGAC	867	3.80 ± 0.53	0.04 ± 0.01	3.76 ± 0.54
sACM	550	5.00 ± 0.80	0.12 ± 0.00	4.87 ± 0.80
Amberlyst-15*	38	6.80 ± 0.35	2.57 ± 0.29	4.22 ± 0.32

* Determined using sulfur content obtained from CHNS analysis.

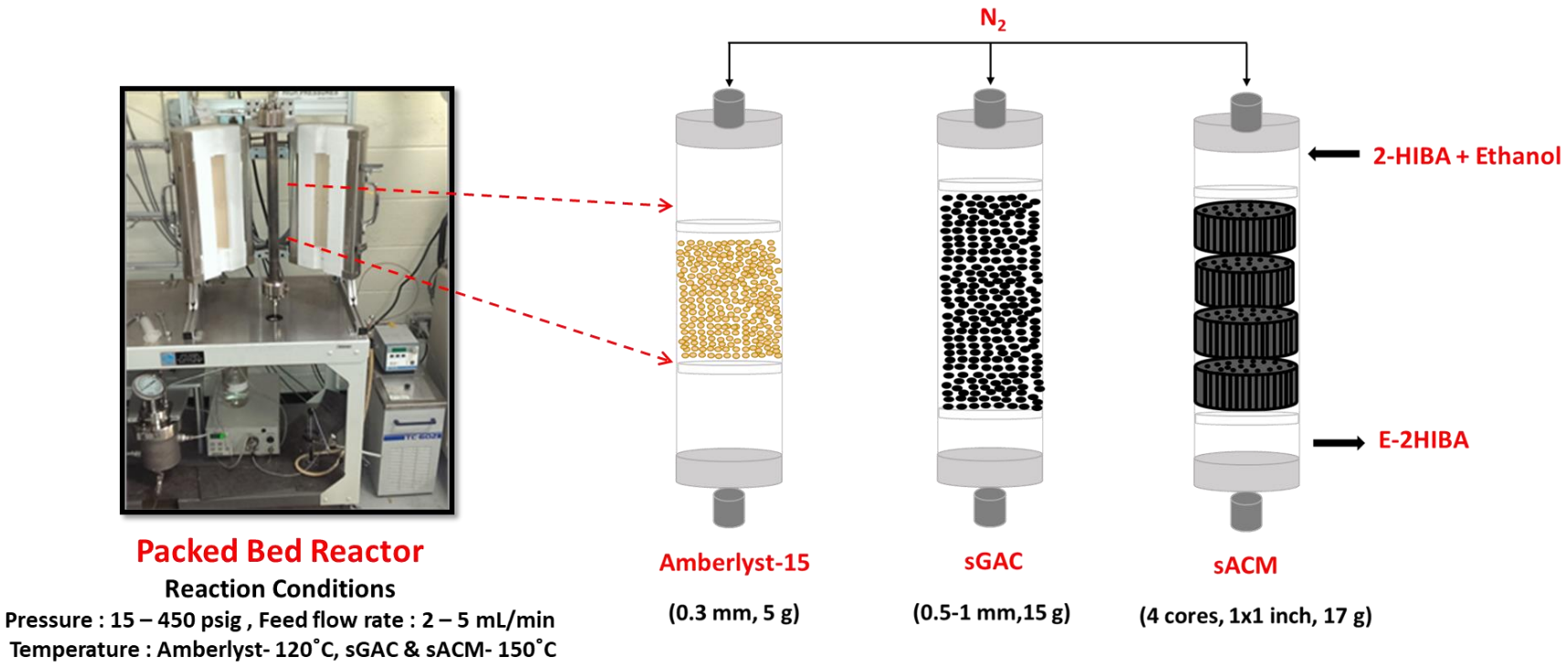

Figure 4.1. Experimental set-up for the continuous flow esterification of 2-HIBA in a Parr packed-bed reactor system with Amberlyst-15, sulfonated GAC (sGAC) and sulfonated ACM (sACM).

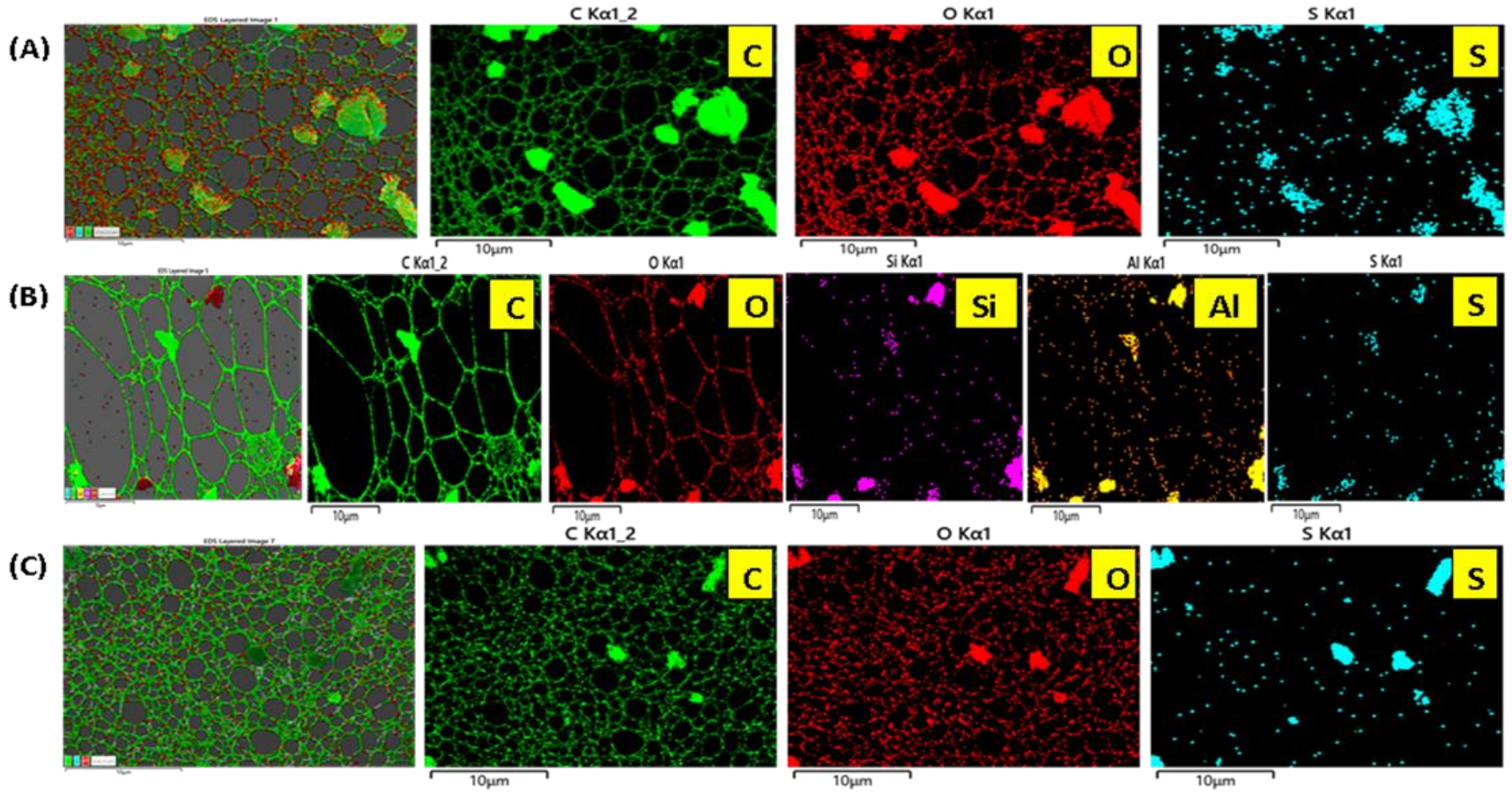

Figure 4.2. STEM-EDS images of the (A) sulfonated GAC (sGAC), (B) sulfonated ACM (sACM) and (C) Amberlyst-15.

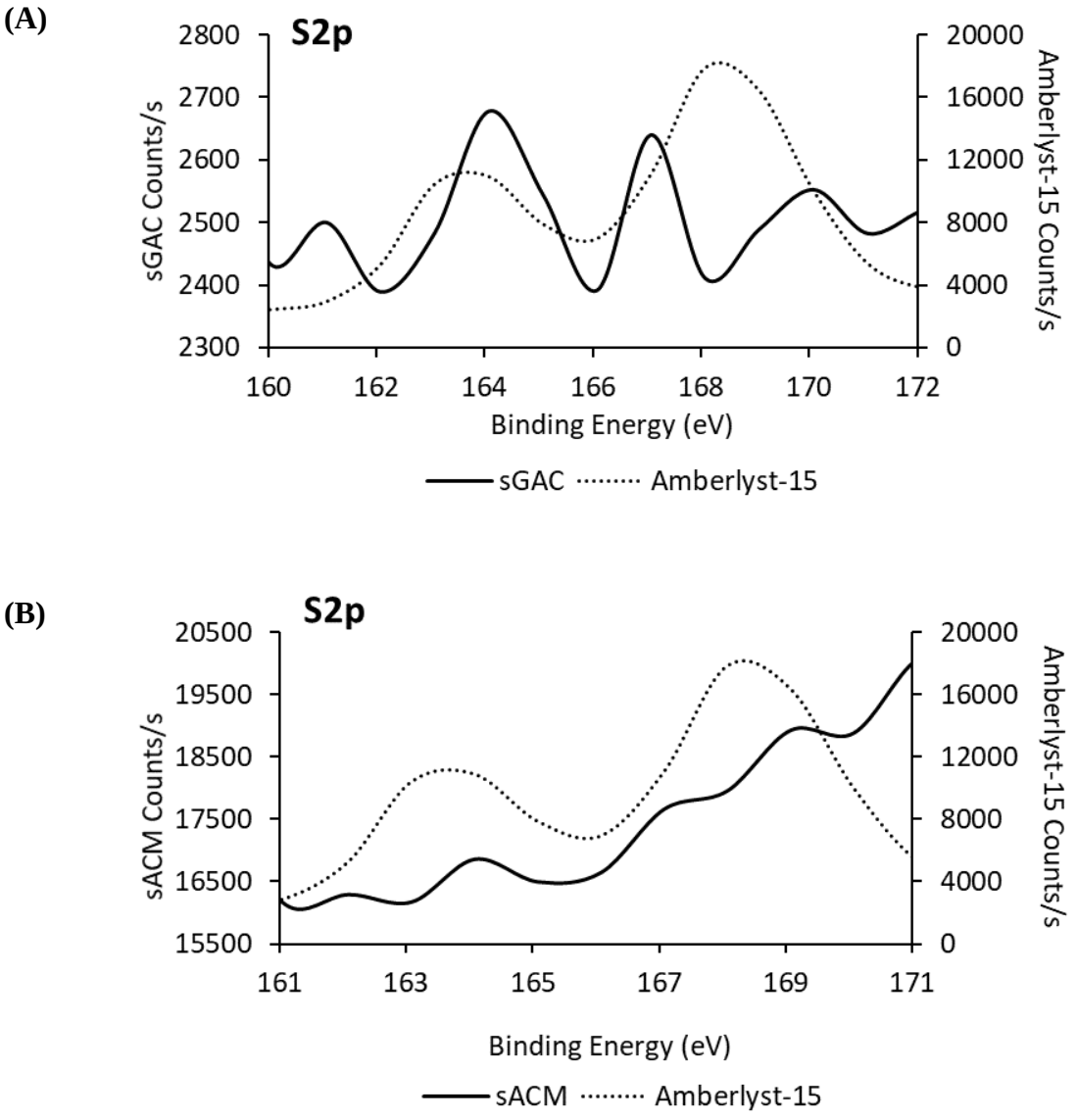

Figure 4.3. XPS Spectra overlay of (A) sulfonated GAC (sGAC) and (B) sulfonated ACM (sACM) with Amberlyst-15.

(A)

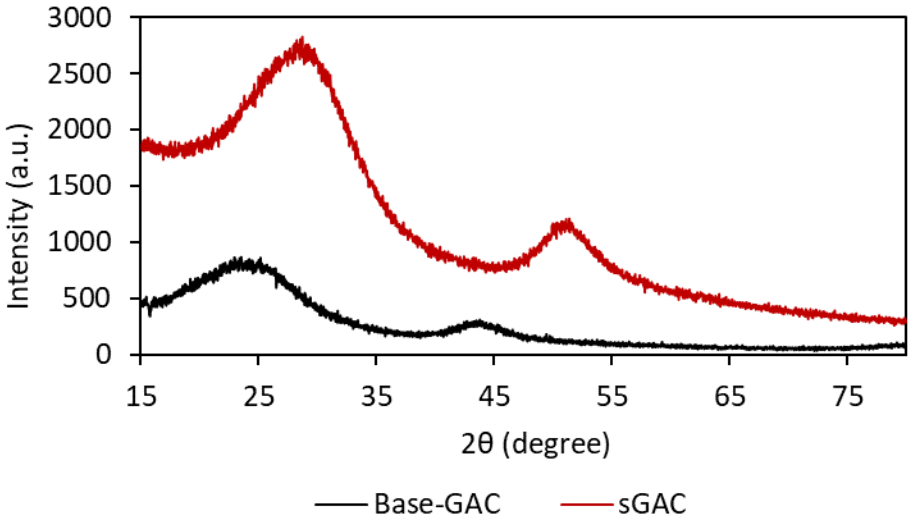

(B)

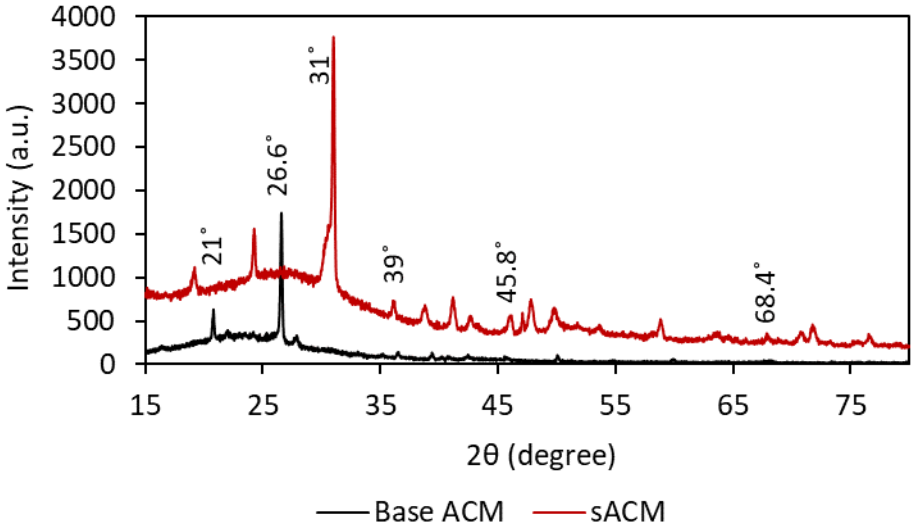

Figure 4.4. XRD analysis of the base (untreated) and sulfonated (A) GAC and (B) ACM.

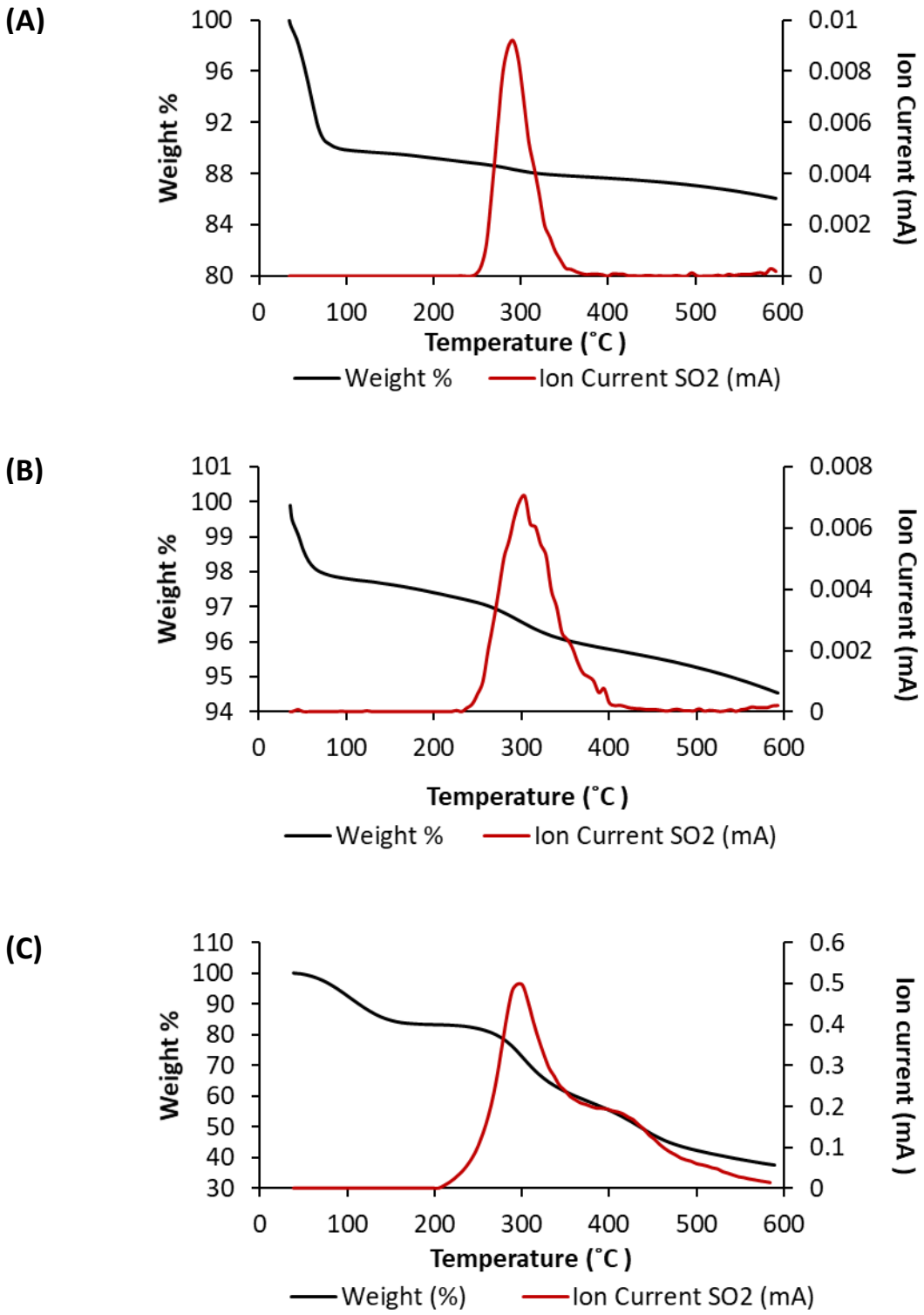

Figure 4.5. TGA analysis and associated mass spectra of sulfur dioxide evolved from the catalysts as a function of temperature for the (A) sGAC, (B) sACM, and (C) Amberlyst-15.

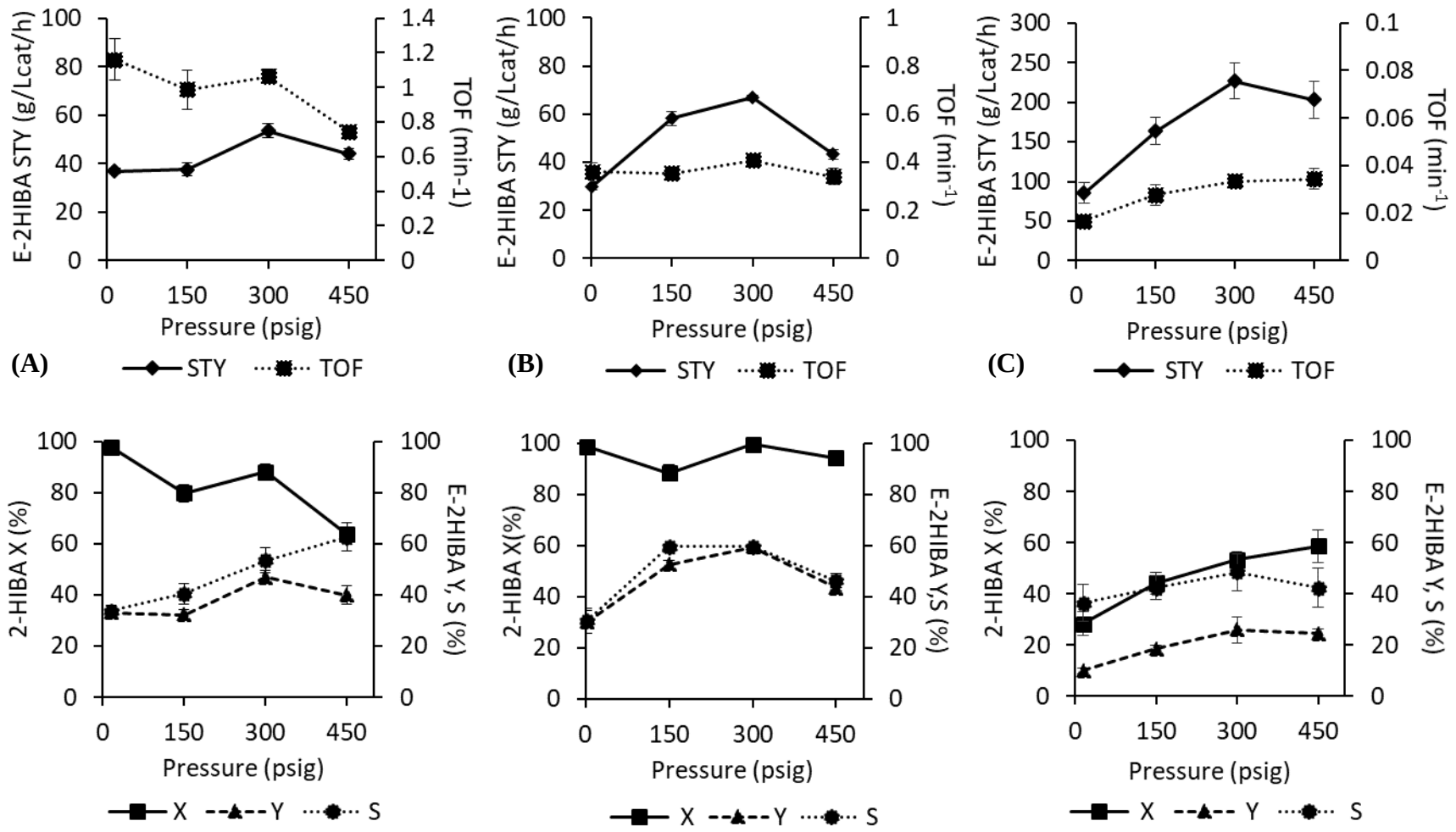

Figure 4.6. Effect of reaction pressure on E-2HIBA space time yield (STY), turn over frequency (TOF), 2-HIBA conversion (X), E-2HIBA yield (Y) and selectivity (S) for (A) sulfonated GAC (sGAC), (B) sulfonated ACM (sACM), and (C) Amberlyst-15. Reaction conditions: Q_l = 2 mL/min, T= 120 °C for Amberlyst-15 and 150 °C for sGAC and sACM.

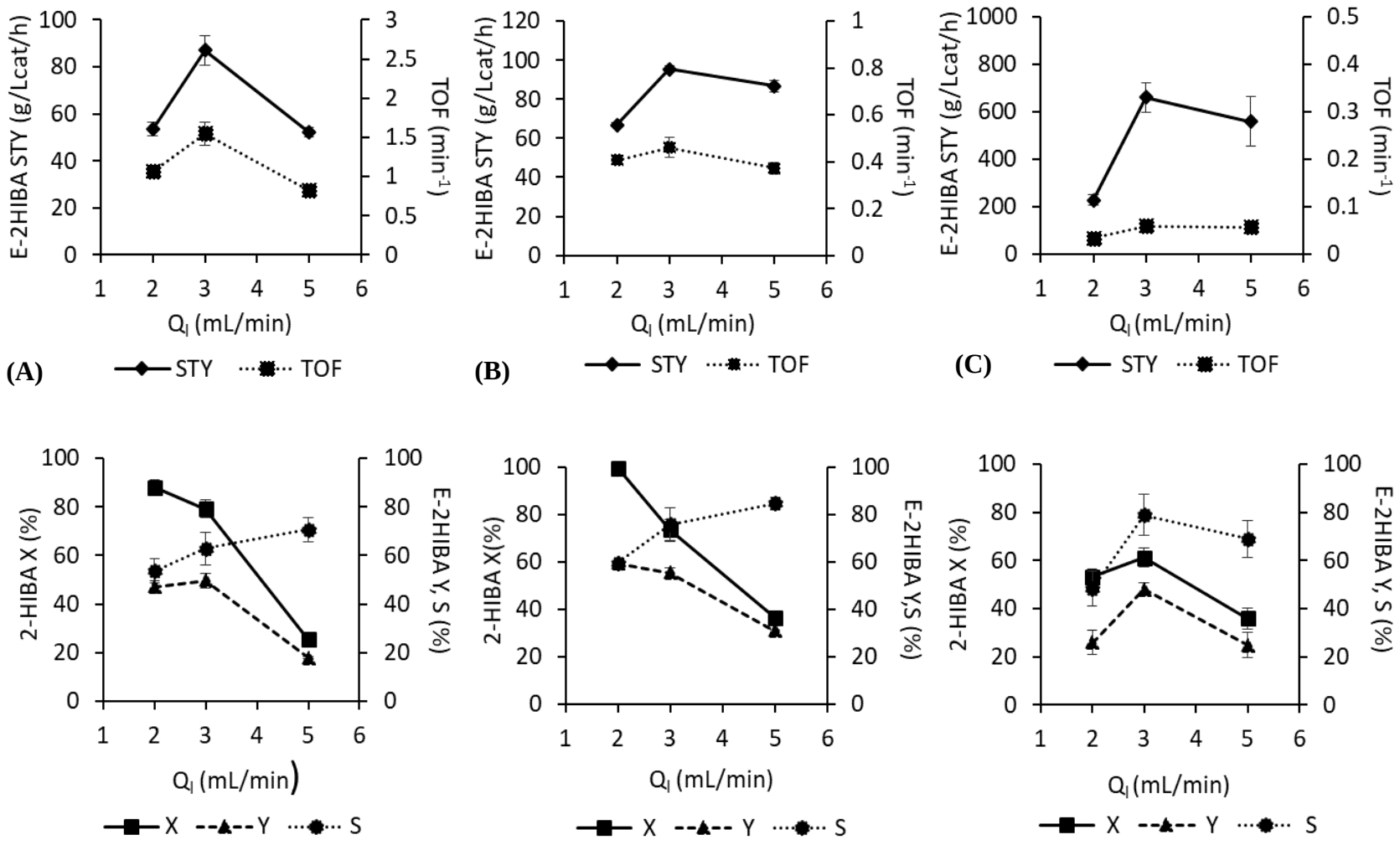

Figure 4.7. Effect of feed flow rate (Q_l) on E-2HIBA space time yield (STY), turn over frequency (TOF), 2-HIBA conversion (X), E-2HIBA yield (Y) and selectivity (S) for (A) sulfonated GAC (sGAC), (B) sulfonated ACM (sACM), and (C) Amberlyst-15. Reaction conditions: P= 300 psig, T= 120 °C for Amberlyst-15 and 150 °C for sGAC and sACM.

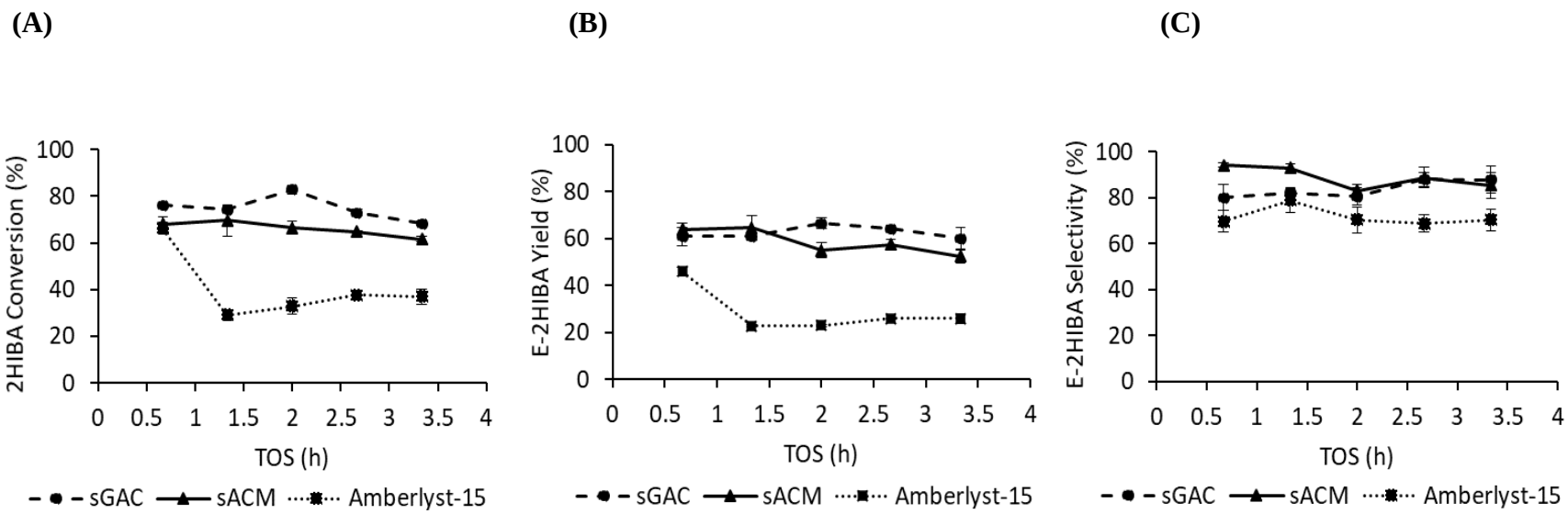

Figure 4.8. (A) 2-HIBA conversion, (B) E-2HIBA yield and (C) E-2HIBA selectivity for sulfonated GAC (sGAC), (B) sulfonated ACM (sACM), and Amberlyst-15. Reaction conditions: Q_l = 3 mL/min, P = 300 psig, T= 120 °C for Amberlyst-15 and 150 °C for sGAC and sACM.

CHAPTER 5

KINETICS OF 2-HYDROXYISOBUTYRIC ACID ESTERIFICATION USING SOLID ACID CARBON CATALYSTS

[1] Sripada S., Kastner J.R., 2023

To be submitted to *Chemical Engineering Journal*

Abstract

The kinetics of 2-hydroxyisobutyric acid (2-HIBA) esterification with ethanol was studied using sulfonated carbon catalysts in granular (sGAC) and monolith (sACM) forms in a continuous flow packed bed reactor. The effect of molar ratio of 2-HIBA and ethanol (1:10, 1:5 and 1:3) at different liquid residence times (τ= 3.09 to 9.24 min, Q_l = 2-6 mL/min) was investigated with the sGAC. The kinetics of the sACM catalyzed esterification were investigated at a 2-HIBA to ethanol molar ratio of 1:5 by varying the residence time (3.09 to 9.24 min) and compared with the GAC. The sACM displayed higher conversions and significantly higher space-time-yields (2.7 ×) compared to the sGAC (Q_l = 3 mL/min, τ = 6.18 min) due to higher surface area to volume ratio, high mass transfer rate, and water stripping effect. Eley-Rideal and Langmuir-Hinshelwood models were applied to fit the kinetic data, and the reaction system parameters were obtained through non-linear regression of the experimental data. Both ER and LH models showed satisfactory agreement with the experimental data with an R^2 of 0.92-0.95 and experimental-model concentration residuals ≤5%. From the LH model, the adsorption/desorption equilibrium constant of 2-HIBA was higher compared to the other reaction parameters, whereas in the ER model, the adsorption/desorption equilibrium constant of 2-HIBA was similar to that of water. Estimation of the external and internal mass transfer criteria indicated negligible effects of mass transfer. The developed kinetic model can be used for reactor design, particularly for solid acid monolith catalysts for the esterification of bio-based organic acids.

Keywords: Kinetics, Langmuir-Hinshelwood mechanism, Eley-Rideal mechanism, continuous esterification, sulfonated carbon

5.1 Introduction

Organic esters find widespread industrial applications in pharmaceuticals, solvents, cosmetics, lubricants, plasticizers, and fuels.[1,2] Esters of hydroxyacids are gaining attention owing to their industrial and medical applications. For instance, the esters of 2-hydroxyisobutyric acid (2-HIBA) have applications as biodegradable fragrance chemicals. The methyl ester of 2-HIBA (methyl 2-hydroxyisobutyrate) is used in electronic materials, and as an intermediate for agrochemicals and medicine, while the ethyl ester (ethyl 2-hydroxyisobutyrate) has applications as an industrial solvent.[3,4] Homogeneous acids such as sulfuric acid, hydrochloric acid and p-toluene sulfonic acid are widely used industrial esterification catalysts. [5] However, concerns related to equipment corrosion, formation of byproducts, difficulty in separation of the products from the catalyst and treatment of the effluent, has generated an interest in employing heterogeneous solid acid catalysts.[6]

Solid acid catalysts including ion exchange resins and zeolites have been widely employed for esterification reactions.[7,8] However, these solid acids are limited by their low surface area, and acidic resins like Amberlyst-15 have low thermal stability,[9] which limits their use in continuous reactions at high temperatures.[10] Sulfonated carbons have emerged as efficient, heterogeneous, solid acid substitutes for sulfuric acid due to their Bronsted acidity, large surface area, and synthesis from renewable and inexpensive woody biomass.[11,12] Currently, most solid acid carbon catalysts are synthesized from carbon in powdered/granular forms. Although such forms of carbon can be employed in batch, slurry, and trickle-bed reactors, their use in continuous processing is difficult as the particles undergo attrition, affecting catalyst recovery and longevity. High pressure drop and mass transfer limitations are among other concerns.[13] With the fine/specialty chemical industry tending towards continuous processes,[14] owing to easier

automation, safer long-term operation,[15] economic viability and high productivity,[16] there is a need for more efficient and reusable structured catalysts.[17] Activated carbon monolith (ACM) can overcome the obstacles with the powdered/granular forms as it combines the benefits of an activated carbon support (large surface area, stability in acidic, basic, and aqueous environments) and the monolithic structure into a single composite catalyst. Moreover, these structured catalysts confer the advantages of a high interfacial mass transfer rate, low pressure drop, and easy scale-up which facilitates their use in continuous processing. [13]

Several authors have studied esterification kinetics using solid acid catalysts including heteropolyacid based ionic liquids, ion exchange resins, and mesoporous silica catalysts and proposed pseudohomogeneous (PH), Eley-Rideal (ER) and Langmuir-Hinshelwood (LH) models. [18,19,20] Few authors have investigated esterification kinetics using sulfonated carbon in granular forms. Shuit and Tan used a PH model to describe the esterification of palm fatty acid distillate with methanol using sulfonated-multi-walled carbon nanotubes.[21] Bhusari and coworkers found that an ER model was a better fit for the experimental data for the esterification of acetic acid with n-butanol using a sulfonated carbon catalyst.[22] However, there is very little information on the kinetics of esterification reactions using solid acid carbon monoliths. Nakhate and Yadav developed a power law model for the esterification of levulinic acid with benzyl alcohol in a batch reactor system using a sulfonated carbon-based graphene oxide monolith. [23]

The above-mentioned kinetic studies were performed in batch reactors. The inherent non-steady state, and the occurrence of concentration and temperature gradients can lead to inaccurate results when assuming an ideal batch reactor kinetic model.[24] Continuous flow reactors allow more accurate measurements of reaction rates and kinetics, as well as product yields, selectivity, and space-time-yields.[10] Chu and coworkers studied the continuous vapor phase esterification of

acetic acid with ethanol and n-butanol using a dodecatungstosilicic acid on activated carbon catalyst and observed a dual site LH mechanism for ethanol and a single site ER mechanism for n-butanol.[25] However, there is limited information on the kinetics of continuous esterification reactions using solid acid carbon monolith catalysts.

Esterification reactions generate water as a byproduct. Since esterification is a reversible, equilibrium-limited reaction, the presence of water may inhibit the activity of the acid catalyst, negatively impacting the conversion and reaction rate. [26] In-situ stripping of water produced during the reaction using a gas flow through the reactor can avoid catalyst deactivation. Further, this water stripping effect may be more pronounced in monoliths compared to granular catalysts since the gas flow through the monolith channels can strip the water that partitions into the vapor phase. Beers and coworkers demonstrated the counter-current stripping of water using nitrogen in the esterification of hexanoic acid and 1-octanol using a zeolite coated monolith catalyst.[26]

While various authors have developed kinetic models for solid acid catalysts such as ion exchange resins,[27,28,29] limited information is available on the kinetics of solid acid carbon catalyzed esterification, particularly using solid acid carbon monolith catalysts. Previously, we developed a continuous process for the esterification of 2-HIBA with ethanol using the sulfonated carbon catalysts in granular (sGAC) and monolith (sACM) forms. The objective of this work was to investigate and compare kinetics and develop a kinetic model for 2-HIBA esterification over the sGAC and sACM catalysts. The experimental kinetic data were correlated with single site Eley-Rideal and dual site Langmuir-Hinshelwood models. In addition, the effect of mass transfer on the reaction kinetics of the monolith relative to the granular carbon was studied. A kinetic model was proposed to aid in scale-up and reactor design for the esterification of bio-based organic acids using granular and monolithic sulfonated carbon catalysts.

5.2 Experimental Section

5.2.1 Materials

2-hydroxyisobutyric acid ($C_4H_8O_3$, purity > 98%) and ethyl 2-hydroxyisobutyrate ($C_6H_{12}O_3$, purity > 98%) were purchased from TCI chemicals. 200 proof ethanol (purity >99.5%), sulfuric acid used for carbon sulfonation, and Amberlyst-15 (hydrogen form) were procured from Sigma Aldrich. Two catalysts were used in this study, a sulfonated granular activated carbon catalyst (sGAC), and a sulfonated activated carbon monolith (sACM). The wood-based granular activated carbon (GAC) (surface area of 1350 m^2/g and pore volume of 1.2 cc/g) and activated carbon monolith (ACM 101-H) were provided by Applied Catalysts (Laurens, SC) and the ACM was manufactured by coextrusion of 50% activated carbon and 50% of a ceramic binder. The monolith properties have been previously reported[13] and each monolith core has a diameter and length of 1 inch, 400 cells/in^2, wall thickness of 0.01- inch, cell spacing of 0.044- inch, geometric surface area of 70.8 in^2/in^3, open frontal area of 0.59 in^2, density of 350 kg/m^3, surface area of 598 m^2/g (BET), pore diameter of 29.8 Å and pore volume of 0.5 cc/g (BJH).

5.2.2 Catalyst Preparation

The sulfonated granular and monolithic catalysts were synthesized as described previously.[30] The base granular activated carbon (GAC) was crushed and sieved to a particle size of 0.5-1 mm, washed until constant pH (3 ×) to eliminate any contaminants (initial pH was ~9.0) and dried at 105 °C. Sulfuric acid (2M) was introduced into the GAC by incipient wetness impregnation at 1.2 mL/g catalyst (1.2:1 [v/w] sulfonating agent: carbon ratio), according to the pore volume of the GAC (1.2 mL/g), to ensure all particles were sufficiently wetted. The monolith cores (ACM) were immersed into 2M H_2SO_4 (100 mL) and sonicated at 30 °C for 30 minutes as reported

previously. [30] Subsequently, the GAC and ACM were treated hydrothermally at 180 °C and 250 °C respectively for 12 h. Post treatment, the sulfonated GAC and ACM cores were washed with deionized water (25-50 mL/g catalyst) at room temperature to remove traces of excess acid (H_2SO_4), to ensure the catalytic activity was solely due to the sulfonated carbon. The sulfonated ACM cores were washed by sonication in deionized water. Washing (8-12 ×, 1 h washes) was carried out until the filtrate displayed a constant pH, (approximately 4.0 for the GAC and ACM catalysts). Post-washing, all catalysts were dried in a hot air oven at 105 °C overnight.

5.2.3 Analytical

The liquid product sample collected from the reactor was analyzed using HP 5890 Series II gas chromatography equipped with a flame ionization detector (GC-FID) and a HP Innowax column (30 m × 0.25 mm × 0.25 mm). The GC-FID was operated with the method of inlet temperature 240 °C, detector temperature 250 °C, initial oven temperature of 45 °C for 2.5 minutes followed by a ramp of 10 °C /min for 21 minutes and then held at 230 °C for 4 minutes. 1 μL of each sample was injected on the GC-FID in triplicate. [30] The concentrations of 2-HIBA, E-2HIBA, and ethanol were determined using 5-point standard curves. The standards for 2-HIBA and E-2HIBA were prepared in ethanol, while standards for ethanol were prepared using methanol as the solvent. The concentrations for water were estimated based on stoichiometry and the conversion of 2-HIBA.

5.2.4 Catalytic Esterification

2-HIBA esterification reactions were performed in a continuous flow reactor system designed by Parr Instrument Company as described previously.[31] The liquid feed (2-HIBA in ethanol) and nitrogen (50 mL/min) were continuously passed through the stainless-steel packed bed reactor

(Parr, Moline, IL) (1-inch inner diameter) concurrently downwards through a T-junction. The gas flow rate was controlled by a Brooks Delta II Smart Mass Flow Controller, while the liquid feedstock was pumped into the reactor using a Scientific Systems LD-Class HPLC pump. The catalyst (5 g sGAC, 5 g sACM-1 core packing height of 3.5 cm) was held in place by a stainless-steel screen and quartz wool above and below the bed. The reactor temperature was controlled by a Thermcraft Lab-Temp 1760-watt furnace powered by a Parr 4875 Power Controller and the pressure was regulated with a TESCOM back pressure regulator. Post reaction, the liquid product was collected in a condenser (stainless steel vessel with a cooling jacket) connected to a Brookfield TC-602 water bath maintained at 6 °C.

To study the kinetics of 2-HIBA esterification with the sGAC, a series of reactions were performed at 150 °C, 300 psig at different liquid residence times (Q_l : 2-6 mL/min) with 2-HIBA to ethanol molar ratios of 1:10, 1:5 and 1:3. These reaction conditions were chosen as they were found to be optimal for achieving high ester space-time yields and selectivity from our previous continuous esterification work. [31] A fresh batch of catalyst was used to study the kinetics at each molar ratio.

For all continuous reactions, the main kinetic parameters including conversion (X = mol 2-HIBA converted/mol 2-HIBA fed), yield (Y= mol E-2HIBA produced/mol 2-HIBA fed), and selectivity (S = mol E-2HIBA produced/mol feed converted) were determined. Liquid hourly space velocity (LHSV, 1/h) was calculated from $[Q_{in} * \rho_{cat}]/W$, and ester space time yield (STY, g/L-cat/h) as $[F_{out} * \rho_{cat} * MW]/W$ where Q_{in} is the inlet volumetric molar flow rate (mL/min), ρ_{cat} is the bulk density of the catalyst, F_{out} is the outlet molar flow rate, W is the catalyst mass, and MW is the molecular weight.

5.2.5 Determination of Equilibrium Constant

To determine the equilibrium constant, batch esterification experiments of 2-HIBA were performed in 75 mL autoclave batch reactors (Parr Series 5000 Multiple Reactor System) at a temperature of 150 °C, pressure of approximately 9 bar and a residence time of 8 h. An 8 h residence time was considered sufficient time to ensure chemical equilibrium had been attained in the reaction system.[32] A working volume of 20 mL (357 gL^{-1} 2-HIBA in ethanol, 2-HIBA: ethanol molar ratio of 1:5) and catalyst (1 g sGAC/sACM) was mixed using a magnetic stir bar (700 rpm). The reactor headspace was pressurized with nitrogen at 1.6 bar, then heated to the set-point at 10 °C /min. Heat up times were approximately 15 min and the reaction pressure increased from 1.6 bar to 9 bar at a temperature of 150 °C. On completion of the reaction, the vessel was cooled down by quenching in ice. After depressurizing the reactor, the reaction mixture and catalyst were recovered and the catalyst was separated via filtration (Whatman, 11 μm pore size). The filtrate was collected and analyzed by GC-FID.[30]

With the assumption of reversible overall second order rate kinetics, the concentration-based equilibrium constant (assuming ideal solution) can be determined using the following equation,[33]

$$K_{eq} = \frac{k_f}{k_r} = \frac{[E2HIBA][H_2O]}{[2HIBA][EtOH]} = \frac{X_{eq}^2}{(1 - X_{eq})(MR - X_{eq})}$$

Equation 5.1

Where K_{eq}, k_f, k_r, X_{eq} and MR are the equilibrium constant, forward rate constant, reverse rate constant, equilibrium conversion and molar ratio of ethanol and 2-HIBA, respectively. [E-2HIBA], [H_2O], [2-HIBA] and [EtOH] are the equilibrium concentrations of E-2HIBA, water, 2-

HIBA, and ethanol, respectively. The equilibrium conversions and equilibrium constants obtained for the sGAC and sACM are presented in Table 5.1.

5.2.6 Kinetic Modeling

To study the kinetics of 2-HIBA esterification with ethanol over the sulfonated carbon catalysts, initially, the effect of acid to alcohol molar ratio on sGAC catalytic activity was investigated. A series of experiments were performed at 2-HIBA to ethanol molar ratios of 1:10, 1:5, and 1:3 (2-HIBA concentrations of 178 g/L, 357 g/L and 594 g/L) at residence times (5 time points) ranging from 3.09 to 9.24 min (Q_l = 2 - 6 mL/min) at 150 °C and 300 psig. A molar ratio of 1:1 could not be studied due to the immiscibility of 2-HIBA in ethanol at such a high 2-HIBA concentration (approximately 1700 g/L). Further the kinetics of the sACM catalyzed esterification was studied at a 2-HIBA to ethanol molar ratio of 1:5 by varying the residence time between 3.09 to 9.24 min. Kinetic modeling was performed by fitting the experimental concentrations obtained as a function of space time (τ) for the 1:5 molar ratio for both catalysts to the Langmuir-Hinshelwood (LH) and Eley-Rideal (ER) models. The LH model assumes that both reactants are adsorbed onto the active sites of the catalyst while the ER model assumes that one of the adsorbed reactants interacts with the other reactant in the bulk phase.

5.2.7 Mass Transfer Calculations

The Mears and Weisz -Prater criteria were used to determine if external or internal mass transfer resistance affected the kinetic analysis. Mears criterion is evaluated using the relation[34]

$$\frac{-r_A' \rho_b Rn}{k_c C_{Ab}} < 0.15$$

Equation 5.2

where $-r'_{2HIBA}$ is the reaction rate for 2HIBA (mmol g^{-1} s^{-1}), ρ_b is the bulk density (kg m^{-3}) , R is the catalyst particle radius (in m, for the sACM, R= wall thickness/2 i.e., 1.27 × 10^{-4} m) n, the reaction order (we calculated the Mears criterion assuming a second order reaction), k_c is the mass transfer coefficient (m s^{-1}) and $C_{2HIBA,b}$ is the bulk liquid phase concentration of 2-HIBA (mol dm^{-3}). A Mears criterion value less than 0.15 indicates the reaction is not externally mass transfer limited. The Wilke-Chang equation was used to determine the liquid phase diffusion coefficient of 2-HIBA in the 2-HIBA/ethanol mixture.

$$D_{\mathrm{AB}} = \frac{1.17 \times 10^{-1} \sqrt[3]{\varepsilon_B M_B} T}{\mu_B v_A^{0.6}}$$

Equation 5.3

Where T is the absolute temperature, M_B is the molecular weight and μ_B is the viscosity of ethanol (cP), ε_B is the association factor of ethanol (1.5) and V_A is the molar volume of 2-HIBA (0.125 m^3 mol^{-1}). Assuming a tortuosity factor (τ) of 4 and internal void fraction (ε) of 0.5, the effective diffusivity D_e was calculated using the relation,

$$D_e = \frac{\varepsilon}{\tau} D_p$$

Equation 5.4

The mass transfer coefficient (k_c) for the sGAC was estimated from the relation,

$$k_C = 0.266 \left(\frac{D_{AB}}{\mathrm{d}_p}\right) \mathrm{Re}^{1.15} Sc^{1/3}$$

Equation 5.5

In this work, the liquid superficial velocity ranged from 6.6 – 19.8 × 10^{-5} m s^{-1}, while the gas superficial velocity was 16.5 x 10^{-4} m s^{-1}. Therefore, the gas/liquid velocity ratio ranged from 25 (Q_l= 2 mL/min) to 8.33 (Q_l= 6 mL/min), indicating that the reactions with the sACM were performed under film flow (Q_g/Q_l = 6 to 200).[13] We thereby assumed that 2-HIBA was

transported from the bulk liquid phase (ethanol) to the solid catalyst through a thin film. The liquid-solid mass transfer coefficient for the sACM was estimated using the film mass transfer coefficient correlation given by Liapis and co-workers.[35]

$$\frac{k_f}{D_e} = Sh = \alpha_1 \mathrm{Pe}^{1/3}$$

Equation 5.6

k_f is the film transfer coefficient, λ is the average pore diameter (nm), Sh is the Sherwood number, α_1 is a proportionality constant and is 1 for monoliths of cylindrical geometry. The Peclet number is given by,

$$Pe = \frac{v_m \lambda}{De}$$

Equation 5.7

where ν_m is the liquid superficial velocity (m/s).

The Weisz-Prater criterion was used to assess the effect of internal diffusion limitations within the catalysts and was calculated according to the equation,

$$C_{WP} = \eta \phi_1^2 = \frac{-r_A'(obs)\rho_c R^2}{D_e C_{As}}$$

Equation 5.8

where $-r'_A$ is the observed rate of reaction (mol/gcat.s), ρ_c is the catalyst density (kg/m^3) , R is the catalyst particle radius (m), D_e is the effective diffusivity (m^2/s) , $C_{A,s}$ is the concentration of 2-HIBA at the catalyst surface (mol/m^3), η is the internal effectiveness factor and ϕ is the Thiele modulus. A $C_{WP} << 1$, indicates the absence of internal diffusion limitations in the catalyst pellet; however, if $C_{WP} >> 1$, then internal diffusion severely limits the reaction.

5.2.8 Statistical Analysis

The GC-FID analyses were performed in triplicate and reported as the mean and sample standard deviation. The sample standard deviation was calculated from the range (R) for small sample size (n) (for $n \leq 5$, R/d_2, where $d_2 = 1.128$).[36] A Student's t-test was performed in the analysis between two means (i.e., catalysts) for the E-2HIBA STY and 2-HIBA conversion, assuming the null hypothesis with the reported level of significance (α).

5.3 Results and Discussion

5.3.1 Effect of Molar Ratio

Figure 5.1 depicts the kinetics of 2-HIBA esterification over the sulfonated GAC at 150 °C and 300 psig at different 2-HIBA to ethanol molar ratios (1:10, 1:5, 1:3). Increasing the 2-HIBA to ethanol to molar ratio (excess of alcohol at 1:10 MR) led to higher 2-HIBA conversion, particularly at the lower flow rates or longer residence time (6.18-9.24 min). Various authors have previously reported an increase in conversion on increasing the alcohol to acid molar ratio. While studying the kinetics of acetic acid esterification with methanol, Sert and Atalay noted an increase in conversion on varying the molar ratio of acetic acid to methanol from 0.5 to 2.[37] Similarly, Mekala and coworkers reported an increase in acetic acid conversion (from 68.9 to 92.9%) with increase in molar ratio of acetic acid to methanol from 1:1 to 1:4.[38] Further, we noted higher E-2HIBA yield (38.1%, 6.18 min) at the higher 2-HIBA to ethanol molar ratio. Lauwaert and co-workers also reported an increase in esterification rate, and higher ester yield on increasing the acid to alcohol molar ratio from 1:1 to 1:10 while studying the kinetics of acetic acid and methanol esterification.[39] Further, higher ester space-time-yields were observed at a residence time of 6.18 min (Q_l= 3 mL/min) at all 2HIBA to ethanol molar ratios which could

be attributed to enhanced fluid-catalyst mass transfer in the system and the possibility of mass transfer limitations at the longer residence time (Q_l = 2 mL/min). Similar results were noted in our previous work on the continuous catalytic esterification of 2-HIBA with the sGAC.[30]

Figure 5.2 depicts the kinetics of 2-HIBA esterification over the sulfonated ACM at 150 °C and 300 psig at a 2-HIBA to ethanol molar ratio of 1:5. We observed an increase in 2-HIBA conversion from 25.6% to 60.7% on increasing the residence time from 3.09 to 9.24 min. A higher E-2HIBA STY of 1675 g/Lcat/h, was observed at 6.18 min (Q_l = 3 mL/min). The lower E-2HIBA STY and selectivity (1060 g/Lcat/h, 45.9%) at 9.42 min could be due to mass transfer limitations at the longer residence time (Q_l = 2 mL/min).[30]A comparison of the sGAC and sACM, indicates higher conversion (α = 0.05, level of significance) and significantly higher space-time-yields (2.7 ×) (α = 0.05, level of significance) with the sACM (Figure 5.3). The higher conversion and STY obtained with the sACM could be due to the larger surface area to volume ratio that resulted in higher acid site density, and improved mass transfer. Further, co-current stripping of water produced during the reaction by the carrier gas nitrogen may have enhanced the performance of the sACM compared to its granular counterpart. Similar results were observed in our previous work comparing the continuous catalytic esterification of the sGAC and sACM at a 2-HIBA to ethanol molar ratio of 1:44.[30] Beers and coworkers also reported higher conversion with a BEA coated monolith in the esterification of hexanoic acid and 1-octanol (160 °C, 130 min, 1 atm) with counter-current stripping of water by nitrogen (87% conversion with counter-current stripping of water vs 75% in the no-stripping configuration.[26]

5.3.2 Mass Transfer Analysis

The external (Mears) and internal (Weisz-Prater) mass transfer criteria were determined for the range of flow rates (Q_l = 2-6 mL/min) applied in this work for sGAC and sACM at a 2HIBA to

ethanol molar ratio of 1:5. For both catalysts at all flow rates, the Mears criterion was below 0.15 suggesting the reaction systems were not externally mass transfer limited under the conditions studied (LHSV range of 6.5-19.4 /h for the sGAC and 8.8-26.5 /h for the sACM). The Weisz-Prater (C_{WP}) values were << 1, indicating the absence of internal mass transfer limitations. The estimated Mears and C_{WP} values for the sGAC and sACM are included in Appendix C (Table S5.1 and Table S5.2).

5.3.3 Kinetic modeling of 2-HIBA esterification

The kinetic model of 2-HIBA esterification with ethanol catalyzed by the sulfonated GAC and ACM was evaluated using LH and ER reaction mechanisms. Both LH and ER kinetic models assuming surface reaction as the rate-limiting step were applied to correlate the kinetic experimental data obtained for the sGAC and sACM by varying the liquid residence time at a 2-HIBA to ethanol molar ratio of 1:5 (150 °C, 300 psig, 50 mL/min N_2). The same batch of catalyst was used for all five runs for both the sGAC and sACM.

The esterification of 2-HIBA with ethanol is a reversible reaction as show below.

$$2HIBA + EtOH \longleftrightarrow E2HIBA + H_2O$$

The LH model assumes that both reactants (2-HIBA and ethanol) are adsorbed onto the active sites of the catalyst (Figure 5.4). The rate of the surface reaction for the LH mechanism can be written as,

$$r = k_f C_{2HIBAs} C_{EtOHs} - k_r C_{E2HIBAs} C_{H_2Os} \qquad \text{Equation 5.9}$$

The rate expression for the LH model can be given by equation,

$$r = k_f K_{2HIBA} K_{EtOH} C_0^2 \frac{C_{2HIBA}C_{EtOH} - \frac{1}{K} C_{E2HIBA}C_{H_2O}}{[1 + K_{2HIBA}C_{2HIBA} + K_{EtOH} C_{EtOH} + K_{E2HIBA}C_{E2HIBA} + K_{H_2O}C_{H_2O}]^2}$$

Equation 5.10

The ER model assumes that the reaction takes place between adsorbed molecules of 2-HIBA and ethanol molecules in the bulk solution and considers the adsorption of water on the catalyst surface (Figure 5.4). The rate of the surface reaction for the ER mechanism can be written as,

$$r = k_f \ C_{2HIBAs}C_{EtOH} - k_r \ C_{E2HIBA}C_{H2Os}$$ Equation 5.11

The rate expression for the ER model can be given by equation,

$$r = k_f C_0 K_{2HIBA} \ \frac{\left[C_{2HIBA}C_{EtOH} - \frac{1}{K} C_{E2HIBA}C_{H2O}\right]}{1 + K_{2HIBA} \ C_{2HIBA} + K_{H2O}C_{H2O}}$$

Equation 5.12

The derivations for the rate equations are provided in the supporting information (Appendix C). In the rate equations, k_f is the forward reaction rate constant (mol/g/min), C_0 is the total concentration of active sites, K_i is the adsorption/desorption equilibrium constant of species 'i' , K is the surface reaction equilibrium constant, C_{2HIBA}, C_{EtOH}, C_{E2HIBA}, C_{H2O} and C_{2HIBAs}, C_{EtOHs}, $C_{E2HIBAs}$, C_{H2Os} are the concentrations of 2-HIBA, ethanol (EtOH), E-2HIBA, and water in the bulk liquid phase and adsorbed on the catalyst surface respectively.

For a packed bed reactor system, with the assumption of constant volumetric flow rate and catalyst mass ($\rho_B \times V_b$)

$$r_i = \left(\frac{1}{\rho_B}\right)\left(\frac{dC_i}{d\tau}\right)$$

Equation 5.13

$$\tau = \frac{V_b}{Q_i}$$ Equation 5.14

Where ρ_B is the bulk density of the catalyst, V_b is the packed bed volume and τ is the reactor space time.

For the rate expression for the LH model, denoting the denominator in equation 5.10 divided by ρ_B as R,

$$R = \frac{[1 + K_{2HIBA}C_{2HIBA} + K_{EtOH}C_{EtOH} + K_{E2HIBA}C_{E2HIBA} + K_{H_2O}C_{H_2O}]^2}{\rho B}$$ Equation 5.15

Defining the consumption of 2-HIBA as – (r_1) and the formation of E-2HIBA as (r_2), two differential equations are obtained for the LH model.

$$\frac{dC_{2HIBA}}{d\tau} = \frac{-kf\ K_{2HIBA}\ C_{2HIBA}}{R}$$ Equation 5.16

$$\frac{dC_{E2HIBA}}{d\tau} = k_f\ K_{2HIBA}\ K_{EtOH}\ \frac{\left[C_{2HIBA}C_{EtOH} - \frac{1}{K}C_{E2HIBA}C_{H_2O}\right]}{R}$$ Equation 5.17

Similarly, for the rate expression for the ER model, denoting the denominator in equation 5.12 divided by ρ_B as S,

$$S = \frac{[1 + K_{2HIBA}\ C_{2HIBA} + K_{H2O}C_{H2O}]}{\rho_B}$$ Equation 5.18

Defining the consumption of 2HIBA as – (r_1) and the formation of E-2HIBA as (r_2), two differential equations are obtained for the ER model.

$$\frac{dC_{2HIBA}}{d\tau} = \frac{-k_f K_{2HIBA}\ C_{2HIBA}}{S}$$ Equation 5.19

$$\frac{dC_{E2HIBA}}{d\tau} = k_f K_{2HIBA} \frac{\left[C_{2HIBA}C_{EtOH} - \frac{1}{K}C_{E2HIBA}C_{H2O}\right]}{S}$$ Equation 5.20

The ODEs were solved to determine the rate constants, and adsorption/desorption constants by fitting the concentration data for the sGAC and sACM (Tables 5.2 and 5.3). MATLAB's ODE45 solver was used to solve the kinetic model, to predict the forward rate constant and adsorption/desorption equilibrium constants. The goodness of fit was calculated as R^2 by minimizing the residual sum of squares (RSS) between the experimental and predicted concentrations of each component with time using equation 5.21.

$$RSS = \sum \left(C_{\exp} - C_{predicted}\right)^2$$ Equation 5.21

The LH and ER surface reaction models showed satisfactory agreement with the experimental data (Table 5.4, Figure 5.5) with R^2 ranging between 0.92-0.95, suggesting that the reaction mechanism depends on the interaction between the reactants and acid sites of the sulfonated carbon catalysts. Very few studies have investigated the esterification kinetics over sulfonated carbon catalysts, yet both ER and LH models have been employed to describe the kinetics of solid acid catalyzed esterification reactions.[40,41] Since we could not obtain kinetic data for 2-HIBA esterification from the literature, we compared our results with reversible esterification performed with other acid-alcohol systems. The predicted adsorption/desorption equilibrium constants agree with previous studies on reversible esterification reactions. An ER model for the esterification of butyric acid with n-butanol over a Dowex 50Wx8-400 catalyst assuming surface reaction as the rate-limiting step gave similar forward rate constants and slightly lower acid equilibrium adsorption constants to the constants obtained over the sGAC and sACM. An LH model over the same Dowex catalyst assuming surface reaction was rate-limiting, gave lower

forward rate constants, yet higher acid, alcohol, and ester equilibrium adsorption/desorption constants. [42] These differences can be attributed due to the lower temperature (110 °C vs 150 °C in this work), and different acid/alcohol system and catalyst used. An ER model for the esterification of acetic acid with 1-octanol over Amberlyst-36 gave a similar water equilibrium adsorption constant (K_{H2O}) yet higher acetic acid equilibrium adsorption constant compared to the 2-HIBA equilibrium adsorption constants (K_{2HIBA}) obtained with the sGAC and sACM.[43] This could be due to the lower temperature (85 °C vs 150 °C) and the smaller size of acetic acid molecules compared to 2-HIBA.

5.4 Conclusions

Kinetics of 2-HIBA esterification with ethanol over sulfonated carbon in granular (sGAC) and monolith forms (sACM) was determined using single site Eley-Rideal and dual site Langmuir-Hinshelwood models. Kinetic models in which both 2-HIBA and ethanol competitively adsorb on an acid site (LH), and only 2-HIBA adsorbs on an acid site (ER) were in satisfactory agreement with the experimental data, with R^2 values ranging between 0.92-0.95 and experimental-model concentration residuals ≤ 5%. However, the residual sum of squares was high, ranging between 29-35 % for the LH and ER models respectively, indicating the need for investigating other reaction mechanisms (rate-limiting-steps). From the model, five reaction parameters including the forward rate constant and 2-HIBA, ethanol, E-2HIBA and water adsorption/desorption equilibrium constants were obtained and were consistent with a few studies reported in the literature on esterification kinetics with ion exchange resins. A mass transfer analysis indicated negligible effects of external and internal mass transfer resistances with both catalysts. Our results suggest the proposed kinetic models can be used in conjunction

with a mass transfer model, for reactor design and scale-up, to estimate the amount of catalyst (number of cores for the sACM) required for a specific ester (E-2HIBA) concentration for the sulfonated carbon catalyzed esterification of 2-HIBA and other bio-based organic acids. Future work would involve employing a volumetric titration method (e.g., Karl Fischer titration) to determine the water concentration of the samples (estimated based on stoichiometry and conversion in this work). In addition, other possible reaction mechanisms (e.g., involvement of two different acid sites in the LH model) will be investigated and an activity-based model (vs concentration-based model in this work) will be developed to account for the non-ideality of the reaction mixture and partitioning between the gas and liquid phases to arrive at a better fit of the experimental data with the kinetic model.

Acknowledgements

Support for this research was provided by the USDA-NIFA Grant (Carbon Monolith Catalysts from Wood for Biobased Platform Chemicals: 2017-67021-26136). The authors thank Applied Catalysts for providing the carbon materials.

References

1. G.D. Yadav, P.H. Mehta, Heterogeneous catalysis in esterification reactions: Preparation of phenethyl acetate and cyclohexyl acetate by using a variety of solid acidic catalysts, Ind. Eng. Chem. Res. 33 (1994) 2198-2208.
2. Y. Liu, E. Lotero, J.G.Goodwin Jr, Effect of water on sulfuric acid catalyzed esterification, J. Mol. Catal. A. Chem., 245 (2006) 132-140.
3. M. Nobuyuki, A. Takafumi, H. Hirofumi, Process for Producing Methyl α-Hydroxyisobutyrate. Patent Application. US005391813A, Oct 12, 1993.
4. A. Okamoto, E. Kushida, U. Yokobori, K. Kimura, α-hydroxyisobutyric acid ester compound, Fragrance material composition and use as fragrance material. Patent Application. EP 3816266A1, May 5, 2021.
5. K. Vasić, G.H. Podrepšek, Z. Knez, M. Leitgeb, Biodiesel production using solid acid catalysts based on metal oxides, Catalysts, 10 (2020) 237.
6. A. Izci, F. Bodur, Liquid-phase esterification of acetic acid with isobutanol catalyzed by ion-exchange resins, React. Funct. Polym. 67 (2007) 1458-1464.
7. D.M. Dal Pozzo, J.A.A. dos Santos, E.S. Júnior, R.F. Santos, A.Feiden, S.N.M. de Souza, I. Burgardt, Free fatty acids esterification catalyzed by acid Faujasite type zeolite, RSC Adv., 9 (2019) 4900-4907.
8. A. Hykkerud, J.M. Marchetti, Esterification of oleic acid with ethanol in the presence of Amberlyst 15, Biomass Bioenergy, 95 (2016) 340-343.

9. J. Guilera, E. Ramirez, C. Fite, M. Iborra, J. Tejero, Thermal stability and water effect on ion-exchange resins in ethyl octyl ether production at high temperature, Appl. Catal. A-Gen., 467 (2013) 301-309.
10. R. Hilten, J. Weber, J.R. Kastner, Continuous upgrading of fast pyrolysis oil by simultaneous esterification and hydrogenation, Energy Fuels, 30 **(**2016) 8357-8368.
11. W. Mateo, H. Lei, E. Villota, M. Qian, Y. Zhao, E. Huo, Q. Zhang, X. Lin, C. Wang, Z. Huang, Synthesis and characterization of sulfonated activated carbon as a catalyst for bio-jet fuel production from biomass and waste plastics, Bioresour. Technol., 297 (2020) 122411.
12. J.R. Kastner, J. Miller, D.P. Geller, J. Locklin, L.H. Keith, T. Johnson, Catalytic esterification of fatty acids using solid acid catalysts generated from biochar and activated carbon, Catal., 190 (2012) 122-132.
13. M. Pirmoradi, N. Janulaitis, R.J. Gulotty, Jr., J.R. Kastner, Continuous hydrogenation of aqueous furfural using a metal-supported activated carbon monolith, ACS Omega, 5 (2020) 7836-7849.
14. N. Al Azri, R. Patel, G. Ozbuyukkaya, C. Kowall, G. Cormack, N. Proust, R. Enick, G. Veser, Batch-to-continuous transition in the specialty chemicals industry: Impact of operational differences on the production of dispersants, Chem. Eng. J., 445 (2022) 136775.
15. Dr. B. Gutmann, Dr. D. Cantillo, Prof. Dr. C.O. Kappe, Continuous-flow technology-A tool for the safe manufacturing of active pharmaceutical ingredients, Angew. Chem. Int. Ed. 54 (2015) 6688-6728.

16. J. A. M. Lummiss, P.D. Morse, R. L. Beingessner, T. F. Jamison, Towards more efficient, greener synthesis through flow chemistry, Chem. Rec. 17 (2017) 667-680.

17. R. Munirathinam, J. Huskens, W. Verboom, Supported catalysis in continuous flow microreactors, Adv. Synth. Catal. 357 (2015) 1093-1123.

18. P.E. JagadeeshBabu, K. Sandesh, M.B. Saidutta, Kinetics of esterification of acetic acid with methanol in the presence of ion exchange resin catalysts, Ind. Eng. Chem. Res., 50 (2011) 7155-7160.

19. B. Guang, Y. Wu, W. Liu, J. Wang, Y. Xiao, Y. Liu, Kinetics study of the esterification reaction of cyclohexene to cyclohexyl acetate catalyzed by novel Bronsted-Lewis acids bifunctionalized heteropolyacid based ionic liquids hybrid solid acid catalysts, Catal. Letters, 152 (2022) 75-86.

20. S. Miao, B.H. Shanks, Mechanism of acetic acid esterification over sulfonic acid-functionalized mesoporous silica, J. Catal., 279 (2011) 136-143.

21. S.H. Shuit, S.H. Tan, Esterification of palm fatty acid distillate with methanol via single-step pervaporation membrane reactor: A novel biodiesel production method, Energy Convers. Manag. 201 (2019) 112110.

22. A.A. Bhusari, B. Mazmudar, A.P. Rathod, R.D. Khonde, Kinetics of catalyzed esterification of acetic acid with n-butanol using carbonized agro-waste, Int. J. Chem. Kinet. 52 (2020) 450-462.

23. A. V. Nakhate, G. D. Yadav, Synthesis and Characterization of Sulfonated Carbon-Based Graphene Oxide Monolith by Solvothermal Carbonization for Esterification and Unsymmetrical Ether Formation, ACS Sustainable Chem. Eng., 4 (2016) 1963-1973.

24. J. P. McMullen, K.F. Jensen, Rapid determination of reaction kinetics with an automated microfluidic system, Org. Process. Res. Dev. 15 (2011) 398-407.

25. W. Chu,X. Yang, X. Ye, Y. Wu, Vapor phase esterification catalyzed by immobilized dodecatungstosilicic acid (SiW12) on activated carbon, Appl. Catal. A- Gen., 145 (1996) 125-140.

26. A.E.W. Beers, R.A. Spruijt, T.A. Nijhuis, F. Kapteijn, J.A. Moulijn, Esterification in a structured catalytic reactor with counter-current water removal, 66 (2001) 175-181.

27. A. Orjuela, A. J. Yanez, A. Santhanakrishnan, C. T. Lira, D. J. Miller, Kinetics of mixed succinic acid/acetic acid esterification with Amberlyst 70 ion exchange resin as catalyst, Chem. Eng. J. 188 (2012) 98-107.

28. F. Hamerski, G.G. Dusi, J. T. F. dos Santos, V.R. da Silva, F. A. P. Voll, M. L. Corazza, Esterification reaction kinetics of acetic acid and n-pentanol catalyzed by sulfated zirconia, Int. J. Chem. Kinet. 52 (2020) 499-512.

29. S. H. Ali, Kinetics of catalytic esterification of propionic acid with different alcohols over Amberlyst 15, Int. J. Chem. Kinet. (2009).

30. S. Sripada, J.R. Kastner, Continuous catalytic esterification using a solid acid activated carbon monolith: Comparison of granular and monolith forms with a commercial catalyst, Chem. Eng. J., 476 (2023)146586.

31. S. Sripada, J.R. Kastner, Catalytic esterification using solid acid carbon catalysts synthesized by sustainable hydrothermal and plasma sulfonation techniques, Ind. Eng. Chem. Res, 61 (2022) 3928-3940.

32. E. Canadell, J.H. Badia, E. Ramirez, C. Fite, M. Iborra, J. Tejero, Determination of thermodynamic properties for the esterification of levulinic acid with 1-butene, Ind. Eng. Chem. Res., 61 (2022) 8313-8322.

33. S.Z. Hassan, M. Vinjamur, Analysis of sensitivity of equilibrium constant to reaction conditions for esterification of fatty acids with alcohols, Ind. Eng. Chem. Res, 52 (2013) 1205-1215.

34. H.S. Fogler, Elements of chemical reaction engineering, Prentice-Hall, 5th ed.; Englewood Cliffs: New Jersey, 1986; pp 600-650.

35. A. I. Liapis, J.J. Meyers, O.K. Crosser. Modeling and simulation of the dynamic behavior of monoliths. Effects of pore structure from pore network model analysis and comparison with columns packed with porous spherical particles, J. Chromatogr. A. 865 (1999) 13-25.

36. I. Miller, J.E. Freund, Probability and Statistics for Engineers. Prentice-Hall, Inc., Englewood Cliffs, NJ, 1985.

37. E. Sert, F.S. Atalay, Kinetic study of the esterification of acetic acid with 1-butanol catalysed by alumina-supported tungstophosphoric acid, Prog. React. Kinet. Mech. 35 (2010) 236-248.

38. M. Mekala, V.R. Goli, Kinetics of esterification of acetic acid and methanol using Amberlyst 36 cation-exchange resin solid catalyst, Prog. React. Kinet. Mech. 40 (2015) 367-382.
39. J. Lauwaert, E. Van de Steene, P. Vermeir, J. De Clercq, J.W. Thybaut, Critical assessment of the thermodynamics in acidic resin-catalyzed esterifications. Ind. Eng. Chem. Res. 59 (2020) 22079-22091.
40. P.Sangsiri, N. Laosiripojana, W. Laosiripojana, P. Daorattanachai, Activity of a sulfonated carbon-based catalyst derived from organosolv lignin towards esterification of stearic acid under near-critical alcohol conditions, ACS Omega, 7 (2022) 40025-40033.
41. Y. Liu, J. Liu, H. Yan, Z. Zhou, A. Zhou, Kinetic study on esterification of acetic acid with isopropyl alcohol catalyzed by ion exchange resin, ACS Omega, 4 (2019) 19462-19468.
42. I. Bum Ju, H-W. Lim, W. Jeon, D.J. Suh, M-J Park, Y-W. Suh, Kinetic study of catalytic esterification of butyric acid and n-butanol over Dowex 50Wx8-400, Chem. Eng. J. 168 (2011) 293-302.
43. S. Akyalcin, M.R. Altiokka, Kinetics of esterification of acetic acid with 1-octanol in the presence of Amberlyst 36, Appl. Catal. A-Gen. 429-430 (2012) 79-84.

Table 5.1. Equilibrium data (equilibrium conversion X_{eq} and concentration-based equilibrium constant K_{eq}) obtained with the sulfonated carbon catalysts under batch conditions (150 °C, 8 h, 9 bar).

Catalyst	**Molar Ratio (2HIBA: EtOH)**	**X_{eq}**	**K_{eq}**
sGAC	1:5	0.87 ± 0.02	1.39 ± 0.28
sACM	1:5	0.91 ± 0.01	2.15 ± 0.17

Table 5.2. Concentration versus residence time experimental data obtained for the sGAC (T= 150 °C, P= 300 psig, Q_l= 2-6 mL/min) and used for kinetic modeling (C_{H2O} was calculated based on stoichiometry and the measured C_{2HIBA}, C_{EtOH}, C_{E2HIBA} concentrations).

Residence time τ (min)	**C_{2HIBA}** (mol/L)	**C_{EtOH}** (mol/L)	**C_{E2HIBA}** (mol/L)	**C_{H2O}** (mol/L)
0	3.42	11.80	0.00	0.00
3.09	2.95	11.63	0.21	2.96
3.72	2.86	11.97	0.27	2.74
4.62	2.99	11.90	0.34	2.93
6.18	2.53	11.36	0.48	2.42
9.24	2.01	11.63	0.69	1.74

Table 5.3. Concentration versus residence time experimental data obtained for the sACM (T= 150 °C, P= 300 psig, Q_l= 2-6 mL/min) and used for kinetic modeling (C_{H2O} was calculated based on stoichiometry and the measured C_{2HIBA}, C_{EtOH}, C_{E2HIBA} concentrations).

Residence time τ (min)	**C_{2HIBA}** (mol/L)	**C_{EtOH}** (mol/L)	**C_{E2HIBA}** (mol/L)	**C_{H2O}** (mol/L)
0	3.28	12.34	0.00	0.00
3.09	2.90	12.30	0.48	2.84
3.72	2.25	11.26	0.56	2.17
4.62	2.02	11.19	0.69	1.94
6.18	1.98	12.34	1.00	1.96
9.24	1.92	11.74	1.35	1.29

Table 5.4. Rate constants and adsorption/desorption equilibrium constants obtained from the LH and ER kinetic models for liquid phase 2-HIBA esterification using sGAC and sACM at 150 °C and 300 psig.

Model	**k_f** **(molgcat^{-1}min^{-1})**	**K_{2HIBA}** **(L/mol)**	**K_{EtOH}** **(L/mol)**	**K_{E2HIBA}** **(L/mol)**	**K_{H2O}** **(L/mol)**	**R^2**
sGAC _LH	0.010	0.043	0.036	0.002	0.006	0.928
sGAC _ER	0.002	0.004	_	_	0.005	0.922
sACM _LH	0.052	0.017	0.061	0.023	0.006	0.949
sACM _ER	0.003	0.006	_	_	0.005	0.938

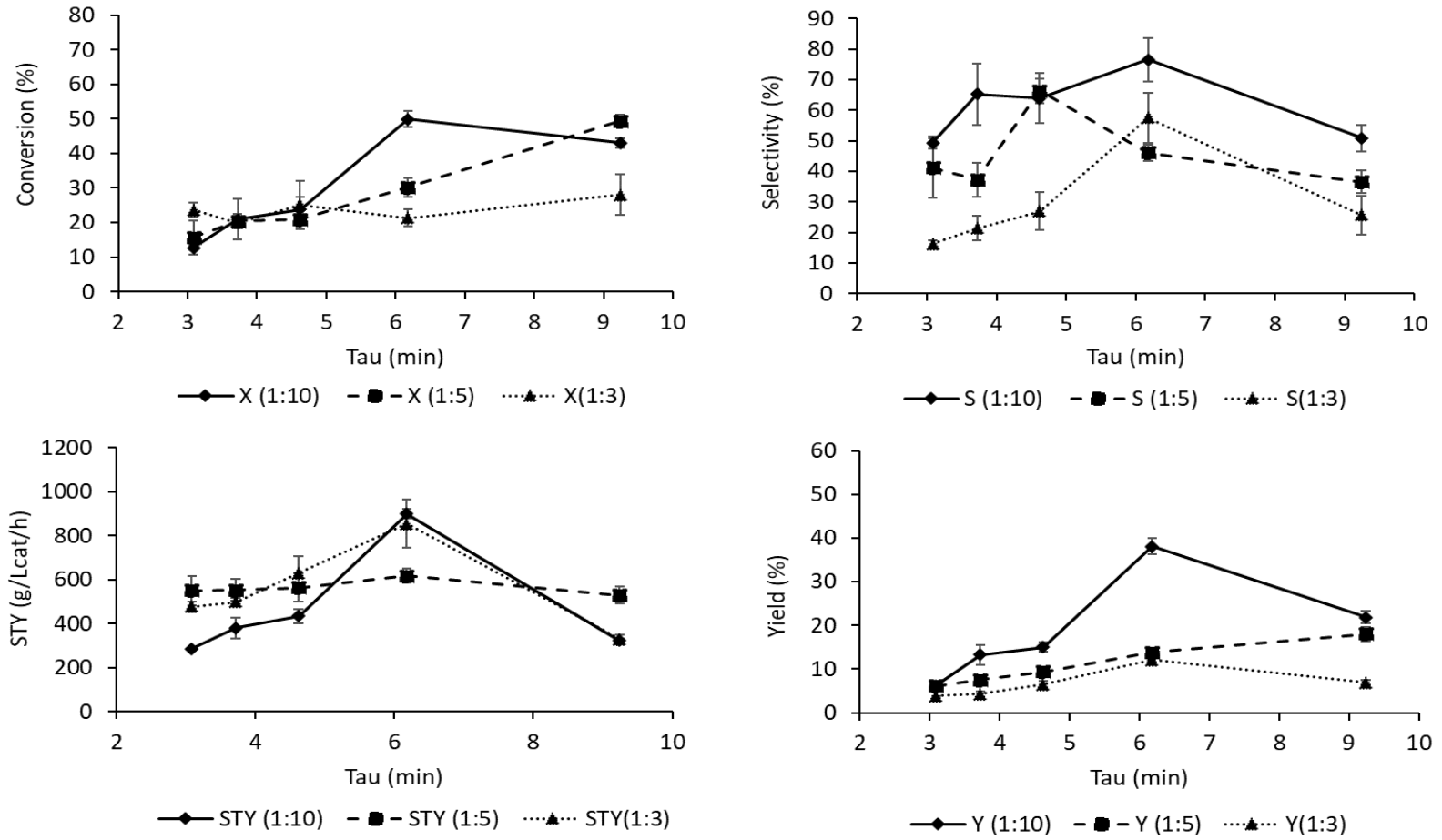

Figure 5.1. Effect of 2-HIBA to ethanol molar ratio on 2-HIBA conversion (X), E-2HIBA selectivity (S), space-time-yield (STY) and yield (Y) with the sulfonated GAC (sGAC). Reaction conditions: Temperature: 150 °C, Pressure: 300 psig, N_2= 50 mL/min, Residence time (Tau) = 3.09-9.24 min, Q_l= 2-6 mL/min. For each molar ratio a different batch of catalyst was used, and the experiments were performed consecutively with an accumulated time-on-stream of 3.33 h.

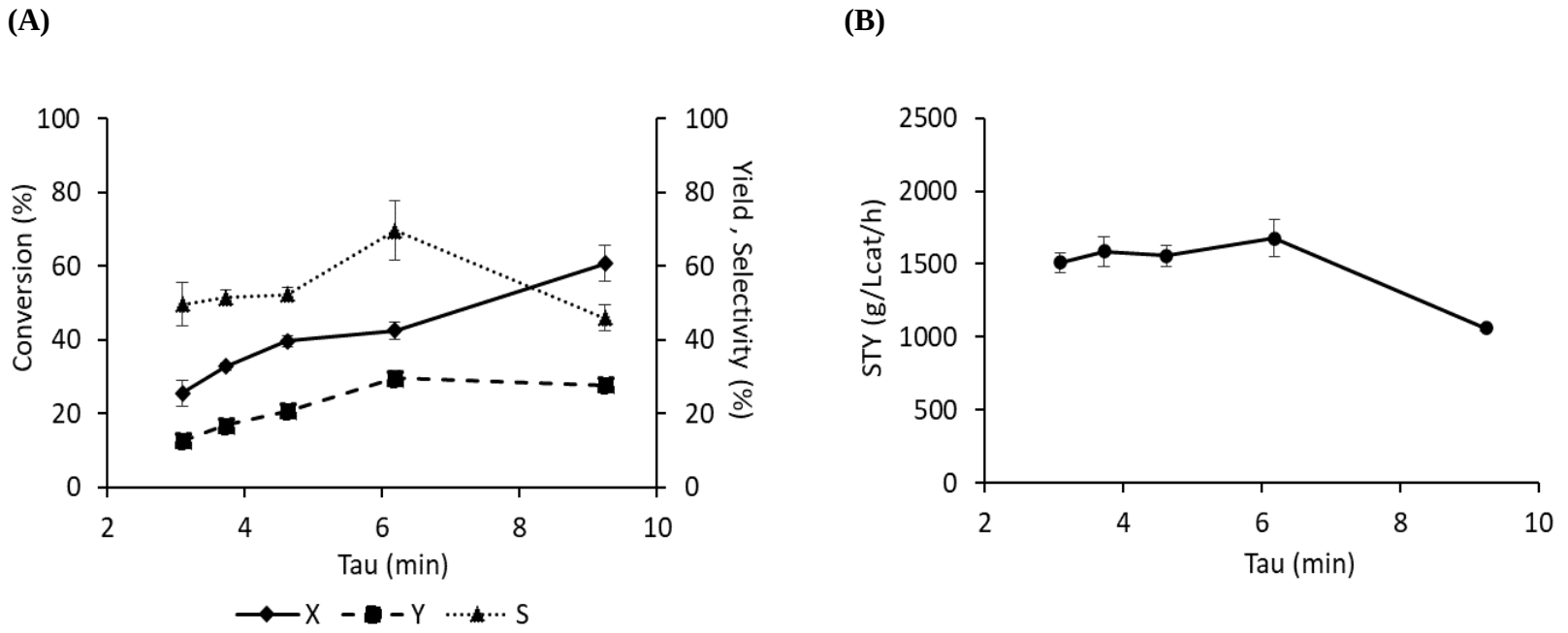

Figure 5.2. (A) 2-HIBA conversion (X), E-2HIBA selectivity (S), and yield (Y), and (B) E-2HIBA space-time-yield (STY) with the sulfonated ACM (sACM) at 2-HIBA to ethanol molar ratio of 1:5. Reaction conditions: Temperature: 150 °C, Pressure: 300 psig, N_2 = 50 mL/min, Residence time (Tau) = 3.09-9.24 min, Q_l = 2-6 mL/min. The experiments were performed consecutively with the same batch of catalyst, with an accumulated time-on-stream of 3.33 h.

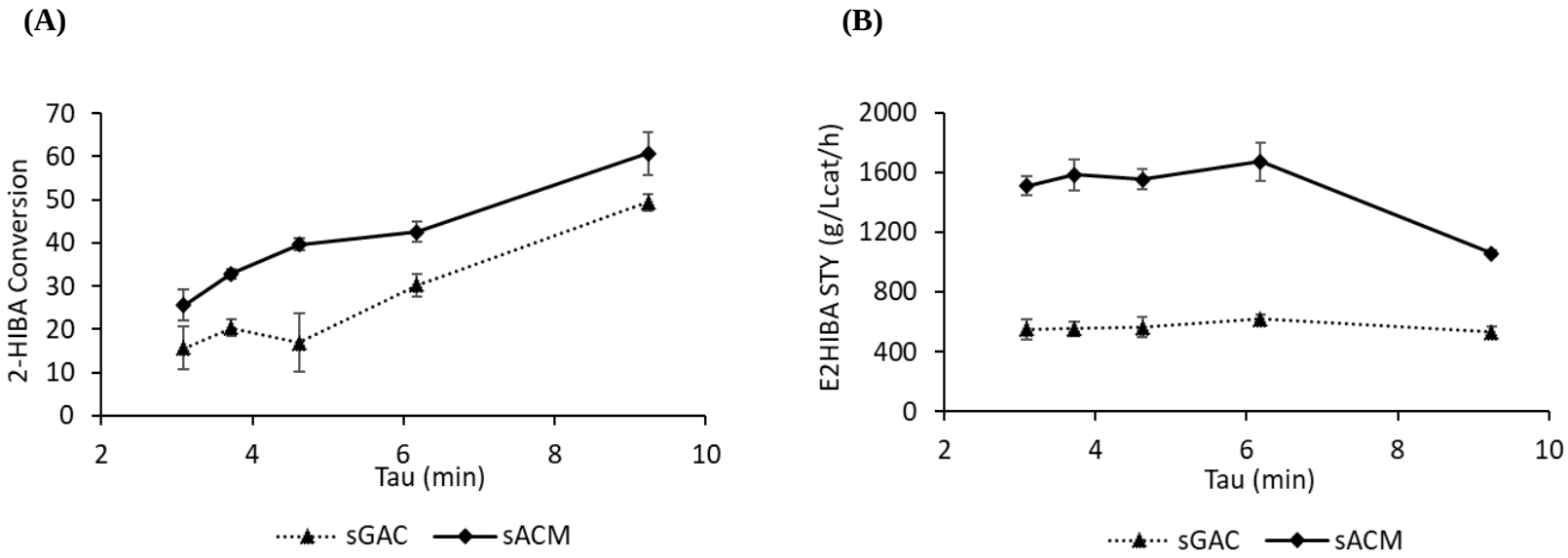

Figure 5.3. Comparison of (A) 2-HIBA conversion and (B) E-2HIBA space-time-yield (STY) for the sGAC and sACM at 2-HIBA to ethanol molar ratio of 1:5. Reaction conditions: Temperature: 150 °C, Pressure: 300 psig, N_2 = 50 mL/min, Residence time (Tau) = 3.09-9.24 min, Q_l= 2-6 mL/min. The experiments were performed consecutively with the same batch of catalyst (5g with the sGAC and 3.8 g with the sACM), with an accumulated time-on-stream of 3.33 h.

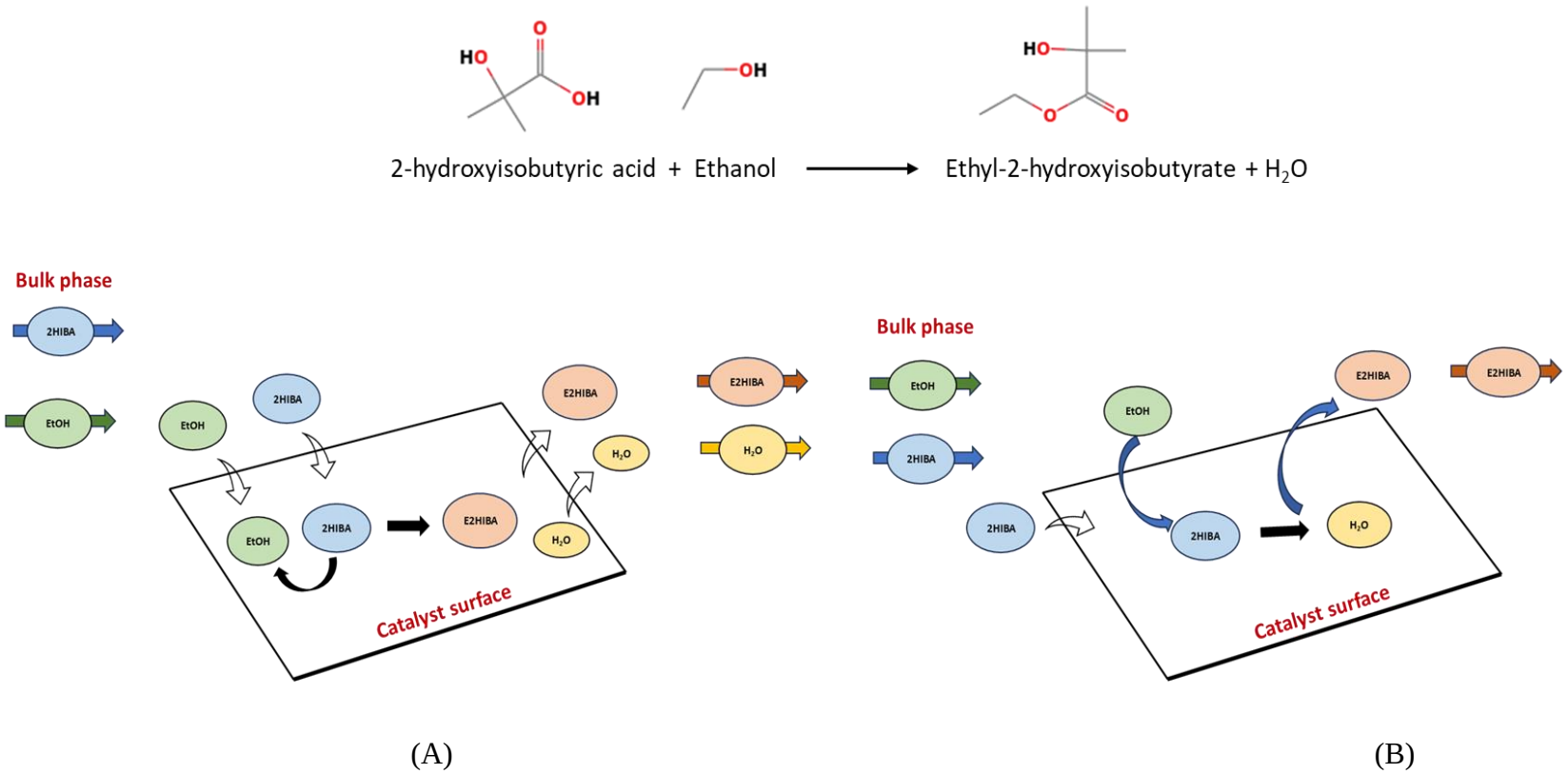

Figure 5.4. (A) Langmuir Hinshelwood and (B) Eley-Rideal reaction mechanisms for the sulfonated carbon catalyzed esterification of 2-HIBA and ethanol.

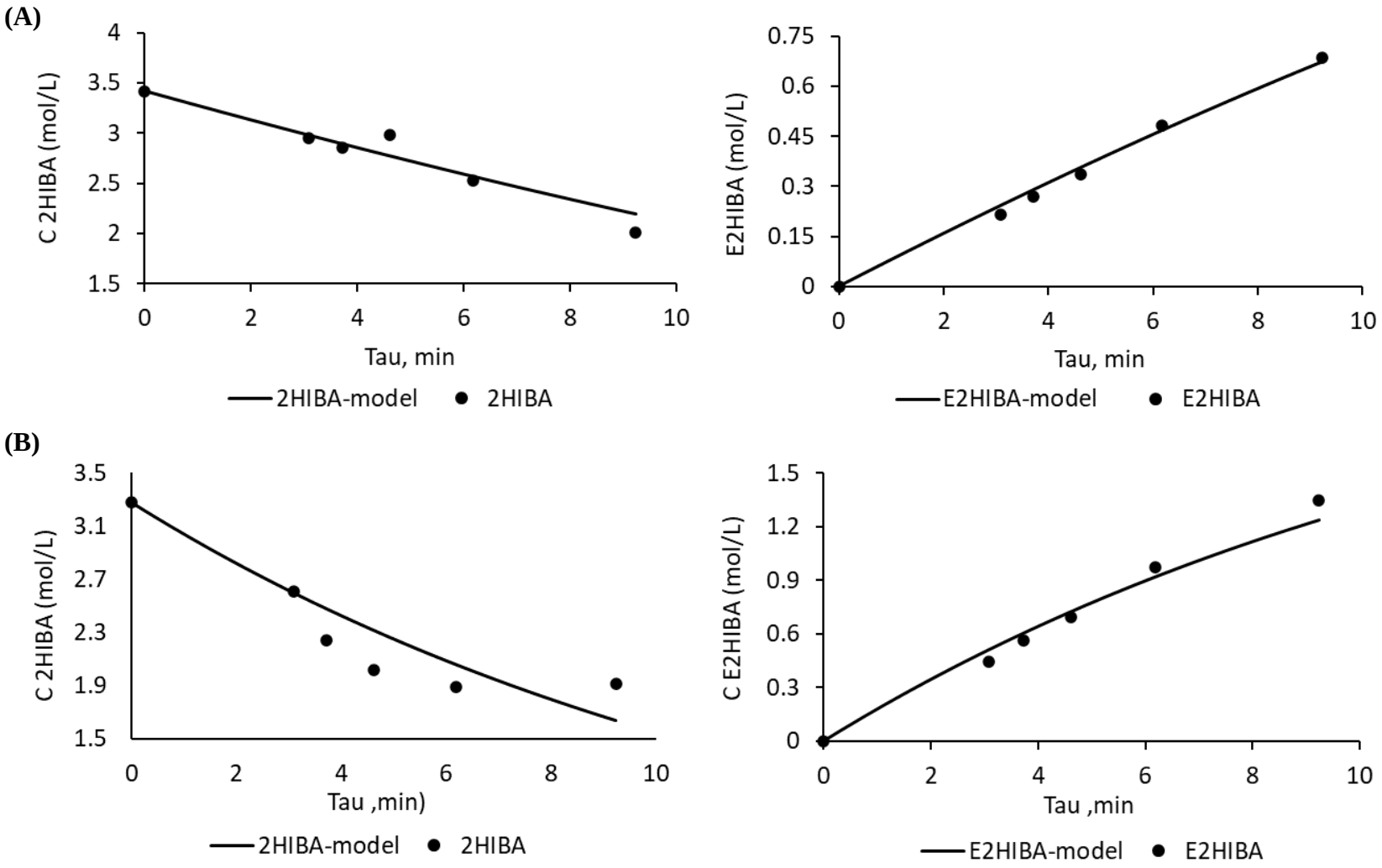

Figure 5.5. Concentration as a function of space time plots for the Langmuir Hinshelwood kinetic model (solid lines) for the (A) sGAC and (B) sACM.

CHAPTER 6

CATALYTIC ESTERIFICATION OF PYRUVIC ACID USING SOLID ACID CARBON CATALYSTS

[1] S. Sripada, [1] H. Rajpurohit, M.A. Eiteman, J.R. Kastner, 2023

To be submitted to *Green Chemistry*

Abstract

Pyruvic acid is an important organic acid widely employed in the pharmaceutical, chemical and agrochemical industries, and its production has been extensively investigated through biotechnological routes. The ethyl ester of pyruvic acid, ethyl pyruvate, is gaining interest in the pharmaceutical and food industries owing to its anti-inflammatory, anti-microbial and antioxidant properties. In this study, solid acid (sulfonated) wood-based activated carbon granular (sGAC) and monolith (sACM) catalysts were employed for the esterification of pyruvic acid with ethanol and compared with commercial petroleum-derived Amberlyst-15. The sGAC and sACM exhibited similar pyruvic acid conversion (96-98%), EP selectivity (95-96%), significantly higher turnover frequencies (22-71 ×), yet lower ester yield (56-59% vs 77.8%) compared to Amberlyst-15 (sGAC and sACM :150 °C, Amberlyst-15: 120 °C, 1 h). Anticipating the challenge of integrating fermentation with catalysis for the catalytic upgrading of pyruvic acid, the effect of fermentation residuals (water, sulfuric and phosphoric acids) was investigated. The effect of water inhibition (10%) was more pronounced in Amberlyst-15 compared to the sGAC, indicating poisoning of acid sites in Amberlyst-15. The addition of sulfuric (13.3 mM) /phosphoric (4.3 mM) acids reduced ester yield and selectivity, suggesting pyruvic acid side reactions and accelerated ester hydrolysis. The solid acid carbons are promising catalysts for upgrading fermentation-derived organic acids.

Key Words: Sulfonated carbon, activated carbon monolith, pyruvic acid, ethyl pyruvate, esterification.

6.1 Introduction

Organic acids are a key group of building blocks that can be used as platform molecules for the industrial production of a wide array of chemicals.[1] They are low-molecular weight compounds comprising one or more carboxyl groups and possess multifarious applications in the chemical, food, cosmetic, pharmaceutical, and fuel industries.[2] For instance, lactic acid finds numerous applications as a food additive, in personal care products, cosmetics, and as a building block for bio-based polymers poly (lactic acid). [3] Butyric and fumaric acids have applications in animal feed supplements.[4,5] Pyruvic acid, a key metabolite in central metabolism, and a potential untapped platform chemical, serves as a chemical precursor for the production of pharmaceuticals and commodity products.[1] Pyruvic acid has been used for the synthesis of citraconic anhydride, an analogue of petroleum derived maleic anhydride and raw material for various chemicals, resins, dyes, and surface-active agents.[6] 2,3-Butanediol and acetoin, bio-based platform chemicals with applications in chemical, cosmetics, food, and polymer sectors have also been synthesized from pyruvic acid.[7] Further, the esters of organic acids have penetrated a wide variety of markets spanning solvents, perfumes, flavoring agents, plasticizers, pharmaceuticals, and specialty chemicals.[8] For instance, the ethyl esters of butyric and lactic acids find applications as green solvents and are promising replacements for halogenated petroleum-based solvents.[9,10] Monoethyl fumarate and dimethyl fumarate have applications in dermatology for the treatment of diseases such as psoriasis and multiple sclerosis.[11] Pyruvate esters find applications in the synthesis of various bio-based polymers. The acylation of pyruvate esters with carboxylic anhydride in the presence of an acid catalyst can yield α-acyloxyacrylate esters, polymers with higher thermal durability compared to poly (methyl methacrylate).[12] The ethyl ester of pyruvate, ethyl pyruvate, can undergo a self-aldol addition, followed by

dehydration to produce 2-methylene-4-oxopentanedioate, a functional itaconic acid ester analogue with applications in lubricants, plasticizers, and polymer intermediates.[13] Figure 6.1 depicts some of the products and polymers that can be produced from pyruvic acid and ethyl pyruvate.

Ethyl pyruvate (EP) has been gaining a lot of interest owing to its versatile medical applications as an anti-inflammatory agent.[14] EP has also been shown to have anti-oxidative[15] and anticoagulant properties.[16] Further, the bifunctional group structure, stability, low cost and toxicity make EP valuable for biomedical applications. EP is also used as a flavoring agent and food additive.[17] EP has been synthesized by the oxidative dehydrogenation of lactates using molecular oxygen or hydrogen peroxide as oxidant and transition metal oxide/ noble metal catalysts. Zhang et al. employed a solid pyridine-rich carbon supported vanadium catalyst for the oxidative dehydrogenation of ethyl lactate (EL). With this catalyst, they observed 80% EL conversion and 90% selectivity to EP (130 °C, 1 atm).[18] Lu and coworkers employed hydrogen peroxide and titanium substituted zeolite and observed 100 % EL conversion and 97.8% EP yield (50 °C, 9 h).[19] While this route can generate high ester yields under mild conditions, it requires the use of expensive noble metal catalysts. Further, the expense and associated explosive risk with peroxides limits their industrial use. Moreover, the formation of byproducts from pyruvate/lactate decarboxylation makes the separation of EP from EL more energy intensive. [20] Alternatively, EP can be synthesized by the acid-catalyzed esterification of pyruvic acid and ethanol.

Pyruvic acid is conventionally synthesized in large volumes from tartaric acid, which is obtained from butane or benzene-derived maleic anhydride (Figure 6.2). [21,22] Since maleic anhydride is a petrochemical product, its cost depends greatly on crude oil prices.[22] Moreover, the dehydrative

decarboxylation of tartarate to pyruvate uses an excess of $KHSO_4$ as dehydrating agent.[20] This route to the synthesis of pyruvate is high in cost and causes serious environmental pollution. Enzymatic biotransformation methods using lactate oxidase and catalase have been explored,[23] however the raw materials for these biotransformations are expensive and unsuitable for a wide range of industrial applications. Another method is the synthesis of pyruvic acid by microbial fermentation, which offers the benefits of low cost and high product quality. [24] Several microbial strains have been studied and engineered for pyruvic acid production including *Candida glabrata*, *Saccharomyces cerevisiae*, *Corynebacterium glutamicum* and *Escherichia coli*. [24,25,26]

The production of EP by the esterification of pyruvic acid with ethanol has been investigated with homogeneous catalysts including sulfuric acid, hydrochloric acid, methanesulfonic acid, and the solid acid ion exchange resins Nafion and Diaion PK208.[27] However, homogeneous acids pose limitations including reactor corrosion, difficulty in catalyst recovery and reuse, and neutralization of the effluent.[28] These drawbacks can be overcome by employing solid acids such as zeolites and ion exchange resins. However, zeolites are limited by their low surface area and porosity,[29] while ion-exchange resins such as Amberlyst-15 present drawbacks such as low surface area, low thermal and operational stability, high cost, and synthesis from petroleum derivatives.[30,31] Sulfonated carbons (SC) are gaining attention as esterification catalysts owing to their high Bronsted acidity, large surface area and well-developed porosity.[32] Further they can be synthesized from activated carbon which has a very high surface area, is stable in acidic, basic and aqueous environments, and can be obtained from renewable biomass.[33] Sulfonated carbons have previously been shown to have high catalytic efficiency in the esterification of both short (e.g., lactic acid) and long-chain (e.g., hexanoic acid, decanoic acid and oleic acid) organic acids.[34,35,36] Further, in monolith form, sulfonated carbon provides a larger surface area to

volume ratio, that enables high mass transfer rates and low pressure drop, facilitating its use in continuous processing.[37]

The catalytic upgrading of fermentation derived organic acids (e.g., lactic acid, pyruvic acid) using heterogeneous solid acid catalysts would serve as an efficient route to producing organic esters. EP can be produced in a single step from pyruvic acid compared to the two-step process (esterification and oxidation) from lactic acid (Figure 6.2). Purification steps including ultrafiltration, activated carbon treatment, cation-exchange and dewatering have previously been performed in succession for the post-fermentation purification of organic acids such as succinic acid and propionic acid.[38] Separation and purification of the organic acid from the fermentation broth can generate a low-water, product stream as feed for catalytic upgrading. However, this aqueous environment can still present challenges for equilibrium-limited esterification reactions, which also generate water as a byproduct.[39] The presence of water can influence the reactivity and selectivity of catalysts by blocking the active sites.[40] Further, heterogeneous catalysts may be poisoned by contaminants present in the feed.[41] During the catalytic reactions, the fermentation-derived product along with residual impurities can diffuse into the pores of the catalyst and interact with/poison the catalyst surface. Poisoning causes blocking of active sites and may also influence the electronic and geometric structure of the catalytic surface.[42] Fermentation broth impurities range from media components to remnants of biomass deconstruction that can cause catalyst deactivation. Some common poisons encountered in fermentation media include amino acids, proteins, vitamins, and sulfur. Poisons such as sulfur can be irreversibly chemisorbed onto the active sites on metal-based catalysts.[42] Although sulfur can be removed by calcination, high temperatures can lead to unfavorable alterations of the catalyst support.[43] To integrate fermentation with catalysis successfully for synthesizing organic esters, it is essential to address

the challenges pertaining to the aqueous environment and evaluate the impact of broth impurities on catalyst performance.[41]

Studies on the effect of biogenic impurities have mostly focused on metal hydrogenation catalysts.[44,45] Holzhauser and co-workers studied the effect of fermentation broth impurities on the hydrogenation of itaconic acid with a Ru/C catalyst. The presence of salts such as $CaCl_2$, $FeCl_3$, $ZnSO_4$, $CuSO_4$, KH_2PO_4, NH_4NO_3, and $MgSO_4$ were found to inhibit the catalyst. Further, glucose was found to plug the pores of the carbon catalyst resulting in deactivation. [46] Very few studies have investigated catalyst deactivation due to biogenic impurities in esterification reactions. Delhomme et al. performed esterification reactions of succinic acid in the fermentation broth using catalysts such as dodecyl benzene sulfonic acid (DBSA) and Nafion. With the actual fermentation broth, using DBSA and Nafion NR-50, they were able to achieve succinic acid conversions of 78% and 70% as opposed to about 91% and 84% with pure succinic acid respectively. They attributed the reduction in conversion and partial catalyst deactivation to the presence of high concentrations of salts, particularly phosphates, in the medium.[39] In addition, Kasinathan et al. observed that amino acids such as tryptophan could inhibit the activity of Amberlyst-36 in the esterification of lactic acid,[47] while Luque et al. discovered that by-products of succinic acid fermentation such as acetic acid, formic acid and pyruvic acid could deactivate a sulfonated mesoporous carbon catalyst.[48]

Few studies have previously investigated the batch esterification of fermentation-derived/ aqueous solutions of organic acids using ion exchange resins and granular solid acid catalysts.[39,34] However, there is limited information in the literature on the catalytic esterification of pyruvic acid using solid acid carbon catalysts. In this work, we studied the esterification of pyruvic acid and ethanol using sulfonated wood-based activated carbon in granular (sGAC) and

monolith (sACM) forms and compared the catalytic performance of the sulfonated carbons to the commercial catalyst, Amberlyst-15. Further, anticipating the challenge of integrating fermentation with catalysis for production of ethyl pyruvate, we investigated the effect of water and potential catalyst poisons (phosphates and sulfates) on catalytic activity. The novelty of this work lies in using solid acid carbon catalysts (granular and monolith) for the synthesis of ethyl pyruvate. The goal of this work is to contribute new knowledge on developing hybrid fermentation-catalytic processes for upgrading biobased organic acids using renewable, wood-based solid acid carbon catalysts for the synthesis of pharmaceuticals and value-added chemicals.

6.2 Experimental Section

6.2.1 Materials and Catalysts

Pyruvic acid ($C_3H_4O_3$, purity > 98%), ethyl pyruvate ($C_5H_8O_3$, purity > 98%), 200 proof ethanol (purity >99.5%), sulfuric acid used for carbon sulfonation, and Amberlyst-15 (hydrogen form) were procured from Sigma Aldrich. Three catalysts were used in this study, a sulfonated granular activated carbon catalyst (sGAC), a sulfonated activated carbon monolith (sACM) and a commercial petroleum-derived acidic resin, Amberlyst-15. The wood-based granular activated carbon (GAC) (surface area of 1350 m^2/g and pore volume of 1.2 cc/g) and activated carbon monolith (ACM 101-H) were provided by Applied Catalysts (Laurens, SC). The ACM was manufactured by coextrusion of 50% activated carbon and 50% of a ceramic binder. Each monolith core has a diameter and length of 1 inch, 400 cells/in^2, wall thickness of 0.01- inch, cell spacing of 0.044-inch, geometric surface area of 70.8 in^2/in^3, open frontal area of 0.6 in^2, density

of 350 kg/$m^{3,}$ surface area of 598 m^2/g (BET), pore diameter of 29.8 Å and pore volume of 0.5 cc/g (BJH).[37]

6.2.2 Catalyst Preparation

The catalysts were synthesized as previously described.[31] The base granular activated carbon (GAC) was crushed and sieved to a particle size of 0.5-1 mm, washed until constant pH (3 ×) to eliminate any contaminants (initial pH was ~9.0) and dried at 105 °C. Sulfuric acid (2M) was introduced into the GAC by incipient wetness impregnation at 1.2 mL/g catalyst (1.2:1 [v/w] sulfonating agent: carbon ratio), according to the pore volume of the GAC (1.2 mL/g), to ensure all particles were sufficiently wetted. The monolith core (ACM) was immersed into 2M H_2SO_4 (100 mL) and sonicated at 30 °C for 30 minutes as reported previously. Post treatment, the sulfonated GAC and ACM were washed with deionized water (25-50 mL/g catalyst) at room temperature to remove traces of excess acid (H_2SO_4). The sulfonated ACM core was washed by sonication in deionized water. Washing (8-12 ×, 1 h washes) was carried out until the filtrate displayed a constant pH (approximately 4.0 for the GAC and ACM catalysts). Post-washing, all catalysts were dried in a hot air oven at 105 °C overnight. The sACM was crushed to a d_p of 0.5-1 mm prior to the catalytic reactions.

6.2.3 Analytical

The liquid sample collected from the reactor was analyzed using high performance liquid chromatography (HPLC). HPLC (Shimadzu LC-20 AT) was performed using a Coregel 64-H Transgenomic column (7.8 × 300 mm) and 2mN H_2SO_4 mobile phase (flow rate) at 40 °C (5 μL injection volume).[49.]

6.2.4 Catalytic Esterification

A series of batch reaction studies were performed with the sGAC, crushed sACM, and Amberlyst-15 to determine the effect of temperature (100 °C - 150 °C) and residence time (0.5 h -3 h) on pyruvic acid (PA) conversion and EP yield (mol of EP formed / mol of pyruvic acid charged). Reactions were performed in 75 mL autoclave batch reactors (Parr Series 5000 Multiple Reactor System). A working volume of 20 mL of 40 g/L pyruvic acid in an excess of ethanol (37.7:1 ethanol to PA molar ratio) and catalyst was mixed using a magnetic stir bar (700 rpm). The reactor headspace was pressurized with nitrogen at 1.6 bar, then heated to the set-point at 10 °C /min. Heat up times were approximately 15 min and residence times are reported from the time the set-point temperature was reached. On completion of the reaction, the vessel was cooled down by quenching in ice. After depressurizing the reactor, the reaction mixture and catalyst were recovered and the catalyst was separated via filtration (Whatman, 11 μm pore size). The filtrate was collected and analyzed by HPLC. Control reactions without catalyst were also carried out. All experiments were performed in duplicate. Esterification reaction rates (mmol g-cat^{-1} h^{-1}), PA conversion (mol converted/mol initial PA), EP yield (mol produced/mol initial PA) and selectivity (mol produced/mol PA remaining and EP) were calculated using the batch data as reported previously.[33] The turnover frequency (TOF, min^{-1}) was estimated from the reaction rate (mmol g^{-1}min^{-1}) and acid site density (mmol g^{-1}). In calculating the reaction rates and TOF, the heat-up time (15 min) was included in the contact time (Table 6.1).

6.2.5 Effect of Fermentation Medium Components

The effect of water content and residual fermentation medium components on pyruvic acid conversion and ester yield and selectivity were investigated with the sGAC and Amberlyst-15. To determine the effect of water, water contents of 5 and 10 % were added to the reaction medium (40 g/L pyruvic acid in ethanol). Anticipating the product stream post fermentation would go through purification (activated carbon treatment, ultrafiltration, cation exchange) and comprise pyruvic acid along with sulfates and phosphates in the form of sulfuric and phosphoric acids (post cation-exchange), H_2SO_4 (13.3 mM) and H_3PO_4 (4.3 mM) were individually added to the reaction medium and their effects on catalytic activity were studied. These concentrations were chosen based on elemental analysis of a modified fermentation medium adopted from Moxley and Eiteman.[26]

6.2.6 Statistical Analysis

The batch reactions were performed in duplicate and reported as the mean and sample standard deviation. The sample standard deviation was calculated from the range (R) for small sample size (n) for TOF, yield, and conversion (for $n \leq 5$, R/d_2, where $d_2 = 1.128$).[50] In the analysis between two means for the TOF, a Student's t-test was performed, assuming the null hypothesis, and the level of significance (α) is reported.

6.3 Results and Discussion

6.3.1 Catalytic Esterification

Batch esterification reaction studies were performed with the sGAC and Amberlyst-15 to determine the effect of temperature (100, 120 and 150 °C) and residence time (0.5, 1, 3 h) on

ethyl pyruvate (EP) yield and pyruvic acid (PA) conversion (Figure 6.3). Some EP was formed at the initial time point with both catalysts, and there was an increase in PA conversion and EP yield and selectivity on increasing the temperature from 100 °C to 150 °C. The sGAC and Amberlyst-15 displayed an increase in conversion from 17% to 71.9% and 61.1% to 94% on increasing the temperature from 100 °C to 150 °C, respectively. Further, with both catalysts, there was an increase in PA conversion, EP yield and selectivity on increasing the residence time to 1 h. With the sGAC, a maximum EP yield of 58.8%, selectivity of 96.1% and PA conversion of 98% were obtained at 150 °C and 1 h residence time (Figure 6.3A). Similar results were reported by Liu and coworkers in the esterification of succinic acid with ethanol. Using a sulfonated carbon catalyst synthesized using concentrated sulfuric acid, they obtained 99% succinic acid conversion and 97% selectivity to diethyl succinate (80 °C, 4 h).[51]

Further, in our work, increasing the residence time to 3 h led to a decline in PA conversion to 86.4% (EP yield: 37%, EP selectivity: 74.2%). In comparison, with Amberlyst-15, a maximum EP yield of 77.8%, selectivity of 94.8% and PA conversion of 95.6 % were obtained at 120 °C and 1 h residence time. Further increasing the temperature to 150 °C, and residence time to 3 h led to a decline in PA conversion, EP yield and selectivity (Figure 6.3B). The decrease in conversion observed on increasing the temperature to 150 °C may be attributed to the low thermal stability of Amberlyst-15 at temperatures above 120 °C.[30] Further, the drop in conversion observed on increasing the residence time to 3 h could be due to the accumulation of the byproduct water. Tao and coworkers reported similar results in the esterification of glycerol and acetic acid using a sulfonated carbon material. The slight decline in conversion these researchers observed on increasing the residence time from 2 to 7 h was attributed to the drop in glycerol concentration and accumulation of water.[52] Our results suggest that the sGAC attained

equilibrium around 150 °C, while Amberlyst-15 attained equilibrium at 120 °C at approximately 1 h residence time. Similar results were observed in our previous work on the batch esterification of 2-hydroxyisobutyric acid (2-HIBA) with ethanol. 2-HIBA conversions of 71% and 81% and ester yields of 64-65% were observed with the sGAC and Amberlyst-15 respectively at 1 h residence time (sGAC :150 °C, Amberlyst-15: 120 °C).[31] Further, the catalytic performance of the crushed sACM was compared to the sGAC and Amberlyst-15 at 1 h residence time (sGAC and sACM :150 °C, Amberlyst-15: 120 °C) (Figure 6.4). The sACM exhibited similar results to the sGAC, with an EP yield of 56.6%, selectivity of 96.1% and a PA conversion of 97.7%.

For almost all reactions, the carbon recovery was above 80%. A few unknowns were detected which based on our previous work and the literature, were hypothesized to be ethanol dehydration products (diethyl ether, ethylene).[31,53] Our results suggest that reaction temperatures of 150 °C for the sGAC/sACM and 120 °C for Amberlyst-15 at 1 h residence time were optimal for pyruvic acid esterification. An analysis of the turnover frequencies (TOF's) of the catalysts indicates a significantly higher TOF of 3.83 min^{-1} with the sGAC, about 71 × that of Amberlyst-15 ($\alpha = 0.05$, level of significance). The sACM also displayed a higher TOF, 22 × that of Amberlyst-15 ($\alpha = 0.05$, level of significance). The low TOF observed with Amberlyst-15 could be due to the low surface area of the catalyst which limits access to the acid sites. The higher TOF's exhibited by the sulfonated carbons despite the low sulfonic acid densities could be due to the higher surface area of these catalysts (sGAC: 867 m^2/g, sACM: 550 m^2/g) (Table 6.1). In addition, our previous work and the literature indicate the presence of weak acidic COOH and OH groups on the sulfonated carbons may enhance catalytic activity. [31,54]

6.3.2 Effect of Fermentation Residuals

One of the major challenges in the catalytic upgrading of biologically derived compounds is the nature of impurities present in the fermentation broth. During heterogeneous catalytic reactions, the fermentation-derived product along with residual impurities can diffuse into the pores of the catalyst and interact with the catalyst surface causing deactivation. Therefore, it is essential to assess the impact of these impurities on catalyst performance prior to catalytic upgrading. Anticipating pyruvic acid could be synthesized by microbial fermentation, we determined the effect of water and potential residual medium components on catalytic activity. The fermentation medium generally comprises cations including sodium and potassium, and anions such as phosphates and sulfates. Alkali metal cations have been shown to poison catalytically active sites [55] and can be eliminated by purification through cation-exchange chromatography.[38] Post fermentation and purification steps including activated carbon treatment, ultrafiltration, and cation exchange with HCl, we presumed the product stream would comprise pyruvic acid along with anions in the form of sulfuric and phosphoric acid. Thus water (5 and 10%), sulfuric acid (13.3 mM) and phosphoric acid (4.3 mM) were added to the reaction medium along with the catalyst in separate experiments and the effect of these components on catalytic activity was determined.

Effect of Water

With sGAC, the addition of 5% water to the reaction medium (40 g/L pyruvic acid in ethanol) resulted in an 8.6%, 9.5% and 12.8% decrease in PA conversion, EP yield and selectivity, respectively (Figure 6.5). Increasing the water concentration to 10% did not affect the conversion and selectivity, however led to a further decrease in ester yield of 10.1%. In the case of Amberlyst-15, the addition of 5% water resulted in a much greater decline of 22.7% in PA

conversion, 46% in EP yield and 34.7% in EP selectivity, compared to the sGAC. Increasing the water content to 10% did not affect the ester yield but led to a further decline in conversion of 14.3% and ester selectivity of 13%. The presence of water in the reaction medium has been found to hinder esterification, and accelerate the reverse reaction i.e., ester hydrolysis.[56] While studying the effect of water content on the esterification of oleic acid and methanol with Amberlyst-15, Park and co-workers observed a rapid decrease in catalytic activity with Amberlyst-15, which was attributed to the poisoning of acid sites by water and poor accessibility of the reactants to the active sites. [57] A water content of 10% in the reaction mixture reduced the EP selectivity from 95-96% to 87% with the sGAC and 54% with Amberlyst-15. Our results suggest the effect of water inhibition was more pronounced in Amberlyst-15 compared to the sGAC. Byproducts (2-3 new peaks) were noted at approximately 22 min, and between 33-39 min with the sGAC and Amberlyst-15 in the presence of water. The decrease in activity observed on the addition of water with both catalysts, particularly Amberlyst-15, may be attributed to the poisoning of sulfonic acid sites, and poor accessibility of the reactants to the acid sites in the presence of water. [57,58] Low ester selectivity upon water addition to the reaction mixture could be due to ester hydrolysis or pyruvic acid dimerization reactions. Previously, Perkins and co-workers reported the interconversion between pyruvic acid and its dimers, parapyruvic acid and zymonic acid, under aqueous conditions.[59]

Effect of sulfur and phosphorus

To test the effect of sulfur and phosphorus on catalytic activity, assuming the residual fermentation broth post cation-exchange would comprise sulfuric and phosphoric acids, 13.3 mM H_2SO_4 and 4.3 mM H_3PO_4 (based on elemental analysis of the fermentation medium) were added separately to the reaction medium along with the catalyst (sGAC, Amberlyst-15). The

control comprised the reaction medium along with liquid H_2SO_4 /H_3PO_4 (no catalyst). As shown in Figure 6.6A, the sGAC displayed slightly higher PA conversion and EP selectivity to the control comprising sulfuric acid, yet a lower yield of 58.8% compared to 71.4% with the control. The addition of 13.3 mM H_2SO_4 to the sGAC resulted in a 22% decrease in PA conversion (EP yield: 46.4 %, selectivity: 70.1%). As shown in Figure 6.6 A, Amberlyst-15 displayed slightly higher EP yield, yet lower EP selectivity and PA conversion compared to the control comprising sulfuric acid. Further a comparison of the controls of the sGAC (150 °C, 1h) and Amberlyst-15 (120 °C, 1h) with H_2SO_4 indicates a higher EP yield of 71.4% and selectivity of 94.3% compared to 40.8% and 89.8% with the Amberlyst-15 control. The results observed can be attributed to the higher reaction rate at 150 °C (10.6 mmoL/g/h) compared to 120 °C (8.04 mmoL/g/h). The addition of H_2SO_4 to Amberlyst-15 resulted in a 19.2% decrease in PA conversion, and a significantly higher decrease of 40.4% in EP yield (compared to a decrease of 21% with the sGAC). Further, byproducts were noted at retention times of approximately 27 and 33 min.

The addition of 4.3 mM H_3PO_4 to the reaction medium with sGAC resulted in a 12.8%, 31.5% and 23.7% decrease in PA conversion, EP yield and selectivity, respectively (Figure 6.6B). Similar results were noted with Amberlyst-15 with a 13.8%, 36.3% and 22.2% decrease in conversion, yield, and selectivity respectively. Delhomme and coworkers observed similar results in the esterification of succinic acid with a Nafion NR-50 catalyst.[39] High concentrations of phosphate salts in the medium negatively impacted conversion (67% in aqueous solutions vs 84% in pure solutions of succinic acid). Further, the low conversion (70%) observed with the fermentation broth was attributed to the exchange of H^+ of the resin with cations including K^+ and Na^+ in the medium, resulting in partial deactivation of the catalyst.[39] With the sGAC and Amberlyst-15, byproducts were also noted at retention times of approximately 27 and 33 min.

Both sulfuric acid and phosphoric acids catalyze ethanol dehydration, suggesting the unknowns could be diethyl ether and ethylene.[56,60] However, our results indicate a decline in EP yield and selectivity with both the sGAC and Amberlyst-15 in the presence of sulfuric and phosphoric acids. This reduction in ester yield and selectivity may be attributed to pyruvic acid side reactions occurring at the low pH conditions in the reaction mixture. Pyruvic acid is known to undergo spontaneous dimerization (aldol condensation), resulting in parapyruvic acid. [61] It has previously been reported that under acidic conditions (0.1 M HCl), parapyruvic acid undergoes an intramolecular esterification reaction, producing a lactone called zymonic acid. Heating the reaction mixture (75 ºC, pH: 0 -10) resulted in the conversion of zymonic acid to *Z*-4-methyl-2-oxopent-3-enedioic acid, which on subsequent decarboxylation produced methylsuccinic acid.[61]

6.4 Conclusions

The esterification of pyruvic acid with ethanol using sulfonated carbon in granular and monolith forms was demonstrated and compared to commercial Amberlyst-15. The sulfonated carbon catalysts displayed similar pyruvic acid conversion (96-98%) and ethyl pyruvate (EP) selectivity (95-96%), yet significantly higher turnover frequencies (22 - 71 ×) than Amberlyst-15. Ethyl pyruvate yields of 58.8% and 56.6% were obtained with the sulfonated GAC and ACM respectively, compared to 77.9% with Amberlyst-15 (sGAC and sACM :150 °C, Amberlyst-15: 120 °C, 1 h). Addition of fermentation residuals including water, sulfuric and phosphoric acids to the reaction medium comprising the sGAC/Amberlyst-15 caused a decline in catalytic activity, suggesting accelerated ester hydrolysis and the formation of byproducts. However, the effect of water inhibition was more pronounced in Amberlyst-15 compared to the sGAC, suggesting poisoning of the acid sites in Amberlyst-15. The solid acid carbons are promising catalysts for upgrading fermentation-derived organic acids. The results of this study provide

valuable insights to guide fermentation medium design and subsequent downstream processing of pyruvic acid prior to chemocatalytic upgrading. Future work will investigate the catalytic activity of the sulfonated carbon catalysts using fermentation-derived pyruvate.

Acknowledgements

Support for this research was provided by the USDA-NIFA Grant (Carbon Monolith Catalysts from Wood for Biobased Platform Chemicals: 2017-67021-26136). The authors thank Applied Catalysts for providing the carbon materials.

References

1) J. Becker, A. Lange, J. Fabarius, C. Wittmann, 2015, Top value platform chemicals: biobased production of organic acids. Curr. Opin. Biotech. 36 (2015)168-175.
2) N. Murali, K. Srinivas, B.K. Ahring, Biochemical production and separation of carboxylic acids for biorefinery applications, Fermentation, 3 (2017) 1-25.
3) J. O. Campos de Franca, D. da Silva Valadares, M. F. Paiva, S. Claudia, L. Dias, J.A. Dias, Polymers based on PLA from synthesis using D,L-Lactic acid (or racemic lactide) and some biomedical applications: A short review, Polymers (Basel), 14 (2022) 2317.
4) L. Jiang. H. Fu, H.K. Yang, W. Xu, J. Wang, S-T. Yang, Butyric acid: Applications and recent advances in its bioproduction, Biotechnol. Adv., 36 (2018) 2101-2117.
5) C.A.R. Engel. A.J.J. Straathof, T.W. Zijlmans, W.M. van Gulik, L.A.M. van der Wielen, Fumaric acid production by fermentation, Appl. Microbiol. Biotechnol, 78 (2008) 379-389.
6) M. Ai, K. Ohdan, Formation of citraconic anhydride by vapor-phase decarboxylase-condensation of pyruvic acid. Stud. Surf. Sci. Catal., 101 (1996) 201-209.
7) S. Maina, A.A. Prabhu, N. Vivek, A. Vlysidis, A. Koutinas, V. Kumar, Prospects on bio-based 2,3-butanediol and acetoin production: Recent progress and advances, Biotechnol. Adv., 54 (2022) 107783.
8) C.R. Khudsange, K.L. Wasewar, Process intensification of esterification reaction for the production of propyl butyrate by pervaporation, Resource-Efficient Technologies 3 (2017) 88-93.

9) J.H. Clark, F.E.I. Deswarte, T.J. Farmer, The integration of green chemistry into future biorefineries, Biofuels Bioprod. Bioref. 3 (2009) 72-90.

10) N. Singh, R. Kumar, P.K. Sachan, Kinetic study of catalytic esterification of butyric acid and ethanol over Amberlyst 15, ISRN Chem. Eng. 2013 (2013) 1-7.

11) U. Wollina, Fumaric acid esters in dermatology, Indian Dermatol. Online J., 2 (2011) 111- 119.

12) W. Ninomiya, M. Sadakane, S. Matsuoka, H. Nakamura, H. Naitou, W. Ueda, An efficient synthesis of α-acyloxyacrylate esters as candidate monomers for bio-based polymers by heteropolyacid-catalyzed acylation of pyruvate esters, Green Chem. 11 (2009) 1666-1674.

13) Y. Wang, J.D. Lewis, Y. Román-Leshkov, Synthesis of itaconic acid ester analogues via self-aldol condensation of ethyl pyruvate catalyzed by hafnium BEA zeolites, ACS Catal. 6 (2016) 2739-2744.

14) R. Yang, S. Zu, T.I. Tonnessen, Ethyl pyruvate is a novel anti-inflammatory agent to treat multiple inflammatory organ injuries., J. Inflamm (Lond) 13 (2016) 37.

15) M.C. Reade, M.P. Fink, Bench-to-bedside review: Amelioration of acute renal impairment using ethyl pyruvate, Critical Care, 9 (2005) 556- 560.

16) H. Haidl, A. Schlagenhauf, A. Krebs, H. Plank, W. Wonisch, V. Fengler, A. Fiegl, G. Horl, M. Koestenberger, T. Wagner, E. Tafeit, G. Cvirn, S. Hallstrom, The anticoagulant effects of ethyl pyruvate in whole blood samples, Plos One, 15 (2020) e0240541.

17) M. Z. Durak, J.J. Churey, M. Gates, G. L. Sacks, R. W. Worobo, Decontamination of green onions and baby spinach by vaporized ethyl pyruvate, J. Food. Prot. 75 (2012) 1012-22.

18) Y. Zhang, S. Liao, H. Zhang, R. Liu, X. Tong, The selective aerobic oxidation of ethyl lactate to ethyl pyruvate mediated by a trace of HBr with visible light, Mol. Catal., 540 (2023) 113066.

19) T. Lu, J. Zou, Y. Zhan, X. Yang, Y. Wen, X. Wang, L. Zhou, J. Xu, Highly efficient oxidation of ethyl lactate to ethyl pyruvate catalyzed by TS-1 under mild conditions, ACS Catal., 8 (2018) 1287-1296.

20) X. Liu, Q. Wang, C. Liu, X. Wang, C. Peng, R. Liu, C. Yang, High-performance vapor-phase selective oxidation of ethyl lactate to ethyl pyruvate over SiO_2 supported PMoVNb oxides, Catalysts, 10 (2020) 197.

21) D. Pal, A. Keshav, B. Mazumdar, A. Kumar, H. Uslu, Production and recovery of pyruvic acid: Recent advances, J. Inst. Eng. India Ser. E., 2017.

22) H. Hronská, S. Micháliková, M. Rosenberg, Microbial production of specialty C4 dicarboxylic acids from maleic anhydride, J. Food Nutr. Res., 56 (2017) 219-231.

23) G. Li, J. Lian, H. Xue, Y. Jiang, M. Wu, J. Lin, L. Yang, Enzymatic preparation of pyruvare by a whole-cell biocatalyst coexpressing L-lactate oxidase and catalase, Process Biochem., 96 (2020) 113-121.

24) Q. Lu, X. Shan, W. Zeng, J. Zhou, Production of pyruvic acid with *Candida glabrata* using self-fermenting spent yeast cell dry powder as a seed nitrogen source, Bioresour Bioprocess., 9 (2022) 109.

25) D. Wang, L. Wang, L. Hou, X. Deng, Q. Gao, N. Gao, Metabolic engineering of Saccharomyces cerevisiae for accumulating pyruvic acid, Ann. Microbiol., 65 (2015) 2323-2331.

26) W.C. Moxley, M.A. Eiteman, Pyruvate production by *Escherichia coli* by use of pyruvate dehydrogenase variants, Appl. Environ. Microbiol., 87 (2021) e00487-21.

27) T. Ono, S. Imamura, Production of ethyl pyruvate, Patent Application. JPH1180088A, Sept 5, 1997.

28) A. Martínez-Castelló, M. Tejeda-Serrano, A. E. Nowacka, J. Oliver-Meseguer, A. Levya-Pérez, Solid-catalyzed esterification reaction of long-chain acids and alcohols in fixed-bed reactors at pilot plant scale, Chem. Eng. Process., 178 (2022) 109038.

29) T. Ennaert, J.V. Aelst, J. Dijkmans, R. De. Clercq, W. Schutyser, M. Dusselier, D. Verboekend, B.F. Sels, Potential and challenges of zeolite chemistry in the catalytic conversion of biomass, Chem. Soc. Rev., 45 (2016) 584-611.

30) J. Guilera, E. Ramirez, C. Fite, M. Iborra, J. Tejero, Thermal stability and water effect on ion-exchange resins in ethyl octyl ether production at high temperature, Appl. Catal. A-Gen., 467 (2013) 301-309.

31) S. Sripada, J.R. Kastner, Catalytic esterification using solid acid carbon catalysts synthesized by sustainable hydrothermal and plasma sulfonation techniques, Ind. Eng. Chem. Res, 61 (2022) 3928-3940.

32) L.J. Konwar, P. Maki-Arvela, J-P. Mikkola, SO_3H- containing functional carbon materials: Synthesis, structure, and acid catalysis, Chem. Rev., 119 (2019) 11576-11630.

33) J.R. Kastner, J. Miller, D.P. Geller, J. Locklin, L.H. Keith, T. Johnson, Catalytic esterification of fatty acids using solid acid catalysts generated from biochar and activated carbon, Catal., 190 (2012) 122-132.

34) V.C. Nguyen, N.Q. Bui, P. Mascunan, T.T. Ha Vu, P. Fongarland, N. Essayem, Esterification of aqueous lactic acid solutions with ethanol using carbon solid acid

catalysts: Amberlyst 15, sulfonated pyrolyzed wood and graphene oxide. Appl.Catal. A: Gen.., 552 (2018) 184-191.

35) X-Y. Liu, M. Huang, H-L Ma, Z-Q Zhang, J-M. Gao, Y-L. Zhu, X-J. Han, X-Y. Guo, Preparation of a carbon-based solid acid catalyst by sulfonating activated carbon in a chemical reduction process, Molecules, 15 (2010) 7188-7196.

36) Y. Pi, W. Liu, J. Wang, G. Peng, D. Jiang, R. Guo, D. Yin, Preparation of activated carbon-based solid sulfonic acid and its catalytic performance in biodiesel preparation, Front. Chem. 10 (2022) 944398.

37) M. Pirmoradi, N. Janulaitis, R.J. Gulotty, Jr., J.R. Kastner, Continuous hydrogenation of aqueous furfural using a metal-supported activated carbon monolith, ACS Omega, 5 (2020) 7836-7849.

38) E.M. Karp, R.M. Cywar, L.P. Manker, P.O. Saboe, C.T. Nimlos, D. Salvachua, X. Wang, B.A. Black, M. L. Reed, W.E. Michener, N.A. Rorrer, G. T. Beckam, Post-fermentation recovery of biobased carboxylic acids, ACS Sustainable Chem. Eng. 6 (2018) 15273-15283.

39) C. Delhomme, S.L.M. Goh, F.E. Kühn, D. Weuster-Botz. Esterification of bio-based succinic acid in biphasic systems: Comparison of chemical and biological catalysts. J.Mol.Catal. B Enzym., 80 (2012) 39-47.

40) D.A. Sievers, L. Tao, D.J. Schell, Performance and techno-economic assessment of several solid-liquid separation technologies for processing dilute-acid pretreatment corn stover, Bioresour. Technol., 167 (2014) 291-296.

41) T.J. Schwartz, B.J. O'Neill, B.H. Shanks, J.A. Dumesic, Bridging the chemical and biological catalysis gap: Challenges and outlooks for producing sustainable chemicals. ACS Catal. 4 (2014) 2060-2069.

42) M.D. Argyle, C.H. Bartholomew, Heterogeneous Catalyst Deactivation and Regeneration: A Review, Catalysts 5 (2015)145-269.

43) C. Sievers, Y. Noda, L. Qi, E.M. Albuquerque, R.M. Rioux, S.L. Scott, Phenomena affecting catalytic reactions at solid-liquid interfaces, ACS Catal. 6 (2016) 8286-8307.

44) Z. Zhang, J.E. Jackson, D.J. Miller, Effect of biogenic fermentation impurities on lactic acid hydrogenation to propylene glycol, Bioresour. Technol. 99 (2008) 5873-5880.

45) T.J. Schwartz, Z.J. Brentzel, J.A. Dumesic, Inhibition of metal hydrogenation catalysts by biogenic impurities. Catal Lett. 145 (2015)15-22.

46) F.J. Holzhäuser, J. Artz, S. Palkovits, D. Kreyenschulte, J. Büchs, R. Palkovits, Electrocatalytic upgrading of itaconic acid to methylsuccinic acid using fermentation broth as a substrate solution. Green Chem. 19 (2017) 2390-2397.

47) P. Kasinathan, D.W. Hwang, U. Lee, Y.K. Hwang, J.S. Change, Effect of solvent and impurity on synthesis of ethyl lactate from fermentation-derived ammonium lactate, Chem. Eng. Sci. 66 (2011) 4549-4554.

48) R. Luque, C.S.K. Lin, C. Du, D.J. Macquarrie, A. Koutinas, R. Wang, C. Wedd, J.H. Clark, Chemical transformations of succinic acid recovered from fermentation broths by a novel direct vacuum distillation-crystallisation method. Green Chem., 11 (2009) 193-200.

49) M.A. Eiteman, M.J. Chastain, Optimization of the ion-exchange analysis of organic acids from fermentation, Anal. Chim. Acta, 338 (1997) 69-75.

50) I. Miller, J.E. Freund, Probability and Statistics for Engineers. Prentice-Hall, Inc., Englewood Cliffs, NJ, 1985.

51) H. Liu, Q. Peng, J. Ren, B. Shi, Y. Wang, Synthesis of a sulfated-group-riched carbonaceous catalyst and its application in the esterification of succinic acid and fructose dehydration to form HMF, J. Iran. Chem. Soc. 18 (2021) 2649-2656.

52) M-L. Tao, H-Y. Guan, X-H. Wang, Y-C. Liu, R-F. Louh, Fabrication of sulfonated carbon catalyst from biomass waste and its use for glycerol esterification, Fuel Process. Technol. 138 (2015) 335-360.

53) E. Chaichana, W. Wiwatthanodom, B. Jongsomjit, Carbon-based catalyst from pyrolysis of waste tire for catalytic ethanol dehydration to ethylene and diethyl ether. Int.J. Chem.Eng. 2019, (2019) 1-10.

54) S. Suganuma, K. Nakajima, M. Kitano, D. Yamaguchi, H. Kato, S. Hayashi, M. Hara, Hydrolysis of cellulose by amorphous carbon bearing SO_3H, COOH, and OH groups, J. Am. Chem. Soc. 130 (2008) 12787-12793.

55) P. M. Mortensen, D. Gardini, H.W.P. de Carvalho, C.D. Damsgaard, J-D. Grunwaldt, P.A. Jensen, J.B. Wagner, A.D. Jensen, Stability and resistance of nickel catalysts for hydrodeoxygenation: carbon deposition and effects of sulfur, potassium, and chlorine in the feed, Catal. Sci. Technol., 4 (2014) 3672-3686.

56) Y. Liu, E. Lotero, J.G.Goodwin Jr, Effect of water on sulfuric acid catalyzed esterification, J. Mol. Catal. A. Chem., 245 (2006) 132-140.

57) J-Y. Park, Z-M. Wang, D-K. Kim, J-S. Lee, Effects of water on the esterification of free fatty acids by acid catalysts, Renew. Energy, 35 (2010) 614-618.

58) S. Sripada, J.R. Kastner, Continuous catalytic esterification using a solid acid activated carbon monolith: Comparison of granular and monolith forms with a commercial catalyst, Chem. Eng. J., 476 (2023)146586.

59) R.J. Perkins, R.K. Shoemaker, B.K. Carpenter, V. Vaida, Chemical equilibria and kinetics in aqueous solutions of zymonic acid, J. Phys. Chem. A, 120 (2016) 10096-10107.

60) M. Zhang, Y. Yu, Dehydration of ethanol to ethylene, Ind. Eng. Chem. Res. 52 (2013) 9505-9514.

61) A.C. Rios, P.P. Bera, J.A. Moreno, G. Cooper, Pyruvate aldol condensation product: A metabolite that escaped synthetic preparation for over a century, ACS Omega, 5 (2020) 15063-15068.

Table 6.1. Physical Properties and Reaction Characteristics of the Sulfonated Carbons and Amberlyst-15.

Catalyst	Surface area (m^2/g)	SO_3H density[c] (mmol g^{-1})	Reaction rate (mmol g^{-1} h^{-1})	TOF (1.25 h) (min^{-1})
sGAC[a]	867	0.04 ± 0.01	9.64 ± 0.31	3.65
sACM[b]	550	0.12 ± 0.00	8.85 ± 0.04	1.19
Amberlyst-15	38	2.57 ± 0.29	8.30 ± 0.35	0.05

Reaction conditions: temperature 150 °C, residence time includes heat-up time, catalyst loading 1 g, reaction volume 20 mL, and pyruvic acid concentration 40 g/L.

[a] GAC treated with 2 M H_2SO_4 by incipient wetness impregnation, followed by hydrothermal treatment at 180 °C.

[b] ACM core treated with 2 M H_2SO_4 by sonication, followed by hydrothermal treatment at 250 °C, and crushed prior to the reaction.

[c] Based on elemental analysis.[31]

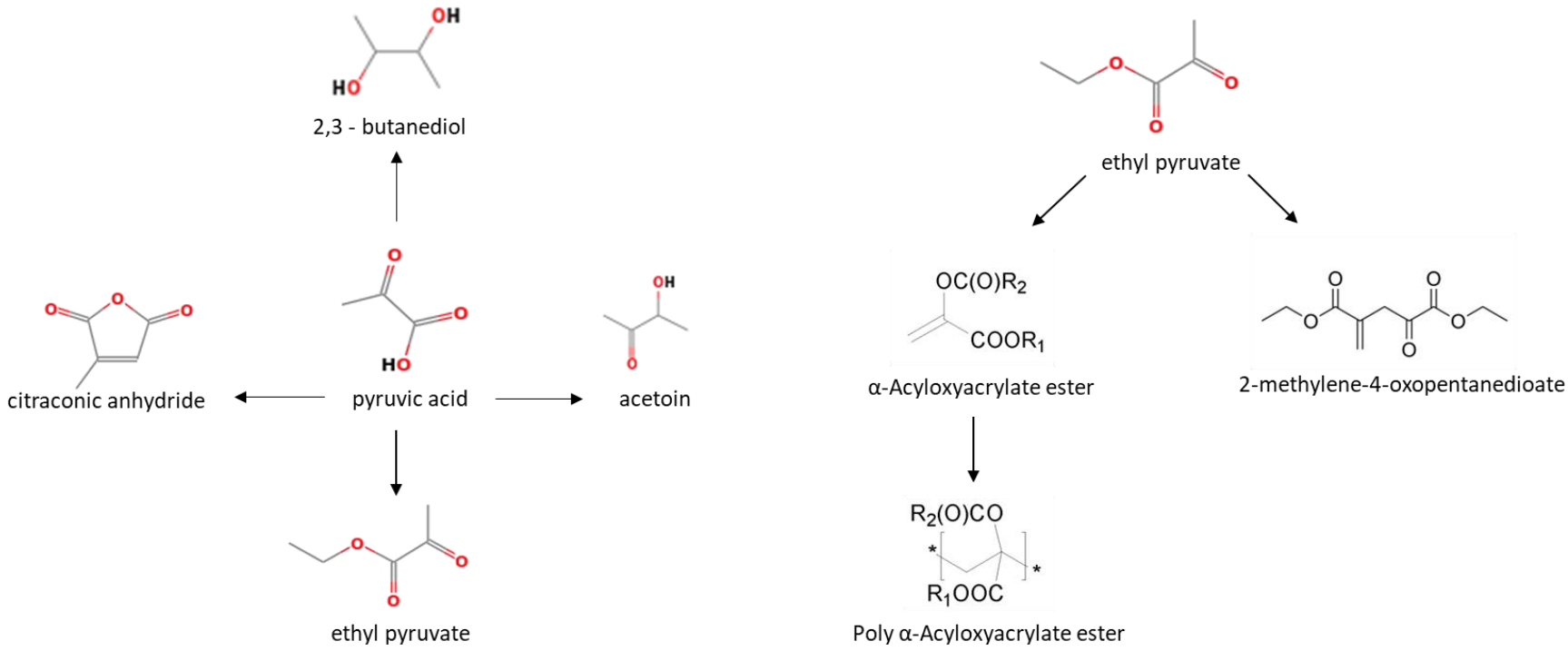

Figure 6.1. Various possible products from pyruvic acid and ethyl pyruvate.

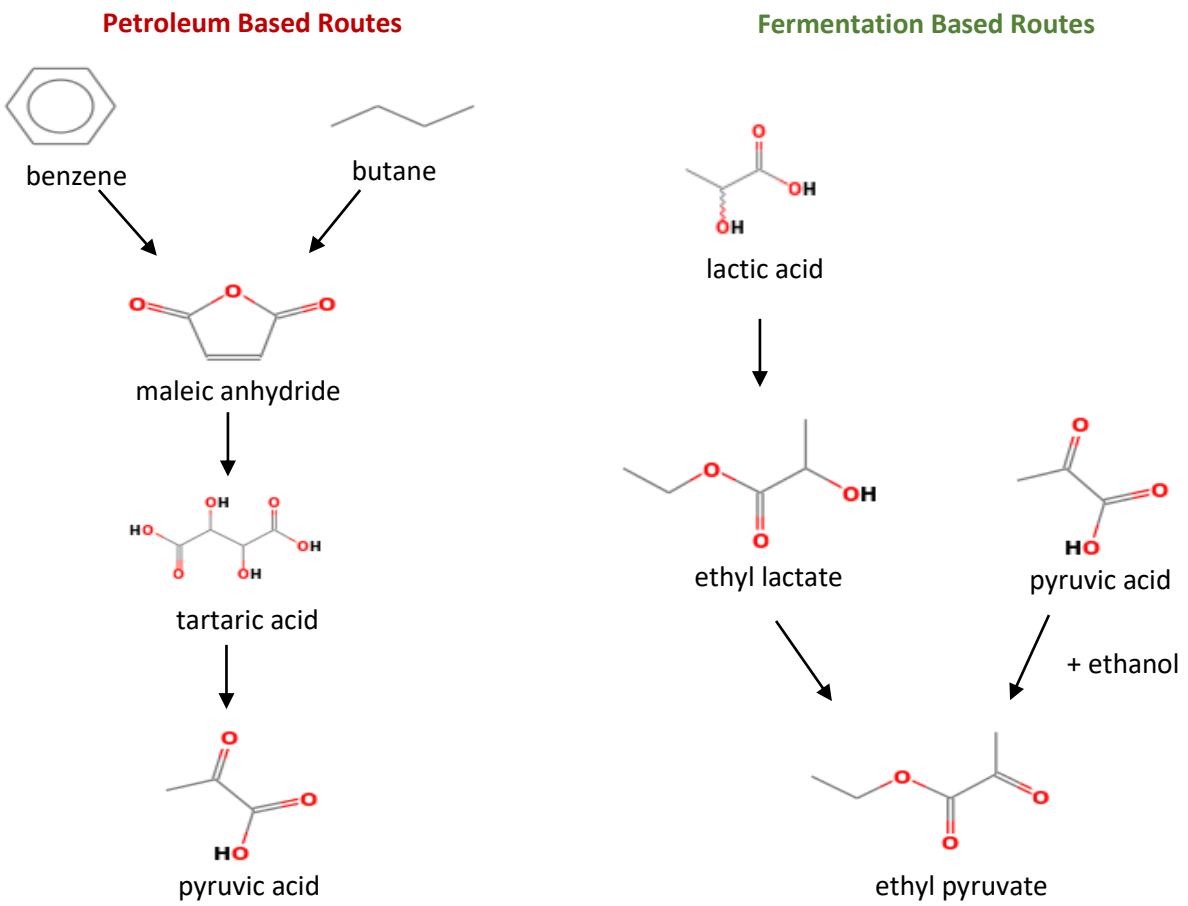

Figure 6.2. Reaction pathways depicting petroleum-based routes to pyruvic acid, and fermentation-based routes to ethyl pyruvate from lactic acid (two-step) and pyruvic acid (single-step).

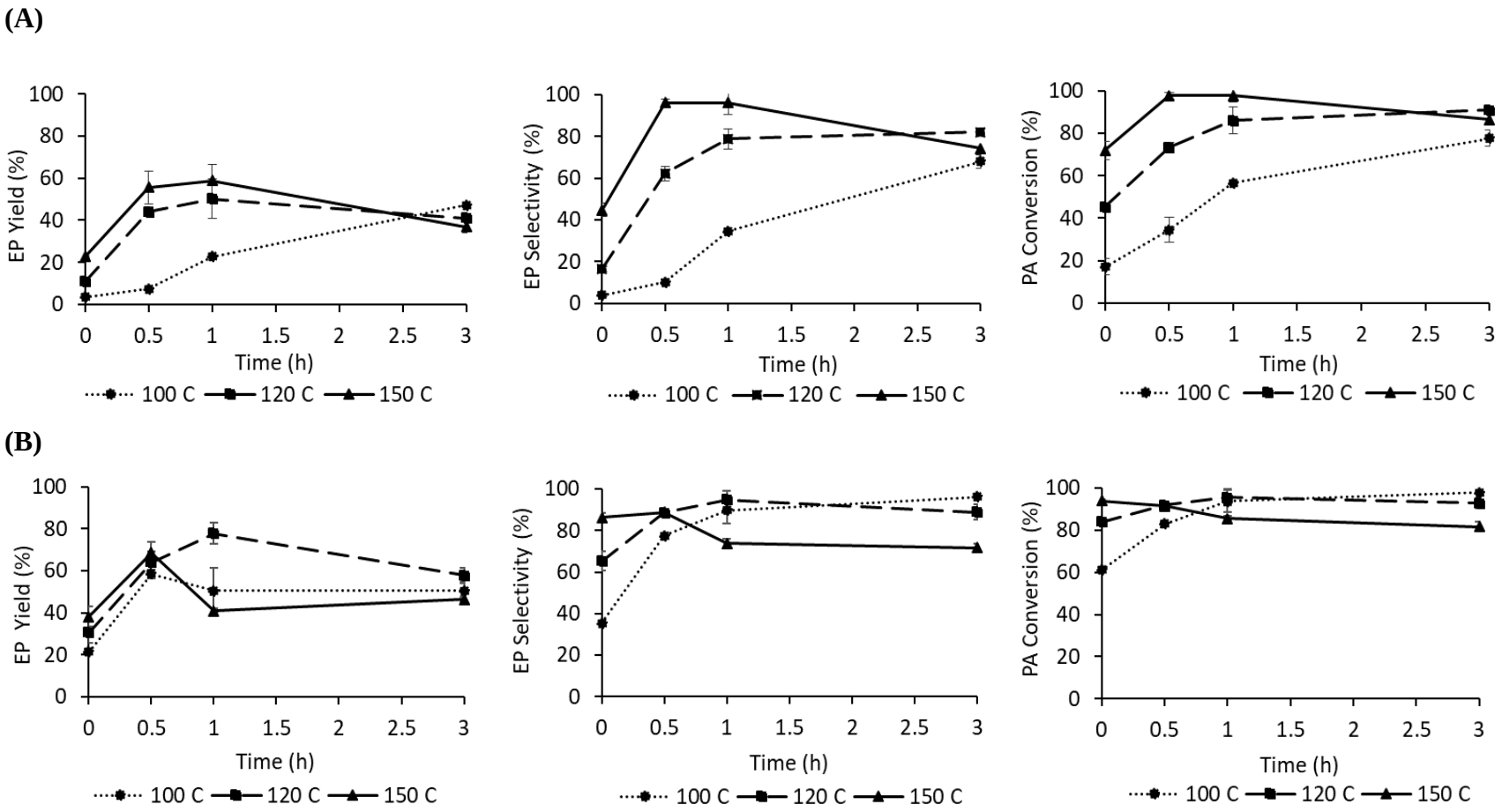

Figure 6.3. Effect of reaction temperature (100-150 °C) and residence time (0-3 h) on ethyl pyruvate (EP) yield and selectivity, and pyruvic acid (PA) conversion for the (A) sGAC and (B) Amberlyst-15.

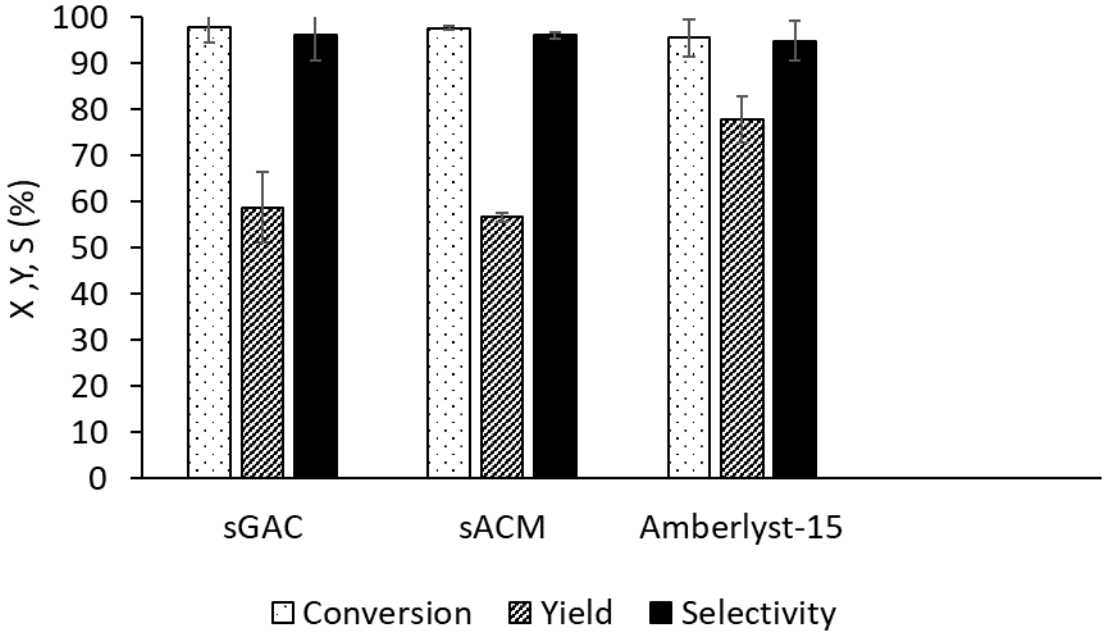

Figure 6.4. Comparison of pyruvic acid (PA) conversion, ethyl pyruvate (EP) yield and selectivity, for the sGAC, sACM, and Amberlyst-15. Reaction conditions: Temperature = 120 °C for Amberlyst-15, 150 °C for the sGAC and sACM, Pressure = 4.3 bar for Amberlyst-15 and 9 bar for the sGAC and sACM, residence time = 1 h, catalyst loading = 5 wt %.

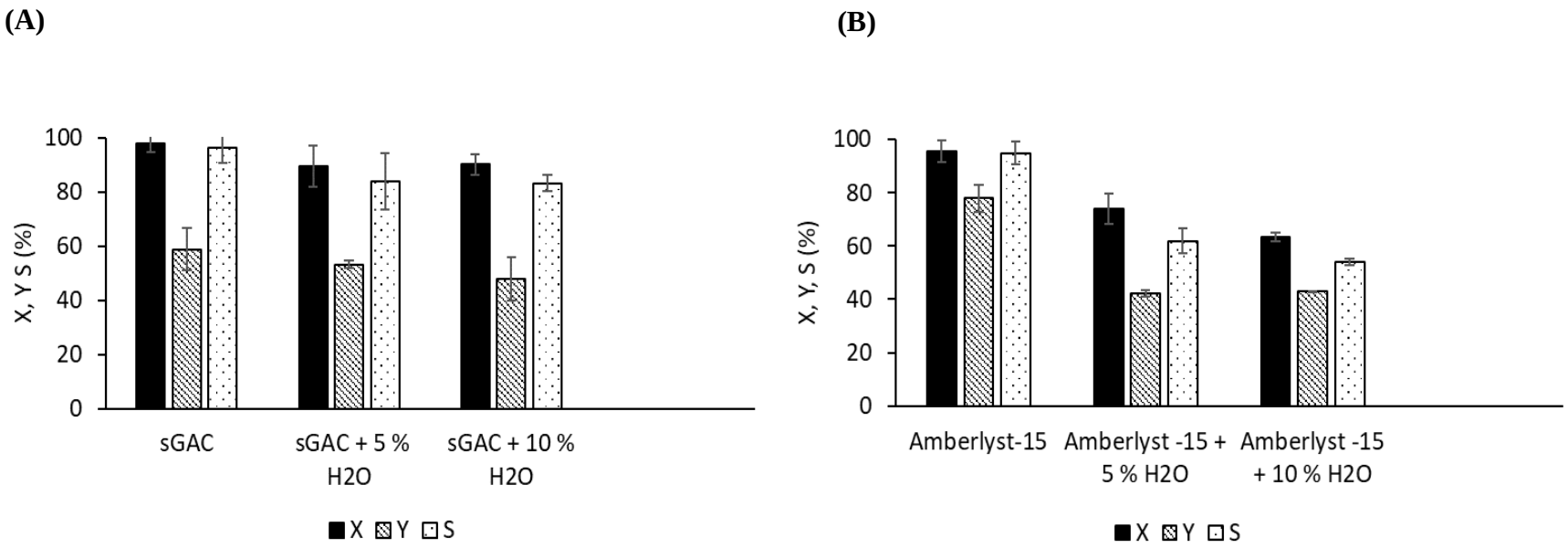

Figure 6.5. Effect of water (5 and 10 %) on pyruvic acid conversion (X), ethyl pyruvate yield (Y) and selectivity (S) for the (A) sGAC and (B) Amberlyst-15. Reaction conditions: Temperature = 120 °C for Amberlyst-15, 150 °C for the sGAC, Pressure = 4.3 bar for Amberlyst-15 and 9 bar for the sGAC, residence time = 1 h, catalyst loading = 5 wt %.

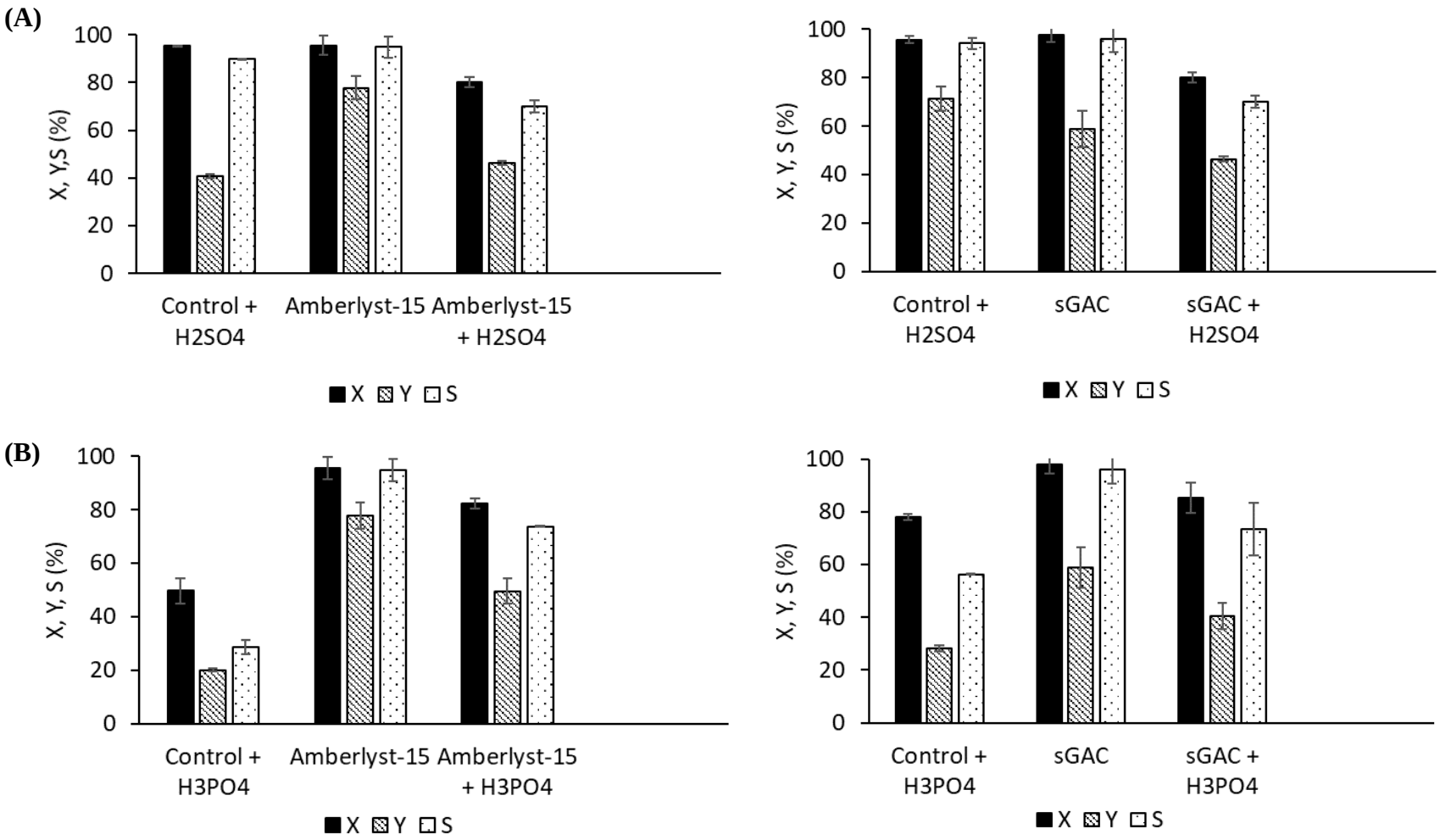

Figure 6.6. Effect of (A) sulfur (13.3 mM H_2SO_4) and (B) phosphorus (4.3 mM H_3PO_4) on pyruvic acid conversion (X), ethyl pyruvate yield (Y) and selectivity (S) for the sGAC and Amberlyst-15. Reaction conditions: Temperature = 120 °C for Amberlyst-15, 150 °C for the sGAC, Pressure = 4.3 bar for Amberlyst-15 and 9 bar for the sGAC, residence time = 1 h, catalyst loading = 5 wt%.

CHAPTER 7

DEVELOPMENT OF SOLID BASE CARBON MONOLITH CATALYSTS FOR THE CONTINUOUS SYNTHESIS OF HIGH-DENSITY AVIATION FUEL PRECURSORS

[1] S. Sripada, J.R. Kastner, 2023

To be submitted to *Catalysis Communications*

Abstract

Cyclopentanone (CP), a cyclic hydrocarbon, is gaining attention as a bio-based platform chemical for the synthesis of high-density jet fuel range cycloalkanes. The base-catalyzed self-condensation of CP yields 2-cyclopentylidene cyclopentanone (2-CP) and 2,5-dicyclopentylidene cyclopentanone (3-CP). 2-CP has applications in fuels, fragrances and flavors, and 3-CP is used as a precursor for diesel-grade products. In this study solid base activated carbon monolith (ACM) supported hydrotalcite catalysts (HT/ACM) were synthesized using traditional thermal calcination, rehydration and sustainable air plasma techniques and demonstrated for continuous cyclopentanone self-condensation. Among the ACM supported hydrotalcites, the HT/ACM activated by air plasma at 100 W for 1 min (PHT/ACM-100W) displayed a higher 2-CP space-time-yield of 641 g/Lcat/h, and selectivity of 27% (220 °C, 1 atm, 0.73 min vapor phase contact time). PHT/ACM-100 W displayed higher CP conversion (42%) compared to the unsupported calcined (22%, 500 °C, 4 h) and rehydrated (37%, 8 h, 105 °C) ACM catalysts, yet significantly lower space-time-yields, suggesting low hydrotalcite distribution and loading on the carbon monolith. The plasma activated carbon monolith supported hydrotalcite catalysts synthesized in this work are promising alternatives to the thermally activated and rehydrated hydrotalcites for the catalytic upgrading of bio-based cyclic and linear ketones.

Keywords: Cyclopentanone, condensation, activated carbon monolith, hydrotalcite, plasma

7.1 Introduction

Aviation fuels account for approximately 12% of the liquid transportation fuels globally. Currently, high-density aviation fuels such as JP-10, RJ-7 and RJ-5 are synthesized from petroleum-based feedstocks.[1] The rising fuel demand of the aviation industry and the energy and environmental concerns surrounding fossil fuel consumption has generated an interest in the catalytic conversion of renewable biomass to aviation fuels. Lignocellulosic biomass has attracted attention as a potential feedstock for jet fuels. However, the carbon content of lignocellulose is C_5-C_6, which is much lower than the minimum carbon number required for diesel and aviation kerosene. C-C- coupling reactions (aldol condensation, hydroxyl alkylation/alkylation, Diels-Alder reactions) have been employed to synthesize jet fuel range alkanes from lignocellulose.[2,3] However, these bio-jet fuels are composed of straight or branched paraffins. Although these paraffins have high cetane number and good thermal stability, they have lower densities (<0.79 g/mL)[4] and heating values compared to conventional jet fuel (a mixture of paraffins and cyclic hydrocarbons), due to which they must be blended with conventional jet fuel to meet the aviation fuel specifications. Therefore, there is a need to develop sustainable and economically feasible routes to produce high-density cyclic hydrocarbons using lignocellulosic platform chemicals that meet aviation fuel standards. [1]

Cyclopentanone (CP), a cyclic hydrocarbon, is an important chemical intermediate used in the manufacturing of pharmaceuticals, insecticides, and rubber chemicals. CP is currently produced by the decarboxylation of adipic acid at high temperatures. [5] However, CP is also an important lignocellulosic platform chemical, with the advantages of wide feedstock availability and low price.[6] CP can be produced at high carbon yields (62-95.8%) by the aqueous-phase selective hydrogenation of furfural, which is obtained by the hydrolysis-dehydration of hemicellulose in

lignocellulosic biomass. [7] CP can be catalytically converted by a self-condensation reaction to 2-cyclopentylidene cyclopentanone (dimer C10) and 2,5-dicyclopentylidene cyclopentanone (trimer C15), which on further hydrodeoxygenation results in high density jet fuel range cycloalkanes bi(cyclopentane) and tri(cyclopentane). [8] The dimer 2-CP has applications in fuels, and in hydrogenated form in fragrances and flavors. The trimer is also used as a precursor for diesel-grade products. The mono-condensed product (dimer) is preferred over the di-condensed product (trimer) for producing high density fuel with suitable viscosity. [8] However, most catalysts show low selectivity towards the dimer, due to the rapid formation of the trimer, indicating the need for catalysts with high selectivity towards 2-CP. [4]

Further, the steric hindrance exhibited by cyclopentanone makes its self-condensation difficult to achieve, requiring a high efficiency catalyst to promote the reaction. [9] Homogeneous catalysts such as NaOH have been studied for the conversion of cyclic ketones to bi and tri-cyclic sustainable aviation fuels by self-condensation reactions. [10] NaOH has been reported to have excellent catalytic activity in the aldol condensation of cyclic ketones and furfural. However, homogeneous catalysts such as NaOH present challenges of separation of the catalyst from the product, reactor corrosion and environmental concerns in terms of disposal. [11] These limitations can be overcome by using heterogeneous solid catalysts, which are advantageous over homogeneous catalysts in minimizing waste streams and reducing equipment corrosion. Solid base catalysts such as Na_2CO_3, $Ca(OH)_2$, $MgO\text{-}ZrO_2$ and solid acids such as zeolites and Amberlyst-15 have been employed for the aldol condensation of aldehydes and ketones, and aldol self-condensation reactions. [12,13,14] However, these weak bases show low catalytic activity due to their inability to activate cyclopentanone to form the carbanion which is necessary for condensation. Solid acids such as Amberlyst-15 and zeolites are limited by low surface area.

Further, Amberlyst-15 has low thermal stability, and presents a risk of leaching of carcinogenic styrene monomers, posing health and environmental concerns. [15,16]

Hydrotalcites (HTs) are gaining interest for aldol condensation reactions. They are advantageous over other solid bases in being more environmentally benign in comparison to heavy metals and cost-effective. HTs are layered double hydroxides (LDH's) comprising positively charged hydroxide layers with charge balancing anions and water molecules in the interlayers. They are represented by the general formula $[M^{2+}_{(1-x)}\ M^{3+}_{x}\ (OH)_2]\ (A^{n-})_{x/n}\ .\ zH_2O$ where M^{2+} represents metallic cations such as Mg^{2+}, Ca^{2+}, Zn^{2+} , while M^{3+} represents Al^{3+}, Fe^{3+}, Mn^{3+}.[17] The interlayer anions are usually carbonates (CO_3^{2-}) in naturally occurring hydrotalcites, however they could also be Cl^-, or NO_3^-.[18] Mg- Al HT's have been employed as mixed oxides Mg (Al) O with Lewis basicity obtained by thermal decomposition/calcination (activation) of the Mg-Al HT precursor. Reconstruction of the mixed oxide by immersion in decarbonated water or contact with water vapor yields meixnerite, a HT analogue with OH^- ions in the interlayer region. [19] A schematic depiction of the calcination and rehydration of Mg-Al hydrotalcites is shown in Figure 7.1.[20] Rehydrated hydrotalcites possess strong basicity and exhibit higher catalytic efficiency in comparison to calcined hydrotalcite. Various authors have studied the liquid and vapor phase rehydration of hydrotalcites. [11,21,22] Abello and co-workers found that gas phase rehydration led to a higher degree of reconstruction of the lamellar structure of the mixed oxide compared to liquid phase rehydration. [23]

Aldol condensation reactions can be catalyzed by both acid and base catalysts. Calcined hydrotalcites have the advantage of bifunctional acid-base pairs of medium-high strength. Further rehydrated hydrotalcites display strong Brønsted base sites (OH^-) in addition to weak Lewis acid sites (Al^{3+}). Aldol condensation follows an enolate mechanism and the stronger

basicity of the rehydrated catalyst is favorable for the generation of the carbanion. The Lewis acid sites on hydrotalcite bring about protonation of the carbonyl group, increasing its electrophilicity. This synergism between the base and acid sites on HTs have been found to be beneficial for aldol condensation.[6]

However, hydrotalcite activation involves traditional long-duration thermal calcination methods which are economically and energetically intensive. Treating these materials at high temperatures may also bring about volume losses causing collapse of the structure [24]. Recently, there has been an interest in the plasma activation of hydrotalcites. Plasma is a partially ionized gas comprising electrons, ions, photons, radicals, and excited species, and is generated by applying a high voltage to a gas/gas mixture for ionization. [25] Low temperature and pressure, short duration plasma methods may serve as a sustainable alternative to the conventional high-temperature calcination methods. [24] Plasma can enhance the concentration of OH^- ions in the interlayer regions of hydrotalcites, which are the active sites for catalytic reactions. [26] In addition, solid bases synthesized by plasma techniques have previously been shown to have high catalytic stability. [27]

Supported hydrotalcites are receiving attention due to their base catalysis activity, enhanced mechanical properties and easier separation. Introducing HT onto an inexpensive support material that will enable high HT loading would be desirable. In this context, activated carbon (AC) can serve as a valuable catalyst support as it can be obtained from inexpensive woody biomass, has high surface area (enabling higher active phase loading), is stable under harsh process conditions and possesses good mechanical properties. [28] Supporting HT on AC would result in better HT dispersion in the pores of AC, increasing the accessibility of active sites, leading to improved catalytic performance and productivity, in comparison to unsupported HT.

Further an AC support would play a key role in improving water tolerance and thereby stability of the catalyst, which would be beneficial in various processes such as condensation reactions. [29] HT has been supported on carbon nanofibers/ multiwalled carbon nanotubes and successfully applied for CO_2 adsorption and the synthesis of methyl isobutyl ketone from acetone. [30,31] Although nanocarbons are significant catalytic support materials, their applications in continuous processes are limited. For multiphase catalysis, a slurry suspension of these carbon catalysts results in particle attrition and difficulty in catalyst recovery post filtration. In gas-solid applications, these carbon granules/powders cannot be employed in packed-beds due to large pressure drop. To overcome these limitations, there is a lot of interest in employing structured catalysts that can avoid the time-consuming filtration process and ensure better active phase dispersion.[32] Activated carbon in monolith form (ACM) offers advantages over powdered/granular forms, including lower pressure-drop, high mass transfer rates and high space time yields, which facilitates its applications in continuous processes. [33] The well-developed porosity and large surface area to volume ratio of the carbon monolith also enables better catalyst dispersion, indicating the numerous advantages of employing the ACM as a support for hydrotalcite. However, there is limited to no knowledge on the application of monolith supported hydrotalcites for continuous processes.

Mg-Al HT has been shown to have high catalytic activity in the self-condensation of cyclopentanone. Yang et al. studied the batch self-condensation of CP using various solid base catalysts including MgO, KF/Al_2O_3, $CaO\text{-}CeO_2$, CaO, LiAl-HT and Mg-Al HT and observed superior catalytic performance with Mg-Al HT.[6] Very few studies have investigated the continuous self-condensation of CP. Sheng and coworkers studied the continuous flow self-condensation of CP in a fixed bed reactor and found that Mg-Al HT outperformed other solid

bases including LiAlHT, MgO-ZrO_2 and CeO_2 .They obtained 73.2% CP conversion and 70% selectivity towards the trimer (C15). [34] The excellent catalytic performance of Mg-Al HT was attributed to the high surface area, strong acidity and basicity, and synergism of acid and base sites on this catalyst. [6,34] However, there has been very limited research on continuous catalytic condensation of CP with solid base carbon monolith catalysts.

In this study, we investigated the continuous self-condensation of cyclopentanone in a packed bed reactor with ACM supported HT (HT/ACM) synthesized by calcination, rehydration, and air plasma methods. We theorize that with the advantages the ACM support has to offer, activated carbon monolith supported hydrotalcite would serve as a green catalyst for the continuous synthesis of jet fuel range cycloalkanes.

7.2. Experimental Section

7.2.1 Materials

Cyclopentanone (C_5H_8O, purity ≥ 99%) and hydrotalcite (HTC) powder with MgO/Al_2O_3 ratio of 3:1 were purchased from Sigma Aldrich and 2-cyclopentylidenecyclopentanone ($C_{10}H_{14}O$, purity 95%) was procured from Astatech. Three catalysts were compared in this study; an activated carbon monolith supported calcined hydrotalcite catalyst (CHT/ACM), an activated carbon monolith supported calcined and rehydrated hydrotalcite catalyst (RCHT/ACM), activated carbon monolith supported plasma-activated hydrotalcite catalyst (PHT/ACM). The wood-based granular activated carbon (GAC) (surface area of 1350 m^2/g and pore volume of 1.2 cc/g) and activated carbon monolith (ACM 101-H) were provided by Applied Catalysts (Laurens, SC). The ACM was manufactured by coextrusion of 50% activated carbon and 50% of a ceramic binder. Each monolith core has a diameter and length of 1 inch, 400 cells/in^2, wall

thickness of 0.01- inch, cell spacing of 0.044-inch, geometric surface area of 70.8 in^2/in^3, open frontal area of 0.59 in^2, density of 350 $kg/m^{3,}$ surface area of 598 m^2/g (BET), pore diameter of 29.8 Å and pore volume of 0.5 cc/g (BJH). [33]

7.2.2 Catalyst Preparation

The ACM supported hydrotalcite was activated by calcination, rehydration, and plasma methods. Raw hydrotalcite (HT) powder (MgO/Al_2O_3 3:1) was calcined in air at 500 °C for 4 hours (HT powder is insoluble in water and must be calcined in air prior to dissolution in dI H_2O). Each ACM core was sonicated in a 100 mL aqueous solution of 5 wt% calcined Mg-Al HT at 30 °C for 30 min, followed by drying in air at 105 °C (HT/ACM). The ACM supported HT was calcined under N_2 at 500 °C for 4 h (CHT/ACM). Rehydration was performed both at room temperature and at 105 °C. The CHT/ACM was rehydrated with water vapor at room temperature under a flow of N_2 (RCHT/ACM-RT). Rehydration at 105 °C was performed under N_2 with decarbonated water for 8 h at a liquid flow rate of 0.5 mL/min (RCHT/ACM-105 °C). Calcination and rehydration steps were performed in a packed bed reactor (Parr Instrument Company). Plasma activation of the HT/ACM was performed at 30 W and 100 W, to determine the effect of plasma power on hydrotalcite activation. Plasma treatment at 30 W was performed in a Harrick expanded plasma cleaner (PDC-001, 115V, chamber size 150 × 170 mm, maximum radiofrequency power 30 W) in air for 10 min (PHT/ACM-30W). Plasma activation at 100 W was performed in a Tergeo-plus plasma cleaner (PIE Scientific, chamber size 160 × 280 mm, maximum radiofrequency power 150 W) in air for 1 min (PHT/ACM-100W). With both plasma cleaners, 1 ACM core was treated at a time.

7.2.3 Catalyst Characterization

The catalysts were characterized by various techniques to study their structure, composition, and surface morphology. Scanning Transmission Electron Microscopy (STEM) Imaging was performed on a Hitachi SU-9000 STEM. Subsequent Energy-dispersive X-ray spectroscopy analysis was conducted on an Oxford Xmax EDS detector. The Mg and Al content on the carbon catalysts was quantified by Microwave Digestions followed by Inductively Coupled Plasma - Optical Emission Spectroscopy (ICP-OES) analysis.

7.2.4 Analytical

The liquid sample collected from the reactor was analyzed using HP 5890 Series II gas chromatography equipped with a flame ionization detector (GC-FID) and a HP Innowax column (30 m × 0.25 mm × 0.25 mm). The GC-FID was operated with the method of inlet temperature 230 ℃, detector temperature 240 ℃, initial oven temperature of 45 ℃ for 2.5 minutes followed by a ramp of 10 ℃ /min for 15.5 minutes and then held at 200 ℃ for 5 minutes. 1 μL of each sample was injected on the GC-FID in triplicate. [35]

7.2.5 Catalytic Reactions

Cyclopentanone self-condensation reactions were performed in a continuous flow reactor system (Parr Instrument Company) at atmospheric pressure. Once the reactor reached the desired temperature and was in steady state regime, the liquid feed (neat cyclopentanone) and nitrogen (50 mL/min) were continuously passed through the stainless-steel packed bed reactor (Parr, Moline, IL) (1-inch inner diameter) concurrently downwards through a T-junction. The gas flow rate was controlled by a Brooks Delta II Smart Mass Flow Controller, while the liquid feedstock was pumped into the reactor using a Scientific Systems LD-Class HPLC pump. The catalyst

(approximately 14-15 g corresponding to 3 cores, packing height of 10-11 cm) was held in place by a stainless-steel screen and quartz wool above and below the bed. The reactor temperature was controlled by a Thermcraft Lab-Temp 1760-watt furnace powered by a Parr 4875 Power Controller and the pressure was regulated with a TESCOM back pressure regulator. Post reaction, the liquid product was collected in a condenser (stainless steel vessel with a cooling jacket) connected to a Brookfield TC-602 water bath maintained at 6 °C.

Reaction Scheme

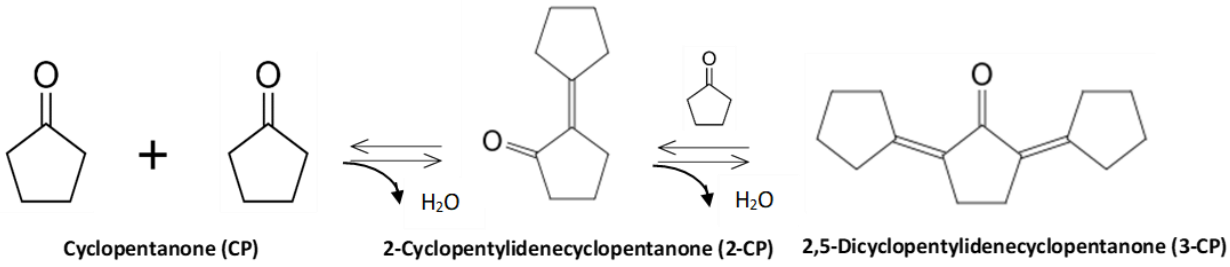

The optimum reaction conditions (temperature, liquid flow rate) for CP self-condensation for the ACM supported calcined hydrotalcite (CHT/ACM) were determined by performing a series of experiments at temperatures ranging from 140-220 °C and liquid flow rates of 1-3 mL/min. The order of performing the optimization experiments to determine the effect of various reaction parameters on product selectivity and space time yield were as follows: (i) testing the effect of varying temperature (T), (ii) varying liquid flow rates (Q_l). To compare the catalytic activity of the ACM supported calcined (CHT/ACM), rehydrated (RCHT/ACM-RT, RCHT/ACM-105 °C) and plasma activated (PHT/ACM-30 W, PHT/ACM-100W) hydrotalcites and the unsupported calcined (CHT) and rehydrated catalysts (RCHT), continuous cyclopentanone condensation reactions were performed at a temperature of 220 °C, pressure of 1 atm, liquid flow rate of 2

mL/min (contact time : 3.5-18.3 min) and N_2 flow rate of 50 mL/min (contact time : 0.14-0.73 min).

For all continuous reactions, the main kinetic parameters including conversion (X = mol CP converted/mol CP fed), yield (Y= mol 2-CP produced/mol CP fed), and selectivity (S = mol 2-CP produced/mol feed converted) were determined. Liquid hourly space velocity (LHSV, 1/h) was calculated from $[Q_{in} * \rho_{cat}]/W$. Gas hourly space velocity (GHSV, 1/h) was calculated as $[Q_{gas,in} * \rho_{cat}]/W$ where $Q_{gas,in}$ = 50 mL/min, and 1/GHSV gives the vapor phase residence time. 2-CP space time yield (STY, g/L-cat/h) was calculated as $[F_{out} * \rho_{cat} * MW]/W$ where Q_{in} is the inlet volumetric molar flow rate (mL/min), ρ_{cat} is the bulk density of the catalyst, F_{out} is the outlet molar flow rate, W is the catalyst mass, and MW is the molecular weight.

7. 2.6 Statistical Analysis

The ICP-OES, and GC-FID analyses were performed in triplicate and reported as the mean and sample standard deviation. The sample standard deviation was calculated from the range (*R*) for small sample size (*n*) (for $n \leq 5$, R/d_2, where $d_2 = 1.128$). [36] A Student's t-test was performed in the analysis between two means (i.e., catalysts) for the 2-CP STY, selectivity, and CP conversion assuming the null hypothesis with the reported level of significance (α).

7.3 Results and Discussion

7.3.1 Catalyst Characterization

The STEM-EDS images of the unsupported calcined (CHT) and rehydrated (RCHT) hydrotalcites indicate the presence of almost spherical aggregates of hydrotalcite platelets (Figure 7.2).[37] EDS analysis of the CHT and RCHT displayed Mg, Al, and oxygen, suggesting

the formation of Mg-Al mixed oxides post calcination. Figure 7.3 (A) and (B) depict the ACM supported calcined (CHT/ACM) and rehydrated (RCHT/ACM-105 °C) catalysts. The ACM supported plasma catalysts activated at 30 W (PHT/ACM-30 W) and 100 W (PHT/ACM-100W) are shown in Figure 7.3 C and 7.3 D. STEM images of all the ACM supported catalysts indicate a porous carbon network with hydrotalcite aggregates dispersed almost evenly on the carbon surface.[38] Further, the rehydrated (unsupported and ACM supported) and plasma activated catalysts displayed a greater aggregation of hydrotalcite platelets compared to the calcined catalysts (CHT and CHT/ACM). The formation of hydrotalcite agglomerates has been previously associated with the formation of hydroxide ions in the interlayers of hydrotalcites.[39] The EDS images of the ACM supported catalysts indicate the presence of Mg and Al hydrotalcite species uniformly distributed over the carbon surface. In addition to carbon and oxygen, the ACM supported hydrotalcites displayed silica, which can be attributed to the ceramic binder comprising silica and alumina used to manufacture the ACM. ICP–OES analysis indicated a Mg^{2+}/Al^{3+} molar ratio of approximately 2:1 for the ACM supported catalysts (except for the RCHT/ACM-105 °C which showed a slightly lower Mg/Al ratio of 1.63) compared to 3:1 with the commercial hydrotalcite used for the synthesis of the catalysts (Table 7.1). The lower Mg/Al ratio of the ACM supported hydrotalcites suggests lower loading of hydrotalcite on the ACM support.

7.3.2 Continuous Condensation of Cyclopentanone

Since there is limited information in the literature on the continuous condensation of cyclopentanone using carbon supported hydrotalcites, particularly activated carbon monolith supported hydrotalcites, we wanted to study the effect of reaction conditions (temperature, feed flow rate) on cyclopentanone conversion and 2-cyclopentylidene cyclopentanone space time

yield (STY) and selectivity. A series of reactions were performed with the ACM supported calcined hydrotalcite (CHT/ACM) at atmospheric pressure and temperatures ranging from 140 - 220 ºC to determine the effect of temperature on CP conversion, 2-CP space-time-yield, yield, and selectivity. As shown in Figure 7.4 A, increasing the temperature from 140 to 220 ºC led to an increase in CP conversion from 12.4% to 25%, 2-CP space-time-yield (STY) from 5.6 to 98.8 g/Lcat/h and selectivity from 0.7% to 7.1%. Further increase in temperature to 220 ºC did not affect the 2-CP selectivity. Increase in condensation temperature was previously reported to increase CP conversion and 2-CP selectivity, and temperatures of 170 ºC were found to be optimal for cyclopentanone self-condensation.[40] As reaction rates, CP conversion, and 2-CP STY and selectivity were higher at 220 ºC at 1 atm pressure, further experiments were performed under these conditions. The effect of feed flow rate on CP condensation was determined by varying the feed flow rate between 1-3 mL/min (N_2 flow rate was held constant at 50 mL/min) (Figure 7.4 B). We observed a decrease in CP conversion on increasing the feed flow rate from 1 to 3 mL/min (liquid residence time). However, there was an increase in 2-CP STY, yield, and selectivity on increasing the flow rate to 2 mL/min. Further increasing the feed flow rate to 3 mL/min resulted in a decline in 2-CP STY, yield, and selectivity. Since a higher STY of 98.8 g/Lcat/h and 2-CP selectivity of 7.1% were observed at Q_l = 2mL/min (220 °C, 1 atm), these conditions were chosen for comparison of the catalytic activity of the CHT/ACM with the ACM supported rehydrated and plasma activated hydrotalcite catalysts.

7.3.3 Comparison of ACM supported Hydrotalcite Catalysts

The self-condensation of cyclopentanone was investigated with the activated carbon monolith supported calcined, rehydrated and plasma activated hydrotalcites and compared to the unsupported bulk calcined and rehydrated hydrotalcite catalysts (220 °C, 1 atm, Q_l = 2 mL/min).

Figures 7.5 A and B depict the conversion of cyclopentanone, and yield, selectivity, and space-time-yield (STY) of 2-cyclopentylidene cyclopentanone obtained with the different catalysts. Among the ACM supported hydrotalcite catalysts, the best catalytic performance was exhibited by the hydrotalcite activated with air plasma at 100 W (PHT/ACM-100W). The PHT/ACM-100W displayed a CP conversion of 42%, and 2-CP STY, yield, and selectivity of 641 g/Lcat/h, 11.5% and 27.3% respectively. Further, the PHT/ACM-100W displayed higher 2-CP STY, selectivity, and CP conversion in comparison to the catalyst activated by air plasma at 30 W (PHT/ACM-30W, 2-CP STY: 269.2 g/Lcat/h selectivity: 17.7%, CP conversion: 27.2%) (α = 0.05, level of significance). Air plasma treatment can enhance the OH^- ions in the interlayers of hydrotalcites, which serve as the active sites for the catalytic reaction.[26,41] We speculate the treatment at 100 W generated a higher concentration of OH^- ions in the interlayers of the layered double hydroxide compared to the 30 W treatment, resulting in a higher concentration of active sites, and thereby improved catalytic performance. Similar results were observed by Hajkova and Tisler in the aldol condensation of furfural and acetone using an unsupported plasma activated hydrotalcite catalyst. With Mg-Al HT subjected to air plasma at atmospheric pressure (120 W, 4 s), they observed a higher furfural conversion of approximately 18 % in comparison to 9% with the calcined catalyst.[26]

Among the HT/ACM catalysts, the calcined ACM supported HT (CHT/ACM) displayed a lower conversion and 2-CP yield of 21.7% and 1.7% respectively. Subsequent rehydration using water vapor at 105 °C (RCHT/ACM-105 °C) improved catalytic performance, resulting in a higher CP conversion of 36.9%, and 2-CP STY, yield, and selectivity of 558.2 g/Lcat/h, 10% and 27.1%, respectively. Calcination of the HT/ACM destroys the layered structure, generating mixed oxides with Lewis base centers, which are further converted to strong Brønsted base sites on

rehydration, resulting in higher catalytic activity.[22] Rehydrated Mg-Al HT has previously been shown to have a higher reaction rate compared to the calcined catalyst in the aldol condensation of benzaldehyde and acetone.[40] As shown in Figure 7.6, the RCHT/ACM-105 °C displayed higher CP, and significantly higher 2-CP (5.6 ×) reaction rates compared to the CHT/ACM. Further, it was observed that the HT/ACM rehydrated in the vapor phase at 105 °C displayed better catalytic performance in comparison to the HT/ACM rehydrated at room temperature for the same 8 h duration (36.9% vs 26.7% conversion). These results suggest that room temperature rehydration of the HT/ACM cores using humidified air was not as effective compared to the high temperature rehydration treatment performed in this study.

A comparison of the ACM supported calcined and rehydrated hydrotalcite catalysts with their unsupported counterparts indicates higher CP conversion, 2-CP STY, yield, and selectivity with the bulk catalysts. The bulk CHT displayed a higher CP conversion of 34.4 % (2-CP yield and selectivity of 6.7% and 19.6%) compared to 25% (2-CP yield and selectivity of 1.7% and 7.1%) with the CHT/ACM. The 2-CP yields observed with the calcined bulk Mg-Al HT in this study are lower in comparison to other reports on batch and continuous CP self-condensation. Yang and coworkers observed about 86% yield of 2-CP with calcined bulk hydrotalcite in the batch self-condensation of CP (180 °C, 8 h).[6] In the continuous self-aldol condensation of cyclopentanone in a fixed-bed continuous flow reactor with calcined Mg-Al HT, Sheng and coworkers observed 73.2% CP conversion, approximately 20% selectivity to 2-CP 70% selectivity to the trimer 3-CP, and 51% 3-CP carbon yield (170 °C, 1 atm, 1 g catalyst Q_l = 0.1 mL/min, H_2= 150 mL/min). The high catalytic activity of Mg-Al HT was attributed to the high specific surface area and strong acidity and basicity of the catalyst and the high 3-CP yield obtained under continuous flow was speculated to be due to the stripping of water from the

catalyst surface by the carrier gas hydrogen.[34] Further RCHT displayed a conversion of 39.6%, slightly lower (6%) than the PHT/ACM-100W yet exhibited maximum 2-CP STY, yield, and selectivity of 5687 g/Lcat/h, 20% and 49.6%, respectively (Figures 7.5 A and B). The RCHT also displayed a lower CP, yet higher 2-CP reaction rate (3 ×) than the PHT/ACM-100W (Figure 7.6). This difference in 2-CP reaction rates with the two catalysts could be due to the lower carbon recovery with the PHT/ACM-100W compared to RCHT (75.2 ± 2.24% vs 95.2 ± 2.34%) suggesting the possibility of the formation of byproducts that were not accounted for in this study. The low 2-CP STY, yield and selectivity observed with the ACM catalysts could be due to the uneven distribution, lower loading of hydrotalcite, and lower Mg/Al ratio on the ACM, as confirmed by the ICP-OES analysis. The catalytic performance of hydrotalcites is dependent on Mg/Al ratio and increases with increasing Mg/Al ratio. The lower Mg/Al ratio (2:1) on the ACM supported hydrotalcites compared to the unsupported catalysts (3:1) may have resulted in lower catalytic activity, indicating the need for further optimization of the catalyst preparation methods. However, an analysis of the performance of the calcined, rehydrated and plasma activated HT/ACM catalysts suggests that 1 min air plasma treatment at 100 W generated better results compared to calcination under N_2 at 500 °C for 4 h, and calcination followed by subsequent rehydration at 105 °C for 8 h under N_2. The results obtained with the PHT/ACM-100 W are promising and indicate the potential of plasma methods in replacing calcination/calcination-rehydration procedures for the activation of carbon supported hydrotalcites.

7.4 Conclusions

The continuous self-condensation of cyclopentanone was demonstrated using activated carbon monolith supported hydrotalcite catalysts. The plasma activated ACM (100 W, 1 min, PHT/ACM-100W) displayed a higher 2-CP space-time-yield of 641 g/Lcat/h, and selectivity of

27.3% compared to the calcined ACM (STY: 98.8 g/Lcat/h, S: 7.1%), and higher STY (STY: 558 g/Lcat/h) yet similar selectivity to the rehydrated ACM catalyst (220 °C, 1 atm). PHT/ACM-100W also displayed higher CP conversion of 42% compared to 21.7% with the calcined and 36.9% with the rehydrated ACM, indicating 1 min air plasma treatment at 100 W generated better results compared to calcination at 500 °C for 4 h, and calcination followed by rehydration at 105 °C for 8 h. The higher catalytic activity of the HT/ACM activated by air plasma at 100 W compared to the 30 W treatment and rehydration procedure was attributed to the generation of a higher concentration of OH^- ions in the interlayers of the hydrotalcite, resulting in a higher concentration of active sites, and thereby enhanced catalytic performance. The unsupported rehydrated calcined hydrotalcite (RCHT) displayed a slightly lower conversion (39.6%) than the PHT/ACM-100W, yet significantly higher 2-CP STY, yield, and selectivity of 5687 g/Lcat/h, 19.6% and 49.6% respectively (220 °C, 1 atm). The plasma methods developed for the synthesis of carbon monolith supported hydrotalcite catalysts in this work are promising alternatives to the thermal/ rehydration activation procedures for synthesizing supported hydrotalcites. Our results suggest the potential of employing structured ACM supported hydrotalcites for the catalytic upgrading of bio-based cyclic ketones. Future work would involve optimization of the catalyst preparation methods to improve hydrotalcite distribution and loading on the carbon monolith.

Acknowledgements

Support for this research was provided by the USDA-NIFA Grant (Carbon Monolith Catalysts from Wood for Biobased Platform Chemicals: 2017-67021-26136). The authors thank Applied Catalysts for providing the ACM material.

References

1. Q. Liu, X. Zhang, Q. Zhang, Q. Liu, C. Wang, L. Ma, Synthesis of jet fuel range cycloalkanes with cyclopentanone and furfural, Energy Fuels, 34 (2020) 7149-7159.
2. S. Sun, X. Zhang, Y. Li, X. Shao, J. Ji, J. Liu, W. Wang, Z. Li, X. Ji, Synthesis of renewable diesel and jet fuel range alkanes using 2-methylfuran and cyclohexanone, RSC Adv., 12 (2022)12932-12937.
3. X. Zhang, Y. Li, C. Qian, L. An, W. Wang, X. Li, X. Shao, Z. Li, Research progress of catalysts for aldol condensation of biomass based compounds, RSC Adv. 13 (2023) 9466-9478.
4. Q. Deng, J. Xu, P. Han, L. Pan, L. Wang, X. Zhang, J-J Zou, Efficient synthesis of high-density aviation biofuel via solvent-free aldol condensation of cyclic ketones and furanic aldehydes, Fuel Process. Technol., 148 (2016) 361-366.
5. C. Xu, Y. Gao, X. Liu, R. Xin, Z. Wang, Hydrotalcite reconstructed by in situ rehydration as a highly active solid base catalyst and its application in aldol condensations, RSC Adv., 3 (2013) 793-801.
6. J. Yang, N. Li, G. Li, W. Wang, A. Wang, X. Wang, Y. Cong, T. Zhang, Synthesis of renewable high-density fuels using cyclopentanone derived from lignocellulose, Chem. Commun. 50 (2014) 2572-2574.

7. W. Wang, S. Sun, F. Han, G. Li, X. Shao, N. Li, Synthesis of diesel and jet fuel range cycloalkanes with cyclopentanone and furfural, Catalysts, 9 (2019) 886.

8. D. Liang, G. Li, Y. Liu, J. Wu, X. Zhang, Controllable self-aldol condensation of cyclopentanone over MgO-ZrO2 mixed oxides: Origin of activity and selectivity, Catal Commun. 81 (2016) 33-36.

9. X. Meng, H. Su, R. Song, J. Su, J. Bian, Solvent-free aldol condensation of cyclopentanone with natural clay-based catalysts: Origin of activity and selectivity, Catalysts, 13 (2023) 530.

10. D. Lorenzo, A. Santos, E. Simon, A. Romero, Kinetic of alkali catalyzed self-condensation of cyclohexanone, Ind. Eng. Chem. Res. 52 (2013) 2257-2265.

11. O. Kikhtyanin, Z. Tisler, R. Velvarska, D. Kubicka, Reconstructed Mg-Al hydrotalcites prepared by using different rehydration and drying time: Physico-chemical properties and catalytic performance in aldol condensation, Appl. Catal. A-Gen., 536 (2017) 85-96.

12. L. Ao, W. Zhao, Y-s. Guan, D-k. Wang, K-s. Liu, T-t. Guo, X. Fan, X-y. Wei, Efficient synthesis of C15 fuel precursor by heterogeneously catalyzed aldol condensation of furfural with cyclopentanone, RSC Adv., 9 (2019) 3661-3668.

13. G. Liang, A. Wang, X. Zhao, N. Lei, T. Zhang, Selective aldol condensation of biomass-derived levulinic acid and furfural in aqueous-phase over MgO and ZnO, Green Chem. 18 (2016) 3430-3438.

14. D. Lorenzo, E. Simon, A. Santos, A. Romero, Kinetic model of catalytic self-condensation of cyclohexanone over Amberlyst 15, Ing. Eng. Chem. Res. 53 (2014) 19117-19127.

15. Dr. B. Gutmann, Dr. D. Cantillo, Prof. Dr. C.O. Kappe, Continuous-flow technology-A tool for the safe manufacturing of active pharmaceutical ingredients, Angew. Chem. Int. Ed. 54 (2015) 6688-6728.

16. J. A. M. Lummiss, P.D. Morse, R. L. Beingessner, T. F. Jamison, Towards more efficient, greener synthesis through flow chemistry, Chem. Rec. 17 (2017) 667-680.

17. A. Sharma, S. Kumari, S. Sharma, T. Singh, S. Kumar, A. Thakur, S.K. Bhatia, A.K. Sharma, Layered double hydroxides: an insight into the role of hydrotalcite-type anionic clays in energy and environmental applications with current progress and recent prospects, Mater. Today Sustain. 22 (2023) 100399.

18. D.P. Debecker, E.M. Gaigneaux Prof., G. Busca Prof., Exploring, tuning, and exploiting the basicity of hydrotalcites for applications in heterogeneous catalysis, Chem. Eur. J. 15 (2009) 3920-3935.

19. J. Perez-Ramirez, S. Abello, N. M. van der Pers, Memory effect of activated Mg-Al hydrotalcite: In situ XRD studies during decomposition and gas-phase reconstruction, Chem. Eur. J. 13 (2007) 870-878.

20. A. Navajas, I. Campo, A. Moral, J. Echave, O. Sanz, M. Montes, J.A. Odriozola, G. Arzamendi, L.M. Gandia, Outstanding performance of rehydrated Mg-Al hydrotalcites as heterogeneous methanolysis catalysts for the synthesis of biodiesel, Fuel, 211 (2018) 173-181.

21. K. Ebitani, K. Motokura, K. Mori, T. Mizugaki, K. Kaneda, Reconstructed hydrotalcite as a highly active heterogeneous base catalyst for carbon-carbon bond formations in the presence of water, J. Org. Chem., 71 (2006) 5440-5447.

22. M. Mokhtar, A. Inayat, J. Ofili, W. Schwieger, Thermal decomposition, gas phase hydration and liquid phase reconstruction in the system Mg/ Al hydrotalcite/ mixed oxide: A comparative study, Appl. Clay Sci., 50 (2010) 176-181.

23. S. Abello, F. Medina Dr., D. Tichit Dr., J. Perez-Ramirez Dr., J.C. Groen, J. E. Sueiras Dr., P. Salagre Dr., Y. Cesteros Dr. Aldol condensations over reconstructed Mg-Al hydrotalcites: structure-activity relationships related to the rehydration method, Chem. Eur. J. 11 (2005) 728-739.

24. V. Medvecká, D. Kováčik, A, Zahoranová, M. Stupavská, M. Černák, Atmospheric pressure plasma assisted calcination of organometallic fibers, Mater. Lett., 162 (2016) 79-82.

25. Z. Wang, Y. Zhang, E.C Neyts, X. Cao, X. Zhang, B. W.-L. Jang, C-j Liu, Catalyst preparation with plasmas: How does it work? ACS Catal., 8 (2018) 2093-2110.

26. P. Hajkova, Z. Tisler, Atmospheric Plasma Treated Hydrotalcite-Type Catalyst. Catal Letter 147 (2017) 374-38.

27. B. R. Vahid, M. Haghighi, S. Alaei, J. Toghiani, Reusability enhancement of combustion synthesized MgO/MgAl2O4 nanocatalyst in biodiesel production by glow discharge plasma treatment, Energy Convers. and Manag., 143 (2017) 23-32.

28. J.R. Kastner, J. Miller, D.P. Geller, J. Locklin, L.H. Keith, T. Johnson, Catalytic esterification of fatty acids using solid acid catalysts generated from biochar and activated carbon. Catal. 190 (2012) 122-132.

29. S. Cimino, J. Apuzzo, L. Lisi, MgO dispersed on activated carbon as water tolerant catalyst for the conversion of ethanol into butanol. Appl. Sci., 9 (2019) 1371.

30. A. Garcia-Gallastegui, D. Iruretagoyena, V. Gouvea, M. Mokhtar, A. M. Asiri, S. N. Basahel, S.A. Al-Thabaiti, A.O. Alyoubi, D. Chadwick, M.S. P. Shaffer, Graphene oxide as support for layered double hydroxides: Enhancing the CO_2 adsorption capacity, Chem. Mater. 24 (2012) 4531-4539.

31. F. Winter, V. Koot, A.J. van Dillen, J.W. Geus, K.P. de Jong, Hydrotalcites supported on carbon nanofibers as solid base catalysts for the synthesis of MIBK. J. Catal. 236 (2005) 91-100.

32. C. Mu, K. Huang, T. Cheng, H. Wang, H. Yu, F. Peng, Ni foams decorated with carbon nanotubes as catalytic stirrers for aerobic oxidation of cumene, Chem. Eng. J. 306 (2016) 806-815.

33. M. Pirmoradi, N. Janulaitis, R.J.Jr Gulotty, J.R. Kastner, Bi-Metal-Supported Activated Carbon Monolith Catalysts for Selective Hydrogenation of Furfural. Ind. Eng. Chem. Res., 59 (2020) 17748-17761.

34. X. Sheng, G. Li, W. Wang, Y. Cong, X. Wang, G.W. Huber, N. Li, A. Wang, T. Zhang, Dual-bed catalyst system for the direct synthesis of high-density aviation fuel with cyclopentanone from lignocellulose. AIChE J., 62 (2016) 2754-2761.

35. S. Vasefi, Development of sustainable solid base hydrotalcite catalyst support by granular activated carbon, [Master Dissertation, University of Georgia], 2021.

36. I. Miller, J.E. Freund, Probability and Statistics for Engineers. Prentice-Hall, Inc., Englewood Cliffs, NJ, 1985.

37. P.K. Sahu, P.K. Sahu, R. Gupta, M. Messali, S.M. Almutairi, P.L. Sahu, D.D. Agarwal, Sustainable synthesis and characterization of Ni-Al containing double-layered nanocatalysts and their catalytic activity, ACS Omega, 3 (12) 18976-18983.

38. L.B. Modesto-Lopez, R.J. Chimentao, M.G. Alvarez, J. Rosell-Llompart, F. Medina, J. Llorca, Direct growth of hydrotalcite nanolayers on carbon fibers by electrospinning, Appl. Clay Sci., 101 (2014) 461-467.

39. S. Shao, W. Dong, X. Li, H. Zhang, R. Xiao, Y. Cai, Solvent-free synthesis of jet fuel by aldol condensation and hydroprocessing of cyclopentanone as biomass-derivatives, J. Clean. Prod. 250 (2020) 119459.

40. K.K. Rao, M. Gravelle, J.S. Valente, F. Figueras, Activation of Mg-Al hydrotalcite catalysts for aldol condensation reactions, J. Catal. 173 (1998) 115-121.

41. R. Debek, M. Motak, T. Grzybek, M.E. Galvez, P. Da Costa, A short review on the catalytic activity of hydrotalcite-derived materials for dry reforming of methane, Catalysts, 7 (2017) 32.

Table 7.1. Mg/Al ratio of the ACM supported hydrotalcite catalysts.

Catalyst	Mg/Al Ratio[a]
CHT[b]	3.00
RCHT[b]	3.00
CHT/ACM	1.99 ± 0.00
RCHT/ACM-105 ˚C	1.63 ± 0.02
PCHT/ACM-30W	2.03 ± 0.02
PCHT/ACM-100W	1.98 ± 0.05

Mg^{2+}/Al^{3+} molar ratio was determined by inductively coupled plasma–optical emission spectroscopy (ICP–OES) for the ACM supported catalysts.

[b] Mg^{2+}/Al^{3+} molar ratio of commercial HT is 3:1.

[a] The Al content of the Base ACM material was deducted from the Al content on the catalysts to determine the Mg/Al ratio.

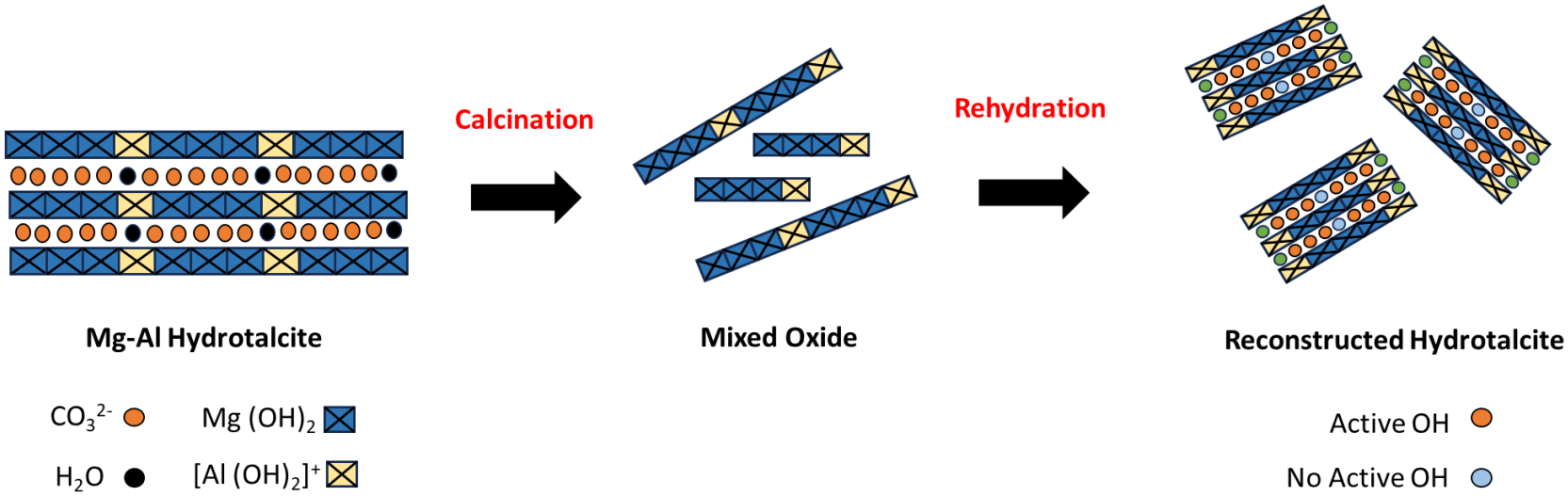

Figure 7.1**.** Schematic depiction of the calcination and rehydration of Mg-Al hydrotalcite.

(A)

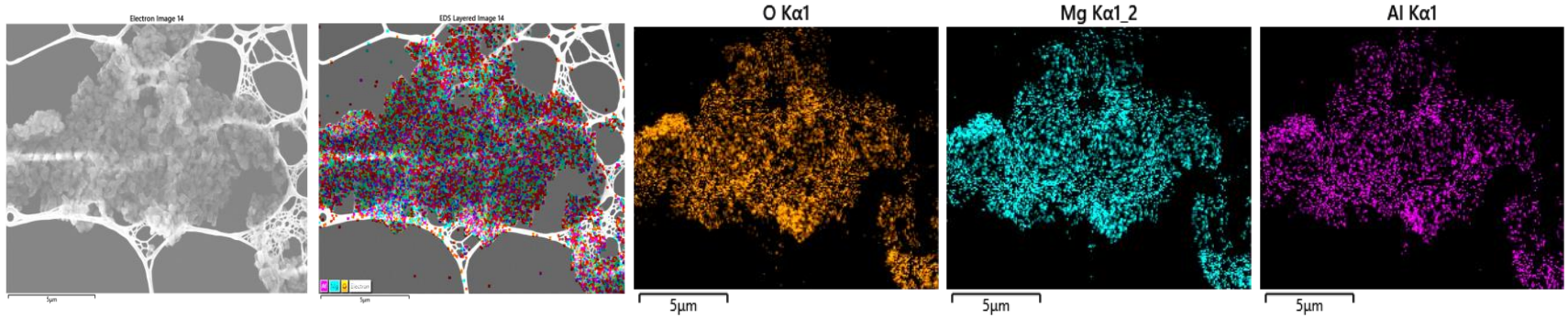

(B)

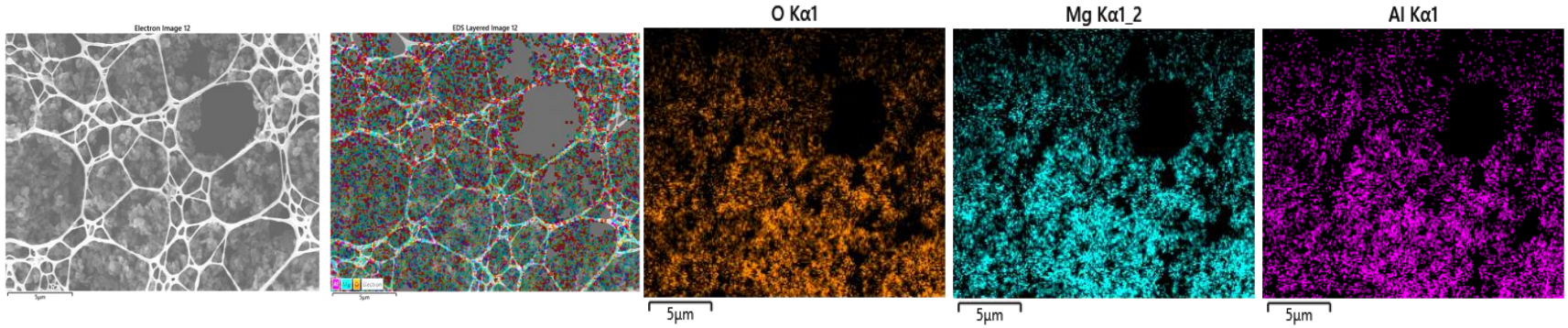

Figure 7.2. STEM-EDS images of (A) calcined hydrotalcite (CHT) and (B) rehydrated (105 °C, 8 h) calcined hydrotalcite.

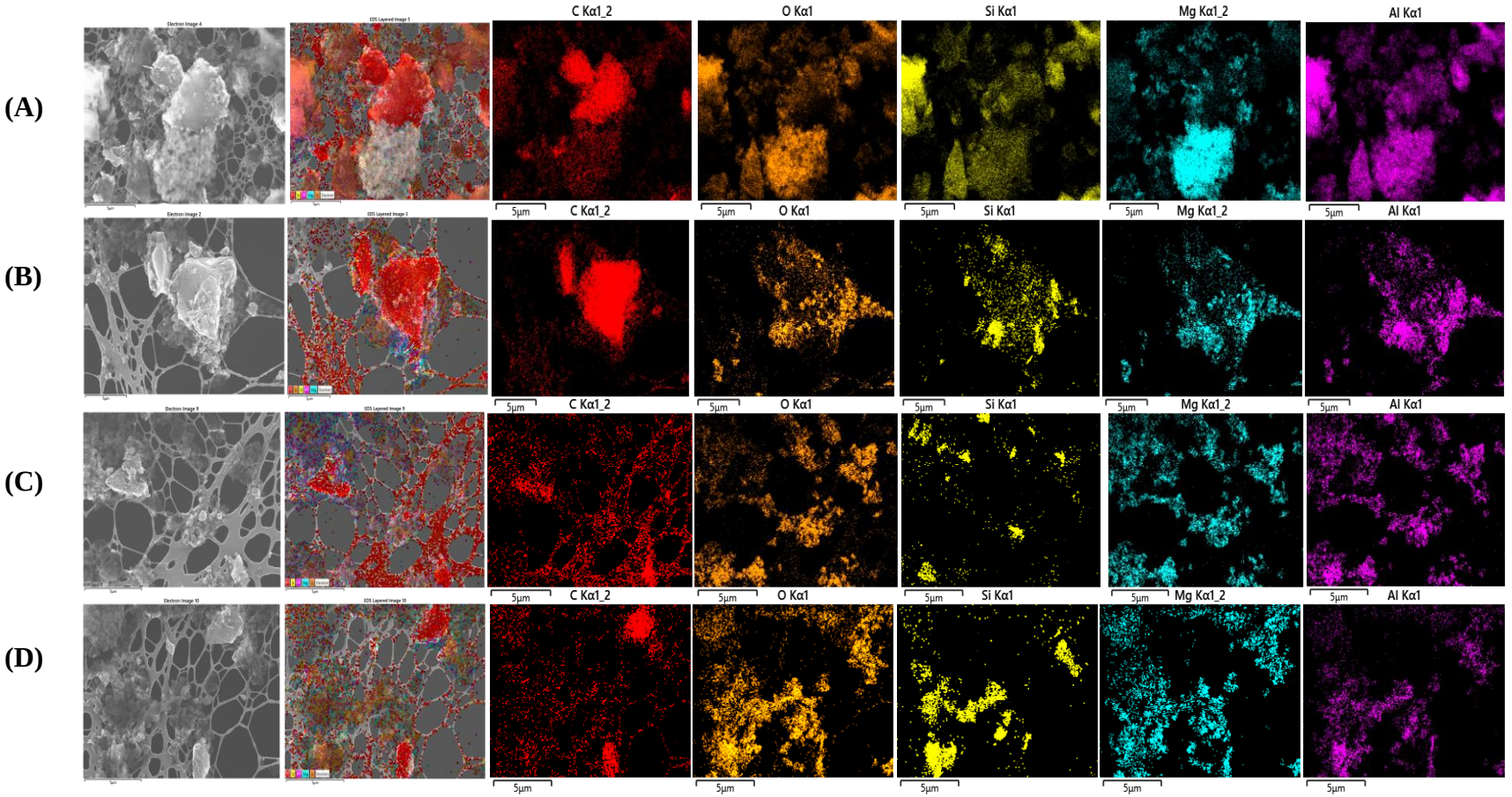

Figure 7.3. STEM-EDS images of ACM supported (A) calcined hydrotalcite (CHT/ACM), (B) rehydrated (105 °C, 8 h) calcined hydrotalcite (RCHT/ACM), (C) plasma activated (30 W, 1 min, PHT/ACM-30W), and (D) plasma activated (100 W, 1 min, PHT/ACM-100W).

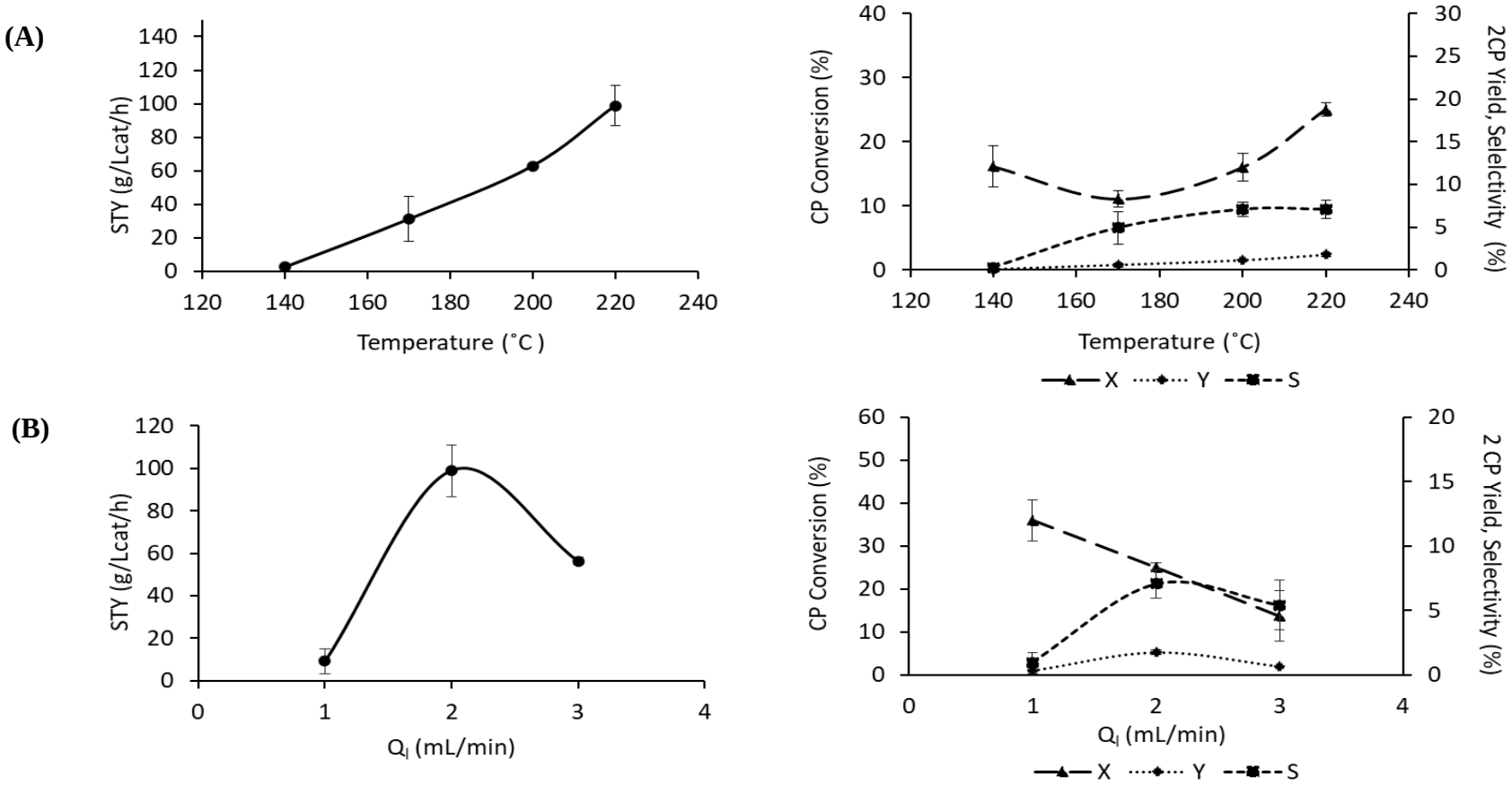

Figure 7.4. (A) Effect of temperature at Q_l= 2mL/min and (B) feed flow rate (Q_l) at T=220 °C on 2-CP space time yield (STY), CP conversion, 2-CP yield, and selectivity for CHT/ACM. Reaction conditions: 220 °C, 1 atm, 15 g catalyst, cyclopentanone flow rate = 2 mL/min, nitrogen flow rate = 50 mL/min. The reactions were performed consecutively (t = 27-30 min) with the same batch of catalyst to study the effect of temperature and Q_l, with an accumulated time on steam of 3 h.

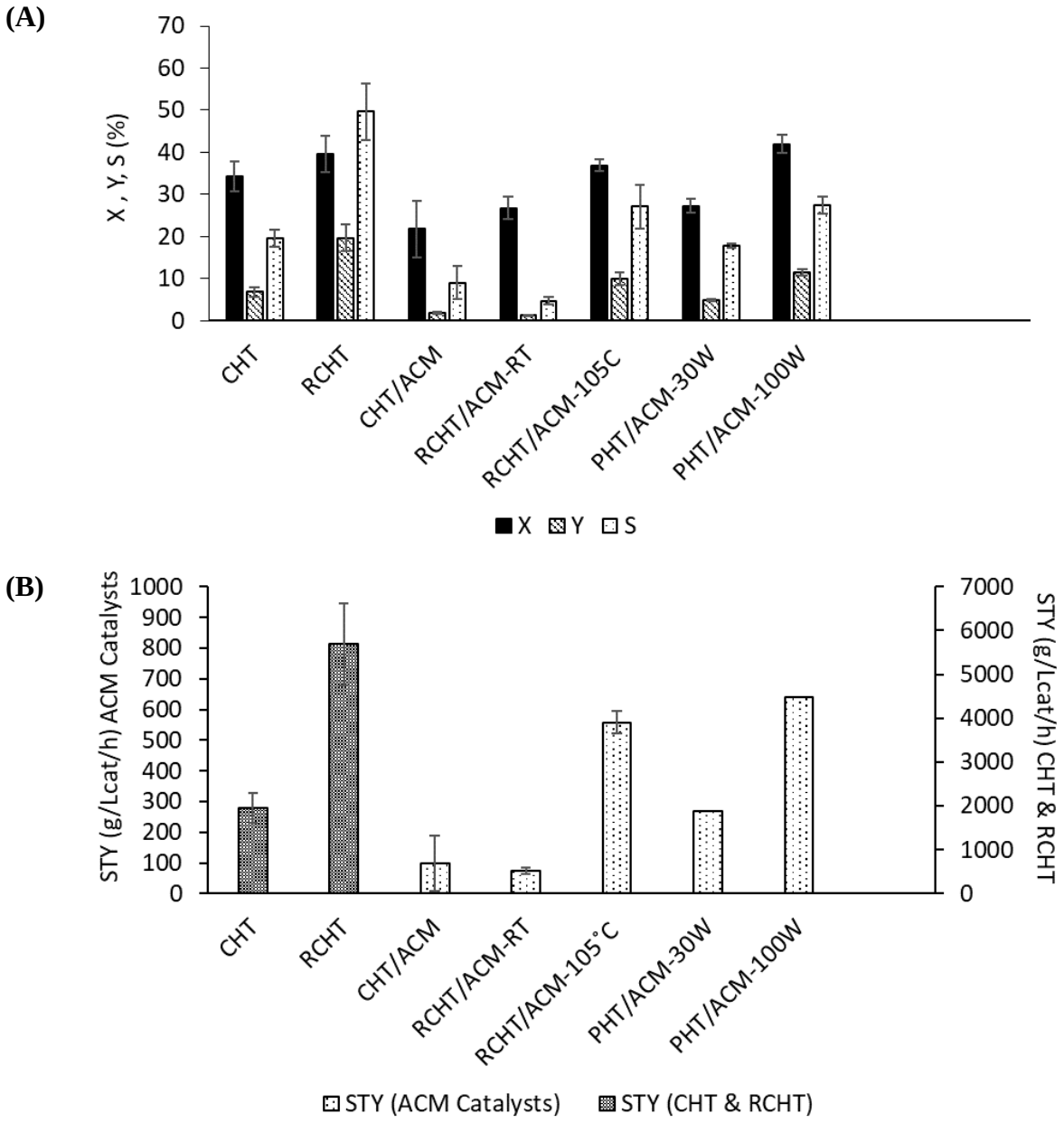

Figure 7.5. (A) Cyclopentanone conversion (X), 2-cyclopentylidene cyclopentanone yield (Y) and selectivity (S) and (B) space-time-yield (STY), in the continuous flow packed bed reactor with the unsupported calcined (CHT) and rehydrated hydrotalcites (RCHT), ACM supported calcined (CHT/ACM), rehydrated at room temperature (RCHT/ACM-RT), rehydrated at 105 °C (RCHT/ACM-105°C), plasma activated at 30 W (PHT/ACM-30W) and 100 W (PHT/ACM-100W). Reaction conditions: 220 °C, 1 atm, 14-15 g catalyst, cyclopentanone flow rate = 2 mL/min, nitrogen flow rate = 50 mL/min.

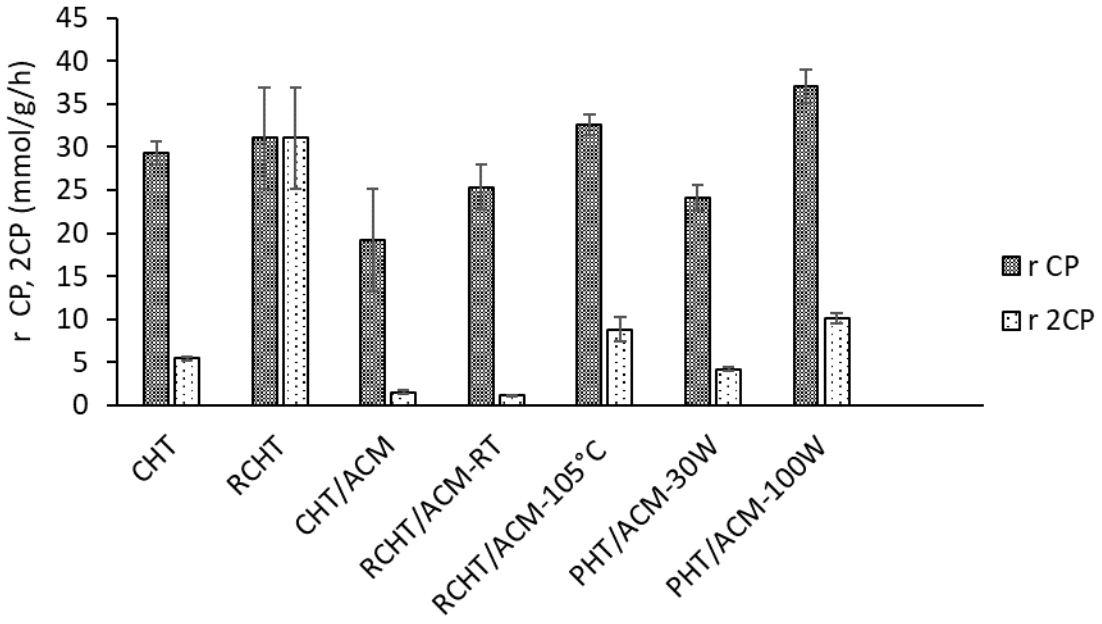

Figure 7.6. Cylcopentanone (CP) and 2-cyclopentylidene cyclopentanone (2-CP) reaction rates (mmol/gcat/h) with the unsupported calcined (CHT) and rehydrated hydrotalcites (RCHT), the ACM supported calcined (CHT/ACM), rehydrated at room temperature (RCHT/ACM-RT), rehydrated at 105 °C (RCHT/ACM-105°C), plasma activated at 30 W (PHT/ACM-30W) and 100 W (PHT/ACM-100W). Reaction conditions: 220 °C, 1 atm, 14-15 g catalyst, cyclopentanone flow rate = 2 mL/min, nitrogen flow rate = 50 mL/min.

CHAPTER 8

CONCLUSIONS AND RECOMMENDATIONS

8.1 Conclusions

This work was aimed at contributing new knowledge to the development of sustainable solid acid and base catalysts, using wood based activated carbon in granular and monolith form by modified hydrothermal and plasma methods. These catalysts were employed in the catalytic upgrading of biomass platform chemicals such as 2-hydroxyisobutyric acid (2-HIBA), pyruvic acid (PA) and cyclopentanone (CP) for the synthesis of value-added chemicals and aviation fuels. The results of this work are classified into five studies. The first study is focused on designing sustainable solid acid carbon catalysts using modified hydrothermal and plasma methods and compares the catalytic performance of the solid acid carbon catalysts with the industrial benchmark catalyst, Amberlyst-15. The sulfonated granular and monolith activated carbon catalysts displayed similar catalytic efficiency to Amberlyst-15, suggesting their potential as sustainable replacements for petroleum derived catalysts. These results also suggested the potential of the sulfonated carbons, particularly the sulfonated monolith, as a structured catalyst for continuous esterification processes. However, while the sulfonated GAC retained 85 % of its initial catalytic performance over the course of the reuse cycles the sulfonated ACM exhibited a constant decline in catalytic efficiency which was speculated to be due to loss of sulfonic acid groups during filtration and catalyst recovery, or attrition of the binder in the ACM. The second study investigated the potential of the sulfonated ACM (sACM) for the continuous esterification

of 2-HIBA in a packed bed reactor and compared the performance of this catalyst to the sulfonated GAC (sGAC) and Amberlyst-15. The sACM (intact monolith cores) displayed higher ester yield and selectivity, and stability compared to Amberlyst-15 in the time-on-stream studies (sGAC and sACM: 150 °C, Amberlyst-15 :120 °C, 300 psig, 3.3 h). The results from this study indicate the potential of the sACM for the continuous catalytic upgrading of biobased organic acids. The third study involves the development of a rate law for continuous 2-HIBA esterification under industrially relevant conditions (higher acid concentrations) over the sGAC and sACM using the Langmuir-Hinshelwood/Eley Rideal models to aid in reactor design and scale-up. A satisfactory agreement between the experimental data and kinetic model was observed for both the LH and ER models, and the adsorption/desorption equilibrium and reaction rate constants were derived from the kinetic model. Further, the sACM displayed higher conversion and significantly higher space-time-yields (2.7 ×) ($\alpha = 0.05$, level of significance) compared to the sGAC which may be attributed to the larger surface area to volume ratio, higher acid site density, enhanced mass transfer and co-current stripping of water from the ACM. The sixth chapter is aimed at expanding the applications of the sulfonated carbon catalysts to other biobased organic acids such as pyruvic acid for the synthesis of ethyl pyruvate, an ester with numerous medical applications. The sGAC and sACM showed promising results in the batch esterification of pyruvic acid, displaying 97% conversion and selectivity and 55-58% ester yield (150 °C, 1 h). Since pyruvic acid has been produced fermentatively and anticipating the challenges of developing an integrated fermentation-catalytic process for the synthesis of ethyl pyruvate, we studied the effect of fermentation residuals (water and salts including phosphate and sulfates) on catalytic activity. The sulfonated carbon catalysts exhibited similar pyruvic acid conversion, ester selectivity, significantly higher turnover frequencies, lower water inhibition,

yet lower ester yields compared to Amberlyst-15. The last chapter involves the development of a continuous process using solid base activated carbon monolith supported hydrotalcites for the continuous self-condensation of cyclopentanone for the synthesis of jet fuel precursors. Plasma activation of the ACM supported hydrotalcite (air plasma, 100 W, 1 min) generated higher 2-cyclopentylidene cyclopentanone (dimer) STY, yield and selectivity compared to the calcination and rehydration treatments. These results suggest the potential of plasma technology as a sustainable alternative for the synthesis of carbon supported hydrotalcites, compared to the traditional calcination/rehydration methods. The solid acid and base carbon catalysts developed in this work are promising green alternatives to the industrially employed petroleum-derived, expensive, and low surface area catalysts. Further they can be employed for the catalytic upgrading of biomass platform chemicals (e.g., 2-HIBA, pyruvic acid, cyclopentanone) for the synthesis of a wide range of fine and specialty chemicals, and aviation fuels.

8.2 Recommendations

The plasma sulfonation methods adopted in this work successfully sulfonated the carbon materials yet resulted in low acid site densities. Further optimization of plasma methods by increasing the hydrogen fraction in the gas mixture (50-70% H_2) and operating the plasma at higher power (100-150 W as opposed to 30 W in this work) may enhance the $H^{\bullet}$ concentration and consequently, the generation of more thermally stable strong acid sites (e.g., thiophenic or S heteroatoms) and sulfonic acid density on the carbon supports. In the 2-HIBA esterification time-on-stream studies, the sulfonated granular and monolithic carbon materials displayed good catalytic stability, retaining 89-91% of their initial activity. However, the catalysts displayed significant leaching of sulfonic acid sites. Improving the plasma catalyst preparation methods

developed in this work (e.g., plasma with 50-70% H_2 at higher power) may stabilize the acid sites against leaching. The esterification kinetic models developed in this work, particularly for the solid acid monolith catalyst, have the potential to be employed for scale up and monolithic reactor design for liquid phase esterification processes. While the models displayed satisfactory agreement with the experimental data, with R^2 values ranging between 0.92-0.95, the residual sum of squares was high, ranging between 29-35% for the LH and ER models. The models were developed with the assumptions of only a liquid phase reaction, surface reaction as the rate-controlling step, and competitive adsorption of the reactants on a single acid site (LH Model). Other reaction mechanisms (such as the vapor liquid partitioning of the products) and activity-based models need to be investigated to account for the non-ideality of the reaction mixture and arrive at a better fit of the experimental data with the kinetic model. Further water concentrations for the kinetic studies were estimated based on stoichiometry and 2-HIBA conversion. Employing a volumetric titration method (e.g., Karl Fischer titration) is recommended to obtain more accurate values for the water concentrations of the samples. In the catalytic esterification of pyruvic acid, the addition of fermentation residuals (water, phosphates, and sulfates) to the reaction medium comprising the sulfonated carbon/Amberlyst-15 resulted in a decline in catalytic activity. Further byproduct analysis would need to be conducted to understand if the addition of fermentation residuals enhances the rate of ester hydrolysis. The plasma methods developed in this work for the synthesis of structured solid base catalysts are promising alternatives to the high-temperature, long duration thermal calcination and rehydration methods employed for the activation of bulk hydrotalcite. However, significantly lower space-time-yields were achieved with the ACM supported plasma activated hydrotalcite (PHT/ACM-100W) compared to the bulk rehydrated hydrotalcite. Further optimization of the catalyst preparation

methods would be required to improve hydrotalcite loading and distribution on the ACM support.

APPENDIX A

SUPLEMENTARY DATA FOR CHAPTER 3

This section comprises the supporting information for chapter 3.

1. Apparatus for plasma treatment
2. Methods – Batch reactions, FTIR and XPS, comparison of plasma treatments
3. STEM-EDS for Base GAC (untreated)
4. STEM-EDS for Base cACM (untreated activated carbon monolith)
5. EDS images for fresh and spent GAC and cACM catalysts
6. FTIR Peak Assignments
7. XPS Peak Assignments
8. FTIR figures

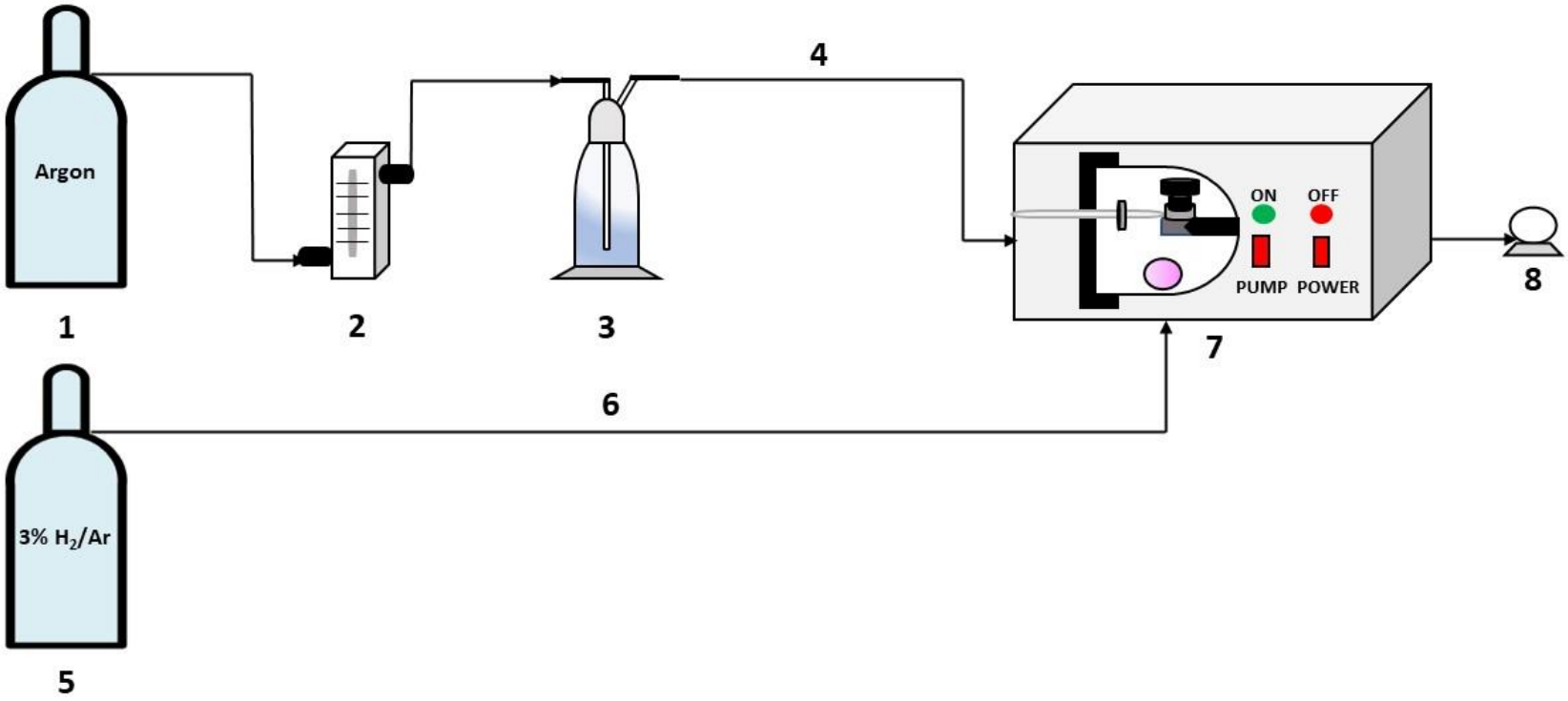

Figure S3.1**.** Schematic of the plasma reactor set up (1) Argon gas tank, (2) rotameter, (3) bubbler apparatus, (4) mixture of Argon-water vapor, (5) 3% H_2/Ar gas tank, (6) mixture of 3% H_2/Ar, (7) plasma reactor, and (8) vacuum pump.

Batch Reactions in Parr Series 5000 Multiple Reactor System

A high agitation rate (725 rpm) was chosen to eliminate external mass transfer resistance. The reactor headspace was pressurized with nitrogen at 1.6 bar, then heated to the set-point at 10 °C /min. Heat up times were approximately 15 min and the reaction pressure increased from 1.6 bar to 8.8-9 bar at a temperature of 150 °C. Residence times are reported from the time the set-point temperature was reached. On completion of the reaction, the vessel was cooled down by quenching in ice. After depressurizing the reactor, the reaction mixture and catalyst were recovered and the catalyst was separated via filtration (Whatman, 11 μm pore size). The filtrate was collected and analyzed by GC-FID, whereas the catalyst was dried in the oven at 105 °C for 2 h and stored for reuse studies. The effect of temperature (100, 120 ,150 °C), residence time (0.5 ,1, 3 h), and catalyst loading (0.25 , 1 g) on conversion and E-2HIBA yield were determined. Based on preliminary experiments, a temperature of 150 °C, residence time of 1h, and a catalyst loading of 1g were found to be optimal. Esterification reactions were performed under these conditions for all treated GAC, crushed ACM (cACM) catalysts, and Amberlyst-15. Control reactions, without catalyst, and with the untreated GAC/cACM, were also carried out. The reuse capacity of the most catalytically efficient hydrothermal and plasma sulfonated carbons and Amberlyst-15 was studied for 4 cycles. After each spent run, the catalysts were separated by filtration and dried in an oven at 105 °C overnight and reused. For the most stable catalysts (GAC-HT-2M, GACHT-18M, GAC-PT-Ar/H2O-15min, and Amberlyst-15), a series of batch reaction studies were performed to determine the effect of temperature (100-150 °C) and residence time (0.5-3 h) on 2- HIBA conversion and E-2HIBA yield.

FTIR Analysis

1mg of catalyst was finely powdered with 300mg of KBr, followed by drying in an oven at 105 °C for 1 h to eliminate moisture. The catalyst samples diluted in KBr were pressed into a disc in a Hydraulic Press (Carver.Inc; Pressure: 20,000 pounds/ 9 metric tons, Time: 10 min). The disc was inserted into the sample holder on the KBr apparatus. On setting the experimental conditions (resolution: 6, number of scans: 64; mode: transmittance), the pellet was analyzed by KBr Fourier Transform Infrared Spectroscopy using a Thermo Scientific Nicolet 6700 FTIR spectrometer in the wave number range of 4000-399 cm^{-1}. For each sample, the background was collected and between analyses, a gap of 5-10 minutes was allowed, to prevent the appearance of carbon dioxide and moisture peaks in the spectrum.

XPS Analysis

The measurement size was 400 μm, and typical detection depth was ~5 nm. Electron and ion flood charge compensation were enabled during the data collection and the surface was milled with an ion gun at 500 keV for 30 sec to remove top surface contamination. Survey scans were collected with a dwell time of 50 ms, pass energy of 200 eV, and step size of 1 eV, at 5 scans for each to improve signal to noise ratio and ensure better resolution. Typical detection limits were at about 1% of the total surface composition for light elements such as Si (Z =14) and below, and heavier elements down to ~ 0.1 % with an accuracy of 20-50 % of the given value. Samples were loaded in a batch and then pumped down to 1e-8 mbar vacuum and the XPS data were collected.

Plasma Method

Argon (2.5 psi) was passed through a water-containing bubbler apparatus at a flow rate of 0.1-0.2 mL/min and allowed to flow through the plasma reactor during operation (Figure S3.1). A gas ballast was used to prevent condensation of water vapor inside the pump. Once the catalyst (GAC/ACM) was placed inside the chamber, a vacuum was created. Using a needle valve, the reactor was flushed with the carrier gas (Ar-H_2O vapor/ 3% H_2/Ar) for 10 min to displace any air at a pressure of 4-6 Torr. The pressure was gradually decreased to 600-900 mTorr and the power was set to 30 W, to generate a stable, bright purple plasma discharge (with 3 % H_2/Ar, the plasma was formed at a slightly higher-pressure range of 800 mTorr-1.3 Torr). Post treatment, the chamber was evacuated, and the sample was stored for further use.

Comparison of Plasma Treatments

(i) Argon-Water Vapor Plasma

Ar/H_2O vapor plasma has been previously studied for the surface etching and modification of polymers. Nikiforov and coworkers investigated an Ar/H_2O vapor atmospheric pressure plasma for the surface modification of polypropylene. They employed a bubbling system with distilled water to modulate the water vapor content in the plasma system.[1] In this work, a mixture of argon and water vapor was used to generate H radicals by passing the gas mixture into the plasma chamber through a bubbler apparatus (Figure S3.1). When argon is used as the carrier gas in the plasma, positively charged Ar^+ and metastable Ar^* are generated. Introducing water vapor into the plasma, causes a transfer of charge between the energetic Ar^* and H_2O molecules, producing H_2O^+ which further dissociates into $OH^\bullet$ and $H^\bullet$ radicals. The dissociation of water vapor by electron bombardment also yields $OH^\bullet$ and $H^\bullet$ radicals. [1] Hydrogen radicals react with

H_2SO_4 to form active SO_3 groups, which may further attack the carbon surface to form sulfonic acid groups ($-HSO_3$). In addition, the $OH^{\bullet}$ can also combine to form H_2O_2, causing oxidation of the carbon surface, to form COOH and OH groups. Based on literature we presume the primary reactions involved in the formation of sulfonic acid groups are as follows:

$Ar + e^- \rightarrow + Ar^* + e^-$

$Ar^* + H_2O \rightarrow Ar + H_2O^+ + e^-$

$H_2O^+ \rightarrow OH^{\bullet} + H^{\bullet}$

$e^- + H_2O \rightarrow e^- + OH^{\bullet} + H^{\bullet}$

$OH^{\bullet} + OH^{\bullet} \rightarrow H_2O_2$

$H^{\bullet} + H_2SO_4 \rightarrow {\bullet}SO_3 + H_3O^+$

$- {\bullet}SO_3 +$ carbon $\rightarrow$ $-C-SO_3-H^+$ (C: carbon surface)

(. – free radical, *- energetic molecule)

Further, Srivastava and Wang observed that increasing the H_2O/Ar ratio above 1.9%, resulted in an unstable plasma that was extinguished within a few minutes.[2] In our preliminary plasma sulfonation studies, we subjected the GAC impregnated with 2M H_2SO_4 (undried), to Ar/ H_2O vapor plasma. However, owing to the high moisture content, the pressure did not reach the permissible range for the plasma to be formed. Therefore, we air-dried our catalysts and operated the Ar/H_2O vapor plasma at low flow rates (0.1-0.2 mL/min) to avoid pressure fluctuations in the plasma chamber. We speculate the gas leaving the bubbler apparatus may not have reached

equilibrium composition, resulting in the lower production of H radicals. This could have resulted in lower sulfonic acid density (<0.1 mmol/g) on the plasma catalysts.

(ii) Hydrogen-Argon Plasma

We also investigated the sulfonation of carbon with hydrogen-argon (3% H_2/Ar), speculating that this mixture (relative to Ar/ H_2O vapor) would generate a higher concentration of H radicals required for sulfonation. The rationale behind using a lower percentage of hydrogen was to use an inflammable gas mixture. Miao et al. used a H_2/Ar plasma for co-doping of nitrogen and sulfur on graphene oxide. While elucidating the plasma mechanism, they showed that the glow discharge plasma of H_2/Ar generates radicals, ions and neutral molecules including Ar^+ , H^+, Ar and H_2. The Ar^+ and Ar species initiate the ionization of H_2. Previously, Bogaerts et al. provided in depth insights into the plasma interactions between H_2 and Ar species. Collisions between Ar^+ and H_2 generates ArH^+, which on subsequent collisions with electrons generates H radicals ($H^\bullet$).[3] The $H^\bullet$ then react with sulfuric acid on the carbon to form active SO_3 groups, which may further attack the carbon surface to form sulfonic acid groups (-HSO_3) on the surface.[3] Based on these studies, we speculate the following H_2/Ar plasma sulfonation mechanism:

$Ar^+ + H_2 \rightarrow ArH^+ + H$ (proton transfer)

$ArH^+ + e^- \rightarrow Ar + H^\bullet$

$H^\bullet + H_2SO_4 \rightarrow \bullet SO_3 + H_3O^+$

$- \bullet SO_3 +$ carbon $\rightarrow$ -C-SO_3-H^+ (C: carbon surface)

It has been found that the density of ArH^+ ions increases at hydrogen fractions lower than 5-10%, and gradually decreases on increasing the hydrogen concentration in H_2/Ar plasmas.[4] Since

we employed 3% H_2/Ar in our plasma sulfonation process and observed slightly lower 2-HIBA conversions in comparison to the Ar/H_2O vapor plasma treated catalysts (indicative of low -SO_3H densities), we suspect this gas mixture was not as effective in generating a sufficient concentration of $H^{\bullet}$ (i.e., there may have been a higher fraction of Ar H^+). It is expected that increasing the hydrogen fraction in the gas mixture would significantly enhance the $H^{\bullet}$ concentration and consequently, the sulfonic acid density on the carbon supports.

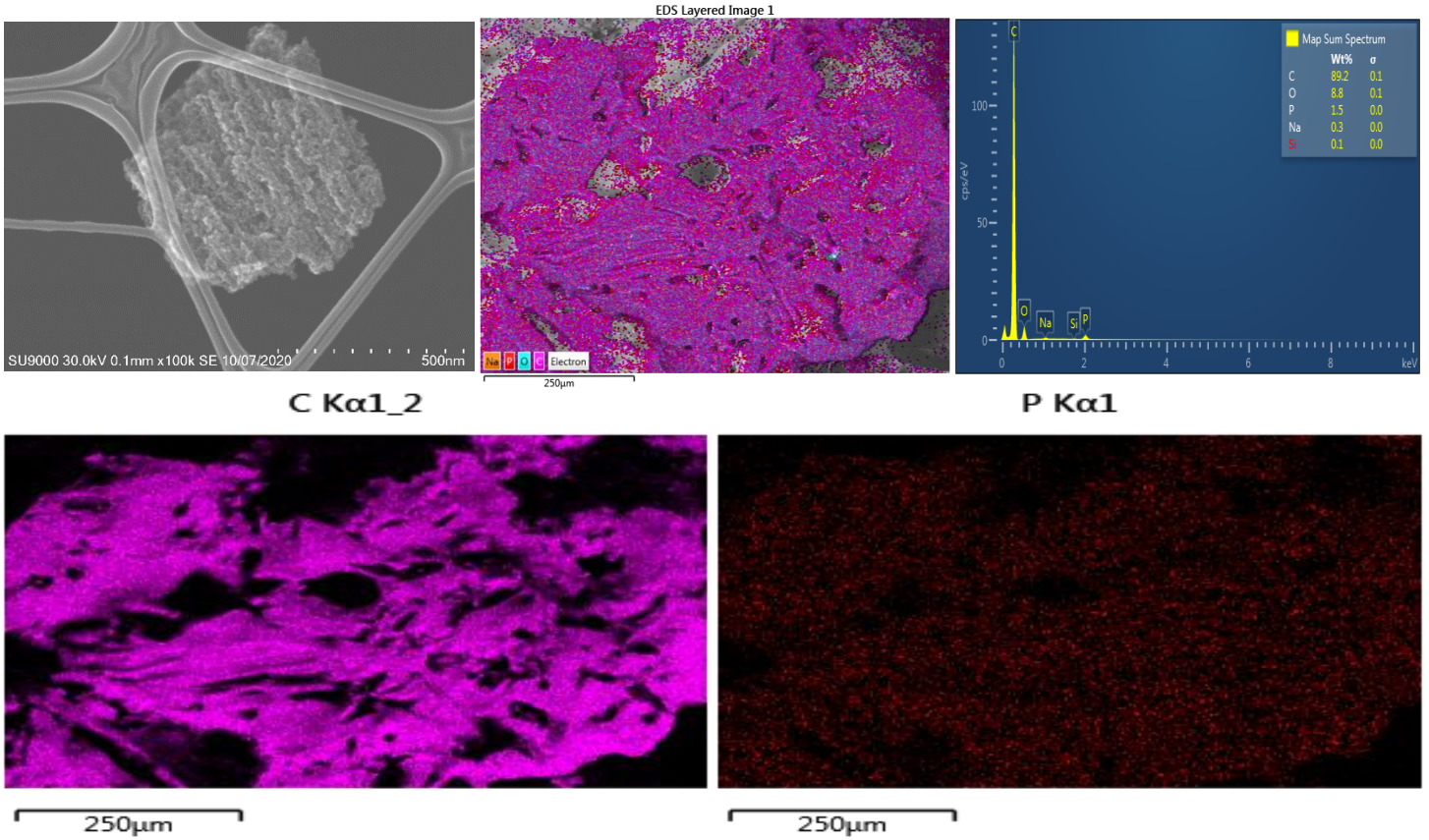

Figure S3.2. STEM-EDS images of Base-GAC.

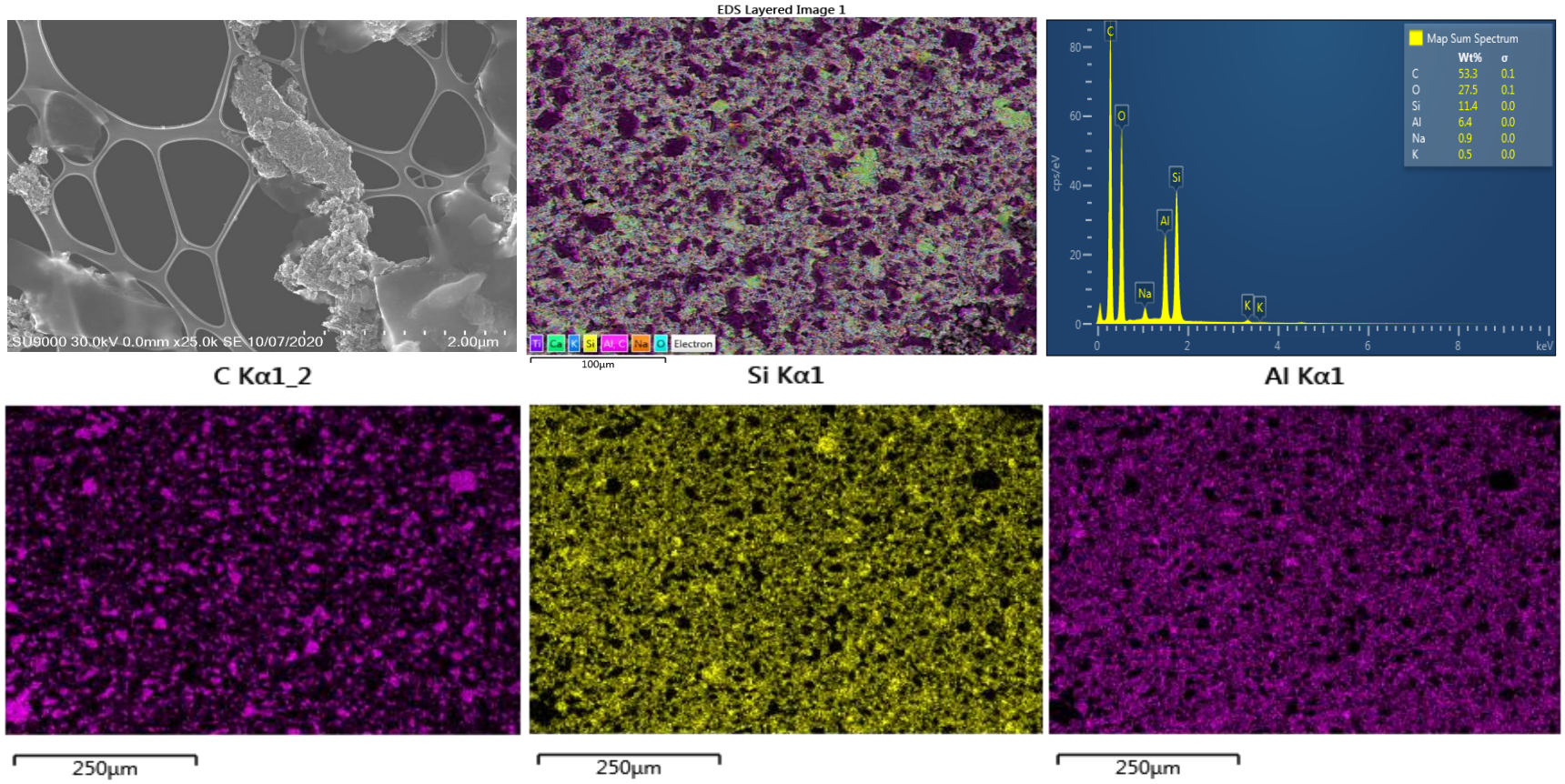

Figure S3.3. STEM-EDS images of Base-cACM.

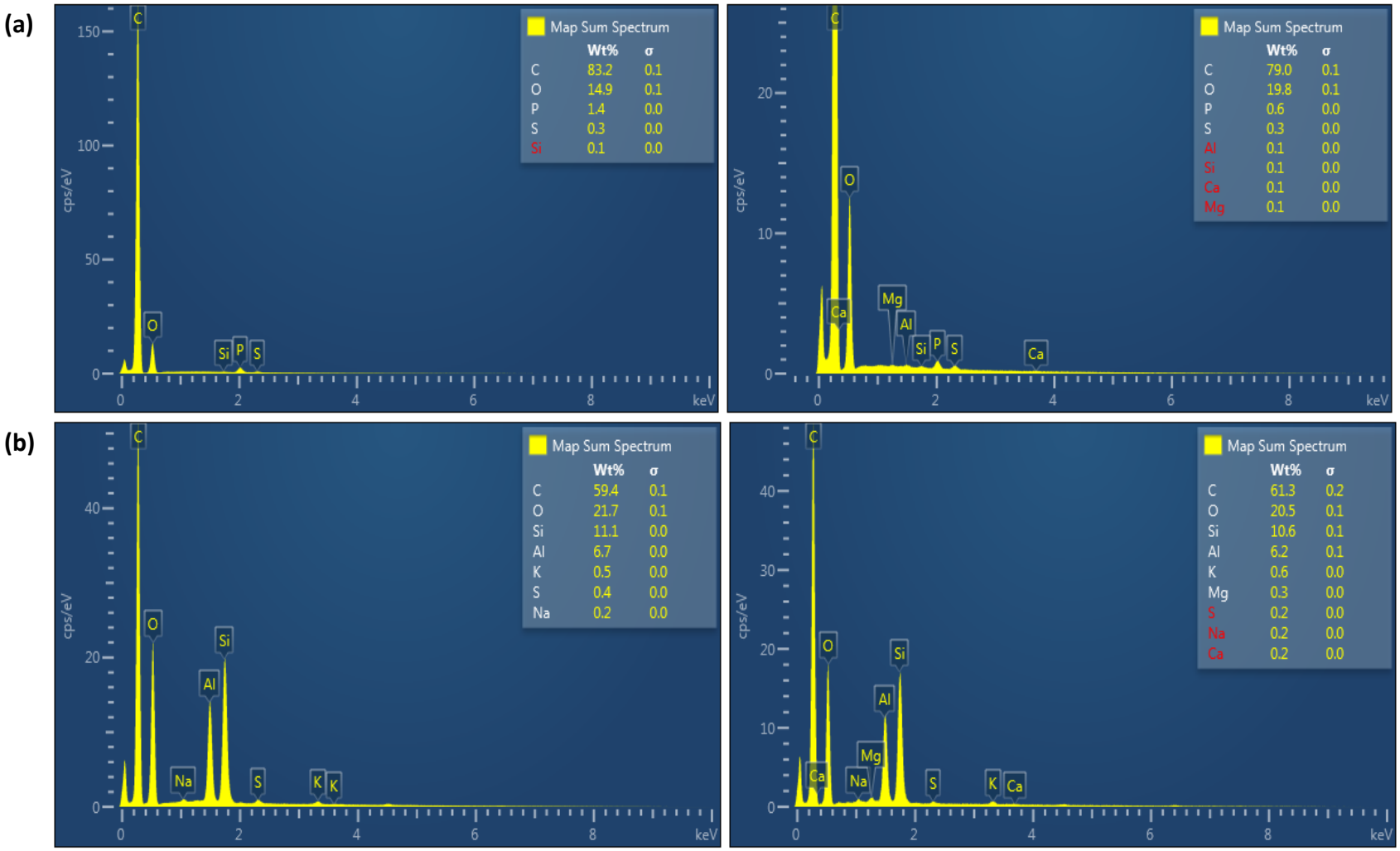

Figure S3.4. EDS images of the fresh and 4th spent (a) GAC-HT-2M and (b) cACM-HT-2M.

Table S3.1. FTIR Analysis of Thermal and Plasma Treated Sulfonated Carbons

Major Peaks cm^{-1}	Amberlyst-15	GAC	cACM	GAC-HT-18M/2M	cACM-HT-2M	GAC-PT	cACM-PT	Assignments	Reference
1008	+	-	-	-	-	-	+	$-SO_3$	Chong et al.,2021
1036	+	-	-	-	-	-	-	(sym O=S=) $-SO_3$/C-S	Liu et al.,2019, Mar and Somsook, 2012
1047	-	+	-	shoulder/+	-	+	-	S=O	Karunagaran et al.,2021
1059	-	-	-	-	+	-	+	-P=O, P-O-C,S=O	Nakhate and Yadav, 2016
1090	-	-	-	-	+	-	+	C-O,P-O	Ma et al.,2021
1105	-	-	-	+/-	-	-	-	S=O	Shaker and Elhamifar, 2020
1128	+	-	-	-/shoulder	-	shoulder	-	$-SO_3$	Kang et al.,2017
1164	-	+	-	+/+	+	+	+	-C-O-C-,P=O	Qin et al.,2020, Zhuang et al.,2020
1170	+	-	-	-	-	-	-	(unsym O=S=O) of $-SO_3$	Mar and Somsook, 2012
1180	-	-	-	-	+	-	+	-S=O	Peng et al.,2017
1272	-	-	-	+/+	+	+	+	C-O	Mengstie and Habtu, 2020
1385	+	-	+	+/+	+	-	+	$-CH_3$	Qin et al.,2020
1414/1450	+	-	-	-	-	-	-	$-CH_2$	Liu et al.,2019
1562	-	-	-	+/+	-	-	-	-C=C-	Wu et al.,2019
1633	+	-	+	-	+	-	+	-C=C-	Mengstie and Habtu, 2020

Table S3.2**.** XPS Analysis of Thermal and Plasma Treated Sulfonated Carbons.[a]

Element	Major Peaks, eV[1]	Amberlyst-15	GAC	cACM	GAC-HT-18M/2M	cACM-HT-2M	GAC-PT	cACM-PT	Assignments
C1s	284	+	+	+	+	-	-	+	-C=C-, C-C
	285	-	-	+	-/+	+	+	+	C-O-C, C=O,
O1s	531	-	+	-	-/-	-	-	-	P=O, C=O, -SO_3
	532	+	+	+	-/-	-	-	+	C=O
	533	-	-	-	+/+	-	+	-	C-O-C
	534	-	-	-	-/-	+	-	-	C-O-C
S2p	163	+	-	-	-/-	-	-	+,weak	C-S-C
	164	-	-	-	+/+	-	-	-	C-S-C
	167	-	-	-	-/-	-	-	-	-SO_3
	168	+	-	-	+/-	-	-	-	-SO_3
	169	Shoulder	-	-	Shoulder/+	-	-	-	-SO_3
P2p	130	-	-	-	+/+	-	+	-	P-O-C
	131	-	-	-	+/+	-	-	-	P-O-C
	132	-	-	-	-/-	-	+	-	P-O-C
	133	-	+,broad	-	+/+	-	+	-	P-O-C, C-P

a, Assignments based on references noted in the text

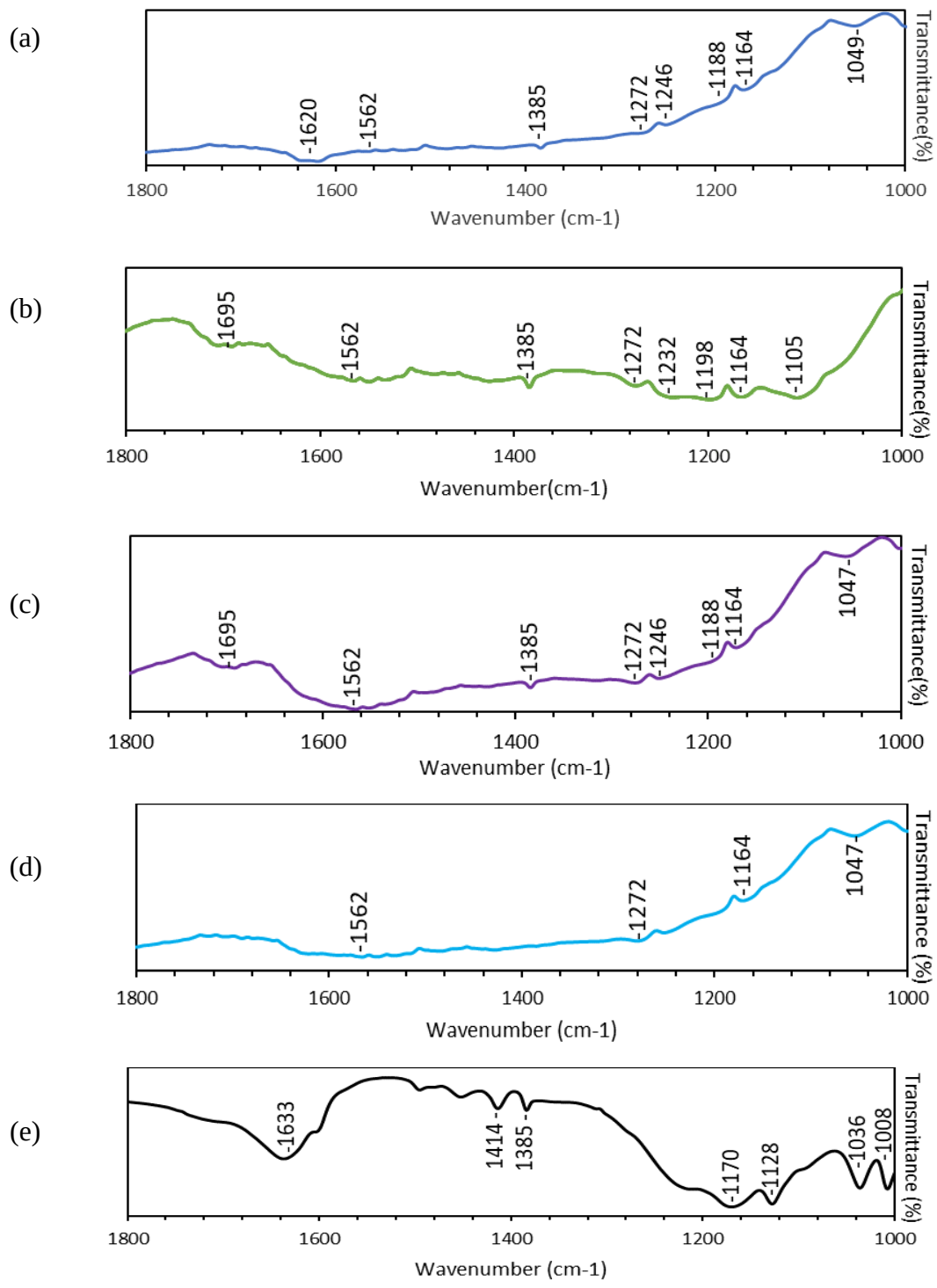

Figure S3.5. (a) FTIR spectra of (a) Base-GAC, (b) GAC-HT-18M, (c) GAC-HT-2M, (d) GAC-PT-Ar/H_2O-15min and (e) Amberlyst-15.

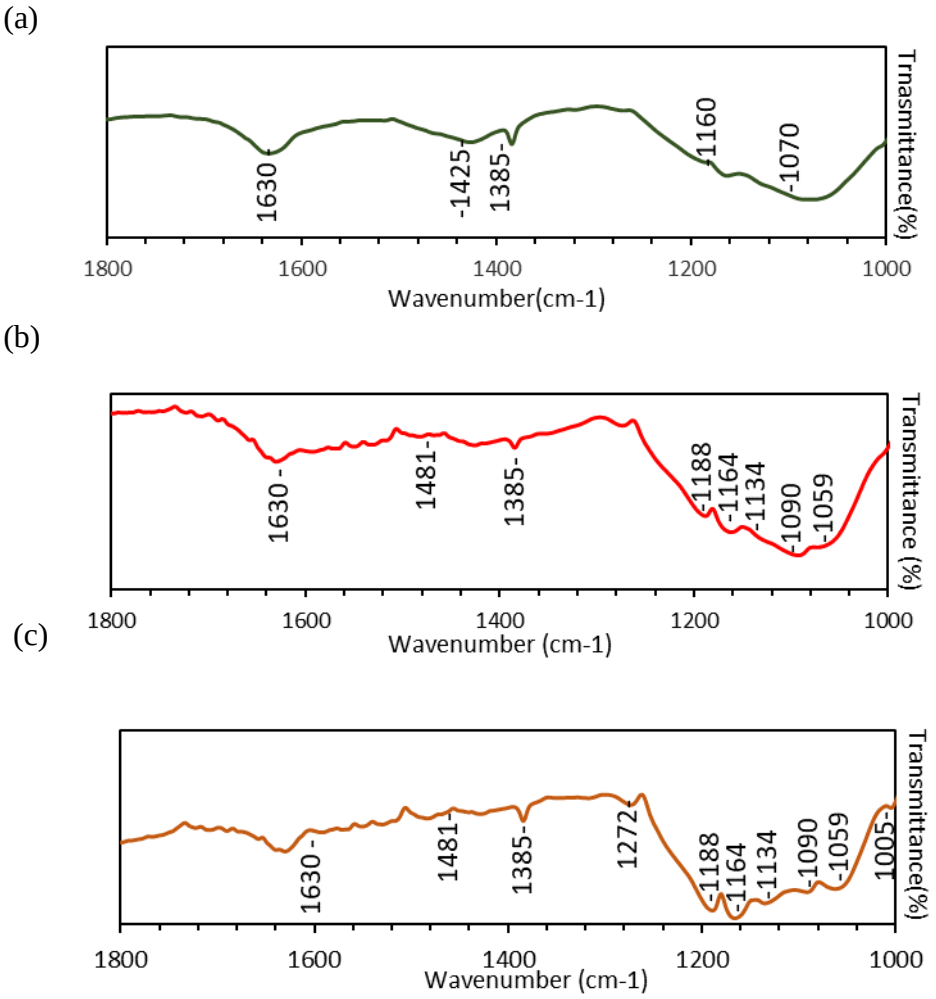

Figure S3.6. FTIR spectra of (a) Base-ACM, (b) cACM-HT-2M, (c) cACM-PT-Ar/H_2O-10min.

References

1) A.Y. Nikiforov, A. Sarani, Ch. Leys, The influence of water vapor content on electrical and spectral properties of an atmospheric pressure plasma jet, Plasma Sources Sci. Technol., 20 (2011) 015014.
2) N. Srivastava, C. Wang, Effects of water addition on OH radical generation and plasma properties in an atmospheric argon microwave plasma jet, J. Appl. Phys., 110 (2011) 053304.
3) A. Bogaerts, E.C. Neyts, Plasma Technology: An Emerging Technology for Energy Storage, ACS Energy Lett., 3 (2018) 1013-1027.
4) T. Kimura, H. Kasugai, Properties of inductively coupled rf Ar/H2 plasmas: Experiment and global model, J. Appl. Phys., 107 (2010) 083308.
5) W.W. Mar, E. Somsook, E, Sulfonic-Functionalized Carbon Catalyst for Esterification of High Free Fatty Acid, Procedia Eng., 32 (2012) 212-218.
6) R. Karunagaran, D. Tran, T.T. Tung, C. Shearer, D. Losic, A Unique Synthesis of Macroporous N-Doped Carbon Composite Catalyst for Oxygen Reduction Reaction, Nanomaterials, 11 (2021) 43.
7) Y. Ma, H. Liang, J. Yin, D. Yao, Y. Xia, K. Zuo, Y-P. Zeng, Air activation of charcoal monoliths for capacitive energy storage, RSC Adv., 11 (2021) 15118.

8) M. Shaker, D. Elhamifar, Sulfonic acid supported on magnetic methylene-based organosilica as an efficient and recyclable nanocatalyst for biodiesel production via esterification, Front. Energy. Res., 8 (2020) 78.
9) S. Kang, G. Zhang, X. Yang, H. Yin, X. Fu, J. Liao, J. Tu, X. Huang, F.G.F Qin, Y. Xu, Effects of *p*-Toluenesulfonic Acid in the Conversion of Glucose for Levulinic Acid and Sulfonated Carbon Production, Energy Fuels, 31 (2017) 2847-2854.
10) J. Zhuang, M. Li, Y. Pu, A.J. Ragauskas, C.G. Yoo, Observation of Potential Contaminants in Processed Biomass Using Fourier Transform Infrared Spectroscopy, Appl. Sci. 10 (2020) 4345.
11) M.A. Mengstie, N.G. Habtu, Synthesis and Characterization of 5-Hydroxymethylfurfural from corncob using solid sulfonated carbon catalyst, Int. J. Chem. Eng., 2020 (2020) 8886361.
12) Z-Y. Wu, P. Yin, H-X. Ju, Z-Q. Chen, C. Li, S-C. Li, H-W. Liang, J-F. Zhu, S-H. Yu, Natural nanofibrous cellulose-derived solid acid catalysts, Research (Wash D C), 2019 (2019) 6262719.

APPENDIX B

SUPLEMENTARY DATA FOR CHAPTER 4

This section comprises the supporting information for chapter 4:

1. Details of the carbon materials used for synthesis of the sulfonated carbon catalysts.
2. Effect of sulfonation time and temperature on sulfonic acid density for the (A) GAC and (B) ACM.
3. Description of external and internal mass transfer calculations.
4. Description of pressure drop calculations.
5. Equilibrium data for the sulfonated carbon catalysts and Amberlyst-15.
6. Physical properties of the spent catalysts.
7. FTIR spectra of (A) Base GAC and sGAC, (B) Base ACM and sACM, and (C) Amberlyst-15.
8. XPS C1s and O1s spectra overlay of the (A) Base GAC and sulfonated GAC and (B) Base ACM and sulfonated ACM.
9. Diethyl ether concentration trends for Amberlyst-15, sulfonated GAC (sGAC) and sulfonated ACM (sACM) on varying the (A) pressure (15-450 psig) and (B) feed flow rate (2-5 mL/min).

10. E-2HIBA space-time yield (STY, g/Lcat/h)), and turnover frequency (TOF, min^{-1}) for the sulfonated GAC (sGAC), sulfonated ACM (sACM), and Amberlyst-15 during time-on-stream.
11. STEM EDS images of (A) Spent-sGAC (B) Spent- sACM and (C) Spent-Amberlyst-15.
12. XPS Spectra overlay of the fresh and spent catalysts of (A) sGAC, (B) sACM and (C) Amberlyst-15.

Details of the carbon materials used for synthesis of the sulfonated carbon catalysts

The wood-based granular activated carbon (GAC) (surface area of 1350 m^2/g and pore volume of 1.2 cc/g) and activated carbon monolith (ACM 101-H) were provided by Applied Catalysts (Laurens, SC) and the ACM was manufactured by coextrusion of 50% activated carbon and 50% of a ceramic binder. Each monolith core has a diameter and length of 1 inch, 400 cells/in^2, wall thickness of 0.01- inch, cell spacing of 0.044- inch, geometric surface area of 70.8 in^2/in^3, open frontal area of 0.59 in^2, density of 350 $kg/m^{3,}$ surface area of 598 m^2/g (BET), pore diameter of 29.8 Å and pore volume of 0.5 cc/g (BJH).

Effect of sulfonation time and temperature on sulfonic acid density

The sulfonation temperature and time are known to impact the catalyst structure and sulfonic acid density. To determine the optimum sulfonation conditions for the GAC and ACM, we treated the carbon materials impregnated with 2M H_2SO_4 hydrothermally at different temperatures (100-250 °C for the GAC and 180-280 °C for the ACM) and times (3 – 12 h). As shown in Figure S4.1, sulfonation temperature had a significant impact on the sulfonic acid density. With the GAC, we noted an increase in sulfonic acid density on increasing the

sulfonation temperature from 100 to 120 °C after which it stabilized and reached a maximum of 0.058 mmol/g at 180 °C. Na and coworkers also noted a similar increased in sulfonic acid density on increasing the sulfonation temperature from 120 to 180 °C. while optimizing the sulfonation temperature of a sulfonated ordered mesoporous carbon catalyst.[1] The ACM, also showed a similar increase in sulfonic acid density on increasing the temperature, reaching a maximum SO_3H density of 0.124 mmol/g at 250 °C. The higher sulfonation temperature requirement of the ACM could be attributed to the more crystalline structure of the ACM in comparison to the GAC. Further increase in temperature to 250 °C with the GAC and 280 °C with the ACM led to a decrease in -SO_3H density, which can be attributed to oxidation or dehydrogenation reactions taking place besides sulfonation.[2,3] Increasing the sulfonation temperature increases the oxidative ability of sulfuric acid, which oversaturates the carbon surface with oxygen-containing groups, thereby preventing further sulfonation.[4] Increase in sulfonation time from 3-12 h led to an increase in both carbon materials with maximum SO_3H densities at 12 h treatment time.

Mass Transfer Calculations for 2HIBA

The Mears and Weisz -Prater criteria were used to determine if external or internal mass transfer resistance affected the kinetic analysis. Mears criterion is evaluated using the relation, [5]

$$\frac{-r_A'\rho_b Rn}{k_c C_{Ab}} < 0.15$$

Equation S4.1

where $-r'_A$ is the reaction rate for 2-HIBA (mmol g^{-1} h^{-1}), ρ_b is the bulk density (kg m^{-3}) , R is the catalyst particle radius (in m, for the sACM, R= wall thickness/2 i.e., 1.27 x 10^{-4} m) n, the

reaction order (we calculated the Mears criterion assuming a second order reaction), k_c is the mass transfer coefficient (m s^{-1}) and $C_{A,b}$ is the bulk liquid phase concentration of 2-HIBA (mol dm^{-3}). A Mears criterion value less than 0.15 indicates the reaction is not externally mass transfer limited.

The Wilke-Chang equation was used to determine the liquid phase diffusion coefficient of 2HIBA in the 2HIBA/ethanol mixture.

$$D_{\mathrm{AB}} = \frac{1.17 \times 10^{-1}\sqrt[3]{\varepsilon_B M_B}T}{\mu_B v_A^{0.6}}$$

Equation S4.2

Where T is the absolute temperature, M_B is the molecular weight and μ_B is the viscosity of ethanol (cP), ε_B is the association factor of ethanol (1.5) and V_A is the molar volume of 2HIBA (0.125 m^3 mol^{-1}).

Effective diffusivity was calculated using the following,

$$De_{ff} = \frac{\varepsilon}{\tau} D_P$$

Equation S4.3

The mass transfer coefficient (k_c) for the sGAC and Amberlyst-15 were estimated from the relation,

$$k_c = 0.266\left(\frac{D_{AB}}{d_p}\right)\mathrm{Re}^{1.15}\, Sc^{1/3}$$

Equation S4.4

In this work, the liquid superficial velocity ranged from 6.6 – 16.5 x 10^{-5} m s^{-1}, while the gas superficial velocity was 16.4 x 10^{-4} m s^{-1}. Therefore, the gas/liquid velocity ratio ranged from 24.9 (Q_l= 2 mL/min) to 9.9 (Q_l= 5 mL/min), indicating that the reactions with the sACM were performed under film flow (Q_g/Q_l = 6 to 200).[6] We thereby assumed that 2-HIBA was

transported from the bulk liquid phase (ethanol) to the solid catalyst through a thin film. Based on this assumption, we estimated the liquid-solid mass transfer coefficient for the sACM, using the film mass transfer coefficient correlation given by Liapis and co-workers[7].

$$\frac{k_f \lambda}{De} = Sh = \alpha_1 Pe^{1/3}$$

Equation S4.5

Where k_f is the film transfer coefficient, λ is the average pore diameter (nm), Sh is the Sherwood number, α_1 is a proportionality constant and is 1 for monoliths of cylindrical geometry. The Peclet number is given by,

$$Pe = \frac{v_m \lambda}{De}$$

Equation S4.6

where ν_m is the liquid superficial velocity (m/s).

The Weisz-Prater criterion was used to assess the effect of internal diffusion limitations within the catalysts and was calculated according to the equation,

$$C_{WP} = \eta \phi_1^2 = \frac{-r_A'(obs)\rho_c R^2}{D_e C_{As}}$$

Equation S4.7

where $-r'_A$ is the observed rate of reaction (mmol/gcat.h), ρ_c is the catalyst density(kg/m^3), R is the catalyst particle radius (m), D_e is the effective diffusivity (m^2/s), $C_{A,s}$ is the concentration of 2-HIBA at the catalyst surface (mol/m^3), η is the internal effectiveness factor and ϕ is the Thiele modulus. A $C_{WP} << 1$, indicates the absence of internal diffusion limitations in the catalyst pellet, however, if $C_{WP} >> 1$, then internal diffusion severely limits the reaction. A summary of the estimated Mears and Weisz -Prater criteria for the three catalysts at the different liquid flow rates studied are presented in Tables S4.1 and S4.2.

Table S4.1. Estimated Mears and Weisz Prater (CWP) criteria for sACM

sACM			
Q_g/Q_l	**Q_l (mL/min)**	**Mears**	**C_{WP}**
24.94	2	1.99×10^{-6}	0.001
16.63	3	1.95×10^{-6}	0.001
9.98	5	1.74×10^{-6}	0.001

Q_g is gas flow rate, Q_l is liquid flowrate, C_{WP} = Weisz -Prater criterion

C_{WP} <<1 indicates that internal mass transfer resistance can be ignored.

$D_{AB(2\text{-}HIBA)} = 1.069 \times 10^{-7}$ m^2/s.

$D_{eff\ (2\text{-}HIBA)} = 1.337 \times 10^{-8}$ m^2/s.

Tortuosity Factor = 4; Internal Void Fraction = 0.5; n or reaction order = 2.

Bulk Liquid Phase Concentrations: $C_{2\text{-}HIBA} = 0.4$ mol/L.

k_f is the film mass-transfer coefficient, m/s.

$\rho_b = 0.28$ g/mL, packing density of sACM, $R = 1.27 \times 10^{-4}$ m, Wall thickness/2 for ACM

Table S4.2. Estimated Mears and Weisz Prater (CWP) criteria for sGAC and Amberlyst-15.

Catalyst	Q_l (mL/min)	Mears	C_{WP}
sGAC	2	0.007	0.006
	3	0.006	0.008
	5	0.001	0.003
Amberlyst-15	2	0.008	0.002
	3	0.006	0.003
	5	0.004	0.003

Q_l is liquid flowrate, C_{WP} = Weisz -Prater criterion

C_{WP} <<1 indicates that internal mass transfer resistance can be ignored.

sGAC

$D_{AB(2\text{-}HIBA)} = 1.07 \times 10^{-7}$ m^2/s; $D_{eff\ (2\text{-}HIBA)} = 1.34 \times 10^{-8}$ m^2/s.

Tortuosity Factor = 4; Internal Void Fraction = 0.5.

ρ_b = 0.27 g/mL, bulk density of sGAC

Amberlyst-15

$D_{AB(2\text{-}HIBA)} = 1.14 \times 10^{-7}$ m^2/s; $D_{eff\ (2\text{-}HIBA)} = 3.17 \times 10^{-8}$ m^2/s.

Tortuosity Factor = 1.3; Internal Void Fraction = 0.36; [8]

ρ_b = 0.69 g/mL, bulk density of Amberlyst-15

Bulk Liquid Phase Concentrations: $C_{2\text{-}HIBA}$ = 0.4 mol/L.

n or reaction order = 2; k_c is the mass-transfer coefficient, m/s.

Pressure Drop calculations

The pressure drop at the optimum reaction conditions for the sulfonated carbons and Amberlyst-15 (Q_l = 3 mL/min, P=300 psig, T= 150 °C for the sulfonated carbons and 120 °C for Amberlyst-15) was calculated and compared. The pressure drop for the sGAC and Amberlyst-15 was estimated using the Ergun equation given below.

$$\frac{dP}{dZ} = -\frac{G}{\rho g_c D_p}\left(\frac{1-\emptyset}{\emptyset^3}\right)\left[\frac{150(1-\emptyset)\mu}{D_p} + 1.75G\right]$$

Equation S4.8

Where $\emptyset$ is porosity, G is superficial mass velocity (ρu), ρ is density, D_p is particle size, u is superficial velocity, P is pressure, Z is bed length and g_c is conversion factor for gravitational acceleration.

For the sACM, the following correlation for pressure drop across a monolithic bed was used.[9]

$$\frac{\Delta p}{L} = \frac{f_0}{2}\frac{\eta_g}{\epsilon_B d_h^2} u_0$$

Equation S4.9

Where f_0 is the friction factor (f_0= 16/Re for monoliths with circular channels), n_g is the viscosity of the fluid (Pa.s), ε_B is the void fraction and d_h is the hydraulic diameter of the monolith channel (m). A summary of the estimated pressure drop values, and comparison between the three catalysts are presented in Table S4.5 and Figure S4.8. Our calculations indicate minimal pressure drop for the small packing heights of the catalysts studied in this work.

Equilibrium data for the sulfonated carbon catalysts and Amberlyst-15

Previously we studied the effect of reaction conditions on 2-HIBA esterification in 75 mL autoclave batch reactors (Parr Series 5000 Multiple Reactor System) and determined the effect of temperature (100, 120, 150 °C), and residence time (0.5, 1, 3 h) on 2-HIBA conversion.[10] It was observed that Amberlyst-15 attained equilibrium conversion at 120 °C, while the sGAC and sACM attained equilibrium conversion at 150 °C, at approximately 1 h reaction time (a further increase in residence time to 3 h did not affect 2-HIBA conversion). An equilibrium conversion of 81% was observed with the sGAC and Amberlyst-15, and 82% with the sACM. Using the equilibrium conversion obtained at the 3 h residence time, the equilibrium constant was estimated from the equation as follows (ideal conditions were assumed).

$$Keq = \frac{X^2}{(1-X)(MR-X)} \qquad \text{Equation S4.10}$$

Where K_{eq}, X and MR are the equilibrium constant, equilibrium conversion and molar ratio respectively. The values of the equilibrium conversion and equilibrium constants obtained with the three catalysts are presented in Table S4.3. The equilibrium constants obtained are lower in comparison to the values reported by other authors [11,12] owing to the high molar ratio of ethanol :2-HIBA used in this work.

Table S4.3. Equilibrium data obtained with the sulfonated carbon catalysts and Amberlyst-15 under batch conditions (120/150 °C, 3 h, 9 bar).

Catalyst	Xeq	Keq	T, °C
sGAC	0.81	0.080	150
sACM	0.82	0.083	150
Amberlyst-15	0.81	0.080	120
Amberlyst-15	0.82	0.084	150

Table S4.4. Physical Properties of the Spent Catalysts.

Catalyst	Total acid density (mmol H^+ g^{-1})	SO_3H Density (mmol g^{-1})	Weak acid groups (COOH/OH) (mmol g^{-1})
sGAC-spent	2.60 ± 0.69	0.005 ± 0.001	2.59 ± 0.69
sACM-spent	2.53 ± 0.31	0.01 ± 0.00	2.52 ± 0.31
Amberlyst 15-spent	5.80 ± 0.92	2.84 ± 0.12	2.96 ± 0.84

Table S4.5. Estimated pressure drop values for the sulfonated carbons and Amberlyst-15.

Catalyst	**ΔP/L (Pa/m)**	**L (m)**	**ΔP(Pa)**
Amberlyst-15	430.68	0.04	15.74
sGAC	28.27	0.11	3.099
sACM	0.069	0.124	0.009

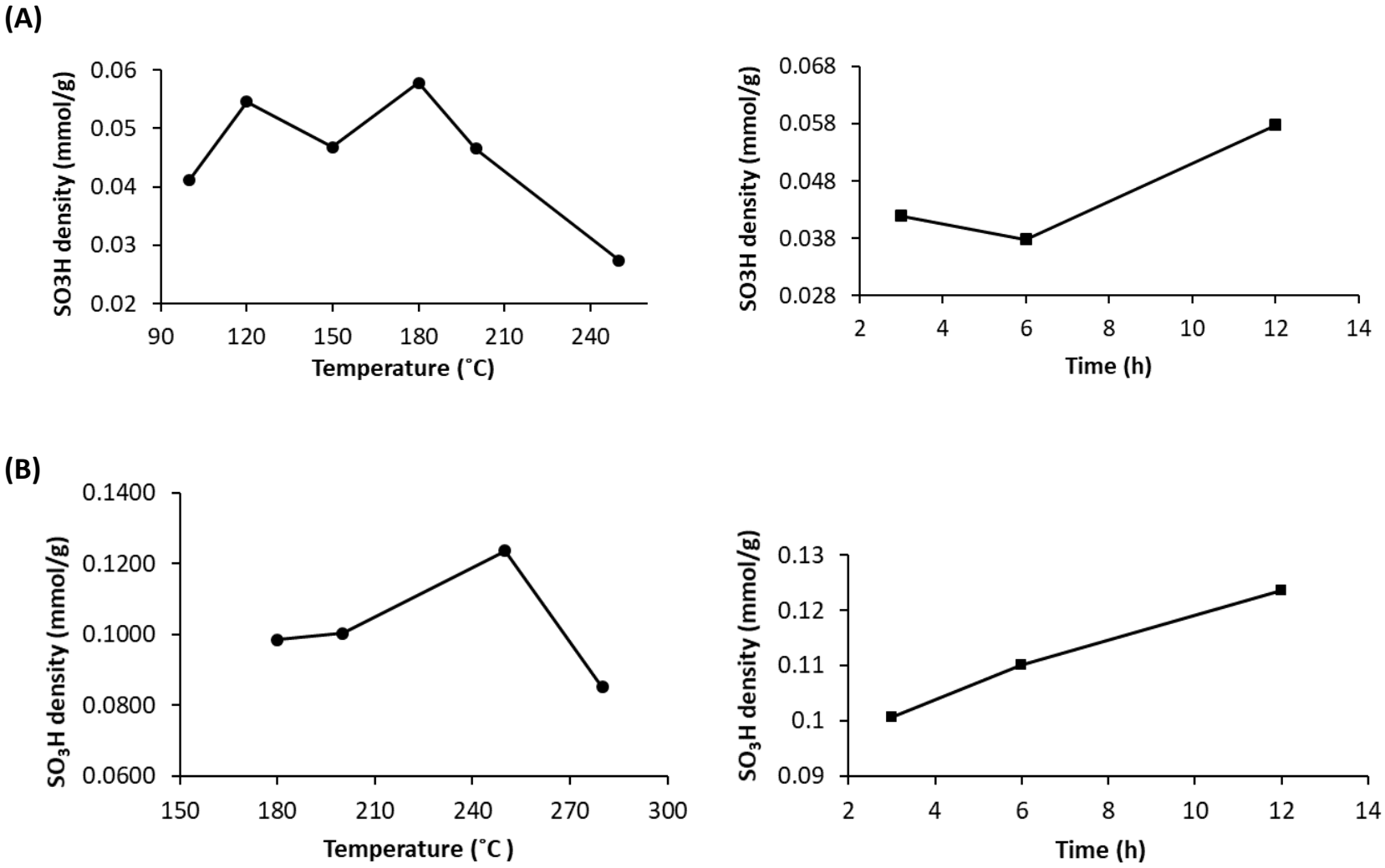

Figure S4.1. Effect of sulfonation time and temperature on sulfonic acid (-SO_3H) density for the (A) GAC and (B) ACM.

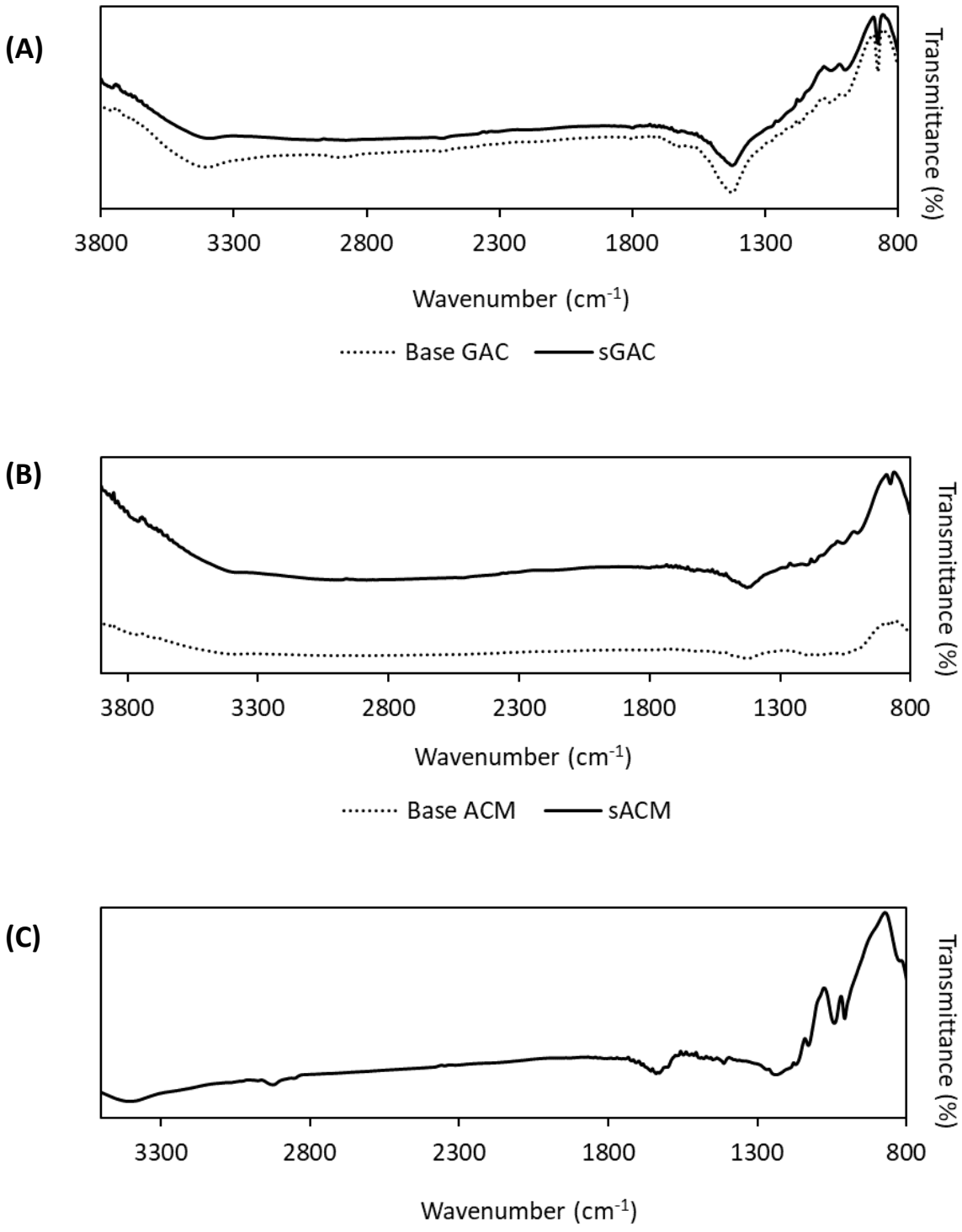

Figure S4.2. FTIR spectra of (A) Base GAC and sGAC, (B) Base ACM and sACM, and (C) Amberlyst-15.

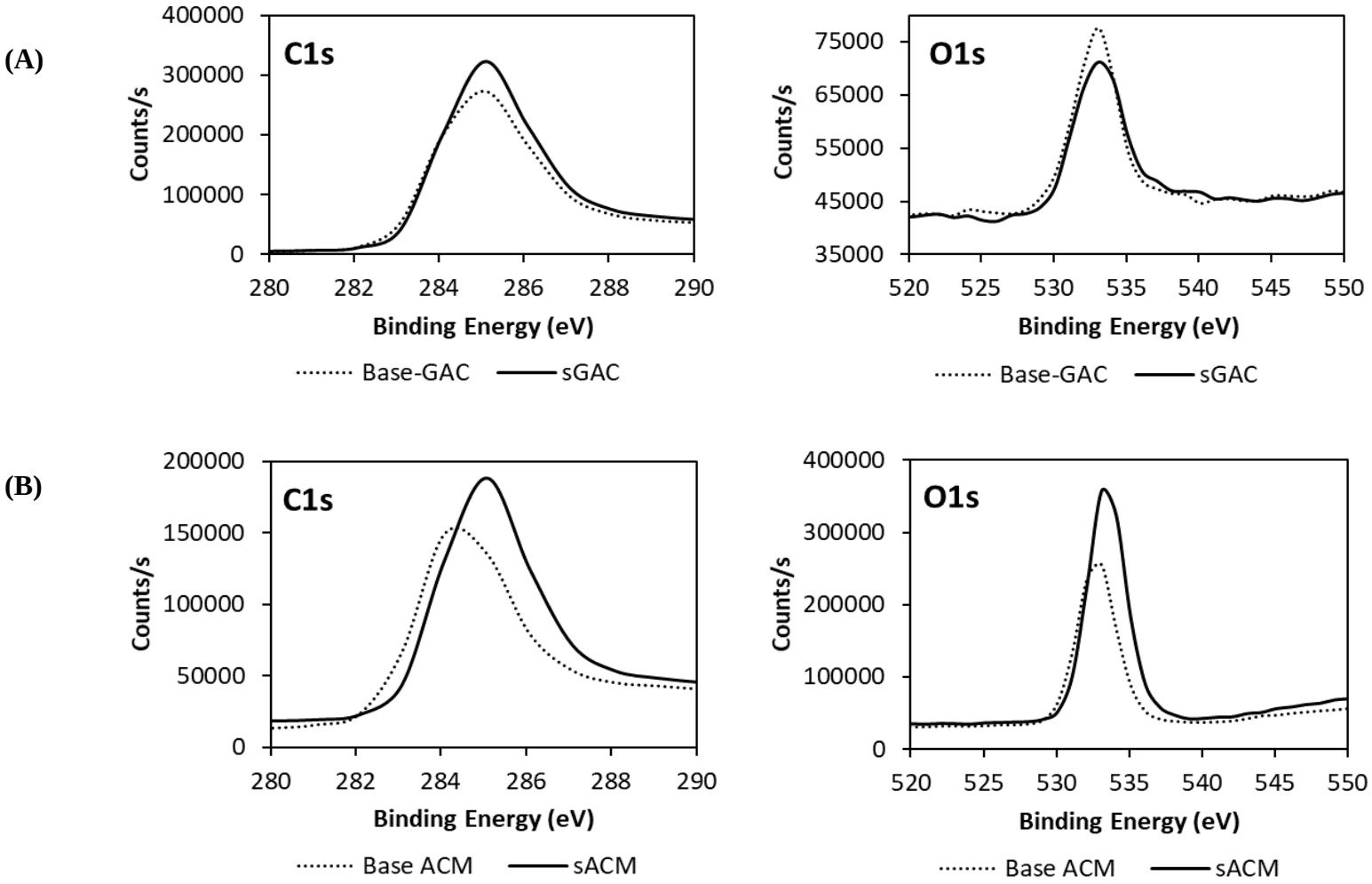

Figure S4.3. XPS C1s and O1s spectra overlay of the (A) Base GAC and sulfonated GAC (sGAC) and (B) Base ACM and sulfonated ACM (sACM).

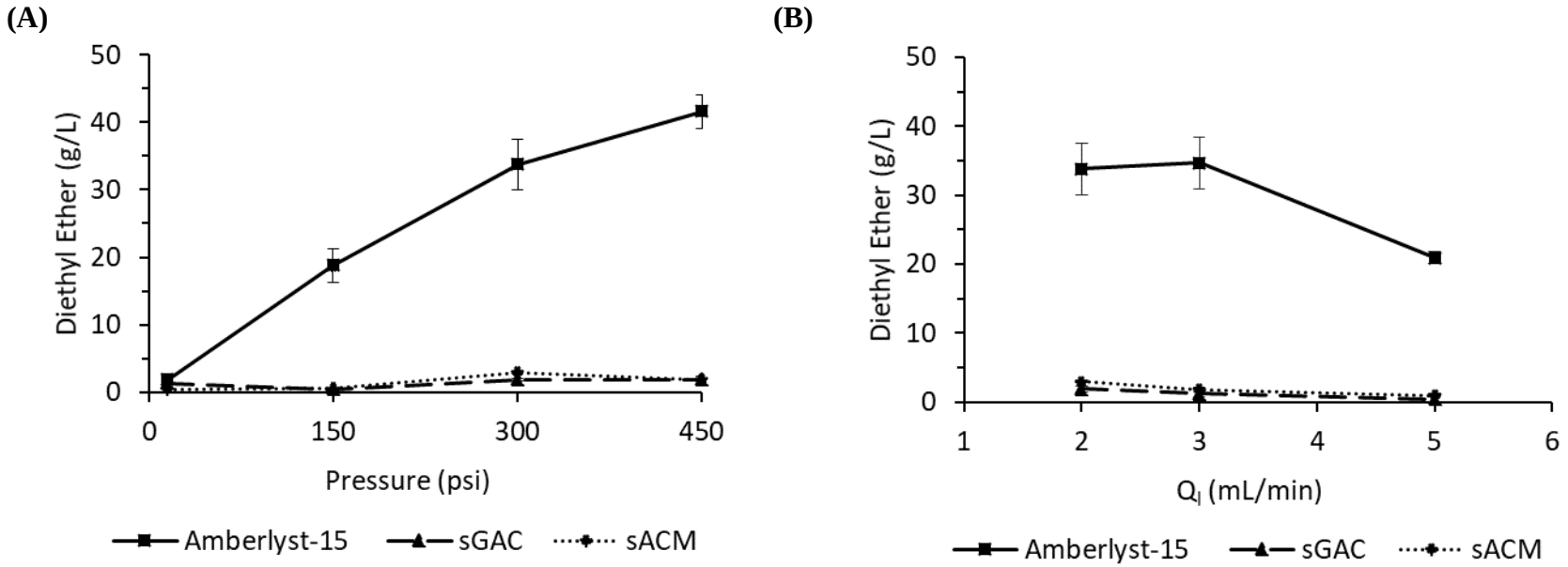

Figure S4.4. Diethyl ether concentration trends for Amberlyst-15, sulfonated GAC (sGAC) and sulfonated ACM (sACM) on varying the (A) pressure (15-450 psig) and (B) feed flow rate (2-5 mL/min). Reaction conditions: T= 120 °C for Amberlyst-15 and 150 °C for sGAC and sACM. The reactions were performed consecutively with the same batch of catalyst with an accumulated time on stream of 4 h.

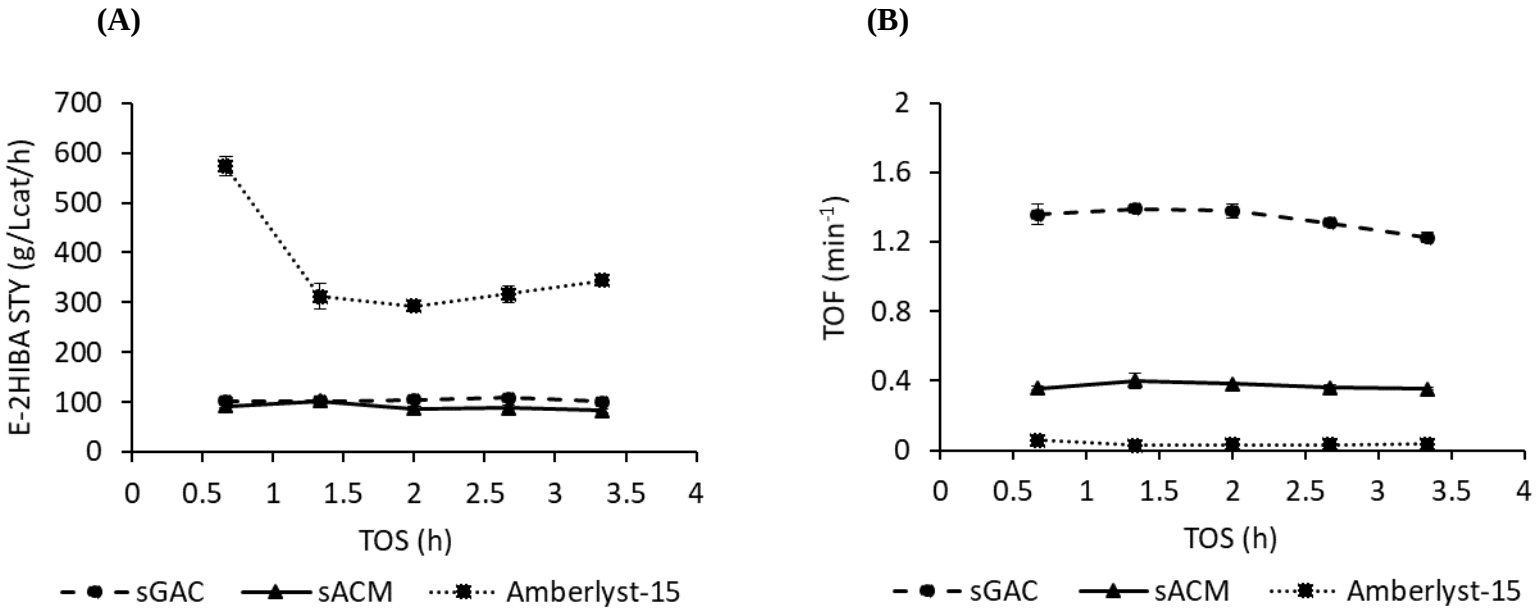

Figure S4.5.(A) E-2HIBA space-time yield (STY, g/Lcat/h), and (B) turnover frequency (TOF, min^{-1}) for the sulfonated GAC (sGAC), sulfonated ACM (sACM), and Amberlyst-15 during time-on-stream. Reaction conditions: Q_l = 3 mL/min, P = 300 psig, T= 120 °C for Amberlyst-15 and 150 °C for sGAC and sACM.

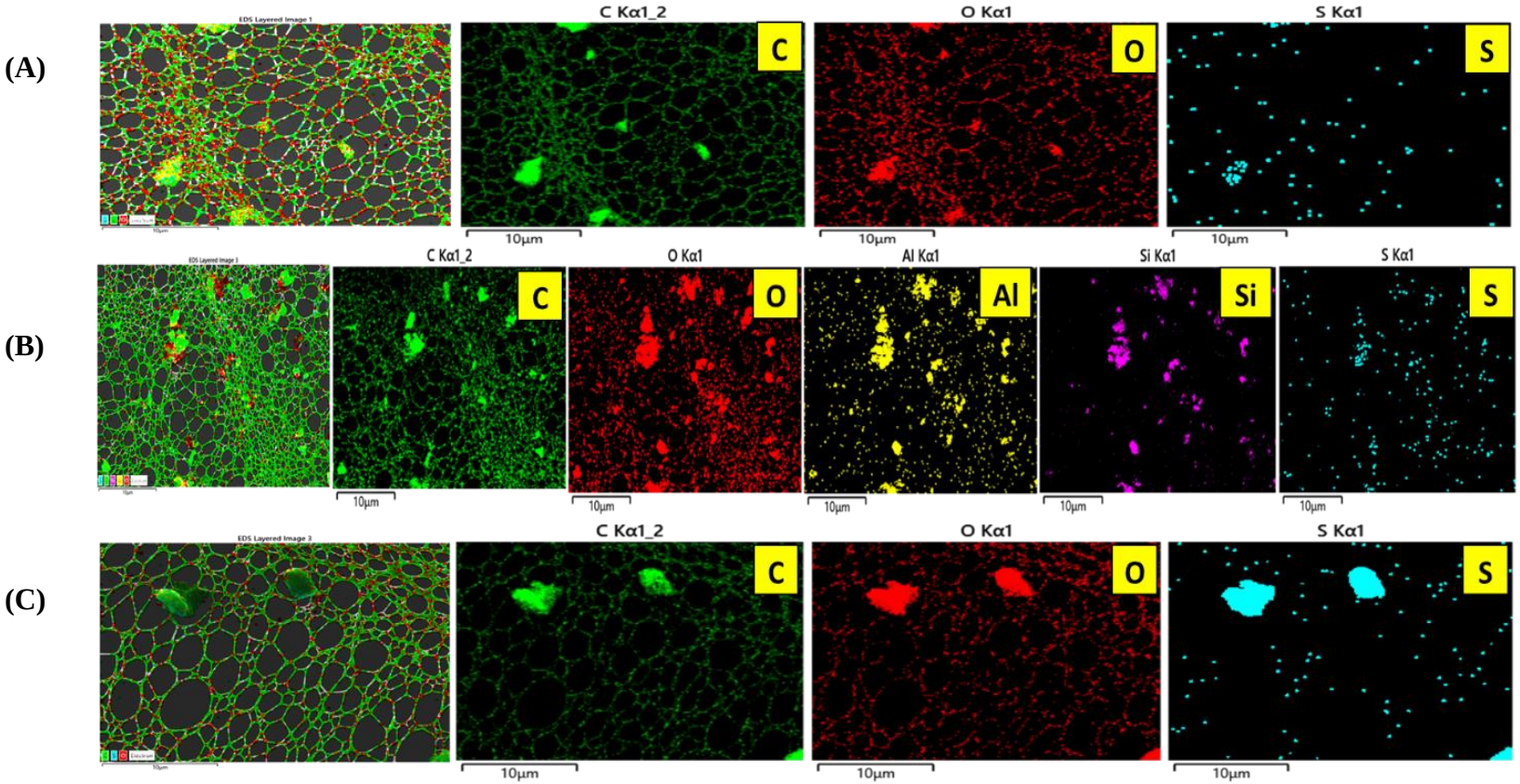

Figure S4.6. STEM EDS images of (A) Spent-sGAC (B) Spent- sACM and (C) Spent-Amberlyst-15

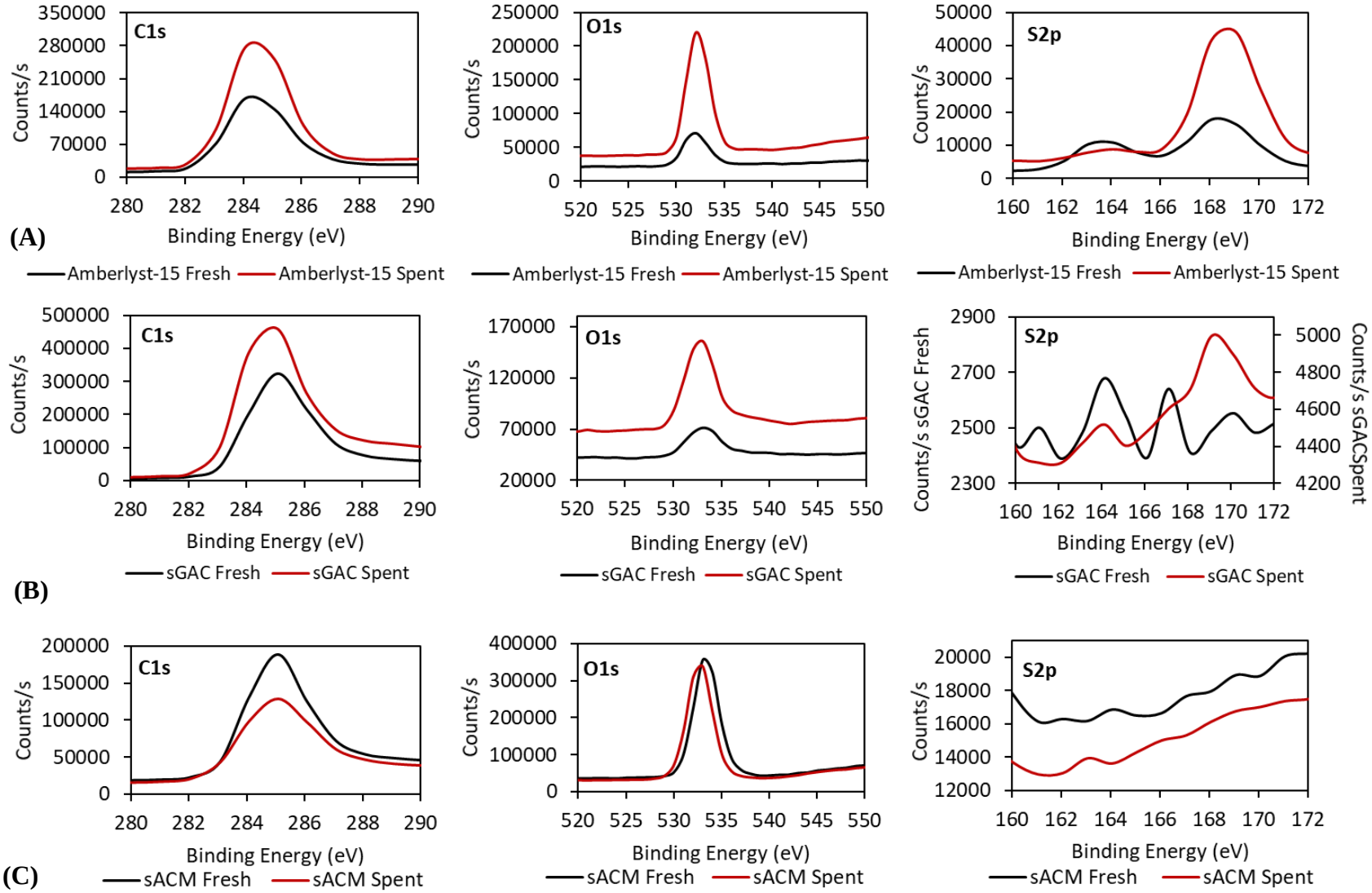

Figure S4.7. XPS Spectra overlay of the fresh and spent catalysts of (A) Amberlyst-15 (B) sGAC, (C) sACM.

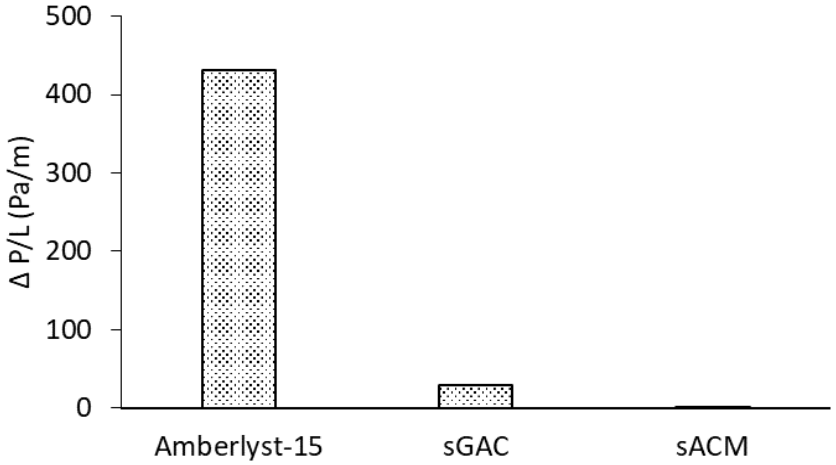

Figure S4.8. Comparison of pressure drop for the sulfonated carbons and Amberlyst-15 (Reaction conditions: Q_l = 3 mL/min, P=300 psig, T= 150 °C for the sulfonated carbons and 120 °C for Amberlyst-15).

References

1) S. Na, Z. Minhua, D. Xiuqin, W. Lingtao, Preparation of sulfonated ordered mesoporous carbon catalyst and its catalytic performance for esterification of free fatty acids in waste cooking oils, RSC Adv., 9 (2019) 15941.
2) K. Ngaosuwan, J.G. Goodwin Jr., P. Prasertdham, A green sulfonated carbon-based catalyst derived from coffee residue for esterification, Renew. Energ., 86 (2016) 262-269.
3) W. Mateo, H. Lei, E. Villota, M. Qian, Y. Zhao, E. Huo, Q. Zhang, X. Lin, C. Wang, Z. Huang, Synthesis and characterization of sulfonated activated carbon as a catalyst for bio-jet fuel production from biomass and waste plastics, Bioresour Technol., 297(2020) 122411.
4) A.P. Koskin, Y. V. Larichev, I. V. Mishakov, M. S. Mel'gunov, A. A. Vedyagin, Synthesis and characterization of carbon nanomaterials functionalized by direct treatment with sulfonating agents, Micropor. Mesopor. Mat. 299 (2020) 110130.
5) H.S. Fogler, Elements of chemical reaction engineering, Prentice-Hall, 5th ed.; Englewood Cliffs: New Jersey, 1986; pp 600-650.
6) M. Pirmoradi, N. Janulaitis, R.J. Gulotty, Jr., J.R. Kastner, Continuous hydrogenation of aqueous furfural using a metal-supported activated carbon monolith, ACS Omega, 5 (2020) 7836-7849.
7) A. I. Liapis, J.J. Meyers, O.K. Crosser. Modeling and simulation of the dynamic behavior of monoliths. Effects of pore structure from pore network model analysis and comparison

with columns packed with porous spherical particles, J. Chromatogr. A. 865 (1999) 13-25.

8) Z. Ziyang, K. Hidajat, A.K. Ray. Determination of adsorption and kinetic parameters for methyl *tert*-butyl ether synthesis from *tert*-butyl alcohol and methanol, J. Catal., 200 (2001) 209-221.

9) W. Liu, W. P. Addiego, C. M. Sorensen, T. Boger, Monolith reactor for the dehydrogenation of ethylbenzene to styrene, Ind. Eng. Chem. Res., 41 (2002) 3131-3138.

10) S. Sripada, J.R. Kastner, Catalytic esterification using solid acid carbon catalysts synthesized by sustainable hydrothermal and plasma sulfonation techniques, Ind. Eng. Chem. Res, 61 (2022) 3928-3940.

11) M-J. Lee, J-Y. Chiu, H-m. Lin, Kinetics of catalytic esterification of propionic acid and *n*-butanol over Amberlyst 35, Ind. Eng. Chem. Res., 41 (2002) 2882-2887.

12) J-W Lin, A.H. Zaki, H-T. Wu, H-m. Lin, M-J. Lee, Kinetics study on esterification of acrylic acid and ethanol over acidic cation-exchange resin beads Amberlyst 35, J. Taiwan Inst. Chem. 102 (2019).

APPENDIX C

SUPLEMENTARY DATA FOR CHAPTER 5

Table S5.1. Estimated Mears and Weisz Prater (CWP) criteria for sGAC.

Catalyst	**Q_l (mL/min)**	**Mears**	**C_{WP}**
sGAC	2	0.011	0.009
	3	0.006	0.009
	4	0.004	0.008
	5	0.004	0.010
	6	0.003	0.009

Q_l is liquid flowrate, C_{WP} = Weisz -Prater criterion

C_{WP} <<1 indicates that internal mass transfer resistance can be ignored.

Mears criterion < 0.15 indicates that external mass transfer resistance can be ignored.

$D_{AB(2\text{-}HIBA)} = 1.069 \times 10^{-7}$ m^2/s; $D_{eff\ (2\text{-}HIBA)} = 1.337 \times 10^{-8}$ m^2/s.

Tortuosity Factor = 4; Internal Void Fraction = 0.5.

ρ_b = 0.27 g/mL, bulk density of sGAC

Bulk Liquid Phase Concentrations: $C_{2\text{-}HIBA}$ = 0.4 mol/L.

n or reaction order = 2; k_c is the mass-transfer coefficient, m/s.

Table S5.2. Estimated Mears and Weisz Prater (CWP) criteria for sACM.

sACM			
Q_g/Q_l	**Q_l (mL/min)**	**Mears**	**C_{WP}**
24.9	2	5.5×10^{-6}	0.002
16.6	3	5.0×10^{-6}	0.002
12.5	4	5.7×10^{-6}	0.002
10	5	5.4×10^{-6}	0.002
8.3	6	4.8×10^{-6}	0.002

Q_g is gas flow rate, Q_l is liquid flowrate, C_{WP} = Weisz -Prater criterion

C_{WP} <<1 indicates that internal mass transfer resistance can be ignored.

Mears criterion < 0.15 indicates that external mass transfer resistance can be ignored.

$D_{AB(2\text{-}HIBA)} = 1.07 \times 10^{-7}$ m^2/s.

$D_{eff\ (2\text{-}HIBA)} = 1.34 \times 10^{-8}$ m^2/s.

Tortuosity Factor = 4; Internal Void Fraction = 0.5; n or reaction order = 2.

Bulk Liquid Phase Concentrations: $C_{2\text{-}HIBA}$ = 3.28 mol/L.

k_f is the film mass-transfer coefficient, m/s.

ρ_b = 0.28 g/mL, packing density of sACM, R = 1.27×10^{-4} m, Wall thickness/2 for ACM

Determination of equilibrium constant

With the assumptions of a second order reversible reaction, the apparent reaction rate of 2-HIBA esterification with ethanol can be given by the expression[1,2],

$$-\frac{dC_{2HIBA}}{dt} = k_1 C_{2HIBA} C_{EtOH} - k_2 C_{E2HIBA} C_{H2O}$$ Equation S5.1

Where C_{2HIBA}, C_{EtOH}, $C_{E\text{-}2HIBA}$ and C_{H2O} are the concentrations of 2HIBA, Ethanol (EtOH), E-2HIBA, and water and k_1 and k_2 are the forward and reverse reaction rate constants.

$$MR = \frac{C_{EtOH_0}}{C_{2HIBA_0}}$$ Equation S5.2

$$C_{2HIBA_0} X_{2HIBA} = C_{EtOH_0} X_{EtOH}$$ Equation S5.3

$$C_{E2HIBA_0} = C_{H2O_0} = 0$$ Equation S5.4

$$\frac{dC_{2HIBA}}{dt} = k_1 C_{2HIBA_0} \left((1 - X_{2HIBA})(MR - X_{2HIBA}) - \frac{X^2_{2HIBA}}{K_{eq}} \right)$$ Equation S5.5

Where MR is the molar ratio of ethanol to 2-HIBA, C_{2HIBA0}, C_{EtOH0}, $C_{E2HIBA0}$ and C_{H2O0} are the initial concentrations of 2HIBA, Ethanol (EtOH), E-2HIBA, and water respectively. X_{2HIBA} is the fractional conversion of 2-HIBA and $K_{eq} = k_1/k_2$ is the equilibrium constant of the reaction. At equilibrium $dC_{2HIBA}/dt=0$, therefore the concentration-based equilibrium constant under ideal conditions can be given by the relation,

$$K_{eq} = \frac{k_f}{k_r} = \frac{[E2HIBA][H_2O]}{[2HIBA][EtOH]} = \frac{X_{eq}^2}{(1 - X_{eq})(MR - X_{eq})}$$ Equation S5.6

Rate Law Development

Langmuir-Hinshelwood (LH) model

The Langmuir-Hinshelwood (LH) model assumes that both reactants are adsorbed onto the active sites of the catalyst. The adsorption, surface reaction and desorption steps are as follows[3]:

$$2HIBA + S \longleftrightarrow 2HIBA \cdot S$$

$$EtOH + S \longleftrightarrow EtOH \cdot S$$

$$2HIBA \cdot S + EtOH \cdot S \longleftrightarrow E\,2HIBA \cdot S + H_2O \cdot S$$

$$E2HIBA \cdot S \longleftrightarrow E2HIBA + S$$

$$H_2O \cdot S \longleftrightarrow H_2O + S$$

In the development of the LH model, the rate equation is derived in terms of surface concentration of the adsorbed species and vacant sites. For the esterification of 2-HIBA and ethanol,

$$2HIBA + Et0H \longleftrightarrow E2HIBA + H_2O$$

C_{2HIBA}, C_{EtOH}, C_{E2HIBA}, C_{H2O} and C_{2HIBAs}, C_{EtOHs}, $C_{E2HIBAs}$, C_{H2Os} are the concentrations of 2-HIBA, ethanol (EtOH), E-2HIBA, and water in the bulk liquid phase and adsorbed on the catalyst surface respectively. C_0 is the total concentration of active sites and C_v is the concentration of vacant sites on the catalyst surface. The rate of surface reaction is given by,

$$r = k_f C_{2HIBAs} C_{EtOHs} - k_r C_{E2HIBAs} C_{H_2Os} \qquad \text{Equation S5.7}$$

Where k_f and k_r are the rate constants for the forward and reverse surface reactions respectively.

$$= k_f \left[C_{2HIBAs} C_{EtOHs} - \frac{k_r}{k_f} C_{E2HIBAs} C_{H_2Os} \right] \qquad \text{Equation S5.8}$$

$$= k_f \left[C_{2HIBAs} C_{EtOHs} - \frac{1}{K_s} C_{E2HIBAs} C_{H_2Os} \right] \qquad K_s = \frac{k_f}{k_r}$$

Equation S5.9

Since all the other steps are assumed to be in equilibrium, the concentration of the adsorbed species is obtained by the following equations. For the adsorption and desorption steps,

$$K_{2HIBA} = \frac{C_{2HIBAs}}{C_{2HIBA} . C_v} \qquad K_{EtOH} = \frac{C_{EtOHs}}{C_{EtOH} . C_v} \qquad K_{E2HIBA} = \frac{C_{E2HIBAs}}{C_{E2HIBA} . C_v}$$

$$K_{H_2O} = \frac{C_{H_2Os}}{C_{H_2O} . C_v}$$

Equation S5.10

Where K_{2HIBA}, K_{EtOH}, K_{E2HIBA} and K_{H2O} are the adsorption equilibrium constants. Further the adsorbed surface concentrations are given as,

$$C_{2HIBAs} = K_{2HIBA} C_{2HIBA} C_V$$ Equation S5.11

$$C_{EtOHs} = K_{EtOH} C_{EtOH} C_V$$ Equation S5.12

$$C_{E2HIBAs} = K_{E2HIBA} C_{E2HIBA} C_V$$ Equation S5.13

$$C_{H_2Os} = K_{H_2O} C_{H_2O} C_V$$ Equation S5.14

Substituting equations S5.10-14 in equation S5.9,

$$r = k_f K_{2HIBA} K_{EtOH} \left[C_{2HIBA} C_{EtOH} - \frac{K_{E2HIBA} K_{H_2O}}{K_s K_{2HIBA} K_{EtOH}} C_{E2HIBA} C_{H_2O} \right] C_V^2$$

Equation S5.15

The total concentration of active sites C_0 is given by,

$$C_0 = C_{2HIBAs} + C_{EtOHs} + C_{E2HIBAs} + C_{H_2Os} + C_V$$ Equation S5.16

$$= C_V\,[1 + K_{2HIBA}C_{2HIBA} + K_{EtOH}C_{EtOH} + K_{E2HIBA}C_{E2HIBA} + K_{H_2O}C_{H_2O}]$$ Equation S5.17

$$C_V = \frac{C_0}{[1 + K_{2HIBA}C_{2HIBA} + K_{EtOH}C_{EtOH} + K_{E2HIBA}C_{E2HIBA} + K_{H_2O}C_{H_2O}]}$$ Equation S5.18

For the esterification of 2-HIBA and ethanol, the equilibrium constant is given by,

$$K = \frac{(C_{E2HIBAs}/K_{E2HIBA}C_V)(C_{H_2Os}/K_{H_2O}C_V)}{(C_{2HIBAs}/K_{2HIBA}C_V)(C_{EtOHs}/K_{EtOH}C_V)} = \frac{C_{E2HIBAS}C_{H_2OS}}{C_{2HIBAS}C_{EtOHS}} \cdot \frac{K_{2HIBA}K_{EtOH}C_V^2}{K_{E2HIBA}K_{H_2O}C_V^2}$$

$$K = \frac{K_{2HIBA}K_{EtOH}}{K_{E2HIBA}K_{H_2O}} \cdot K_s$$ Equation S5.19

Substituting equation S5.18, and S5.19 in S5.15, the rate expression is obtained.

$$r = k_f K_{2HIBA} K_{EtOH} C_0^2 \frac{C_{2HIBA}C_{EtOH} - \frac{1}{K}C_{E2HIBA}C_{H_2O}}{[1 + K_{2HIBA}C_{2HIBA} + K_{EtOH}C_{EtOH} + K_{E2HIBA}C_{E2HIBA} + K_{H_2O}C_{H_2O}]^2}$$

Equation S5.20

Eley-Rideal Model

The E-R model assumes that the reaction is taking place between adsorbed molecules of 2HIBA and ethanol molecules in the bulk solution. Considering negligible adsorption of the ester, yet taking into account the adsorption of water, and assuming surface reaction is the rate determining step, the reaction mechanism is given as follows:[4]

$$2HIBA + S \longleftrightarrow 2HIBA \cdot S$$

$$2HIBA \cdot S + EtOH \longleftrightarrow E2HIBA + H_2O \cdot S$$

$$H_2O \cdot S \longleftrightarrow H_2O + S$$

The rate of the surface reaction can be given as,

$$r = k_f \ C_{2HIBAs} C_{EtOH} - k_r \ C_{E2HIBA} C_{H2Os} \qquad \text{Equation S5.21}$$

$$K_S = \frac{k_f}{k_r} \qquad \text{Equation S5.22}$$

Where C_{2HIBA}, C_{EtOH}, C_{E2HIBA}, C_{H2O} and C_{2HIBAs} and C_{H2Os} are the concentrations of 2-HIBA, ethanol (EtOH), E-2HIBA, and water in the bulk liquid phase and adsorbed on the catalyst surface respectively. k_f and k_r are the rate constants for the forward and reverse surface reactions, respectively.

Assuming all other steps are in equilibrium, the concentrations of adsorbed 2HIBA and water can be given as,

$$C_{2HIBAs} = K_{2HIBA} \ C_{2HIBA} C_v \qquad \text{Equation S5.23}$$

$$C_{H2Os} = K_{H2O} C_{H2O} C_v \qquad \text{Equation S5.24}$$

Where K_{2HIBA} and K_{H2O} are the adsorption/desorption equilibrium constants and C_v is the concentration of vacant sites on the catalyst surface.

C_0 , the total concentration of active sites is given as

$$C_0 = C_{2HIBAs} + C_{H2Os} + C_V \qquad \text{Equation S5.25}$$

$$= C_V (1 + K_{2HIBA}\ C_{2HIBA} + K_{H2O} C_{H2O}) \qquad \text{Equation S5.26}$$

$$C_V = \frac{C_0}{(1 + K_{2HIBA}\ C_{2HIBA} + K_{H2O} C_{H2O})} \qquad \text{Equation S5.27}$$

$$C_{2HIBAs} = \frac{K_{2HIBA}\ C_{2HIBA} C_0}{(1 + K_{2HIBA}\ C_{2HIBA} + K_{H2O} C_{H2O})} \qquad \text{Equation S5.28}$$

$$C_{H2Os} = \frac{K_{H2O} C_{H2O} C_0}{(1 + K_{2HIBA}\ C_{2HIBA} + K_{H2O} C_{H2O})} \qquad \text{Equation S5.29}$$

Substituting the above equations in S5.21, the following rate expression is obtained.

$$r = k_f C_0 \frac{\left[K_{2HIBA}\ C_{2HIBA} C_{EtOH} - \frac{1}{K_s} C_{E2HIBA} K_{H2O} C_{H2O}\right]}{(1 + K_{2HIBA}\ C_{2HIBA} + K_{H2O} C_{H2O})} \qquad \text{Equation S5.30}$$

$$r = k_f C_0 K_{2HIBA} \frac{\left[C_{2HIBA} C_{EtOH} - \frac{1}{K} C_{E2HIBA} C_{H2O}\right]}{1 + K_{2HIBA}\ C_{2HIBA} + K_{H2O} C_{H2O}} \qquad K = K_S \frac{K_{H2O}}{K_{2HIBA}} \qquad \text{Equation S5.31}$$

References

1) C.R. Khudsange, K.L. Wasewar, Kinetics study and parametric sensitivity analysis of esterification of butyric acid with benzyl alcohol: A Taguchi methodology approach, Int. J. Chem. React. Eng., 2018, 20170146.

2) S.Z. Hassan, M. Vinjamur, Analysis of sensitivity of equilibrium constant to reaction conditions for esterification of fatty acids with alcohols, Ind. Eng. Chem. Res, 52 (2013) 1205-1215.

3) H.S. Fogler, Elements of chemical reaction engineering, Prentice-Hall, 5th ed.; Englewood Cliffs: New Jersey, 1986; pp 600-650.

4) S. Akyalcin, M.R. Altiokka, Kinetics of esterification of acetic acid with 1-octanol in the presence of Amberlyst 36, Appl. Catal. A-Gen. 429-430 (2012) 79-84.